COMPARATIVE STUDY OF PHYSICAL PROPERTIES OF ZIRCONIA BASED DENTAL CERAMICS

Thesis submitted by

Piyapanna Pittayachawan

For the degree of

DOCTOR OF PHILOSOPHY

Eastman Dental Institute

Division of Biomaterials and Tissue Engineering

University College London

256 Gray's Inn Road

London

WC1X 8LD

-2008-

Abstract

The aim of this project was to evaluate and compare the mechanical properties of commercial yttria partially stabilized tetragonal zirconia polycrystalline (Y-TZP) ceramics, which have generated interest in restorative dentistry because of their high strength and high resistance to fracture.

Mechanical properties of three commercial Y-TZP ceramics (Lava™, Cercon® and Invizion™) were investigated including the biaxial flexural strength, hardness, fatigue, and subcritical crack growth. Crown shaped specimens (Kavo Everest ZS-blanks with IPS e.max® Ceram and IPS e.max® Zirpress) were submitted to the fatigue followed by biaxial flexural strength test. The microstructure was analysed using AFM, and elemental analysis and fracture pattern were analysed via SEM. Additionally, stress induced transformation toughening was studied using Vickers indentation (load 20-50 kg) and Raman spectroscopy. The phase transformation was also analysed on fracture surfaces of specimens that failed after biaxial flexural strength and subcritical crack growth test.

The results of this project showed no significant difference in the mean biaxial flexural strength of uncoloured and coloured Lava™; however, Cercon® (823±115 MPa) and Invizion™ (828±87 MPa) had significantly lower flexural strength than Lava™ groups (~1100 MPa). All groups had similar hardness values (>1300 Hv). The survival strength of three commercial ceramics ranged from 60 to 70% of their mean biaxial flexural strength at 500,000 cycles. The types of sintering processes (heat pressed and sintered methods) did not influence the flexural strength of crown shaped specimens after fatigue for 50,000 cycles. The subcritical crack growth parameter ranged from 30-197. There were differences in the appearance of the microstructure and the amount of elemental components between the three Y-TZP ceramics. The XRD showed that the as-received surface had three phases, which were tetragonal cubic1 and cubic 2 (slightly larger than cubic 1). The polished surface contained two phases, which were tetragonal and cubic 1. The Raman spectroscopy revealed that the variation of loads had little effect on the level of transformation toughening per unit area; however, the transformation was varied by the distance from the centre to outside the indentation area. The cubic phase had the highest level at the centre while the tetragonal phase was found at a higher level outside the indentation. The monoclinic phase was only detected within the indentation area. For the fractured specimens, monoclinic and cubic phase were found at a higher level at the fracture origin, tension and compression sites.

Further study examined the biaxial flexural strength and shear bond strength of zirconia containing 1, 2 and 5 wt% titanium phosphate glasses in order to identify whether glass affected the flexural and bond strengths. The results showed that the addition of glass 5 wt% or greater lead to the dramatic decrease of the biaxial flexural strength. There was also no significant difference in biaxial flexural strength and shear bond strength between titanium phosphate glass zirconia 0 wt%, 1 wt% and 2 wt% glasses zirconia etched for 2 and 5 minutes.

Therefore, this project concluded that there was a difference in properties and phase transformation between Lava™ Cercon® and Invizion™ groups.

Acknowledgements

Firstly, I would like to sincerely thank my supervisors: Professor Jonathan Knowles for his invaluable advice and guidance throughout the project. I would like to express my gratitude for his help whenever I had a problem with my experiments. I would also like to thank Dr. Ailbhe McDonald for her support and in the clinical aspect of this work as well as use of her industrial contacts. I am very grateful for the time that they dedicated to this project and also the advice regarding my writing.

I would like to thank Dr. Mike Cattell who is a lecturer at Queen Mary's University of London for advice on Weibull analysis and Ms Tsalouchou, former masters degree student at Queen's Mary School of Dentistry, for making zirconia based crowns for this project.

I would like to acknowledge 3M ESPE, Dentsply, and Panadent who supplied the materials for this project.

The Royal Thai Government is also acknowledged for their financial support during this project.

I am very grateful to the Biomaterials staff, Dr. George Georgiou, Dr. Graham Palmer, Dr. Anne Young and Mrs. Nicky Mordan for their invaluable assistance: technical advice and help whenever machines had a problem. I also would like to thank my colleagues, Xin, Paul, Idris and Azadeh, for their encouragement and friendships during PhD.

I would like to thank Meng, Aun, Patimaporn, Eve, Ning, Nong, etc for their friendships, support and encouragement during this PhD.

Finally, I would like to take this opportunity to thank my family for supporting and encouraging me to complete this PhD.

Table of contents

List of Tables

List of Figures

CHAPTER 1

Introduction

The increased popularity of all-ceramic materials as an alternative to metal ceramic restorations is attributed to their excellent aesthetics, chemical stability, and biocompatibility (Craig and Powers 2002; van Noort 2002). However, the brittleness and low tensile strength of conventional glass-ceramics has limited their clinical applications (Craig and Powers 2002; van Noort 2002). Several developed glass-ceramics have been introduced such as high alumina-content glass-infiltrated ceramic core material (In-Ceram® Alumina) and disilicate glass-ceramic (Empress 2®), which have been used successfully for crowns (Marquardt and Strub 2006), anterior fixed partial dentures (FPDs) and three-unit FPDs replacing the first premolar (Sorensen *et al.* 1998; Sorensen *et al.* 1999). However, these materials do not have sufficient strength to withstand high loads in posterior sites especially in the molar region (Sorensen *et al.* 1998; Sorensen *et al.* 1999).

Recently, the development of advanced dental ceramics has led to the application of partially stabilised zirconia in Restorative Dentistry, which can be produced from a computer-assisted design/computer-aided manufacture (CAD/CAM) system. The use of zirconia-based ceramics for dental restorations has risen in popularity due to their superior fracture strength (Curtis *et al.* 2005; Denry and Kelly 2008; Denry and Holloway 2005; Guazzato *et al.* 2005a) and toughness compared with other dental ceramic systems (Guazzato *et al.* 2005b). Zirconia is a polymorphic material that exists in three allotropes: monoclinic, tetragonal and cubic. It can be transformed from one crystalline phase to another during firing. Pure zirconia is monoclinic (m) at room temperature and this phase is stable up to 1170°C (Scott 1975). Above this temperature, it transforms into the tetragonal phase (t) and then into the cubic phase (c) at 2370°C, which exists up to its melting point of 2680°C (Scott 1975). However, this transformation produces crumbling of the material on

cooling (Kelly 2004). In 1951 onward, researchers found that zirconia alloying with lower valance oxides such as CaO, MgO, Y_2O_3, or CeO can retain tetragonal or cubic phases in the room temperature depending on the amount of dopant (Duwez *et al.* 1951; Duwez *et al.* 1952; Fu-Kang *et al.* 1963). However, the tetragonal form is in fact 'metastable' at the room temperature. External stresses such as sandblasting (Kosmac *et al.* 1999), grinding (Garvie *et al.* 1975; Kitazaki *et al.* 2001; Kosmac *et al.* 1999), and thermal ageing (Chevalier 1999) can trigger the transformation of partially stabilised tetragonal zirconia polycrystalline ceramics from a tetragonal into a monoclinic state (Garvie et al, 1975). This transformation is associated with 3-5% volume expansion (Porter and Heuer 1977), which induces compressive stresses, thereby closing the crack tip and preventing further crack propagation (Porter and Heuer 1977). This unique characteristic confers zirconia with superior mechanical properties compared to other dental ceramics.

Currently, several CAD/CAM systems which use zirconia-based ceramics for frameworks are available in the market such as Lava™ system (3M ESPE), KaVo Everest® (Kavo Dental Excellent), and Cercon smart Ceramic® (Degu Dent GmbH, Dentsply). These ceramic systems have improved mechanical properties when compared with high alumina ceramics and it is claimed that they are strong enough to produce 4-unit bridges to replace missing molars (Sorensen 2003). However, the mechanical properties of these systems have not been widely studied. Strength is usually one of the first parameters assessed when trying to understand the clinical potential and limits of a dental ceramic (Guazzato *et al.* 2002). Flexural strength is generally considered as a meaningful and reliable method to assess the tensile strength of brittle materials (as one surface is loaded in tension) as ceramics are in general, much weaker in tension than compression (Bona *et al.* 2003; Duckworth

1951). In addition, the strength reliability and variability of materials should be studied as the failure stresses of brittle materials are statistically distributed as a function of the flaw size distribution in the material (Bona *et al.* 2003). Weibull analysis, which was first developed by Weibull as a statistical method to study the strength reliability and variability (Weibull 1951). The main parameters involved are the Weibull modulus and the characteristic strength (Weibull 1951). A high Weibull modulus indicates a smaller defect population and greater structural reliability (Bona *et al.* 2003). High force and repetitive stresses during chewing cycles may lead to fatigue of the material and premature fracture in the oral environment. Fatigue testing is another method to evaluate the mechanical performance of a material. Fatigue refers to the slow growth of cracks, aided by the combination of water and stress (Morena *et al.* 1986). It has been known that the presence of water will degrade the strength of silicate glasses and other ceramic materials (Morena *et al.* 1986). In the oral environment, the influence of water and fatigue caused by cyclic loading, such as mastication, are considered important factors in the long-term durability of all-ceramic restorations (Ohyama *et al.* 1999a); therefore, it is important to understand what stresses a material can withstand to aid material selection.

The phase transformation of the yttria partially stabilised tetragonal zirconia ceramic is also an interesting area that warrants investigation. The stress-induced phase transformation and phase compositions can be analysed using X-ray diffraction analysis (XRD) and/or Raman spectroscopy; however, XRD tends to be used for bulk analysis or large area surface analysis. Even the new focussing systems have relatively large incident spot sizes. Raman microspectroscopy; however, has the ability to analyse very small and specific areas on a sample surface without any sample preparation (Kailer *et al.* 1999) and it can discern the

phases present (Casellas *et al.* 2001). Hardness indentation has been used to induce phase transformations during loading as a material is subjected to highly localised stresses. The stresses not only cause crack formation by dislocation gliding, but a complete change of the crystal structure and formation of amorphous phases (Kailer *et al.* 1999). Raman spectroscopy combined with hardness indentation testing has been used in some studies (Casellas *et al.* 2001; Colomban and Havel 2002; Kailer *et al.* 1999; Behrens *et al.* 1993) in order to examine pressure-induced phase transformations. One study (Behrens *et al.*, 1993) examined the $t \rightarrow m$ transformation of the yttria partially stabilised tetragonal zirconia ceramic around and below the indent, which was annealed at different temperatures and loaded with 500N via a Vickers indenter. They found that various annealing temperatures affected the transformation. Another study (Casellas *et al.*, 2001) investigated the effect of transformation at different distances from the centre of the indentation along a propagated crack. However, these studies had not investigated the effect of loads and the distance of the transformation toughening of the yttria partially stabilised tetragonal zirconia ceramic within and around the indentation.

Zirconia glass composite such as In-Ceram Zirconia, which contained mainly alumina (approximately 70 wt%) and zirconia (30 wt%) has been studied (Anusavice 2003a). However, the properties and phase configuration of zirconia ceramic that contain small amounts of glass have not been widely investigated.

Therefore, this present study will focus on the properties and phase transformation of commercially available high strength zirconia cores and some experimental glass zirconia ceramics.

CHAPTER 2

Literature review

2.1 Definition of Dental Ceramics

Dental ceramics may be defined as an inorganic compound with non-metallic properties consisting of oxygen and one or more metallic or semimetallic elements, e.g. aluminium, calcium, magnesium, silicon, titanium and zirconium (Anusavice 2003c; Sunnegårdh-Grönberg *et al.* 2003). They can appear as either crystalline or amorphous solids, being called glasses (van Noort 2002). Although the characteristic translucency of ceramics enhances the ability to produce natural-appearing restorations (Isgro *et al.* 2003), they are very susceptible to fracture when they are exposed to tensile or flexural stresses. Ceramics can be classified into four categories: (1) silicates, (2) oxides, (3) non-oxides, and (4) glass (Anusavice 2003c). Silicate ceramics are characterized by an amorphous glass phase and can have a porous structure. The main component is SiO_2 with small additions of crystalline Al_2O_3, MgO, ZrO_2 and/or other oxides. Dental porcelain falls into this category (Anusavice 2003c). Oxide ceramics contain a principal crystalline phase (Al_2O_3, MgO, ZrO_2) with either no glass phase or a small amount of a glass phase (Anusavice 2003c). Non-oxide ceramics are impractical for use in dentistry because of high processing temperatures, complex processing methods, and unaesthetic colour and opacity (Anusavice 2003c). Glass-ceramics are partially crystallised glasses, which occur by nucleation and growth of crystals in the glass matrix (Anusavice 2003c). An example of a glass ceramic is the Dicor glass-ceramic, which contains tetrasilicic fluormica ($KMg_{2.5}Si_4O_{10}F_4$) as the major crystalline phase (Anusavice 2003c).

2.2 History of Dental ceramics

Ceramic comes from the Greek *Keramos*, which means pottery or burnt stuff. Historically, three basic types of ceramic materials have been developed (Jones 1985). Earthenware is fired at low temperatures and is relatively porous. Stoneware, which appeared in China in about 100 B.C., is fired at a higher temperature than earthenware; in both materials, firing increases strength and renders it more impervious to water (Jones 1985). The third material is porcelain, obtained by fluxing white china clay with *China stone* to produce white translucent stoneware. This porcelain was developed in King-te-tching in China in about 1000 A.D. and is much stronger than earthenware and stoneware (Jones 1985).

The French apothecary, Alexis Duchateau, introduced the first ivory denture in 1774 (Anusavice 2003c; Jones 1985). However, the denture became badly stained, porous and absorbed mouth fluids (Jones 1985). In collaboration with Duchateau, the first porcelain tooth material was patented in 1789 by a French dentist, Nicholas Dubois de Chemant (Anusavice 2003c). The product was improved from the previous version that was produced in 1774; however, the method of attaching the teeth to a denture base was still ineffective (Anusavice 2003c). In 1808, Fonzi, an Italian dentist, invented a *terrometallic* porcelain tooth that was held in place by a platinum pin or frame (Anusavice 2003c; Jones 1985). Planteau, a French dentist, introduced porcelain teeth to the United States in 1817, and, Peale, an artist in Philadelphia, developed a baking process for them in 1822 (Anusavice 2003c). Dr. Charles Land introduced the first successful fused feldspathic porcelain inlay and crowns to dentistry in 1886 (Kelly *et al.* 1996). Land described a technique for fabricating ceramic crowns using a platinum foil as a substructure with the high controlled heat of a gas furnace. These crowns exhibited excellent aesthetics but the

low flexural strength of porcelain resulted in a high incidence of failure (Anusavice 2003c). Since then, feldspathic porcelains with reliable chemical bonding have been used in metal-ceramic prostheses for more than 35 years. However, feldspathic porcelains have been too weak to use reliably in the construction of all-ceramic crowns without a cast-metal or metal foil coping (Anusavice 2003c). Furthermore, their firing shrinkage causes significant discrepancies in fit and adaptation of margins. Significant improvement in the fracture resistance of porcelain crowns was introduced by McLean and Hughes, who developed a high-alumina reinforced porcelain restoration in 1965 (McLean 1965). They fabricated alumina of 95% purity as an aluminous core ceramic consisting of a glass matrix containing 45-50% Al_2O_3 (McLean 1967). Because of the inadequate translucency of the aluminous porcelain core material, a veneer of feldspathic porcelain was required to achieve acceptable aesthetics. Aluminous porcelain crowns provided low flexural strength of approximately 131 MPa; therefore, this type of porcelain crown was only used for anterior restorations. Recently, there has been development in both dental ceramic materials and fabrication techniques. For example, higher strength substructure materials such as lithium-disilicate, alumina, and zirconia have been used. Additionally, fabrication techniques such as slip-casting and copy milling techniques have been improved.

2.3 Classification of dental ceramics

Dental ceramics can be classified according to their fusion temperature, chemical composition, application, processing method, and substructure material (Anusavice 2003c; Craig and Powers 2002). According to the firing temperature, dental ceramics can be divided into high-fusing (1300°C), medium fusing

(1101-1300°C), low fusing (850-1100°C), and ultra-low fusing (<850°C) ceramics (Anusavice KJ 1996). This classification was employed more intensively with earlier dental ceramic compositions, which contained three major ingredients: quartz, feldspar, and clay (or kaolin) (Craig and Powers 2002). The fusion temperature is dictated by the relative amount of these three ingredients. In addition, ceramics can be classified by *chemical composition,* such as feldspathic porcelain (high and low leucite), glass-ceramic (lithium disilicate and mica), and core reinforcement (alumina and magnesia) (O'Brien 2002); by *application* such as denture teeth, metal ceramics, veneers, inlays, crowns, anterior bridges, and posterior bridges; by *processing method* such as pressable, sintering, casting, or machining; or by *substructure material* such as cast metal, glass-ceramic, CAD/CAM porcelain, or sintered ceramic core (Anusavice 2003c). A classification of dental ceramics in this review will focus on types of ceramics, which are metal ceramic and all-ceramic and then the latter group will be classified by the processing method.

2.3.1 Metal ceramic (Porcelain-fused-to-metal)

Ceramic-metal restorations consist of a cast metallic framework (or core) on to which at least two layers of ceramic are baked. The first layer to be applied is the opaque layer, consisting of ceramic, rich in opacifying oxides (Craig and Powers 2002). Its role is to mark the darkness of the oxidized metal framework to achieve adequate aesthetics (Craig and Powers 2002). The next layer is opacious dentine then dentine and enamel to obtain an aesthetic appearance similar to that of a natural tooth. After it has been built, the ceramic-metal crown is sintered in a porcelain furnace (Craig and Powers 2002). The alloys used for casting the substructure are usually gold-based, containing tin and indium. Gold-palladium,

silver-palladium, and nickel-chromium alloys were initially developed as lower cost alternatives (Craig and Powers 2002).

It has been shown that metal-bonded ceramic crowns are up to three times stronger than conventional all-ceramic crowns (van Noort 2002). One of the common causes of failure with this system is the separation of the ceramic from the metal due to an interfacial breakdown of the metal-ceramic bond (van Noort 2002). Most ceramics have a coefficient of thermal expansion less than that of metals. The metal tries to contract more than the ceramic during cooling because of its higher coefficient of expansion. If the mismatch between the metal and ceramic is too big, internal stresses may be created during cooling, which in turn may cause the ceramic to fracture (van Noort 2002). The coefficient of thermal expansion of feldspathic glasses used in the construction of the porcelain jacket crowns is 7-8 ppm.°C^{-1}. This value is lower than alloys, which are typically in the range of 14-16 ppm.°C^{-1} (van Noort 2002). To overcome the mismatch in thermal coefficients, soda (Na_2O) and potash (K_2O) are added to the ceramic composition to increase the thermal expansion (van Noort 2002; Craig and Powers 2002). The addition of these oxides leads to the formation of the crystalline phase in the glassy ceramic (van Noort 2002). This crystalline phase is known as tetragonal leucite. Additionally, the introduction of soda and potash leads to a reduction in the firing temperature, which reduces distortion due to creep of the alloy (van Noort 2002).

2.3.2 All ceramics

2.3.2.1 Alumina-reinforced porcelain jacket crown

The alumina-reinforced feldspathic core was developed by Hughes and McLean in 1965 (McLean 1965). The material consists of a feldspathic glass containing 45-50% alumina. The alumina ceramic is strengthened by dispersion of a crystalline phase in the glassy matrix (Craig and Powers 2002). Traditionally, the core was baked on a platinum foil and later veneered with matched-expansion porcelain; however, it is now more commonly baked directly on a refractory die (Craig and Powers 2002). The alumina particles are stronger than the glass and more effective at preventing crack propagation than quartz (van Noort 2002). However, the flexural strength of feldspathic porcelain is at best 60 MPa, which is raised to 120-150 MPa for the aluminous core porcelain. This strength is insufficient in posterior sites and is suitable only in anterior sites (van Noort 2002).

2.3.2.2 Leucite-reinforced feldspathic porcelain

Leucite-reinforced feldspathic porcelain contains 45% by volume tetragonal leucite, which acts as a reinforcing phase (Craig and Powers 2002). The thermal contraction mismatch between leucite (22 to 25 x 10^{-6}.°C^{-1}) and the glassy matrix (8x10^{-6}.°C^{-1}) results in the development of tangential compressive stresses in the glass around the leucite crystals, which can act as crack deflectors with increased resistance to crack propagation (Craig and Powers 2002). However, the flexural strength is still low at about 104 MPa (Craig and Powers 2002).

2.3.2.3 Magnesia based core porcelain

Magnesia core material is compatible with the high expansion porcelain normally bonded to metals. Magnesia has a higher expansion coefficient than alumina (MgO: $13.5x10^{-6}$.°C; Al_2O_3: $8x10^{-6}$.°C). Strengthening is achieved by dispersion of the magnesia crystals in a vitreous matrix, and also by crystallisation within the matrix. Additionally, a magnesia core can be significantly strengthened by glazing (Craig and Powers 2002). Normally, a magnesia core has a modulus of rupture strength of 131 MPa after firing; however, the strength can be doubled to 269 MPa by applying glaze (O'Brien 2002; Craig and Powers 2002). Another advantage of this material is that it is considered to be aesthetically superior to a PFM and provides no metal margin. However, it is only used for anterior crowns and is unsuitable for use as a fixed partial denture restoration (O'Brien 2002).

2.3.2.4 Castable ceramics

The first commercially available castable ceramic material was Dicor ceramic, which was introduced in the early 1980s. It is a micaceous glass-ceramic, which contains 45% volume glass and 55% crystalline tetrasilicate mica. It is produced by a conventional lost-wax investment techniques and glass casting (Grossman 1985). A full contour transparent glass crown was cast at 1350°C then heat treated at 1075°C for 10 hours to form a partial crystallisation (55%) of fluorine mica silicate (Anusavice 2003c). The crystals not only create an opaque material out of a transparent crown; they also increase the fracture resistance and strength of the ceramic. It has been reported to have a flexural strength of 152 MPa (O'Brien 2002).

2.3.2.5 Slip-cast ceramic

The core is made from fine grained alumina particles that are mixed with water to form a suspension referred to as a 'slip'. The slip is then placed on a gypsum die, which absorbs the water from the slip by capillary action (Sadoun 1988). This is then heated in a furnace to produce a sintered coping or framework. It is later infiltrated with glass at 1100°C for 4 hours to eliminate porosity and to strengthen the core (Probster and Diehl 1992). The rest of the crown is then formed by traditional firing using a body porcelain over the core (O'Brien 2002). Examples of materials that have used this technique are In-Ceram Alumina, In-Ceram Spinell, In-Ceram Zirconia (Vita Zahnfabrik, Bad Säckingen, Germany). In-Ceram Alumina was developed by Sadoun as a core material in 1988 (Sadoun 1988). In-Ceram Alumina was introduced as a dental glass-infiltrated core material containing about 70% alumina infiltrated with 30% sodium lanthanum glass for crown and bridge substructures (Anusavice 2003c). In-Ceram Spinell was introduced as an alternative to In-Ceram Alumina. It contains magnesium and aluminium oxide. This type of In-Ceram seems to improve translucency in the final restoration (Anusavice 2003c; Denry 1996), while In-Ceram Zirconia is a zirconia-based dental ceramic containing approximately 30 wt% zirconium dioxide and 70 wt% aluminium oxide. In-Ceram Zirconia is available as either slip or dry-pressed. The flexural strength values of the glass-infiltrated core materials are approximately 350 MPa for In-Ceram Spinell, 500 MPa for In-Ceram Alumina, and 700 MPa for In-Ceram Zirconia (Anusavice 2003c). Although the strength of the glass-infiltrated alumina cores is high, the alumina cannot be etched and silane treated for resin bonding; therefore, it cannot bond easily to tooth structure (O'Brien 2002). Also, this material is relatively costly and has a long processing time (O'Brien 2002). In-Ceram ceramic can be used for single

anterior and posterior crowns (In-Ceram Alumina and In-Ceram zirconia), anterior three-unit bridges (In-Ceram Alumina), and three-unit posterior bridges (In-Ceram Zirconia) (Anusavice 2003c).

2.3.2.6 Pressable ceramics

The method for producing pressable ceramics, which was first described by Wohlwend *et al* (Wohlwend *et al.* 1989), utilises the lost wax technique. A wax pattern of the restoration is invested in a phosphate-bonded investment material. Following the burn out procedure, a glass-ceramic is pressed into the mould at a temperature of 1050°C in a custom furnace. An example of the material used is leucite-reinforced feldspathic porcelains strengthened by incorporating leucite (K_2O Al_2O_3 $4SiO_2$) crystals, approximately 45% volume, in the glass matrix (Isgro *et al.* 2003). Flexural strength for these materials has been reported to be 120 MPa (Isgro *et al.* 2003). Conventional feldspathic porcelains designed for metal ceramic restorations contain 12 to 25% volume leucite and have a flexural strength in the range of 60 MPa. The increase in strength has been achieved through a heat treatment that enhances the formation of a highly crystallised microstructure and resists crack propagation under stress (Isgro *et al.* 2003). Also, large pore formation can be avoided due to the better distribution of the crystalline phase within the glass matrix (Isgro *et al.* 2003). The final restoration can use either the leucite-reinforced core material alone or a 2-layer all-ceramic crown veneered with low fusing porcelain (Isgro *et al.* 2003).

Some of the most representative pressable glass ceramics are IPS Empress (EM1) and Empress 2 (EM2) (Albakry *et al.* 2003b). EM1 is a leucite-reinforced glass ceramic produced in the early 1990s (Wohlwend *et al.* 1989). It obtains its strength

from the finely dispersed leucite crystal reinforcement and is recommended for restoring single units including veneers, inlays, onlays, and anterior crowns (Albakry *et al.* 2003b; Sobrinho *et al.* 1998a). The strength values of EM1 range from 95 to 180 MPa and the fracture toughness is approximately 1.3 $MPa.m^{1/2}$ (Sobrinho *et al.* 1998a). In 1998, Ivoclar released EM2, which is lithium disilicate-reinforced glass ceramic processed with the same procedure and equipment used for EM1. EM2 has been recommended for core material suitable for 3 unit-fixed partial dentures up to second premolar (Sobrinho *et al.* 1998a; Albakry *et al.* 2003b). The chemical composition of EM2 is 60 % by weight lithium disilicate, which represents the main crystalline content (Albakry *et al.* 2003b). The improved mechanical properties of this material compared to most other pressable ceramics are attributed to its chemical composition, which comprises dense multi-elongated lithium disilicate crystals within the glass matrix. In such a structure, a crack would be trapped by these distributed crystals, resulting in improved strength and fracture toughness (Albakry *et al.* 2004). The strength and fracture toughness values of EM2 has been reported to range from 340-400 MPa and 2 to 3.3 $MPa.m^{1/2}$, respectively (Sobrinho *et al.* 1998a).

2.3.2.7 Machinable ceramic or CAD/CAM systems

Traditional methods for the production of indirect restorations usually include impression taking, die or model making and final manufacture. Recent technology developments have enabled digitisation and replication of the tooth surface by using CAD/CAM (computer assisted design/computer assisted machining) technology, which can facilitate a restoration. After the tooth is prepared, it is scanned by an optical scanner and a restoration is designed with the aid of a computer and milled by a milling machine (Drummond 1991). An advantage of the CAD/CAM system is

that it can produce a restoration in one visit, which not only minimises the inaccuracies of the hand/laboratory fabrication process (Mörmann *et al.* 1989); it can also reduce the time taken to produce the restoration (Trost *et al.* 2006). Additionally, a temporary restoration is not used; therefore, there can be no loss or re-cementation of temporary restorations, leading to a reduction in laboratory fees (Trost *et al.* 2006). Another advantage is that disposable supplies, such as impression material, wax, stone, and temporary bridge resin, can be eliminated (Trost *et al.* 2006). Clinicians can also spend the majority of their time on tooth preparation and on seating of the final restoration (Trost *et al.* 2006). In addition, the system can produce a higher strength core material compared to conventional ceramic (Qualtrough and Piddock 1999).

However, CAD/CAM requires costly equipment and a trained dentist. Furthermore, the system produces larger internal gaps compared with conventional methods ranging from 100-200 μm (Sertgöz *et al.* 1995; Thordrup *et al.* 1994); and marginal gaps ranged from 50-80 μm (Denissen *et al.* 2000; Yeo *et al.* 2003). The latest versions of CAD/CAM systems such as CEREC® 3 have been improved to provide smaller marginal gaps, 53-67 μm for crowns (Nakamura *et al.* 2003) and 39.1-52.2 μm for inlays (Estafan *et al.* 2003). However, one study reported the marginal gap of CEREC® 3 was between 75 and 102 μm when resin composite was used (Tsitrou *et al.* 2006). These findings are far from the theoretically based requirement of cementation film thickness, which should be between 25 and 40 μm (Christensen 1971). Zirconia crown framework was reported to have marginal opening ranging between 36.6 to 45.5 μm; however, the internal gaps are still large (50-75 μm for axial walls and 74-100 μm for occlusal gaps) (Beuer *et al.* 2008).

During the last 10 years, the use of CAD/CAM in ceramic manufacture has increased significantly, e.g. the Cerec, Celay, Procera, and Lava systems.

2.4 Classification of CAD/CAM systems

2.4.1 CEREC Systems

CEREC stands for *computer-assisted CERamic REConstruction*. The CEREC CAD/CAM (Siemens/Sirona Dental Systems, Bensheim, Germany) method was first developed at the University of Zurich by Mörmann and Brandestini in 1980. CEREC 1 functioned for the first time in 1985 to produce the first chairside inlay and the material was Vita Mark I feldspathic ceramic (Vita Zahnfabrik) (Mörmann 2006). In 1994, CEREC 2 was launched to give more options for restorations such as 1-3 partial and full crowns and copings. It was equipped with an additional cylinder diamond enabling form-grinding for partial and full crowns instead of using only a diamond-coated wheel like CEREC 1. The software design was still displayed two-dimensionally. In 2000, CEREC 3 omitted the wheel and introduced a two-bur-system, consisting of a cylindrical diamond and tapered burs. It divided the system into an acquisition/design unit and a machining unit. The software for three-dimensional virtual display became available in 2003 using CEREC 3 & inLab, which makes the handling illustrative and easy both in the office and the laboratory (Mörmann 2006). The *step bur* that was introduced in 2006, reduced the diameter of the top one-third of the cylindrical bur to a small diameter tip enabling high precision form-grinding with reasonable bur life (Mörmann 2006).

The CEREC system can produce a restoration in a single appointment (Mörmann *et al.* 1989). To make a restoration with the CEREC CAD/CAM chair side system (Sirona), the following sequence is carried out. First, a titanium dioxide

powder is applied to the patient's prepared tooth to provide contrast for the optical scanner. The prepared tooth is scanned with an optical probe and the image is stored in a computer as a positive digital XYZ data model. The restoration is designed on a monitor screen, a block of a machinable glass-ceramic is selected by shade and the restoration is milled at the chair side. The materials used with the CEREC system are Vita Mark II fine-grained, feldspathic ceramic (Vita Zahnfabrik, Bad Säckingen, Germany), ProCAD leucite reinforced ceramic (Ivoclar Vivadent, Amherst, N.Y.) and Paradigm™ MZ100 composite block (3M ESPE). Four types of strong and aesthetic CEREC inLab materials are also available: SPINELL™, ALUMINA™, ZIRCONIA™ and new Yttrium-stabilised Zirconia (YZ™). The latest material is Invizion™, which is milled on CEREC inLab system and combines VITA In-Ceram YZ cubes with the VITAMV9 ceramic veneering material.

2.4.2 Celay System

The Celay system (Mikrona Technologie, Spreitenbach, Switzerland), introduced in 1992, is a machinable ceramic system that is capable of milling inlays, onlays, and veneers from prefabricated industrial ceramic blocks. A technique for manufacturing crowns was then introduced in 1993 using Vita-Celay alumina blocks (Qualtrough and Piddock 1995). Direct intra-oral or indirect patterns may be used to make ceramic restorations (Siervo *et al.* 1994). Celay enables the dentist to produce a restoration during either a single treatment, or a two-session procedure (Kreulen *et al.* 2000).

2.4.3 DCS System

The Digitising Computer System (DCS) can be mechanically programmed to produce a computer-milled restoration using three-dimensional computer models (Schlegel *et al.* 1991). The DCS Precident system comprises a Preciscan laser scanner and Precimill CAM multitool milling center. The DCS Dentform software automatically suggests connector sizes and pontic forms for bridges. It can scan 14 dies simultaneously and mill up to 30 framework units in 1 fully automated operation. Materials used with DCS include porcelain, glass ceramic, In-Ceram, dense zirconia, metals, and fibre-reinforced composites. This system is one of the few CAD/CAM systems that can mill titanium and fully dense sintered zirconia (Liu 2005).

2.4.4 CICERO System (Computer Integrated Ceramic Reconstruction)

Computer-aided design (CAD) and computer-aided manufacturer (CAM) in dentistry offer an alternative to lessen the variability of coloured reproduction in the fabrication of ceramic restorations. However, most of the CAD/CAM systems depend on the process of milling a restoration from porcelain blocks, which may make them less aesthetic then layered restorations. Therefore, improvement in the cosmetic appearance of this type of CAD/CAM restoration is made manually (Dozic *et al.* 2003).

CICERO systems can produce a ceramic coping and 2 porcelain layers (opaque and translucent porcelain) with determined thickness, which may improve the predictability of the final shade of the restoration (Dozic *et al.* 2003). All-ceramic restorations produced by the CICERO CAD/CAM system consist of a glass-impregnated aluminium oxide ceramic core (Synthoceram, Elephant Dental BV) with a thickness 0.6 to 0.8 mm and veneering porcelain which combines 2 porcelains,

a less translucent version and a more translucent version. The 2 types of veneering porcelains can be applied in 16 different shades and various thickness ratios (Dozic *et al.* 2003).

The CICERO method of crown fabrication consists of optically digitising a gypsum die, designing the crown layer build-up, and subsequently pressing, sintering, and milling consecutive layers of a shaded high-strength alumina-based core material, a layer of dentin porcelain, and a final layer of incisal porcelain. Final finishing is performed in the dental laboratory (van der Zel *et al.* 2001). The CICERO system differs from the CEREC and DCS systems in that the ceramic is sintered and milled in a centralized laboratory whereas the CEREC and DCS are produced from ceramic blocks either in the dental laboratory or in the dental practice (van der Zel *et al.* 2001).

2.4.5 Procera All Ceramic System

Procera/AllCeram (Nobel Biocare, Goteborg, Sweden) was first described by Anderson and Odén (Anderson and Odén 1993). The Procera AllCeram crown is composed of densely sintered, high-purity aluminium oxide core combined with compatible AllCeram veneering porcelain (Zeng *et al.* 1996). This ceramic material contains 99.9% alumina, and its hardness is one of the highest among the ceramics used in dentistry (Anusavice 2003c). Procera AllCeram can be used for anterior and posterior crowns, veneers, onlays, and inlays. A unique feature of the Procera system is the ability of the Procera scanner to scan the surface of the prepared tooth and transmit the data to a milling unit to produce an enlarged die through a CAD/CAM process. The core ceramic form is dry-pressed onto the die, and then sintered and veneered. Thus, the usual 15-20% shrinkage of the core ceramic during

sintering will be compensated by constructing an oversized ceramic pattern, which will shrink during sintering to the desired size to accurately fit the prepared tooth (Anusavice 2003c). Some studies confirm that Procera restorations have high strength and excellent longevity (Ödman and Andersson 2001). After 5 and 10 years, a cumulative survival rate of 97.7% and 93.5% was reported. The mean flexural strength for Procera alumina and zirconia is 639 (Itinoche *et al.* 2006) and 1158 MPa respectively (Sierraalta *et al.* 2003).

2.4.6 Cercon

The Cercon system is commonly referred to as a CAM system because it does not have a CAD component (Liu 2005). After the die is prepared, a wax pattern of coping or pontic with a minimum thickness of 0.4 mm is made. The system scans the wax pattern and mills a zirconia bridge coping from presintered zirconia blanks in an enlarged size to compensate for the 20% shrinkage. The processing time for milling is approximately 35 minutes for a crown and 80 minutes for a 4-unit bridge (Anusavice 2003c). The coping is then sintered in the Cercon heat furnace (1,350°C) for 6 to 8 hours (Liu 2005). This method of milling presintered blanks reduces milling time and increases the service life of the unit and instruments. The mean flexural strength of Cercon core using three-point bending test was 1305 MPa and the fracture strength of Cercon crown from one study (Miura *et al.* 2005), which was fabricated simulating a maxillary central incisor, was 1850 MPa.

2.4.7 LAVA ™ system

The Lava system was introduced in 2002. The Lava™ All-Ceramic System utilizes CAD/CAM technology to produce a densely sintered and high-strength

zirconia framework with 3 mol% yttria partially stabilised zirconia polycrystal content. The dental laboratory includes a special scanner (Lava scan), a computerized milling machine (CAM) (Lava Form), and a sintering oven (Lava Therm) plus CAD/CAM software technology. Tooth preparations and any edentulous areas are scanned by a contact-free optical process that uses white light triangulation. The entire scanning process takes approximately 5 minutes for a crown preparation and 12 minutes for 3-units FPD (Piwowarczk *et al.* 2005). After scanning, the crown or bridge framework is designed on the computer and subsequently milled from a green blank (partially sintered zirconia block). This green blank is much softer than a sintered zirconia, allows reduced milling times, minimal tool wear, and demands less load from the milling unit (Suttor *et al.* 2001). Additionally, in order to compensate for shrinkage during the sintering process (20-25%), the CAM produces an enlarged framework structure. The average milling time for crown coping is approximately 35 minutes for a crown preparation and 75-90 minutes for a 3-unit FPD substructure (Piwowarczyk *et al.* 2005; Suttor *et al.* 2001). After milling, the framework can be coloured in 7 shades by the dental technician before sintering. Sintering is accomplished using the special automated oven, which is programmed to run for 8 hours, including heating and cooling phases. Yttrium stabilised zirconia is used for the Lava framework because of its high strength (Suttor *et al.* 2001) and was reported to have a flexural strength exceeding 1000 MPa (Curtis *et al.* 2005).

2.5 Dental ceramics used with CAD/CAM Systems

Many ceramic materials are available for use as CAD/CAM restorations (Table 2.1). Ceramics used in earlier CAD/CAM restoration were machinable glass-ceramic such as Dicor and Vita Mark II (Liu 2005). They have been

successfully used as inlays, onlays, veneers, and crowns. In-Ceram spinell is an ideal choice for very high aesthetics and is indicated for single anterior crowns with a strength of 350 MPa (Liu 2005). In-Ceram alumina has high strength (525 MPa) and high translucency, which can be considered for anterior/posterior crowns and three-unit anterior bridges. However, the materials mentioned above are not strong enough to sustain an occlusal load when used for posterior areas (Liu 2005). For this reason, alumina and zirconia are a better choice for posterior restoration because of their high strengths of 750 MPa and 1000 MPa, respectively (Liu 2005). In-Ceram Zirconia and Yttrium-reinforced Zirconia can be used for posterior crowns and multiple-unit posterior cases in high-stress areas. Fully sintered alumina or zirconia can be difficult to mill; therefore, milling normally occurs at a presintered stage

Table 2.1. Restorative materials used for CAD/CAM systems (Liu 2005)

Restorative material	CAD/CAM system	Indications	Flexural strength (MPa)
Dicor MGC (fluoromica)	Cerec	Inlays, onlays, veneers	<100
Vita Mark II (feldspathic)	Cerec	Inlays, onlays, veneers, anterior crowns	150
ProCAD (leucite reinforced)	Cerec	Inlays, onlays, veneers, anterior crowns	150
In-Ceram Spinell (magnesium oxide)	Cerec 3D, Cerec inLab	Anteiror crowns	350
In-Ceram Alumina (aluminum oxide)	Cerec 3D, Cerec inLab, DCS Precident	Crowns and anterior bridges	500
Alumina (aluminium oxide)	Procera	Crown and bridge	600
In-Ceram zirconia (zirconium oxide)	Cerec 3D, Cerec inLab, DCS Precident	Crown and bridge	750
Partially sintered zirconia (zirconium oxide) (Curtis *et al.* 2005; Denry and Kelly 2008; Denry and Holloway 2005; Guazzato *et al.* 2005a)	DCS Precident, Lava, Procera, Everest, Cercon	Crown and bridge	800-1300
Fully sintered zirconia (zirconium oxide)	DCS Precident, Everest	Crown and bridge	>1000

2.6 Zirconia-based ceramic

2.6.1 Definition and history of zirconia

Zirconium is represented by the chemical symbol **Zr** and has the atomic number 40. It is one of the transition metals (elements whose atom has an incomplete d sub-shell) of the D.I. Mendeleev's periodic chart. Zirconium exits in two forms: the crystalline form, a soft, grayish-white, lustrous metal; and the amorphous form, a bluish-black powder. From ancient times, zirconium has been known as *zircon*, which probably originated from the Persian word *zargun* (golden in colour)

(Kreidl 1942; Christie and Brathwaite 1999). Zircon or zirconium silicate, $ZrSiO_4$ (67.2% of ZrO_2 and 32.8% of SiO_2), is the most important zirconium mineral (Kreidl 1942). The mineral was discovered by Martin Henrich Klaproth, a German chemist, who analysed a zircon from Ceylon (Sri Langa) in 1789 (Kreidl 1942; Christie and Brathwaite 1999; Venetskii 1965). The impure metal (metallic zirconium) was first isolated by Jöns Jakob Berzelius, a Swedish chemist, in 1824 by heating a mixture of potassium and potassium zirconium fluoride in a small iron tube. However, it was impossible to obtain pure zirconium at that time until the beginning of the 19th century. The pure zirconium oxide was first prepared in 1914 by Herzfield (Herzfield 1916). He invented the process of crystallising zirconium oxychloride octahydrate from a concentrated solution of hydrochloric acid to remove large amounts of silica and the oxychloride octahydrate then crystallised out upon cooling (Herzfield 1916). Very pure zirconium was first produced in 1925 by van Arkel and de Boer by an iodide decomposition process (Heiserman 1992). However, Hafnium is always found in zirconium ores because separation is very difficult (Venetskii 1965). Commercial-grade zirconium contains from 1 to 3% Hafnium (Heiserman 1992).

At the beginning of 19th century, a solid solution of yttria-stabilised tetragonal zirconia polycrystal ceramic (Y-TZP) was widely used in the refractory as Nernst lighting element rods and later used as a solid electrolyte (Fu-Kang *et al.* 1963). It was considered for biomedical implants from as early 1969 (Helmer and Driskell 1969), and from 1985 onwards, the majority of zirconia balls were made for total hip arthroplasty. Zirconia ceramic was extended into dentistry in the early 1990s as endodontic posts (Meyenberg *et al.* 1995) and more recently as implant abutments (Kohal and Klaus 2004; Kohal *et al.* 2006) and hard framework cores for crowns and fixed partial dentures (Luthardt RG et al 2004; Luthy *et al.* 2005; Tinschert *et al.*

2001). Zirconia has unique a characteristic called *transformation toughening*, which can give it higher strength and toughness compared with other ceramics.

2.6.2 Transformation toughening

The transformation is believed to be martensitic (Subbarao, 1974). The martensitic transformation occurs by the systematic coordinated shearing of the lattice of the old phase in such a way that the distance moved by any atom is less than one atomic space. This means that the atom retains the same neighbours. Martensitic transformation can only lead to changes in crystal structure, and not in composition of the phases (Anderson *et al.* 1990).

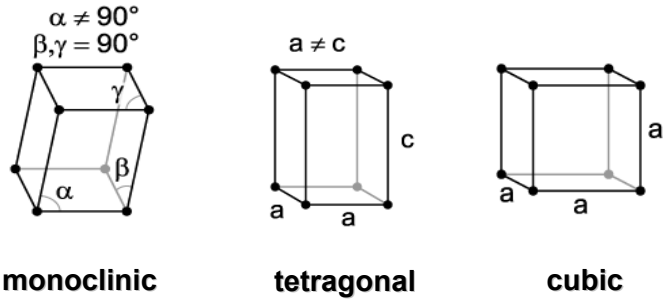

Figure 2.1. Crystallographic phases of zirconia dioxide

Zirconium dioxide can exist in one of three crystallographic phases (Figure 2.1); monoclinic phase (a deformed prism with parallelepiped sides); tetragonal phase (t) (a straight prism with rectangular sides) and cubic phase (c) (square sides). The monoclinic phase (m) appears from room temperature up to 1170°C (Figure 2.2). Above this temperature, it transforms into the tetragonal phase and then at 2370°C into the cubic phase, which exists up to its melting point of 2680°C (Figure 2) (Scott 1975). Volume changes on cooling associated with transformation are substantial enough to make the pure material unsuitable for applications requiring an intact solid structure: $c \rightarrow t$ approximately 2.31% (Kelly and

Denry 2007); *t→m* approximately 3-5% (Porter and Heuer 1977). Researchers have studied the phase relationships between zirconia and metal oxides (Duwez *et al.* 1951; Duwez *et al.* 1952; Fu-Kang *et al.* 1963). They discovered that zirconia alloying with lower valance oxides such as CaO, MgO, Y_2O_3, or CeO can retain tetragonal or cubic phases at room temperature depending on the amount of dopant (Duwez *et al.* 1951; Duwez *et al.* 1952; Fu-Kang *et al.* 1963). In the case of 8 mol% Y_2O_3 dopant, the cubic is stabilised at room temperature while tetragonal phase is stabilised when using 2-5 mol% Y_2O_3 (Scott 1975). The stabilised tetragonal phase has satisfactory properties when compared to other phases and it also provides an advantage because of its martensitic transformation to a monoclinic phase (Gupta *et al.* 1977).

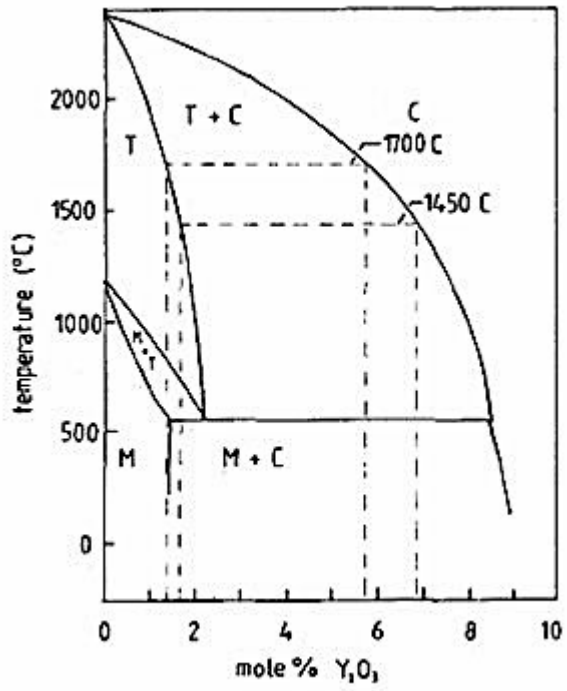

Figure 2.2. Phase Diagram by Scott (Scott 1975)

The transformation from tetragonal into monoclinic form can occur by absorption of mechanical or thermal stress such as grinding (Garvie *et al.* 1975; Kosmac *et al.* 1999; Curtis *et al.* 2005), sandblasting (Kosmac *et al.* 1999; Curtis *et al.* 2005), and high temperature (thermal ageing) (Chevalier 1999; Deville *et al.* 2005), and is associated with a volume increase (Porter and Heuer 1977). This transformation leads to the development of localised compressive stresses being generated around and at the crack tip preventing further crack propagation (Porter and Heuer 1977). This mechanism is known as transformation toughening and makes zirconia-based ceramics exhibit high strength (Garvie *et al.* 1975; Gupta *et al.* 1977) and toughness compared to other ceramics (Guazzato *et al.* 2004b). However, severe transformation to the monoclinic phase can induce a deterioration of materials such as a reduction in the strength and the fracture of the materials. Gupta *et al* (1977) reported that as-sintered specimens containing high amounts of the monoclinic phase (~90%) exhibited low strength in a range of 50-100 MPa with the evidence of microcracks in the materials. In contrast, high amounts of the tetragonal phase (~90%) showed high strength, which was approximately 700 MPa (Gupta *et al.* 1977). Therefore, transformation toughening can provide either advantage or disadvantage depending on the degree of transformation.

2.6.3 Characteristics of zirconia-based ceramic

Zirconia ceramics have superior properties compared to other ceramics and (Guazzato *et al.* 2005b) shows their biocompatibility (Garvie *et al.* 1984; Scarano *et al.* 2003). However, the properties of zirconia ceramic may be reduced when it contacts thermal and humid environments (Chevalier 1999; Lawson 1995).

2.6.3.1 High strength and toughness

Because ceramics are weak in tension; this aspect should be tested. However, the direct tensile test is difficult to perform. This is due to the difficulty in preparing specimens to have the required geometry and it is also difficult to hold the brittle specimens without pre-stressing and fracturing them (Callister 2005). The flexure test is an alternative test to investigate the stress at fracture of brittle materials, which is known as flexural strength (Callister 2005). Fracture toughness identifies the resistance of the brittle materials to the catastrophic propagation of flaws under an applied stress.

Yttria partially stabilised tetragonal zirconia polycrystal ceramics exhibit flexural strength ranging from 800-1300 MPa (Table 2.2) (Curtis *et al.* 2005; Denry and Kelly 2008; Denry and Holloway 2005; Guazzato *et al.* 2005a) with a toughness of approximately 5-10 $MPa.m^{1/2}$ (Michel *et al.* 1983) depending on processing methods, composition and microstructures (Ardlin 2002; Casellas *et al.* 2001; Milleding *et al.* 2003; Nakayama and Sakamoto 1998; Ruiz and Readey 1996). Guazzato *et al* (2004) found DC-Zirkon (5% Y-TZP) had a flexural strength of 1150 (±150) MPa. Similarly, Curtis *et al* (2005) reported that as-received Lava™ specimens tested in a wet environment had a flexural strength of 1308 (±188) MPa, which was not significantly different from the specimens tested in a dry condition (1267±161 MPa). However, Denry and Holloway (2005) found the biaxial flexural strength of the as-sintered Cercon® was 944 (±156) MPa.

Other dental ceramics have lower flexural strength and toughness compared with yttria stabilised tetragonal zirconia ceramics. Empress 2 has flexural strength in a range of 250-350 MPa (Albakry *et al.* 2004; Cattell *et al.* 2002) and fracture toughness approximately 2.8 $MPa.m^{1/2}$ (Quinn *et al.* 2003). In-Ceram Alumina

ceramic has been reported to have flexural strength ranging from 300-600 MPa (Guazzato *et al.* 2004b; Seghi and Sorensen 1995; Tinschert *et al.* 2000; Wagner and Chu 1996; Wen *et al.* 1999; Zeng *et al.* 1996) and a fracture toughness approximately 3.1-4.8 $MPa.m^{1/2}$ (Guazzato *et al.* 2004b; Quinn *et al.* 2003; Wagner and Chu 1996; Wen *et al.* 1999). In-Ceram Zirconia has been reported to have flexural strength and fracture toughness in a range of 475-630 MPa (Apholt *et al.* 2001; Guazzato *et al.* 2005b; Seghi and Sorensen 1995) and 4.8-4.9 $MPa.m^{1/2}$ (Apholt *et al.* 2001; Guazzato *et al.* 2005b) respectively. High alumina content ceramics or Procera has a mean flexural strength in a range of 469-699 MPa (Itinoche *et al.* 2006; Wagner and Chu 1996; Wen *et al.* 1999; Zeng *et al.* 1996) and fracture toughness 3.84-4.48 $MPa.m^{1/2}$ (Wagner and Chu 1996; Wen *et al.* 1999).

Table 2.2. Comparison of flexural strength and fracture toughness of ceramics from different systems

Systems	Core materials	Flexural strength (MPa)	Fracture toughness ($MPa.m^{1/2}$)
Empress II	Lithium disilicate	250-350	2.8
In-Ceram Alumina	Glass-infiltrated alumina	300-600	3.1-4.8
In-Ceram Zirconia	Glass-infiltrated alumina with 35% partially stabilised zirconia	475-630	4.8-4.9
Procera AllCeram	Densely sintered high-purity alumina	469-699	3.84-4.48
Cercon, Lava, Invizion	Yttria partially stabilised tetragonal zirconia	800-1300	5-10

2.6.3.2 Fatigue resistance

2.6.3.2.1 Fatigue failure

Fatigue is the mode of failure, whereby a structure eventually fails after being repeatedly subjected to loads that are so small that one application does not cause failure. All-ceramic materials are susceptible to fatigue mechanisms that can considerably reduce their strength over time. The reduction of mechanical strength due to fatigue is caused by the propagation of natural cracks initially present in the component's microstructure (Studart *et al.* 2007a). The influence of moisture contamination has also previously been identified to affect the fracture strength of ceramic-based dental ceramics, resulting in a 20% decrease in the mean fracture strength (Studart *et al.* 2007a). However, Curtis *et al*. (2007) highlighted that the biaxial flexural strength of Y-TZP ceramic was not detrimentally influenced by water immersion during simulated masticatory forces of 500, 700 and 800 N at 2000 cycles. However, the duration of the fatigue test they performed was rather short to allow water to affect the properties of zirconia. Similarly, one study mentioned that a loading of 100,000 cycles (force of 50 N) did not affect the strength of YTZP framework (Sundh *et al.* 2005). The maximum stress, which was recommended to apply during cycling tests due to higher mechanical strength of zirconia was 500 MPa (Studart *et al.* 2007b) and for In-Ceram and Empress II, 300 MPa and 160 MPa respectively (Studart *et al.* 2007b).

Kim *et al* (Kim *et al.* 2007) studied the fracture patterns during fatigue on flat porcelain veneers on gold-infiltrated alloy (P/Au), porcelain on palladium silver alloys (P/Pd) and porcelain on a Y-TZP (P/Zr) bilayers. They used a spherical tungsten carbide indenter with mouth-motion simulator using 200 N force and a chewing frequency of 1.5 Hz. At 10,000-15,000 cycles for the P/Au system, cracks reached at the porcelain/metal interface and a radial crack (cracks that emanate

outward from the contact axis) initiated at the lower surface of the porcelain veneer at 20,000-25,000 cycles. For the P/Pd system, inner cone cracks (cracks that initiated inside the contact circle and form only in cyclic loading in water) reached the interface at 25,000-50,000 cycles and no radial cracks were found even after 400,000 cycles and increased force of 600 N. Inner cracks in P/Zr system reached the veneer/core interface after 550,000 cycles. These cracks did not penetrated either the Y-TZP core or along the porcelain/Y-TZP interface. There was also no evidence of the radial crack at the lower surface even when a 600 N force was used.

2.6.3.2.2 Fracture resistance after fatigue

All ceramic crown and bridge restorations are subjected on a daily basis to masticatory loading which places the restoration under repeated loading throughout its service-life. Repetitive stresses during the chewing cycle may lead to fatigue of the material and eventually fractures when they are exposed to the oral environment (Chen *et al.* 1999).

Previous studies showed that ceramic containing glass such as ProCAD, In-Ceram, and IPS Empress had a decrease in fracture strength after cyclic loading (Attia and Kern 2004; Chen *et al.* 1999; Sobrinho *et al.* 1998b). Chen *et al* (1999) reported a significant decrease in fracture strength and considerable increase in failure probability of ceramic crowns (Vita MarkII, ProCAD and IPS Empress I, II) when subjected to the cyclic loading at 50,000 cycles using a force of 200 N. Similarly, the fracture strength of In-Ceram and IPS Empress was significantly reduced after 10,000 cyclic using 300 N force (Sobrinho *et al.* 1998b). One study reported that fatigue (20,000 cycles) slightly reduced the flexural strength of glass-

infiltrated zirconia (In-Ceram Zirconia) and high purity alumina (Procera AllCeram) but it was not statistically significant (Itinoche *et al.* 2006).

On the other hand, the reduction of the fracture strength of high purity zirconia ceramic after cyclic loading has not been reported. A recent study showed that when using high forces of 500, 700 and 800 N at low numbers of cycles (2,000 cycles) and also low force of 80 N at 10,000 and 100,000 cycles, there was no significant difference in the mean biaxial flexural strength between unloaded and zirconia discs that had undergone cyclic loading in both dry and wet conditions (Curtis *et al.* 2006). However, Weibull modulus was lower in zirconia discs when loaded for 100,000 cycles due to accumulation of microcrack damage (Curtis *et al.* 2006). Sundh *et al* (2005) found that cyclic loading (100,000 cycles) of zirconia three-unit bridges using 50 N force in water did not significantly affect fracture resistance whereas heat-treatment or veneering zirconia bridges resulted in significantly lower fracture resistance (Sundh *et al.* 2005).

In summary, zirconia has a high resistance to fatigue and there was no evidence of cracks after fatigue testing of porcelain/zirconia bilayered ceramics.

2.6.3.3 Subcritical crack growth resistance

Brittle materials are susceptible to time-dependent failure under static loads, caused by the subcritical growth of cracks to critical lengths (Reese and Cox, 1992). The subcritical crack growth refers to environmentally enhanced crack propagation at subcritical stress levels. The propagation of the pre-existing natural defects occurs at low rates (slow crack growth), and causes delayed failure of ceramics when the flaw size reaches a critical value (Benaqqa *et al.* 2005). The subcritical parameter *A and n* are usually examined for estimating crack growth resistance and lifetime of materials. Where *A* is a constant in metre per second and *n* is an

exponent, which in most ceramics has a value >10 (Reese and Cox 1992). The *n* value can vary from 20-100 (Chevalier *et al.* 1995; Chevalier *et al.* 1999; Studart *et al.* 2007b) dependant on the test methods. Previous studies reported that two common methods, double torsion and flexural tests, show a difference in subcritical *n* values of zirconia ceramics (Chevalier *et al.* 1995; Li and Pabst 1980). Li and Pabst (1980) reported that the *n* value of as-received ZrO_2 specimens tested using the double torsion test (*n*=80) was higher than the flexural test (*n*=51). In contrast, Chevalier *et al* found the *n* value produced from the double torsion method (*n*=19) was lower than the *n* value obtained from dynamic fatigue test (*n*=100).

It is difficult to give a definite conclusion whether zirconia has a higher subcritical parameter than other ceramics as the results from studies differ. One study calculated the *n* and *A* values of 3Y-TZP, In-Ceram Zirconia and Empress 2 ceramic and found that 3Y-TZP, In-Ceram Zirconia and Empress 2 ceramics had *A* values of $3.15x10^{-24}$, $2.61x10^{-25}$ and $1.69x10^{-21}$ $m.s^{-1}$ and *n* values of 28.9, 26.3 and 38.0, respectively (Studart *et al.* 2007b). Conversely, Morena *et al* (1986) found fine-grain ceramic (Cerestore) had a high *n*-value of 80.8 compared with feldspathic (14.6) and aluminous porcelain (28.9) (Morena *et al.* 1986).

One study found that the subcritical crack growth parameter *n* tested in air and water was not significantly different (Studart *et al.* 2007a). Studart *et al* (2007) studied the fatigue properties of three unit zirconia bridges using prismatic beams to simulate the bridges. They found no significant difference in an exponent *n* between the specimens tested in the air (29) and water (28.95). They indicated that the operative mechanism of cyclic degradation and water-assisted crack growth are the same for both environmental conditions (Studart *et al.* 2007a). However, the faster crack growth observed in the presence of water (as n_{water} value is lower than n_{air}) can, therefore, be attributed to the higher concentration of corrosive water

molecules surrounding the propagating crack. Studart *et al* (2007a) also reported that zirconia has a failure probability of only 5% after 20 years if the maximum stress does not exceed 346 MPa. Therefore, they suggested that dental prostheses in patients with parafunctional behaviour such as clenching and grinding, which can reach forces as high as 800 N, should have increased connector dimensions for extending life time (Studart *et al.* 2007a).

2.6.3.4 Thermal and environmental ageing

The major issue concerning zirconia ceramics is their sensitivity to low temperature degradation (LTD) (Chevalier 2006). Ageing occurs by a slow surface transformation from metastable tetragonal phase to a more stable monoclinic phase in a humid environment such as humid air, water vapour and aqueous fluids at a relatively low-temperature (Lawson 1995) ranging from 65-500°C (Sato and Shimada 1985).The tetragonal to monoclinic transformation can be of benefit due to the compressive layer on the surface of the ceramic, which improves its properties. However, further ageing can result in the reduction of material properties (Watanabe *et al.* 1984). The transformation of one grain is accompanied by a volume increase causing stresses on the neighbouring grains and microcracking. This offers a path for the water to penetrate and exacerbate the process of surface degradation and the transformation process (Chevalier 1999; Kelly and Denry 2007). The growth of the transformation zone results in severe microcracking and grain pull out and finally surface roughening which leads to strength degradation (Kelly and Denry 2007). Several factors influence the ageing rate such as ageing temperature, grain size and stabilising agent (Lawson 1995). If the temperature rises up to 200-300°C, the transformation proceeds most rapidly (Yoshimura 1988) (Chevalier 1999). Chen and Lu (1988) found the highest amount of monoclinic

presented at the ageing temperature of 250°C, which led to the lowest flexural strength 340 MPa compared with the as-received specimen (600 MPa) (Chen and Lu 1988). Chevalier studied ageing of zirconia in distilled water at different temperatures from 70-100°C. He found the amount of monoclinic phase increased with ageing time and temperature. However, some studies reported zirconia showed no loss of strength both *in vitro* and *in vivo* (Cales *et al.* 1994; Shimizu *et al.* 1993). Cales *et al* examined ageing of zirconia in Ringer's solution at 37°C at pH7 for 1 year and also implanted zirconia ceramic in animals (rats, rabbits and sheep) for 2 years. They found zirconia ceramics were stable after *in vitro* and *in vivo* long-term ageing. There was also no mechanical degradation caused by the different conditions of *in vitro* ageing and implantation in animals. Similarly, Shimizu *et al* (Shimizu *et al.*, 1993) found no significant decrease of flexural strength when specimens were placed in saline solution at 50 and 95°C for 3 years and also in distilled water at 121°C for 2000 hr. Papanagiotou *et al* (Papanagiotou *et al.* 2006) found that the transformation $t \rightarrow m$ was higher on the In-Ceram YZ ceramics boiled for 7 days than as-sintered and boiled for 24 hours. The transformation presented the highest rate on the specimens after storage in humidified air at 250°C for 7 days. However, the low-temperature ageing treatments in their study did not affect the flexural strength (Papanagiotou *et al.* 2006).

In addition, the critical tetragonal grain size, which is Y_2O_3 dependent, affects the ageing degradation behaviour (Lawson 1995). Lange (1982) reported that the critical grain size increased from 0.2 to 1 μm for compositions ranging between 2 and 3 mol%, respectively. However, Watanabe *et al* (1984) identified that critical grain size increased from 0.2 to 0.6 um as the Y_2O_3 content increased from 2 to 5 mol%. The monoclinic phase increased with ageing when the grain size was larger than the critical value. Conversely, the transformation to monoclinic phase was

either induced or resisted when the grain size was lower than critical value. The level of stabilisation also affected the ageing resistance. A higher stabilisation reduced the phase transformation during ageing.

Therefore, this review concluded that there was transformation toughening of zirconia due to thermal and environmental ageing, which lead to the degradation process of zirconia. However, this process was found to have either reduced or no affect on its flexural strength both *in vitro* and *in vivo* within the limited time of the studies.

2.6.3.5 Biocompatibility

Biocompatibility has been defined as the ability of a material to perform with an appropriate host response in a specific application. Biocompatibility of zirconia has been studied both *in vitro* and *in vivo*, but most of the biocompatibility studies concentrated on femoral ball head implantation. *In vitro* tests used cell cultures with cells such as fibroblasts, blood cells (Piconi and Maccauro 1999) and osteoblast cells. *In vitro* tests using cell cultures were performed on ceramic materials in different physical forms such as powders and dense ceramics (Piconi *et al.* 2003). Josset *et al* (1999) investigated human osteoblasts in culture with zirconia and alumina discs and they found that cells showed good adhesion and spreading properties (Josset *et al.* 1999). The cells can preserve their capacity to proliferate and differentiate into ostogenic pathways. Uo *et al* studied cytotoxicity of dental ceramics cultured with human gingival fibroblast cells using Alamar Blue assay (the activity of the metabolic reaction of cells) and DNA quantification (number of cell growth and activity). They found no cytotoxicity of various ceramics including Denzir (YTZP) (Uo *et al.* 2003). Aidlin (Ardlin 2002) studied the chemical stability and

ageing of zirconia ceramic using 4% acetic acid at 80°C for 168 hours. No chemical solubility above the limit values of ISO 6872 (1995) standard were found.

Some of the *in vivo* tests investigated implanting zirconia ceramics into bone and soft tissue. Scarano *et al* (2003) reported high biocompatibility and osteoconductivity of zirconia implant. They studied the bond response to zirconia implants inserted into tibia of white mature rabbits when the implants were retrieved after 4 weeks (Scarano *et al.* 2003). Newly formed bone was observed in close contact with zirconia ceramic surfaces and osteoblasts were present directly on zirconia. No inflammation was observed. Garvie *et al.* (1984) implanted magnesia-partially stabilised zirconia (Mg-PSZ) in paraspinal muscles of rabbits, which were examined at 1 week, 1 month, 3 months and 6 months (Garvie *et al.* 1984). They reported no significant adverse soft tissue response to implants. No degradation of the properties of Mg-PSZ occurred in contact with living tissue. There was no change in the surface phase content, surface roughness and strength of the implants. Christel *et al* (1989) published a study on *in vivo* effects of zirconia ceramic. Yttria stabilised zirconia and alumina cylinders were implanted into paraspinal muscles of rat. From 1 to 12 weeks after placement, no significant difference was observed between materials. The membrane thickness of macrophage and fibroblast were all higher in alumina mainly at 1 week; however, there was no significant difference with zirconia (Christel *et al.* 1989). Therefore, it can be concluded that there appears to be no cytotoxicity of zirconia ceramic when tested both *in vitro* and *in vivo*

2.6.3.6 Longevity

A restoration's longevity is an important factor when discussing treatment options with a patient. Survival and success rates are commonly used to assess

longevity (Ahmad 2006). Survival indicates that a restoration is functioning without all the initial desired parameters (Ahmad 2006). Success implies that the restoration remains unchanged without any treatment over the observation period (Ahmad 2006). The successful outcome is presence of all three aspects: health, function and aesthetics (Ahmad 2006).

In order to be successful clinically, all-ceramic reconstructions need to achieve longevity and ideally a high survival rate similar to metal ceramic restorations, which are currently used for high strength aesthetic posterior restorations. From meta-analysis, the 5-year survival rate of metal ceramic crowns was 95.6% (95% confident interval) and 93.3% (95% confident interval) for all-ceramic crown (Pjetursson *et al.* 2007). The most common complications found in all-ceramic and metal ceramic were loss of pulp vitality and caries (Pjetursson *et al.* 2007). Single unit zirconia based crowns have been evaluated; however, these studies do not provide details of the success or survival rates of single unit zirconia crowns. Most of the clinical publications relate to zirconia fixed partial dentures (Denry and Kelly 2008; Kelly 2007).

Zirconia ceramic fixed partial dentures have been reported to have survival rates ranging from 73.9-100% at 2-5 years follow up periods (Raigrodski *et al.* 2006; Sailer *et al.* 2007a; Vult von Steyern *et al.* 2005; Zembic *et al.* 2002) (Table 2.3). However, 5 years is considered relatively short. A systematic review reported that metal-ceramic fixed partial dentures had a mean survival rate of 94.4% estimated after 5 years (ranging from 91-97.9%) (Sailer *et al.* 2007b). Survival rate of IPS Empress 2 fixed partial dentures was 70% at 5 years, which was slightly lower than other restorations (Marquardt and Strub 2006). In-Ceram fixed partial dentures had a survival rate of 90% after 5 years (Vult von Steyern *et al.* 2001).

Zirconia restorations offer sufficient stability and good clinical performance in terms of fracture resistance, marginal integrity, marginal discolouration, and secondary caries (Raigrodski *et al.* 2006; Sailer *et al.* 2007a; Vult von Steyern *et al.* 2005; Zembic *et al.* 2002). Two studies found that all zirconia ceramic fixed partial dentures were still in use with no caries detected after 2-3 years with a 100% survival rate (Raigrodski *et al.* 2006; Vult von Steyern *et al.* 2005) (Table2.3). Only minor complications were found such as chipped veneer, marginal crevice (can catch by an explorer) and/or endodontic problem but no restorations needed to be replaced (Raigrodski *et al.* 2006; Vult von Steyern *et al.* 2005). However, some studies reported major complications including framework fracture, root fracture, endodontic complications, extensive fracture of veneering ceramic (Sailer *et al.* 2007a), and secondary caries due to marginal discrepancies and inappropriate cementation (Sailer *et al.* 2007a; Zembic *et al.* 2002). One case report of a 5-unit bridge described how it fractured through the connector area because of chewing stone piece. They assumed that the fracture was attributed to the trauma or fatigue of the ceramic rather than the connector dimensions, which were already adequate for the span of the restoration (18.49-19.28 mm^2) (Sailer *et al.* 2007a).

The most frequent technical problem found in all studies of zirconia restorations was minor chipping or fracture of the veneering ceramic (Raigrodski *et al.* 2006; Sailer *et al.* 2007a; Vult von Steyern *et al.* 2005; Zembic *et al.* 2002). The high incidence of chipping of veneer ceramic may be due to the use of new low-fusing ceramics that have a thermal expansion coefficient compatible with zirconia ($>11x10^{-6}K^{-1}$). These possess poor mechanical properties, in particular low fracture toughness and flexural strength (Raigrodski *et al.* 2006; Sailer *et al.* 2007a). In addition, the framework produced from the CAD/CAM may result in an insufficient occlusal shape to support the veneer ceramic. An unsuitable thickness ratio

between veneer and the framework is also possible (Vult von Steyern *et al.* 2005). One study indicated that a weak bond exists between veneer and zirconia ceramics when compared to metal ceramics, which may cause the veneer to chip (Guess *et al.* 2008). In addition, a systematic review reported that the chipped veneer of zirconia restorations occurred more frequent than glass ceramic and metal ceramic restoration whereas the fractured framework of glass ceramic restoration occurred more frequently than zirconia restoration (Sailer *et al.* 2007b). However, Raigroski *et al* (2006) reported that none of their restorations demonstrated an adhesive failure between veneering porcelain and the zirconia framework after a 3 year observation (Raigrodski *et al.* 2006). One *in vitro* study also found no difference in the bond strength of veneer and framework between all-ceramic and metal restorations (Al-Dohan *et al.* 2004). The difference in bond strength outcomes of veneer and zirconia framework in various studies may be due to types of zirconia frameworks, types of veneering materials and surface finishing on zirconia framework before veneering (Aboushelib *et al.* 2007).

However, it is difficult to compare the success rate or survival rate between different studies that set different criteria for failure of a restoration. The failure they set can be varied from decementation of a restoration to fracture. If minor fracture of a restoration was considered a failure, many restorations would be deemed unsuccessful (Raigrodski *et al.* 2006; Vult von Steyern *et al.* 2005). Vult von Steyern *et al* (2005) suggested that if patients were satisfied and unaware of a minor fracture to a veneer restoration, the chipped veneer was not a failure. One study focused on the condition of zirconia frameworks rather than the restorations (Sailer *et al.* 2007a). They reported that zirconia framework had a success rate of 97.8%; however, there were several complications such as secondary caries and major fractures of veneer ceramic that they did not include in the failure criteria.

Additionally, several studies presented the survival rates in different ways and rendered comparison difficult. Use of percentages at certain time intervals is less informative than median survival as many studies include restorations of differing ages. There are only a few studies evaluating the clinical results of zirconia framework based ceramics for fixed prostheses and may have short observation times.

When examining the medical literature, a high fracture rate of zirconia hip prostheses due to ageing sensitivity of zirconia has been reported (Clarke *et al.* 2003; Hummer *et al.* 1995) and early zirconia products (Prozyr) were recalled and suspended by the United States food and drug administration (FDA) in 2001 (Clarke *et al.* 2003). Due to the short time that zirconia has been used as a substructure in dental restorations. It is difficult to make a definite conclusion regarding longevity. However, short term complications have been reported and discussed in this section. Long-term evaluation will be important to assess the ageing susceptibility of zirconia.

Table 2.3. Characteristics of major clinical studies investigating zirconia-based prostheses

Investigators	Follow up patients	Follow up prostheses (numbers)	Mean (years)	Range observe (years)	Complications (numbers)	Survival rate (percent)	Success Rate (percent)
Sailer *et al* (2007a)	27	3-5 unit posterior (33)	4.5	5	Fractured framework (1) Loss of retention (1) Secondary carries (6) Endodontic problem (1) Root fracture (2) Fracture of veneering ceramic (1) Chipped veneer (7)	73.9	97.8
Raigroski *et al* (2006)	16	3 unit posterior (20)	2.7	1.5-3	Chipped veneer (5) Marginal integrity (1)	100	Not reported
Vult von Steyern *et al* (2005)	18	3-5 unit posterior (20)	2	2	Chipped veneer (3) Endodontic therapy (1)	100	Not reported
Zembic *et al* (2002)	13	1-3 unit posterior (18)	Not reported	3	Endodontic problem (1) Loss of retention (1) Inappropriate cementation (1) Chipped veneer (1) Marginal discrepancies of abutments (6)	83	Not reported

2.7 Factors influenced mechanical properties of zirconia ceramics

Mechanical strength is an important factor that controls the clinical success of dental restorations (Ban and Anusavice 1990). Strength values in ceramics are affected by several factors such as chemical composition, manufacturing and sintering process, test methodology, clinical procedures.

2.7.1 Chemical composition

The strength of zirconia can be varied depending on its chemical composition such as colouring agents and stabilising agent. Because zirconia is off white in colour, the zirconia frameworks can be shaded before sintering in order to achieve an aesthetic and natural appearance for the veneering of fixed partial dentures. Colouring oxide such as Fe, Cu, Co, and Mn can be added to dental ceramics (Milleding *et al.* 2003); however, whether these oxides affect the strength of zirconia ceramics depends on the manufacturing process (Ardlin 2002), amount of colouring oxide (Shah *et al.* 2008) and duration of colour shading (Hjerppe *et al.* 2008). Ardlin (Ardlin 2002) found coloured zirconia (P17) had higher strength than white shaded zirconia (P0). He suggested that the difference in strength might be related to components such as CeO_2, Fe_2O_3 and Bi_2O_3 that were added to obtain different shades. However, he found higher porosities in white shaded specimens which indicated that coloured and uncoloured specimens had different manufacturing processes. However, two studies reported that there was no significant difference in flexural strength between coloured and uncoloured zirconia specimens (Behrens *et al.* 2004; Farsi *et al.* 2006). Shah *et al* (2008) reported that an increase in amounts of cerium acetate, cerium chloride, and bismuth chloride to 5 wt% and 10 wt%

reduced the biaxial flexural strength of zirconia specimens (Shah *et al.* 2008). In contrast, a small amount (1 wt%) of these colouring agents did not affect the biaxial flexural strength. They also found that colouring agents did not induce phase transformation; however, there was a slight increase in lattice parameters compared to the control group (from a= 3.60, b= 5.17 to a= 3.61, b= 5.18 Å), which agrees with one study (Hjerppe *et al.* 2008). Longer shading time also reduced the flexural strength of zirconia (Hjerppe *et al.* 2008).

Another factor that has been reported to influence properties is an alloy added in zirconia. One study (Kim 1990) examined various alloying oxides mixed with 2-3% Y-TZP. They found tantalum pentoxide (Ta_2O_5), niobium pentoxide (Nb_2O_5) and hafnium oxide (HfO_2) enhanced transformability of the Y-TZP. HfO_2 had the lowest effect on transformability compared with Ta_2O_5 and Nb_2O_5 and conversely the addition of Y_2O_3 decreased transformation. In addition, the amount of stabiliser also affected the phase content in zirconia. High tetragonal phase-content could not be achieved for the composition containing 1.5 mol% Y_2O_3 (Lange 1982). Gross and Swain also reported that Y_2O_3 content below 2.3 mol% produced microcracks in all samples. Additional components have been added to Y-TZP in order to improve the strength.

Some studies tried to improve the strength of zirconia by adding some other components to zirconia powder. One study (Nakayama and Sakamoto 1998) reported that there was an increase in flexural strength (from 950 MPa to >1000 MPa) of 2.5 mol% Y-TZP by adding B_2O_3-Al_2O_3-SiO_2. Bamba *et al* (2003) also found that 3 mol% yttria doped zirconia/silicon carbide had similar strength and higher

fracture toughness and Young's modulus than 3Y-TZP; however, 3Y-TZP/SiC used a sintering temperature higher than 3Y-TZP to reach maximum strength.

2.7.2 Manufacturing and sintering process

Manufacturing and sintering processes have a major effect on the properties of zirconia ceramic. One of the important steps for producing materials is powder pressing. There are three basic powder compaction procedures: uni-axial, isostatic (or hydrostatic), and hot pressing. For uni-axial pressing, the powder is compacted in a metal die by pressure that is applied in a single direction (Callister 2005). The formed piece takes on the configuration of die and platens (metal cylinder) through which the pressure is applied. This method and the process is confined to shapes that are relatively non complicated and the technique is simple (Callister 2005). In addition, production rates are high and the process is inexpensive (Callister 2005). For isostatic pressing, the powdered material is contained in a rubber envelope and the pressure is applied by a fluid, isostatically (it has the same magnitude in all direction) (Callister 2005). Isostatic pressing yields denser compacts compared with uni-axial pressing, and results in better quality specimens (Pashchenko *et al.* 1994). More complicated shapes are possible than with uni-axial pressing; however, the isostatic technique is more time consuming and expensive (Callister 2005). For both uni-axial and isostatic procedures, a firing operation is required after the pressing operation. With hot pressing, the powder pressing and heat treatment are performed simultaneously (Callister 2005). Powder is compacted at the elevated temperature. The procedure is used for materials that do not form the liquid phase except at very high and impractical temperatures (Callister 2005). It is costly in terms of time, since

in both methods the mold and die must be heated and cooled during each cycle. Additionally, the mold is usually expensive to fabricate and ordinarily has a short lifetime (Callister 2005). A powder mass usually containing a small amount of water or binder is compacted into the desired shape by pressure (Callister 2005). One function of the binder is to lubricate the powder particles as they move past one another in the compaction process (Callister 2005).

The sintering temperature and the duration of the sintering process have been reported to affect grain size and phase content, which influence the strength of zirconia (Casellas *et al.* 2001; Ruiz and Readey 1996). Ruiz and Ready proposed that the grain size increased with increasing sintering temperature, which led to an increase in fracture toughness, owing to larger transformation zones. However, no significant difference in biaxial flexural strength of various grain size zirconia ceramics was reported in this study. This contrasts with the results of Casellas *et al* (2001) who found that a decrease in grain size gave a slight increase in flexural strength. This is attributed to greater phase transformation around the crack in coarser microstructures than smaller grain materials.

The factors caused by the manufacturing and sintering processes affecting the property of zirconia are flaws or defects and crack initiation, which can lead to early restoration failures (Isgro *et al.* 2003). The strength of ceramic specimens and prostheses depend on the size of microscopic cracks and pores. One article (Denry *et al.* 1993) reported that the presence of numerous surface flaws, including submicroscopic Griffith flaws can lead to failure. This flaw can act as stress concentrators when the object is under load, with microscopic stress occurring at the flaw tip and causing fracture as soon as a critical breaking stress is reached (Denry

et al. 1993). Crack initiation may be influenced by the quality of the ceramic surface and the internal structure of ceramic materials, which can provide resistance to crack growth (Isgro *et al.* 2003). The strength of material is dependent on the size of the pre-existing initiating cracks present in a particular sample or component (Bona *et al.* 2003). In addition, a large number of cracks together with a low fracture toughness of materials will limit the strength of ceramics and cause a large variability in strength (Bona *et al.* 2003).

2.7.3 Experimental design

Experimental design can affect properties of zirconia such as specimen preparation, equipment and geometry, or environmental condition. Specimen preparation required for the test may affect the results; for example, pre-loading on the surface of a specimen or containing a notch, groove, and hole. Some test methods such as the crack growth measurements require an indentation notch before testing, which may affect the results when using higher indentation loads. Zhang and Lawn (2005) found Y-TZP ceramic had high sensitivity to sharp-indenter damage in cyclic flexural stressing. An indented specimen under a force of 10 N caused significant degradation in strength after 10 cycles compared to those with natural flaws, 0.1 and 1 N forces. The strength was also reduced after 100 cycles when using 1 and 0.1 N forces compared with natural flaws.

In addition, strength variation can be caused by different designs of equipment. Albakry *et al* (2003b) studied the biaxial flexural strength of ceramic using a piston on three balls. They suggested that the small piston tip (0.75 mm) may improve the strength values because only a smaller area of the specimen was subjected to the

maximum tensile stresses. Consequently, there was less chance of the specimen having a critical flaw in that area (Albakry *et al.* 2003b). In addition, a difference in geometry for the strength tests such as uni-axial (3 or 4 point bending test) and biaxial test leads to a variation in strength values. Ban and Anusavice (1990) studied failure stress of four brittle materials (zinc phosphate, opaque porcelain, body porcelain and resin composite) using biaxial flexural test (piston on three balls) compared with a four point flexural test. They found that the mean strength obtained from biaxial flexural test was higher than a four-point flexural test. Shetty *et al* (1981) reported that there was no significant difference between the strength value of glass ceramic tested by three and four point bending; however, biaxial flexural test (ball-on-ring) provided a higher strength value in comparison. One of the reasons that the different geometries provide different results is the specimen preparation. The specimens for uni-axial flexural test are prepared in bar shape whilst those for biaxial tests are prepared in disc shaped. Undesirable edge fracture could occur when preparing bar specimens and this may ultimately affect strength.

2.7.4 Clinical related mechanical property

2.7.4.1 Flexural strength related to surface treatment

A requirement for the successful function of low strength ceramic restorations over the years is an adequate adhesion between ceramic and tooth substance. To achieve the best fit between the prosthetic work and the prepared tooth structure, a final adjustment by dental grinding may be required. Sandblasting is frequently used to improve the bond between the luting agent and the prosthetic material. Several researchers have studied the effect of surface treatments such as grinding,

sandblasting, and polishing on the strength and microstructure of zirconia (Guazzato *et al.* 2005a; Kosmac *et al.* 1999; Denry and Holloway 2005; Kosmac *et al.* 2000; Garvie *et al.* 1975).

Garvie *et al* (1975) first reported that grinding increased the strength of zirconia compared with a polishing process. This difference was associated with an increase in the monoclinic content at the surface on grinding while polishing removed some of the monoclinic material and this reduced the surface strain. A similar reduction of the strength can be achieved by annealing, which removes the strain without reducing the surface content of monoclinic phase (Garvie *et al.* 1975). Denry and Holloway found grinding with a 20 micron diamond bur increased the biaxial flexural strength of zirconia because a rhombohedral phase and strained tetragonal phase was formed, which can increase resistance to crack propagation but may be associated with surface and subsurface damage (Denry and Holloway 2005). Kondoh (2004) suggest that the shoulder or hump observed in XRD peak, which others indicated it was rhombohedral phase, was caused by lattice distortion of tetragonal phase (Kondoh 2004). Kosmac *et al* (1999) reported that grinding using a coarse grit (150 μm) diamond bur at high rotation speed lowered the mean strength and reliability whereas sandblasting improved the mean strength at the expense of lower reliability. Therefore, grinding has the ability to introduce compressive stress and enhance the transformation toughening of the zirconia surface with a resultant increase in strength (Garvie *et al.* 1975). However, coarse grinding or severe grinding introduces deep surface flaws which can lower the strength and reliability of zirconia (Curtis *et al.* 2005; Kosmac *et al.* 2000). On the other hand, sandblasting is considered to be a more gentle process and less

material is removed from the surface. Some studies found that sandblasting increased the strength of Y-TZP ceramics (Kosmac *et al.* 1999; Kosmac *et al.* 2000). They suggested that sandblasting is an efficient technique for strengthening zirconia-based ceramic in clinical practice. However, Curtis *et al.* (2005) found alumina abrasion regimes did not significantly alter the mean biaxial flexural strength of zirconia specimens.

2.7.4.2 Bonding capacity related to surface treatment

Long-term clinical success of ceramic restorations depends on successful adhesion between ceramic and tooth substance. To achieve a high bond strength of luting cement to the ceramic, a micromechanical interlocking and chemical bonding to the ceramic surface are required (Blatz *et al.* 2003). To enhance the bond strength of luting cements to ceramics, a number of techniques have been reported; however, different types of ceramics need different surface treatment techniques in order to gain maximum bond strength.

Glass-based ceramics or silica-based ceramics such as feldspathic, leucite and lithium disilicate ceramics are acid-sensitive ceramics; therefore, the common treatment options are acid etching, silanisation, airborne particle abrasion with aluminium oxide or combinations of any of these methods. Acid etching with a solution of hydrofluoric acid (HF) and acidulated phosphate fluoride (APF) are commonly used in dental literatures because they can induce the proper surface texture and roughness of glassy ceramics (Brentel *et al.* 2007; Chen *et al.* 1998; Kukiattrakoon and Thammasitboon 2007; Tylka and Stewart 1994). The acid dissolves the glassy phase and produces a porous irregular surface. This leads to an

increase in surface area and wettability of ceramics enhancing the micromechanical retention (Brentel *et al.* 2007). Examples of acid etching used in the clinic are 5-10% HF and 1.23% APF. HF acid gel has been reported to produce a higher bond strength than APF (Brentel *et al.* 2007; Della Bona *et al.* 2002). In addition, the application of HF acid gel generates more adequate micromorphological surface topography for micromechanical retention of the resin cement (Brentel *et al.* 2007). However, HF is more hazardous than APF with extreme caustic effects to soft tissues (Brentel *et al.* 2007). The danger for its clinical use is also well known due to its rapid vaporisation and the danger of inhalation (Brentel *et al.* 2007). Therefore, HF can only be used in clinical procedures if sufficient care during handling is taken in order to avoid its side effects (Chen *et al.* 1998). For this reason, some studies questioned whether 1.23% APF gel might serve as a safe and effective substitute for etching ceramic surfaces before bonding resin composite. Tylka and Stewart (1994) supported the use of APF as they found no significant difference of shear bond strength between 9.5% HF (5 minnutes) and 1.23% APF acids (10 minutes) (Tylka and Stewart 1994) and these results were similar to another study (Kukiattrakoon and Thammasitboon 2007). Although, they found that 1.23% APF etching produced lower bond strength than 9.6% HF overall, etching with 1.23% APF for 7-10 minutes did not produce a significant difference in shear bond strength compared to etching with 9.6% HF for 4 minutes. Another study (Bona and van Noort 1995) also reported that etching with 9.6% HF for 2 minutes had comparable tensile bond strength to etching with 4% APF for 2 minutes.

In addition, the etching period and addition of a silane coupling agent affects the bond strength of glass ceramics. Etching time depends on the type of acid and

manufacturer recommendation. For example, etching time of HF acid ranging from 5-30 minutes has been used for bond strength tests (Awliya *et al.* 1998; Brentel *et al.* 2007; Chen *et al.* 1998; Della Bona *et al.* 2002; Della Bona *et al.* 2007; Kukiattrakoon and Thammasitboon 2007; Özcan and Vallittu 2003; Tylka and Stewart 1994). However, it is often applied between 1-2 minutes in several studies (Awliya *et al.* 1998; Brentel *et al.* 2007; Della Bona *et al.* 2002; Della Bona *et al.* 2007; Özcan and Vallittu 2003). Additionally, the etching time of APF acid is longer than that of HF etch (Brentel *et al.* 2007; Kukiattrakoon and Thammasitboon 2007; Tylka and Stewart 1994). Over-etching did not improve the bond strength and it may decrease the bond strength because the ceramic surface becomes over-etched and the resin cannot penetrate into the deep microporous surface (Chen *et al.* 1998).

Apart from acid etching, an application of a silane coupling agent is commonly used after the etching process. Silane contains hybrid organic-inorganic compounds, which act as a mediator to promote adhesion between inorganic and organic substrates (Matinlinna *et al.* 2004). It can bond silicone dioxide with the OH groups on the ceramic surface and also have a degradable functional group that copolymerises with the organic matrix of the resin (Matinlinna *et al.* 2004). Therefore, it has chemical bonding ability to both ceramic and composite resin. Use of a silane coupling agent in combination with acid etching has been proved to increase the bond strength (Calamia and SImonsen 1984; Stangel *et al.* 1987) and bonding durability (Brentel *et al.* 2007) of composite to the silica-based ceramics. Brentel *et al* (2007) found that microtensile bond strength was increased by silanisation of the feldspathic ceramic surface after APF and HF acid etching.

After thermocycling for 12,000 times and water storage for 150 days, the bond strength reduced dramatically when the ceramics were not silanised.

Although the etching has been successfully used to increase the bond strength of silica-based ceramics, this technique does not improve the bond strength of glass-infiltrated alumina and zirconia and high purity alumina and zirconia ceramics. Özcan and Vallittu (2003) reported that acid etched glass ceramics exhibited significantly higher shear bond strength (26.4-29.4 MPa) than glass infiltrated alumina ceramics (5.3-18.1 MPa) or zirconia dioxide (8.1 MPa). Bona *et al* reported that 9.5% HF etching on alumina and zirconia-based reinforced ceramic surfaces for 1 minute achieved low tensile and shear bond strength (3.5 and 10.4 MPa) compared with sandblasting (7.6 and 13.9 MPa) and silica coating (10.4 and 21.6 MPa).

Sandblasting using aluminium oxide particles is a surface treatment option that produces irregularities in acid-resistant ceramics. It results in initially relatively low bond strength when cemented with conventional BisGMA resin composite (Kern and Wegner 1998; Lüthy *et al.* 2006); however, the bond strength reduced after long-term thermocycling in distilled water (Kern and Wegner 1998). The reason for this can be assumed that sandblasting of zirconia ceramic produces a certain roughness but only limited or minimal undercuts (Kern and Wegner 1998). Therefore, the bonding between BisGMA resin and zirconia were not water resistant and the sample debonded.

Addition of a silane did not enhance the bond strength of the BisGMA resin composite to zirconia. In addition, the silane did not improve the durability of the bond in water (Kern and Wegner). This indicates that silane does not bond to zirconia. In conventional dental ceramics, it is thought that silane bonding is

mediated through the silica at the ceramic surface. As zirconia contains no silica, the silane cannot promote a resin bond to zirconia.

Using a tribochemical silica coating system has been reported to produce a significant increase in the initial bond strength of the conventional BisGMA resin to YTZP ceramic (Kern and Wegner 1998; Lüthy *et al.* 2006; Ozcan and Vallittu 2003); however, the resin bond was decreased after thermocycling (Kern and Wegner 1998; Ozcan and Vallittu 2003; Lüthy *et al.* 2006). Della Bona *et al* (2007) reported that silica coating produces the highest tensile (10.4 ±1.8 MPa) and shear bond strength (21.6 ± 1.7 MPa) of In-Ceram Zirconia ceramic compared with sandblasting (7.6±1.2 and 13.9± 3.1 MPa) and HF etching (3.5± 1 and 10.4± 3.1 MPa) (Della Bona *et al.* 2007)

The bond strengths of the phosphate monomer containing resin composites (such as Panavia F and Panavia 21), which is 10-methacryloxy-decry dihydrogenphosphate (MDP), to sandblasted zirconia ceramic surface were significantly higher when compared with other techniques and other resin cements (Kern and Wegner 1998; Lüthy *et al.* 2006). Kern and Wegner (1998) reported that tensile bond strength decreased about 17% over storage time but was not statistically significant. Kern and Wegner (1998) used conventional resin composite for control and silanisation groups. However, Lüthy *et al* found shear bond strengths of Panavia F and Panavia 21 were higher after thermocycling (10,000x) for 14 days. Nevertheless, Lüthy *et al* (2006) suggested that their study was too short (14 days) to provide the information on long-term bonding stability compared with Kern and Wegner (1998) who used a longer ageing time (150 days). Therefore, the results from several researchers indicate MDP promotes a water-resistant chemical bond to

zirconia ceramics. The phosphate ester group of the monomer is reported to bond directly to metal oxides (Wada 1986). However, Atsu *et al* (2006) found that MDP-containing composite resin luting agent alone or with silane coupling agent had significantly lower shear bond strength compared with the combination of silica coating and MDP-containing composite resin groups. Therefore, they recommended the application of silica-coating, MDP-bonding, and silanisation combination to increase the bond strength. However, thermocyling test was not performed in this study.

Although chemical-cured polyacid-modified resin composite initially provided relatively high bond strength to sandblasted YPSZ, it decreased statistically significantly over long-term storage with thermal cycling (Kern and Wegner 1998).

The anhydride group of 4-META such as Superbond C&B was reported to have chemical affinity to metal oxides. One study found that 4-META provided initially high bond strength (44.5 MPa); however, the bond strength decreased statistically after thermocycling (Lüthy *et al.* 2006). This reduction could be explained by water absorption of Polymethylmethacrylate (PMMA) during the thermocycling test, which seemed to weaken the chemical bond (Lüthy *et al.* 2006). Dérand and Dérand found 4-META provided the highest bond strength (~17-20 MPa) compared with Panavia 21 (~5-8.9) and Twinlook (autocuring cement) (~2-3 MPa). Superbond also presented the same bond strength regardless of whether the ceramic surface was etched, sandblasted or ground while Panavia and Twinlook had a stronger bond if the ceramic surface was coated with Rotatec (Derand and Derand 2000).

2.8 Mechanical property measurements

Mechanical properties of a material play an important role in the clinical success of dental restorations. The properties of materials should be measured to predict the stability and longevity of the material and prevent the failure.

2.8.1 Flexural strength

Usually, complex stress distributions that are induced by compressive, tensile and shear stresses are present in most specimens. However, brittle materials are much weaker in tension than in compression (Ban and Anusavice 1990). Therefore, tensile strength is generally considered as the more meaningful property for brittle materials for assessment of the failure potential of dental restorations (Ban and Anusavice 1990).

Flexural strength is a fracture-related mechanical property since it is a measure of the resistance of restorations to tensile forces. Materials with high flexural strength provide restorations with less susceptibility to bulk fracture (Sunnegårdh-Grönberg *et al.* 2003). Different methods are available to assess the flexural strength of ceramic materials. These test methods included three-point bending, four-point bending and biaxial flexural tests (Figure 2.3)

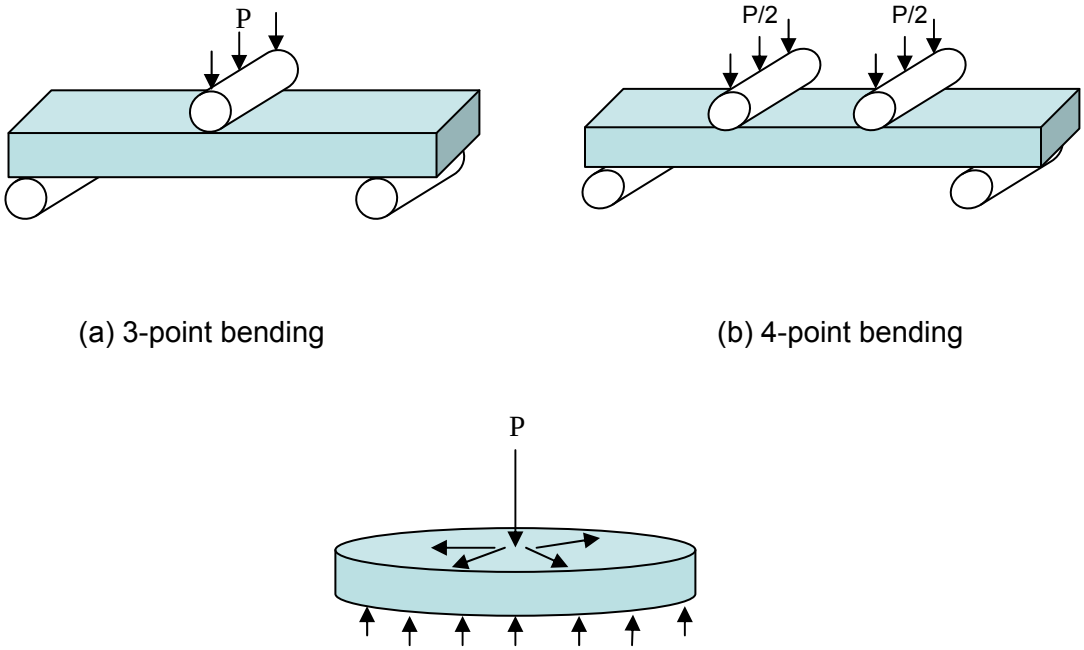

(a) 3-point bending (b) 4-point bending

(c) Biaxial flexure

Figure 2.3. Flexural test methods

2.8.1.1 Uni-axial strength (three-point or four-point flexure test)

Three-point and four-point flexure tests have also been used for strength evaluation of brittle materials and metal-ceramic structures (Ban and Anusavice 1990). For these uni-axial flexure tests, the principle stress on the lower surfaces of the specimens is tensile, and it is usually responsible for crack initiation in brittle materials.

- ***Four point bending***

The four-point flexure test is a method of assessing mechanical properties of materials. It has been used for strength evaluation of single component brittle

materials and bilayered structures such as glass veneer on core ceramic specimens and metal-ceramic structures (Bona *et al.* 2003). For the four-point flexure test, rectangular specimens are supported by two 3-mm-diameter rods set 21 mm apart (Figure 2.3b). The load is applied by two rods that are set 7 mm apart. A cross-head loading rate of 0.2 mm/min is used. The maximum tensile stress is calculated by the equation 2.1

$$\sigma = PL/wt^2 \qquad 2.1$$

Where is *P* is the applied force at failure, *L* is the length of outer span, *w* is the width of the specimen, and *t* is the thickness of the specimen.

Ban and Anusavice (1990) studied flexural strength of zinc phosphate cement for orthodontics, feldspathic opaque porcelain, feldspathic body porcelain and light-cured composite resin using biaxial flexural test compared with four-point bending test. The results showed that groups submitted to four-point bending test exhibited lower strength values than biaxial flexural test.

- ***Three point bending***

The three-point flexural test is one of the standards for strength testing of dental ceramics (Figure 2.3a). Shetty *et al* (Shetty *et al.* 1981) studied the flexural strength of glass-ceramic comparing among 4-point, 3-point bending and biaxial flexural test (ball-on-ring test). They found mean strength values from 4-point and 3-point bending were similar where as ball-on-ring tests exhibited higher mean strength than uni-axial tests.

Although the three-point and four-point flexural tests are one of the standard tests of dental materials, the strength results may be affected by edge flaws and defects (Seal *et al.* 2001; Albakry *et al.* 2003b; Ban and Anusavice 1990). Consequently, the strength value obtained from these methods is lower than the actual strength of the materials (Seal *et al.* 2001). This problem is overcome by the use of biaxial flexural strength test because it is not affected by edge flaws and defects (Albakry *et al.* 2003b; Ohyama *et al.* 1999b; Wagner and Chu 1996) as they are not directly loaded (Wagner and Chu 1996). Therefore, the biaxial test should produce less variation in data for strength determination compared with uni-axial tests (Ohyama *et al.* 1999b).

2.8.1.2 Biaxial flexural strength

The biaxial strength testing has been used for many years (Morrell et al, 1999) and is considered a more reliable method of assessing the strength of brittle dental ceramic materials than uni-axial flexural tests (Figure 2.3c) (Ban and Anusavice 1990; Isgro *et al.* 2003; Wagner and Chu 1996). There are several advantages claimed for biaxial flexural testing of discs compared with uni-axial testing of bars including ease of test piece preparation and ability to test a large effective surface area (Morrell *et al.* 1999; Seal *et al.* 2001). Additionally, the test provides an equibiaxial stress distribution, which is more searching for defects than a uni-axial distribution as found in a bar test (Morrell *et al.* 1999). The specimen is loaded on the opposite sides with radically symmetrical bending forces (Seal *et al.* 2001) and the maximum tensile stress occurs at the central loading area rather than at the edges. Hence, the cracks propagate from the centre of the disc toward the edges (Ban and

Anusavice 1990; Ohyama *et al.* 1999a; Seal *et al.* 2001). The 'edge effect' on the strength data is eliminated or minimised (Ban and Anusavice 1990; Ohyama *et al.* 1999a; Seal *et al.* 2001). Biaxial strength testing has some disadvantages compared with uni-axial testing. First, it is unclear what the optimum test geometry in terms of test piece aspect ratio and edge overhang should be. The use of thin plate analytical solutions for the stress field may have limitations, especially regarding thin materials such as electrolyte membranes (Morrell *et al.* 1999).

A wide variety of loading arrangements have been developed for biaxial flexure tests such as ring-on ring, piston-on-ring, ball-on ring, ring-on-ring, and piston-on-three balls.

- ***Ring-on-ring***

The ring supported/ring loaded geometry, has been agreed as a revision in ISO 6474 for orthopaedic alumina ceramics (Morrell *et al.* 1999). A disc shape specimen is supported by a concentric ring of smaller diameter. Ring-on–ring test has been standardised and extensively used for strength measurements on glass. Whilst bending bars exhibits additional flaws at the edges generated by machining process, the edge of circular discs are nearly free of stress and will not contribute to failure (Fett and Rizzi 2004). However, highly plane-parallel disc-shaped specimens are required.

- ***Ball-on-ring***

In the ball-on-ring test, the specimen is supported by the rings and loaded centrally with a ball. This test configuration was proposed by Shetty *et al* (1981).

Isgro *et al* (2003) studied the biaxial flexural strength test of ceramic core, veneering porcelain, and 2- layer discs which was determined by the ball-on ring test method (ASTM F394-78) using a universal testing machine at cross-head speed of 0.5 mm/min at room temperature. In the ASTM standard, the supporting ring (16 mm in diameter) consists of a series of balls (5mm in diameter) resting on a circular groove in a steel block. This test requires the load be distributed uniformly over the supporting balls; therefore, the specimen discs must be absolutely flat (Isgro *et al.* 2003).

- ***Piston-on- three-ball tests***

Three balls support/guided punch loading, has been standardised as ASTM F394-78 (Morrell *et al.* 1999; Cattell *et al.* 1999) and EN ISO 6872. The EN ISO 6872 outlined that the machine should be capable of a rate of crosshead speed of 1±0.5 mm/min. For the support of the test specimen, provision of three hardened steel balls with a diameter of 3.2±0.5 mm, positioned 120° apart on a support circle with a diameter of 10 mm to 12 mm, are required. The sample shall be placed concentrically on these supports and the load shall be applied with a flat punch with a diameter of 1.2 mm to 1.6 mm at the centre of the specimen. The prepared specimen should have a thickness 1.2±0.2 mm and a diameter of 12 mm to 16 mm (EN ISO 6872:1998 1999).

2.8.2 Fatigue test

Fatigue is the loss of strength and energy resulting from physical work. Fatigue testing is the application of continuous loading to a test specimen in order to

determine how it performs under repeated vibration or strain conditions. Clinically, an accumulation of the microstructure damage during mastication may induce a catastrophic failure. Therefore, fatigue is an aspect of clinical performance of restorations. *In vitro* fatigue tests have been conducted either by means of the Woehler-curve (S-N curve) (Figure 2.4) or alternatively using a stair-case approach. The Woehler-curve method requires a long period to reach a high cycle regime; however, a large sample size is required for the staircase technique in which a series of specimens are tested in sequence. The specimens for fatigue testing can be produced as discs or bar shapes for dynamic fatigue or crown or bridges shape to simulate the restoration. The later group is usually designed for investigating the strength reduction after submission to fatigue testing.

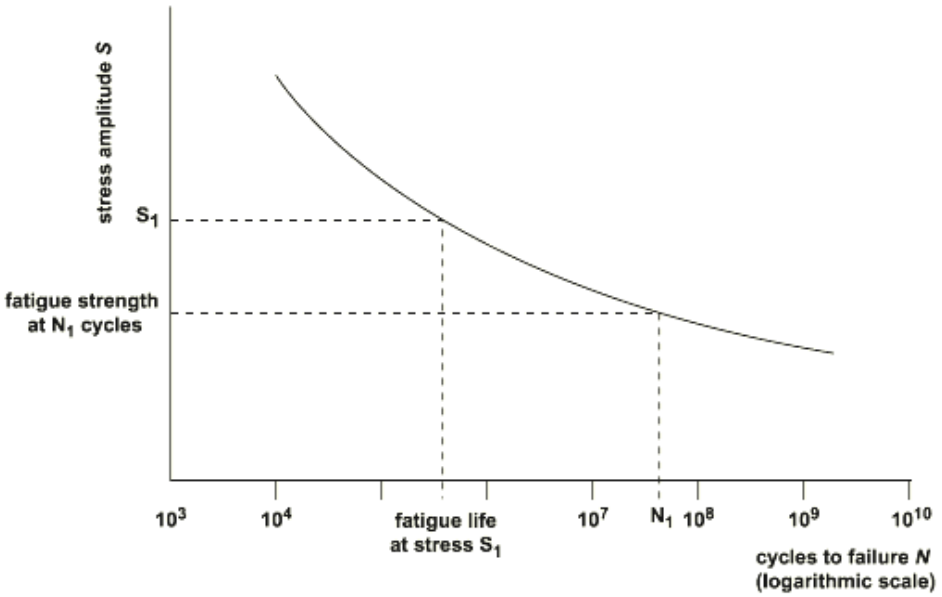

Figure 2.4. S-N curve

2.8.2.1 Fatigue limit and fatigue life

The fatigue life of the specimen is the number of cycles of fluctuating stress and strain that a specimen can withstand before failure occurs. The fatigue life will change for each specimen because it's dependant on the magnitude of the fluctuating stress, the specimen geometry and testing conditions. Dynamic fatigue testing is preferred over fracture-mechanic-based crack propagation tests because it yields more conservative lifetime estimates, and the flaws causing failure are more realistic. The fatigue test can be performed by using a uni-axial (Liu and Chen 1991; Jung *et al.* 2000) or biaxial test (Jung *et al.* 2000; Zhang *et al.* 2004; Zhang and Lawn 2005) with or without small flaws induced by a sharp indenter. Sharp indenter flaws are used to simulate the damage patterns encountered from contacts with hard particulates in surface machining, sandblasting, and scratching (Zhang and Lawn 2005). The damage is readily controlled and quantified via the indentation load (Zhang and Lawn 2005). However, the fatigue property and strength will be reduced if using too high an indentation load because it may damage the ceramic surface. Zhang and Lawn (2005) found that using indentation forces of 0.1N and 1N produced less damage while 10 N force produced a reduction in strength thus reducing fatigue properties. Another method for fatigue testing is the stair-case method. The investigators pre-select a cyclic lifetime and then cycle the material at a stress level. If the specimen fails, a lower stress is chosen, and the experiment is repeated; if the specimen survives to the selected number of cycles, the next experiment is performed at a higher stress level. The concern with this method is that its use virtually implies a fatigue limit; the assumption of a fatigue limit, i.e., a

stress level below which no specimens will fail, is not useful for statistically based lifetime prediction efforts.

2.8.2.2 Flexural strength after fatigue

As reviewed in previous pages, the study of fatigue on fracture strength has been studied in discs or crown shapes or bridges. The biting force in the molar region varies from 400-800 N (Anusavice 2003b; Craig and Ward 1997) and the rate was used as equivalent to the average masticatory cycle of 0.8-1.0 s (DeLong *et al.* 1984). The method is performed the same way as fatigue testing and is followed by the biaxial flexural test.

2.8.3 Subcritical crack growth

Brittle materials are susceptible to time-dependent failure under static loads, caused by the subcritical growth of cracks to critical lengths. It is now widely accepted that subcritical crack growth in ceramics is produced by stress enhanced chemical reactions that occur at the crack tip (Reese and Cox 1992). The crack velocity depends on the applied stress intensity factor, but in most ceramics the time to failure is essentially controlled by crack growth behaviour, where the crack velocity, *v*, has a power-law dependence on the stress intensity factor, K (equation 2.2):

$$v=AK^{n} \qquad 2.2$$

Where *A* is a constant and n is an exponent. Both *A* and *n* are dependent on the chemical environment and its activity at the crack tip. A higher subcritical crack

growth resistance or higher *n* value means slower strength degradation and higher remaining strength, thus longer lifetime (Zhu *et al.* 2003).

The types of the tests that have been used to study subcritical crack growth behaviour in ceramics fall into two categories: those based on the growth of long, induced crack (>100 μm); and those based on short, natural flaws (<100 μm) (Reese and Cox 1992). The experiments involving long cracks enable the direct observation of the growing cracks and the evaluation of the velocity of the crack, *v*, as a function of the applied stress intensity factor, K. While the short crack testing is usually unobservable cracks. It involves either long term tests to measure time-to-failure under a static stress or the effect of subcritical behaviour on the strength of specimens stressed at different rates, in what are known as 'dynamic' fatigue experiments (Reese and Cox 1992). The test is performed using natural flaws; therefore, it will relate to the nature of distribution and size of the flaw population. Whereas in long crack experiments the statistical variation in data results from direct measuring errors (Reese and Cox 1992).

2.8.3.1 Experiments with long crack

Experiments with long cracks are performed by using direct loading, which initiates the crack growth (Reese and Cox 1992). These tests are often performed using crack line loaded specimens, such as, the double torsion, double cantilever beam, or compact tension method, where cracks can grow over distances > 10 mm. The same experiments are also commonly performed using pre-cracked test bars in flexural loading. The major disadvantage of using long cracks is that they may not behave in the same way as short, natural flaws (Reese and Cox 1992). The

indentation method is the easiest and most reliable to produce stable and fairly reproducible crack geometry. However, it produces residual stresses and fatigue damage within the specimen. Chevalier *et al* (1996) suggested that the residual stress caused by the indentation can be reduced by heat treatment of the specimen at 1200°C for 30 minutes (Chevalier *et al.* 1996).

2.8.3.2 Experiment with short crack

Subcritical crack growth behaviour of short, natural flaws can be studied using any method that can be used to measure mechanical strength such as uni-axial and biaxial flexure and direct tension loading. There are two types of tests; static fatigue (performed under constant load) or dynamic fatigue (loading at a range of different stress rates). Failure stress can be expressed as follows (equation 2.3)

$$\log \sigma_f = \log B + \frac{1}{n+1} \log \beta \qquad 2.3$$

Where σ_f is the nominal fracture strength of test piece in MPa;

B is a constant for the batch of test specimens;

β is the stressing rate employed in MPa per second;

Therefore n can be determined by measuring the slope of a log[σ] versus log[β] plot.

2.8.4 Hardness test

Hardness is considered an important property when comparing restorative materials. It is a measure of the resistance to permanent surface indentation or penetration (Albakry *et al.* 2003a). It is defined as the resistance to penetration

displayed by a material by hard indenter of defined geometry and forced into the test surface in a prescribed manner (BSI ENV 843-4:1994). Albakry *et al.* (2003a) suggested that a force of 1.5 N should be used for ceramics as it can prevent the formation of radial cracks as recommended by ASTM C 1327-99 (Albakry *et al.* 2003a).

2.8.4.1 Knoop hardness

A hardness test similar to the Vickers test, but where an elongated indentation is produced by a rhombic-based sharp diamond indenter having specified face angles (BSI ENV 843-4:1994). Only the long diagonal length of the indentation is measured (Figure 2.5), and the result is calculated as the mean force per unit projected area of indentation (equation 2.4).

$$HK\ F = 14.229\ F/d^2 \qquad 2.4$$

Where HK F is the knoop hardness number at applied force F (expressed as the mass in kg from which F is derived), and d is the length of the long diagonal of the indentation in mm. Knoop hardness tests are normally conducted at applied forces derived from masses of less than 1 Kg. This method can be used as an indirect method to evaluate the relative degree of conversion of a material (Cesar *et al.* 2001). However, hardness values cannot be used to compare the degree of conversion among the different materials (Cesar *et al.* 2001).

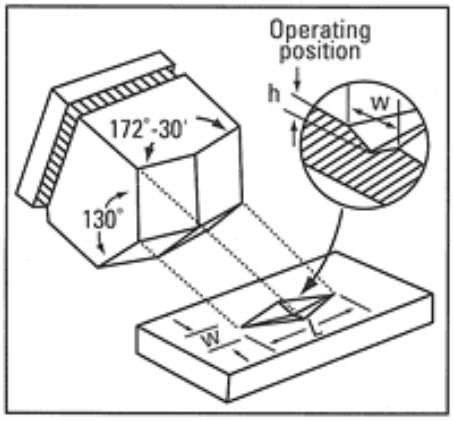

Figure 2.5. Knoop Hardness

2.8.4.2 Vickers Hardness

A hardness test in which a square-based sharp pyramidal diamond indenter having specified face angles is forced into the test-piece surface under a defined force, held for a defined duration and removed (Figure 2.6). The indentation diagonal lengths are measured, the mean result calculated, and this value then employed to calculate a hardness number which is equivalent to the mean force per actual unit area of indenter surface contacting the test surface (BSI ENV 843-4:1994) (equation 2.5).

$$HVF = 1.8544\ F/d^2 \qquad 2.5$$

Where HVF is the Vickers hardness number at applied force F (express as the mass in Kg from which F is derived), and where d is the mean length of the diagonals of the indentation (expressed as mm) (BSI ENV 843-4:1994).

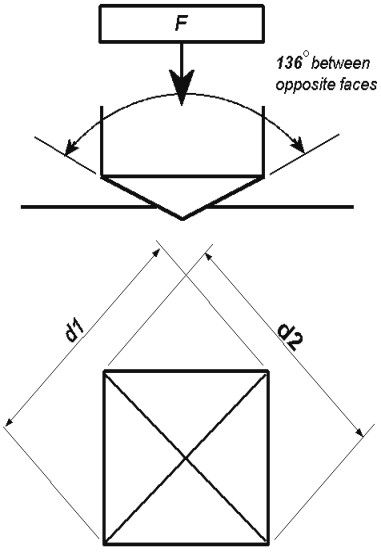

Figure 2.6. Vickers Hardness

2.8.5 Bond strength test

There are two common methods used for bond strength tests; tensile and shear bond strength tests.

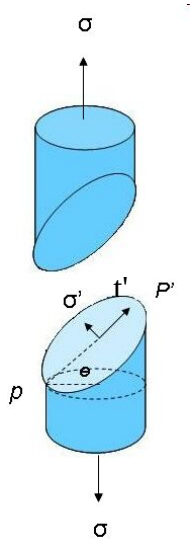

Figure 2.7. Schematic representation showing normal (σ') and shear (t') stresses that act on a plane orientated at an angle ɵ relative to the plane taken perpendicular to the direction along which a pure tensile stress (σ) is applied.

2.8.5.1 Tensile bond strength

The ability of a material to resist breaking under tensile stress is one of the most important and widely measured properties of materials used in structural applications. The force per unit area required to break a material in such a manner is the ultimate tensile strength or tensile strength at break (Callister 2005). In the SI system, the units are newtons per square (N/m^2) or pascals (Pa). Tensile bond strength specimen design consists of two rod specimens of uniform cross-section,

bonded together on their ceramic surfaces and pulled apart in a universal tester (Della Bona and van Noort 1995).

2.8.5.2 Shear bond strength

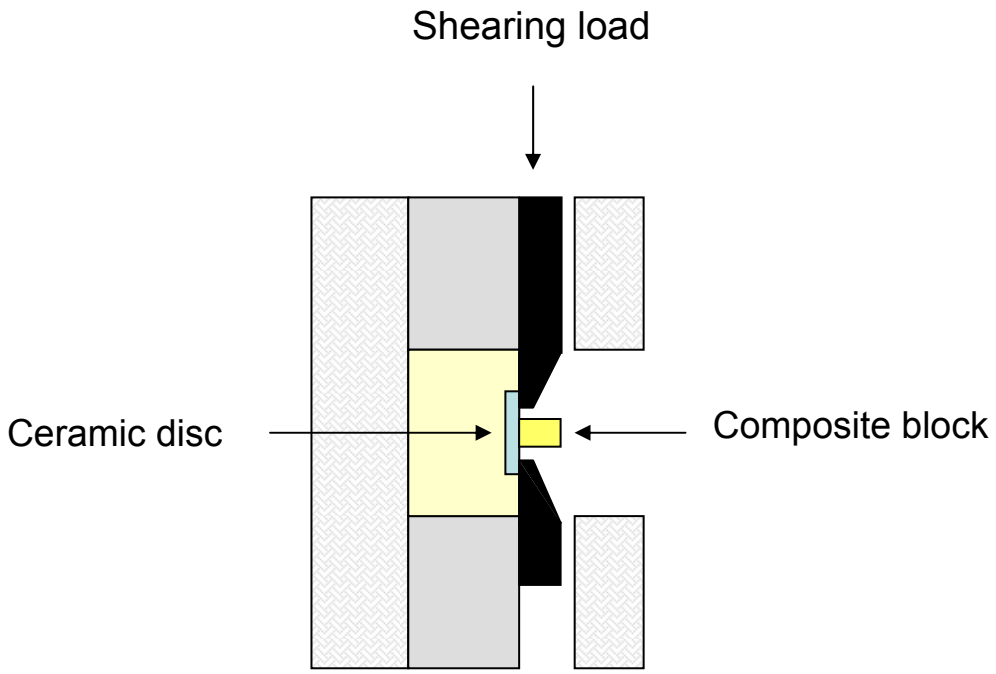

Figure 2.8. Assembly used for determination of shear test

To prepare shear bond test, the ceramic disc was embedded in epoxy resin. The composite cylinder was built and then the preparation sample was placed into the testing rig as illustrated in the diagram (Figure 2.8). For tests performed using a pure shear force, the shear stress t is computed according to equation 2.6.

$$t = \frac{F}{A} \qquad 2.6$$

Where F is the force imposed parallel to the upper and lower faces each of which has an area A. The unit for shear stress is the same as for their tensile counterparts.

Della Bona and van Noort (1995) found that the tensile bond strength test was more appropriate for evaluating the adhesive capabilities of resin composites to ceramics than the shear bond strength test (Della Bona and van Noort 1995). They identified that various sample configurations of shear bond strength test provided a difference in shear bond strength values even though geometric design and adhesive interface were identical. Their results showed that a ceramic base, bonded to a composite cylinder had lower shear bond strength (10.37± 1.99 MPa) compared to a composite base bonded to a ceramic cylinder (18.02± 2.52 MPa) (Della Bona and van Noort 1995). In addition, they reported that the shear bond strength test did not actually identify the quality of the adhesive bond because the failure mode occurred predominantly at the base materials (Della Bona and van Noort 1995). However, some recent studies still use shear bond strength tests (Chen *et al.* 1998; Lüthy *et al.* 2006; Özcan and Vallittu 2003; Atsu *et al.* 2006; Kukiattrakoon and Thammasitboon 2007) because stronger ceramic material bases were used and the failure mode did not usually occur in the base materials.

Long-term water storage and thermal cycling are the conditions that are most often used to test the durability of resin bonds. The bond strength of cements after thermocycling was lower than before thermocycling (Lüthy *et al.* 2006; Kern and Wegner 1998); however, some cements such as Pavania F and Pavania 21 were found to have the higher bond strength value after thermocycling (Lüthy *et al.* 2006). In contrast, Brentel *et al* (2007) reported that thermocycling and long term water

storage did not affect the microtensile bond strength of resin cement to feldspathic ceramic. However, the type of etching agent and silanisation were the factors that influenced the bond strength. Panavia F was used for their test, which would affect the bond strength result after thermocycling. Kern and Wegner (1998) studied the bonding durability to zirconia ceramics using different adhesive methods such as sandblasting (with BisGMA), silica coating (with BisGMA), phosphate monomer resin composite (Panavia F and 21) and polyacid-modified resin composite (Dyract Cem). They found that long-term storage (150 days) with thermocycling reduced the bond strength of cements compared with short storage (3 days) without thermocycling. However, only the bond strength of Panavia F and 21 groups was not significantly reduced after thermocycling (Kern and Wegner 1998).

2.8.6 Phase transformation study

The stress-induced phase transformation and phase configurations can be analysed using X-ray diffraction analysis (XRD) or Raman spectroscopy; however, XRD tends to be used for large area surface analysis. Raman microspectroscopy, however, has the ability to analyse very small and specific areas on a sample surface without any sample preparation (Kailer *et al.* 1999) and it can detect the phases present (Casellas *et al.* 2001). Hardness indentation is the common method that has been used to induce phase transformation as, during loading, the material is subjected to highly localised stresses. The stresses not only cause crack formation by dislocation gliding, but a complete change of the crystal structure and formation of amorphous phases (Kailer *et al.* 1999).

Raman spectroscopy combined with hardness indentation testing has been used in some studies (Casellas *et al.* 2001; Colomban and Havel 2002; Kailer *et al.* 1999; Behrens *et al.* 1993) in order to examine pressure-induced phase transformations. Behrens *et al* (1993) (Behrens *et al.*, 1993) examined the *t→m* transformation of Y-TZP around and below the indent using a force of 500 N of Vickers indentation, which was annealed at different temperatures (400 to 1300 K). They found that various annealing temperatures affected the monoclinic fraction. Annealing up to 500 K increased the size of the transformation zone and the amount of monoclinic phase within the zone. Annealing above 600 K caused a gradual decrease in the monoclinic content. In addition, they found the monoclinic content was highest at the edge of indentation and slightly lower in the core, which was the compressed zone. They suggested that the *t→m* transformation is more easily induced by tensile and shear stresses than by the compressive stresses in the core (Behrens *et al.* 2004). Reese *et al* (1992) also proposed that the highest transformation occurred near the indent edge of Ce-TZP material; however, the highest monoclinic fraction was found at the centre of YTZP ceramics and showed a linear decrease in phase transformation with distance from the centre of indentation. However, these studies did not investigate the effect of loads and the distance to the transformation toughening of Y-TZP ceramic within and around the indentation.

Transformation on the fracture surface was previously observed by Ruiz and Readey using XRD (Ruiz and Readey 1996). Details on which areas had high monoclinic content, however, were not determined in their work. Leach (Leach 1989) examined the transformation of 9 mol% MgO-PSZ specimens after fracture in three-point bending using a Raman microprobe. He reported that monoclinic content was

greatest on the tension side. There was a steady decrease in monoclinic zirconia content, and then it increased again at the compression face.

2.9 Aims and Objectives

This project focused on the mechanical properties and phase transformation of yttria partially stabilised tetragonal zirconia (Y-TZP) specimens, and was divided into two main parts: commercial zirconia and experimental titanium phosphate glass zirconia ceramics. The mechanical properties considered included biaxial flexural strength, hardness, fatigue and subcritical crack growth. Although the biaxial flexural strength and hardness of Y-TZP ceramics have been examined in recent studies (Curtis *et al.* 2005; Guazzato *et al.* 2005a; Kosmac *et al.* 2000), the fatigue and subcritical crack growth behaviour of Y-TZP dental ceramics have not been widely investigated, especially when following ISO or British Standards. Additionally, the comparison of the properties of zirconia ceramics from different systems has not been reported.

The sensitivity of ceramics to slow crack growth is one of their major limitations (Benaqqa *et al.*, 2005). Cyclic loading from mastication could cause subcritical crack growth in dental restorations and the strength will decrease with increasing service time. Higher subcritical crack growth resistance of ceramics leads to slower strength degradation and higher remaining strength for the lifetime of the dental ceramic (Reese and Cox 1992). Therefore, besides biaxial flexural strength and reliability, fatigue and subcritical crack growth resistance are important parameters to consider for designing reliable dental restorations.

Phase transformation is a unique characteristic of zirconia ceramics and this phenomenon will be investigated in this study. The bulk phase compositions of the specimen can be analysed by X-ray diffraction (XRD) while a localised stress-induced phase transformation will be analysed using Raman spectroscopy. Although the pressure-induced phase transformations have been examined in some studies (Casellas *et al.* 2001; Colomban and Havel 2002; Kailer *et al.* 1999; Behrens *et al.* 1993) using Raman spectroscopy combined with hardness indentation testing, the effect of loads and the distance to the transformation toughening of Y-TZP ceramic within and around the indentation has not been investigated.

Phosphate based glasses will be investigated in this study as a sintering aid. The potential benefits may be a material with good strength that sinters at much lower temperatures than zirconia alone and also the glass will allow the zirconia to be more susceptible to etching prior to cementation, thus increasing its potential bond strength. There is a requirement to ensure that the glass has very low solubility and this will be achieved by the addition of titanium dioxide to the glass. This is an interesting route to pursue and may not achieve significant improvements, but it may give an insight into how phosphate glasses react with zirconia.

2.9.1 Aims

The aim of the present study was to evaluate and compare the properties and phase configurations of three commercially available high strength zirconia cores (Lava™, Cercon®, Invizion™) and experimental non-glass and titanium phosphate glass zirconia ceramics. The transformation toughening of the commercial zirconia ceramics in and around a hardness indent, induced by various loaded indentations

was studied using Raman microspectroscopy. The aim was to assess how the relative amounts of tetragonal, cubic and monoclinic phases varied within the indented areas and upon application of different loads.

2.9.2 Objectives

The objectives of the project were as follows:

1. Biaxial flexural strength and Weibull analysis of three commercial zirconia systems (Lava™, Cercon® and Invizion™) were studied in order to compare the strength and reliability between groups. The comparison of these properties with an experimental non-glass zirconia and zirconia containing titanium phosphate glass were also performed. The fracture surfaces of specimens after testing were analysed using scanning electron microscope (SEM) in order to study the fracture pattern and defects at the fracture origin.
2. Hardness study was performed on polished and as-received surfaces of the specimens using Vickers Hardness indentation with 1.5 Kg applied load in order to compare the hardness values between polished and as-received surfaces among groups.
3. A fatigue study (a classical stress-number curve generation method) of three commercial zirconia systems was performed at 37°C distilled water and the cycle limit was set at 500,000 in order to investigate the survival strength and compare the values between the three groups. The fracture surfaces of specimens after testing were analysed using SEM in order to study the fracture pattern and defects at the fracture origin.

4. Subcritical crack growth was investigated in order to find the subcritical crack growth parameter using different loading rates ($N.s^{-1}$). The fracture surfaces of specimens after testing were analysed using SEM in order to study the fracture pattern and defects at the fracture origin.
5. Phases for the commercial and experimental zirconia specimens were analysed using X-ray diffraction (XRD). Polished and unpolished surfaces of specimens were analysed to compare phase transformations.
6. Stress induced phase transformation of three commercial zirconia systems was investigated using Raman spectroscopy. Vickers indentation was performed by using different loads (20-50 kg) in order to study the effect of the applied load to the phase transformation and the distance from the centre of the indentation was also examined on the phase change. In addition, the phase transformation on the fractured surfaces of specimens after biaxial flexural and subcritical crack growth tests was investigated.
7. Shear bond strength and bonding failure of experimental non-glass and titanium phosphate glass zirconia ceramics were investigated in order to identify whether the glass contents affected the shear bond strength. The pilot study of biaxial flexural strength of titanium phosphate glass zirconia ceramics sintered at different temperatures was also performed to examine the effect of percentage of glass on the sintering temperature.
8. Phase transformation of non-glass zirconia and zirconia containing titanium phosphate glass was analysed using XRD in order to study the difference in the phases between groups.

2.9.3 Hypothesis

The hypotheses of this project were as follows:

1. There is no difference in the properties between three commercial zirconia systems and between experimental non-glass and titanium phosphate glass zirconia ceramics. In addition, there is no difference of these properties between coloured and uncoloured Y-TZP ceramic.
2. Phase transformation is not influenced by the level of load applied and the distance from the centre of the indentation.

CHAPTER 3

Analytical techniques

Some of the main analytical techniques used to elucidate information and characterise the specimens including Raman spectroscopy, X-ray diffraction analysis (XRD) and atomic force microscopy (AFM), will be described in this chapter.

3.1 Raman Spectroscopy

Raman spectroscopy is a useful technique for the identification of a wide range of substances - solids, liquids, and gases. It is a non-destructive technique requiring no sample preparation. Raman spectroscopy is a light scattering technique, and can be thought of in its simplest form as a process where a photon of light interacts with a sample to produce scattered radiation of different wavelengths and using a spectrometer to examine light scattered by the sample. Raman bands arise from a change in the polarisation (Horiba Jobin Yvon 2008).

3.1.1 Raman scattering

When a beam of light is incident upon a sample, photons are absorbed by the material and scattered. The vast majority of these scattered photons have exactly the same wavelength as the incident photons and are known as Rayleigh scatter, but a tiny portion (approximately 1 in 10^7) of the scattered radiation is shifted to a different wavelength. These wavelength-shifted photons are called Raman scatter. Most of the Raman scattered photons are shifted to longer wavelengths (Stokes shift), but a small portion are shifted to shorter wavelengths (anti-Stokes shift). Figure 3.1 shows a diagram of Rayleigh scattering, Stokes Raman scattering, and anti-Stokes Raman scattering. In each case, the incident

photon excites an electron into a higher virtual energy level (or virtual state) and then the electron decays back to a lower level, emitting a scattered photon.

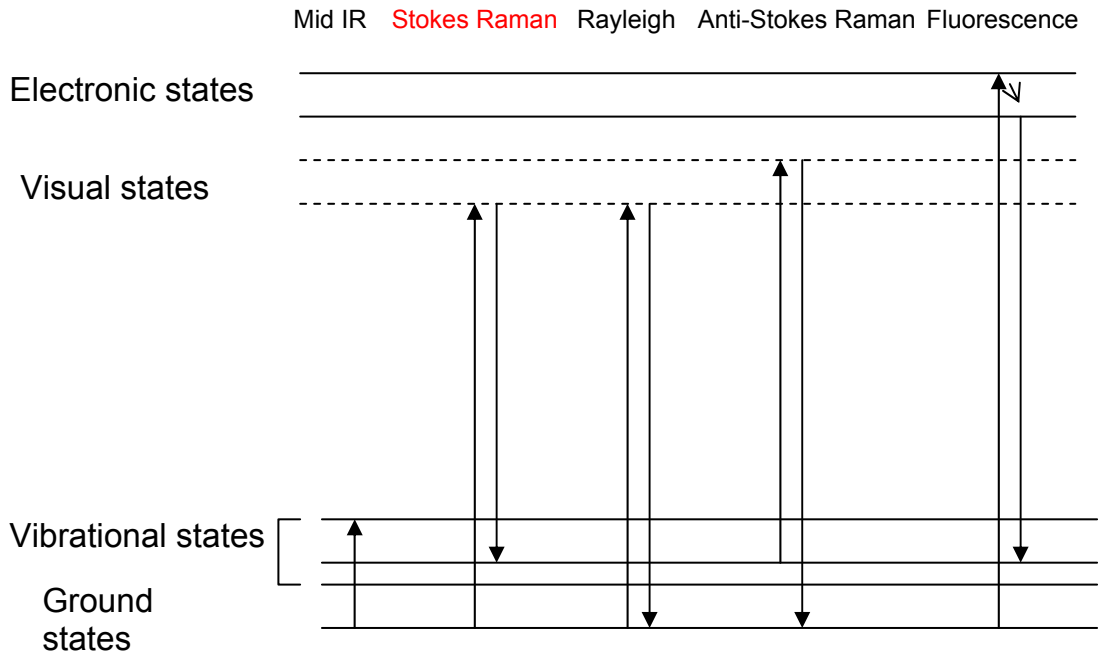

Figure 3.1. Energy level diagram showing the states involved in Raman signal. The line thickness is roughly proportional to the signal strength from the different transitions.

In Rayleigh scattering, the electron decays back to the same level from which it started. In both types of Raman scattering the electron decays to a different level than that where it started. Stokes Raman scattering occurs when the final energy level is higher than the initial level, while anti-Stokes Raman scattering occurs when the final energy level is lower than the starting level. Stokes scattering is much more common than anti-Stokes scattering because at any given time an electron in the most common temperature range is most likely to be in its

lowest energy state, in accordance with the Boltzmann distribution. Only Stokes Raman scattering is commonly used in spectroscopy.

Raman is a form of vibrational spectroscopy. This means that these energy transitions arise from molecular vibrations. Because these vibrations involve identifiable functional groups, when the energies of these transitions are plotted as a spectrum, they can be used to identify the molecule.

3.1.2 The Raman Spectrum

A Raman spectrum is a plot of the intensity of Raman scattered radiation as a function of its frequency difference from the incident radiation (usually in units of wavenumbers, cm^{-1}). This difference is called the *Raman shift*. Because it is a difference value, the Raman shift is independent of the frequency of the incident radiation. Typically, only the Stokes region is used (the anti-Stokes spectrum is identical in pattern, but much less intense). Figure 3.2 present an example of the Raman spectra of three different areas of indent surface of zirconia specimen plotted on the same set of axes. Green coloured spectrum presented the phases at the centre of the indentation. Blue spectrum presented the phases at the edge of the indentation and the red spectrum identified the phases outside indentation area. Each spectrum has a characteristic set of peaks that allows it to be distinguished from others.

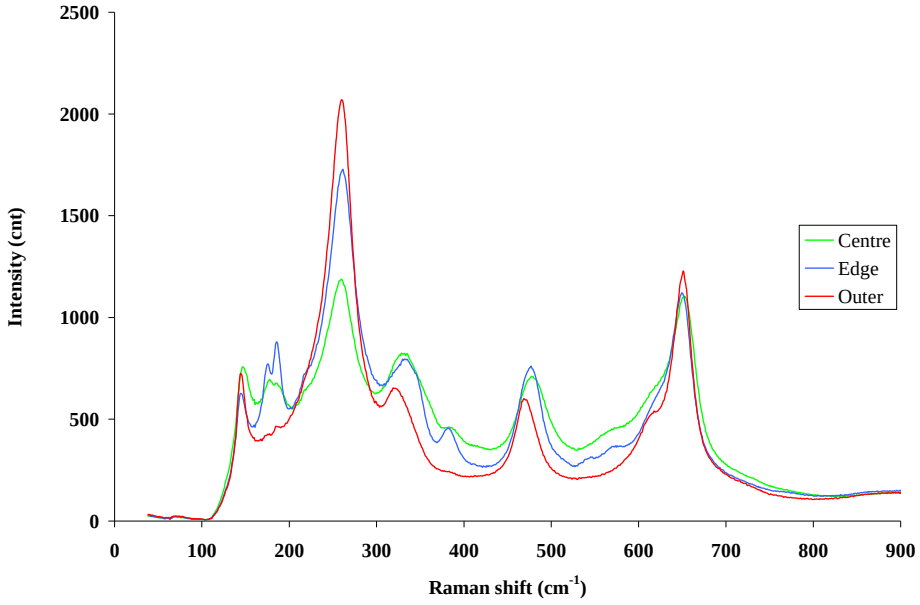

Figure 3.2. Example Raman spectra (from the 50kg loaded specimen) at the centre (green), edge (blue) and outer (red) regions of an indentation.

3.1.3 Raman Instrumentation

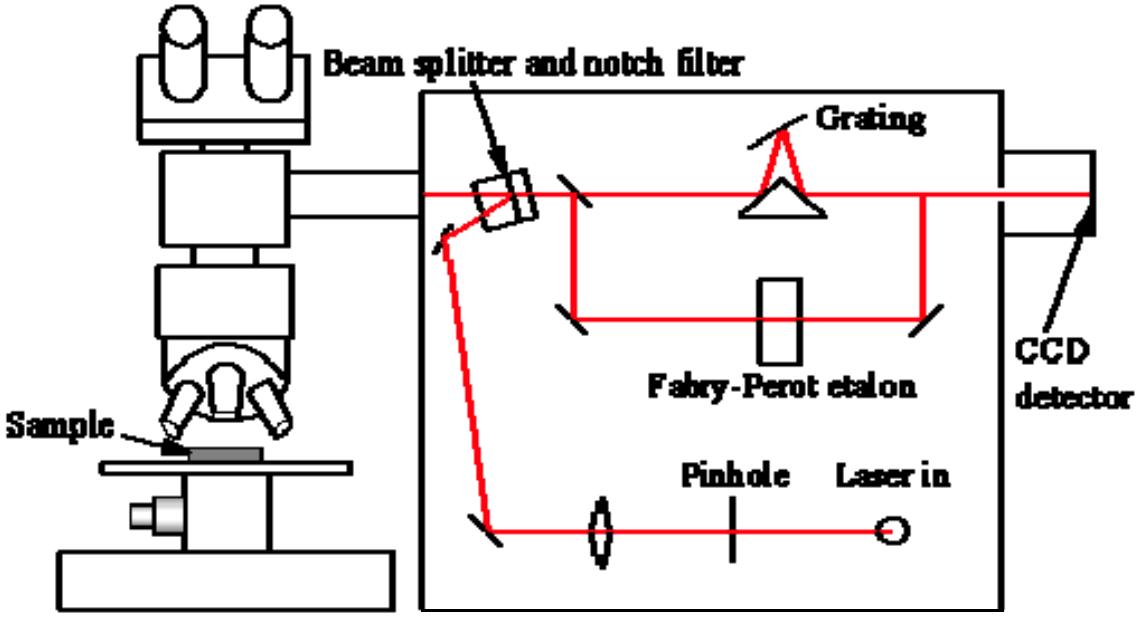

Figure 3.3. Schematic diagram of a Raman spectrometer.

In modern Raman spectrometers (Figure 3.3), lasers are used as a photon source due to their highly monochromatic nature, and high beam fluxes. This is necessary as the Raman effect is weak, typically the Stokes lines are ~10^5 times weaker than the Rayleigh scattered component. In the visible spectral range, Raman spectrometers use notch filters to cut out the signal from a very narrow range centred on the frequency corresponding to the laser radiation. Most Raman spectrometers for material characterisation use a microscope to focus the laser beam to a small spot (<1-100μm diameter). Light from the sample passes back through the microscope optics to reach the spectrometer. Raman shifted radiation is detected with a charge-coupled device (CCD) detector and a computer is used for data acquisition and curve fitting. This data is eventually plotted as the Raman

spectrum. These factors have helped Raman spectroscopy to become a very sensitive and accurate technique.

3.1.4 Application of Raman Spectroscopy

Raman spectroscopy is being successfully applied to the analysis of a wide-ranging number of materials and systems. In zirconia analysis, Raman spectroscopy combined with Vickers hardness indentation is useful method to study phase transformation of the zirconia ceramic. It can distinguish the three phases (tetragonal, cubic and monoclinic) on the different surface areas of the zirconia. In addition, the difference of three phases of the zirconia before and after sintering can be examined.

3.2 XRD Analysis

X-ray diffraction (XRD) is a versatile, non-destructive technique that reveals detailed information about the chemical composition and crystallographic structure of natural and manufactured materials. It can be used not only to determine the separations of layers of atoms but also to determine the locations of the atoms.

3.2.1 Crystal lattice

A crystal lattice is a regular three-dimensional distribution (cubic, rhombic, tetragonal etc.) of atoms in space (Figure 3.4). These are arranged so that they form a series of parallel planes separated from one another by a distance, which

varies according to the nature of the material. For any crystal, planes exist in a number of different orientations - each with its own specific spacing.

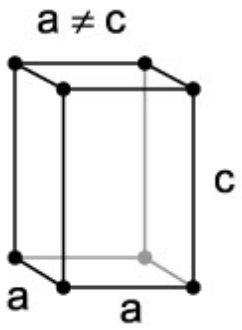

Figure 3.4. Example of one crystal form called tetragonal structure

3.2.2 Bragg's law and basic geometry of x-ray diffraction

X-rays are electromagnetic radiation similar to light, but with a much shorter wavelength. They are produced when electrically charged particles of sufficient energy are decelerated. In an X-ray tube, the high voltage maintained across the electrodes draws electrons toward a metal target (the anode). X-rays are produced at the point of impact, and radiate in all directions. Tubes with copper targets, that produce their strongest characteristic radiation ($K_{\alpha 1}$) at a wavelength of about 1.5 angstroms, are commonly used for geological applications (Coastal and marine Geology program 2001).

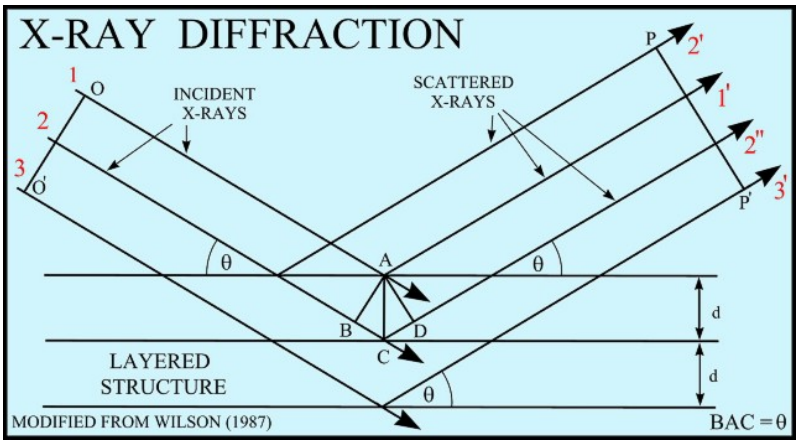

Figure 3.5. The proof of Bragg's law

If an incident X-ray beam encounters a crystal lattice, general scattering occurs. Although most scattering interferes with itself and is eliminated (destructive interference), diffraction occurs when scattering in a certain direction is in phase with scattered rays from other atomic planes. Under this condition the reflections combine to form new enhanced wave fronts that mutually reinforce each other (constructive interference). The relation by which diffraction occurs is known as the Bragg's law or equation. Because each crystalline material has a characteristic atomic structure, it will diffract x-rays in a unique characteristic pattern. The Bragg's law equation is given as follow (equation 3.1);

$$2d(\sin\theta) = \lambda_0 \qquad 3.1$$

Where:

d=lattice interplanar spacing of the crystal

ɵ = x-ray incidence angle (Bragg angle)

λ =wavelength of the characteristic x-rays

The basic geometry of an x-ray diffractometer involves a source of monochromatic radiation and an X-ray detector situated on the circumference of a graduated circle centred on the powder specimen. Divergent slits, located between the X-ray source and the specimen, and divergent slits, located between the specimen and the detector, limit scattered (non-diffracted) radiation, reduce background noise, and collimate the radiation. The detector and specimen holder are mechanically coupled with a goniometer so that a rotation of the detector through 2x degrees occurs in conjunction with the rotation of the specimen through x degrees, a fixed 2:1 ratio (Coastal and marine Geology program 2001).

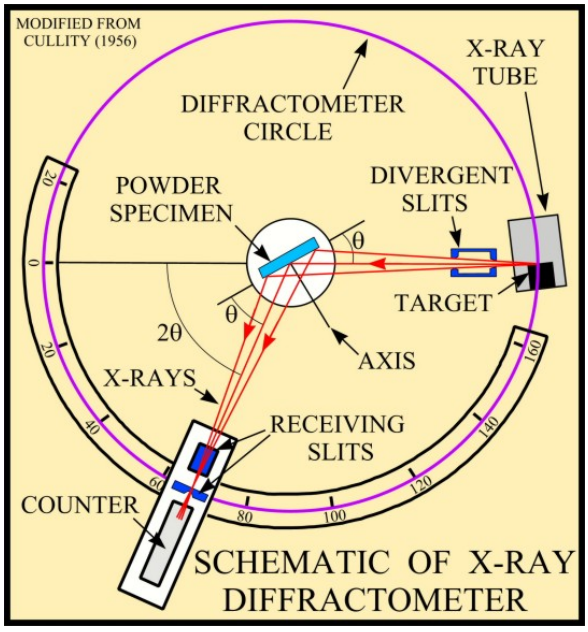

Figure 3.6. Schematic of x-ray diffractometer

3.3 Atomic force microscopy

The atomic force microscope (AFM) or scanning force microscope (SFM) is a very high-resolution type of scanning probe microscope, with demonstrates resolution of fractions of a nanometre, more than 1000 times better than the optical diffraction limit. Bining, Quate and Gerber invented the first AFM in 1986 (Binnig and Quate 1986). AFM consists of a microscale cantilever with a sharp tip (probe) at its end that is used to scan the specimen surface. The cantilever is typically silicon or silicon nitride with a tip radius of curvature on the order of nanometres. AFM images are obtained by measurement of the force on a sharp tip created by the proximity to the surface of the sample (Binnig and Quate 1986). This force is kept small and at a constant level with a feedback mechanism. Depending in the situation, forces that are measured in AFM include mechanical contact force, Van der Waal forces, capillary forces, chemical bonding, and electrostatic forces. To prevent the cantilever tip from damaging the surface of the sample, it is maintained at a constant angular deflection so that the force applied by the tip on the surface is also kept constant. This is achieved using a feedback mechanism that adjusts the distance between the tip and the surface to keep the applied force constant. Applied forces between the tip and the sample typically range from 10^{-11} to 10^{-7} N. By monitoring the motion of the probe as it is scanned across the surface, a three dimensional image of the surface is constructed.

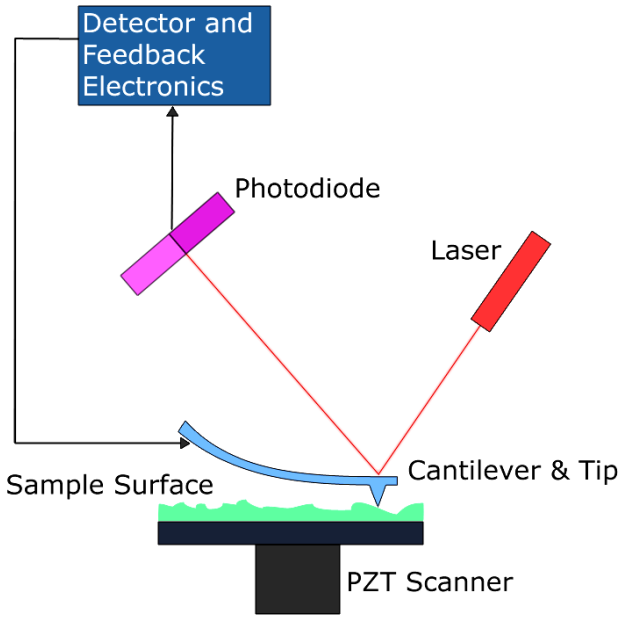

Figure 3.7. A schematic diagram of AFM

When scanning a sample with an AFM, a constant force is applied to the surface by the probe at the end of a cantilever. Measuring the force with the cantilever in the AFM is achieved by two methods. In the first method, the deflection of the cantilever is directly measured. In the second method, the cantilever is vibrated and changes in the vibration properties are measured.

3.3.1 Deflection mode (or contact mode)

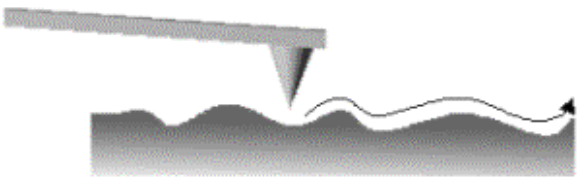

Figure 3.8. Contact mode

Using the feedback control in the AFM, it is possible to scan a sample with a fixed cantilever deflection. Because the deflection of the cantilever is directly proportional to the force on the surface, a constant force is applied to the surface during a scan (Figure 3.8). This scanning mode is often called "contact" mode. However, because the forces of the probe on the surface are often less than a nano-newton, the probe minimally touches the surface.

3.3.2 Vibrating Mode (or non-contact mode)

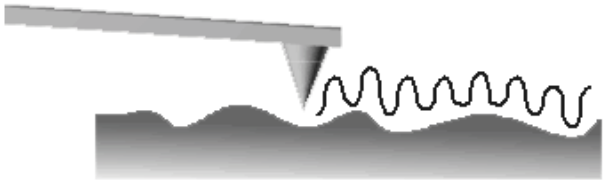

Figure 3.9. Non-contact mode

The cantilever in an AFM can be vibrated using a piezoelectric ceramic. When the vibrating cantilever comes close to a surface, the amplitude and phase of the vibrating cantilever may change (Figure 3.9). Changes in the vibration amplitude or phase are easily measured and the changes can be related to the force on the surface. This technique has many names including non-contact mode, and intermittent contact mode. It is important that the tip not "tap" the surface because the probe may be broken or the sample may be damaged.

CHAPTER 4

Materials and Methods

4.1 Overview of materials and methods

Yttria (3 mol%) partially stabilised zirconia polycrystal (3Y-TZP) ceramics used in this study were divided into 2 major groups; commercial 3Y-TZP and 3Y-TZP containing titanium phosphate glass ceramics. For the commercial 3Y-TZP, three systems (Lava™, Cercon®, and Invizion™) were investigated using the same tests (Figure 4.1). However, limited specimens were available for Cercon® and Invizion™ systems; and the subcritical crack growth test was performed on Lava™ specimens only. Additionally, Kavo Everest® zirconia samples were only subjected to a crown-shaped fatigue test and were not used for other tests. Strength and bonding properties were evaluated for Titanium phosphate glass contained within zirconia.

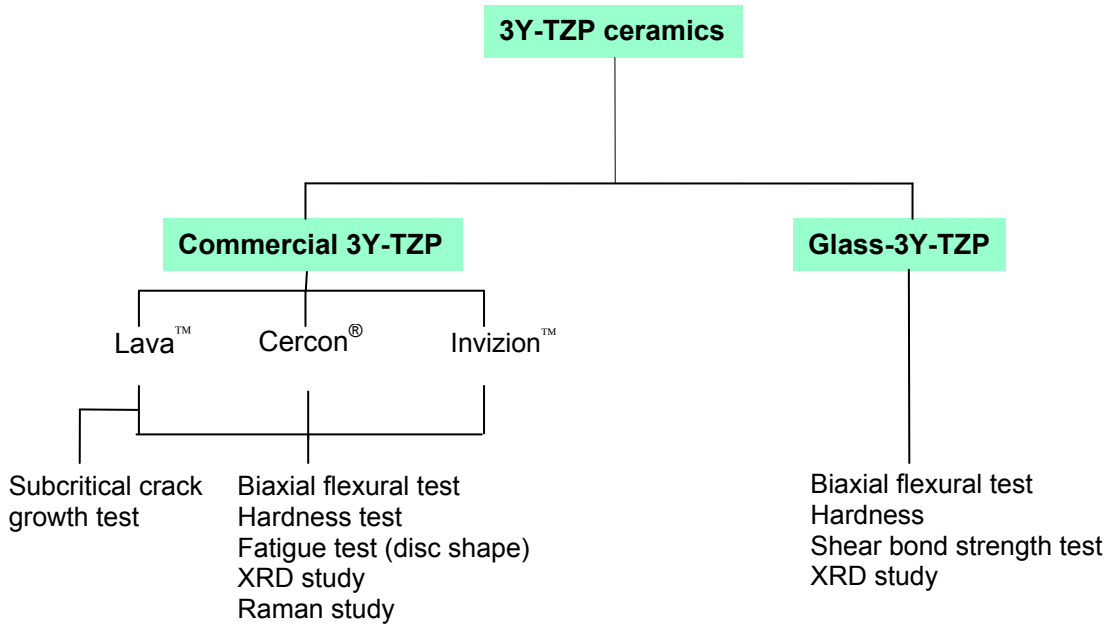

* Kavo Everest®: crown shaped fatigue test

Figure 4.1. Main diagram of experiments on zirconia specimens

4.2 Commercial 3Y-TZP

Standardised Lava™ discs (15x 1.3 mm) (3M ESPE, Seefeld, Germany), Cercon® discs (15x 1.25 mm) (Dentsply, Germany), and Invizion™ discs (VITA In-Ceram 2000 YZ CUBES) (Panadent Ltd, Kent, UK) (14.95x 1.25 mm) were provided by the manufacturers according to the ISO 6872 standard (ISO 6872 1995). The standard described that a test piece should have a thickness of 1.2 ± 0.2 mm and a diameter of 12 mm to 16 mm. For the Lava™ specimens, the final sintering temperature was 1500°C and specimens had been ground with 10 μm diamond paper on both sides by the manufacturer. The final sintering temperature of Cercon® and Invizion™ were 1350°C and 1530°C, respectively. To standardise specimens, all specimens were fine ground and polished on the side exposed to the tension in order to eliminate flaws and defects on the surface.

4.2.1 Specimen preparation

Lava™ specimens were divided into eight groups according to shade: uncoloured and FS1-FS7 (the colour was related to Vita shade A1-D4) (Figure 4.2). Cercon® and Invizion™ (VITA In-Ceram 2000 YZ CUBES) specimens only one shade (uncoloured). Firstly, a pilot study was performed in order to establish a protocol for grinding and polishing and the Proscan 1000 (Scantron Industrial Products Ltd, Taunton, England) was used to measure the surface roughness. The results were recorded every 1 minute after polishing with DP-suspension (Struers, UK) containing polycrystalline diamond of 9 μm size until the specimen surfaces had similar roughness values, and there were no scratches with direct vision. After the pilot study, all specimens were prepared in sequence, first by grinding with 1000 grit

silicon carbide papers (Struers, UK) for 10 minutes, then polishing with DP-suspension (Struers, UK) containing polycrystalline diamond of 9 μm size for 20 minutes and finally polycrystalline diamond of 3 μm size for 10 minutes. All grinding and polishing used one of two Struers RotoPol-11 machines (Struers, UK) at a speed of 150 rpm and a force of 30 N. The Cercon® group was ground with 300, 500 and 800 grit silicon carbide papers (Struers, UK) to eliminate the manufacturing surface defects; followed by the above polishing sequence. All grinding and polishing also used one of two Struers RotoPol-11 machines (Struers, UK). Following grinding and polishing, the diameter and thickness (mm) of each specimen was measured three times at several places on the specimens using a micrometer (Moore&Wright, UK) before testing.

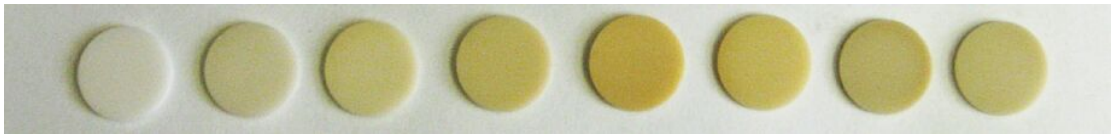

Figure 4.2. Uncoloured and FS1-FS7 shaded discs of Lava™ system

4.2.2 Density measurement

Density measurements were performed on each sintered specimen using the Archimedes principle. The measurements were carried out in distilled water on a Mettler Toledo AG204 balance and associated density kit (Figure 4.3) (Wembley, UK). For the commercial YTZP, twenty five uncoloured Lava™ specimens were selected for testing in order to compare its density with that of zirconia containing titanium phosphate glass. The mass (g) of each specimen was measured three

times in air and water. The means of these air and water masses (g) were used as actual and suspended weights, respectively, and the density was calculated using the equation 4.1.

$$\rho = \frac{actual\ weight}{(actual - suspended)} \times \rho_w \qquad 4.1$$

Where ρ is the density of a sample (g/cm^3) and ρ_w is the density of water (g/cm^3). Temperature in water ($^\circ$C) was recorded and ρ_w obtained from the chart.

Figure 4.3. Density kit

4.2.3 Biaxial flexural strength (BFS) test

Thirty specimens of each group (except Invizion™, which had 15 specimens) were subjected to a biaxial flexural strength test according to ISO 6872 standard. A Dartec HC10 servohydraulic testing frame (Zwick Ltd., UK) and 10 kN load cell (R.D.P. Electronics Ltd, UK) were used and operated by Workshop 96 software program (9600 series). The rig and loading pin for the test were made by Rotary Engineering (Reading, UK) according to the ISO 6872 specifications. Three hardened steel balls on the rig with a ball diameter of 3 mm, positioned at 120° angles giving a support circle with a diameter of 11 mm (Figure 4.4) were used to support the specimens. The loading pin had a length of 2 mm and a diameter of 1.5 mm. When mounting the rig on to the Dartec frame, the lower support rig and loading pin were fixed and checked for axial alignment using a steel sleeve.

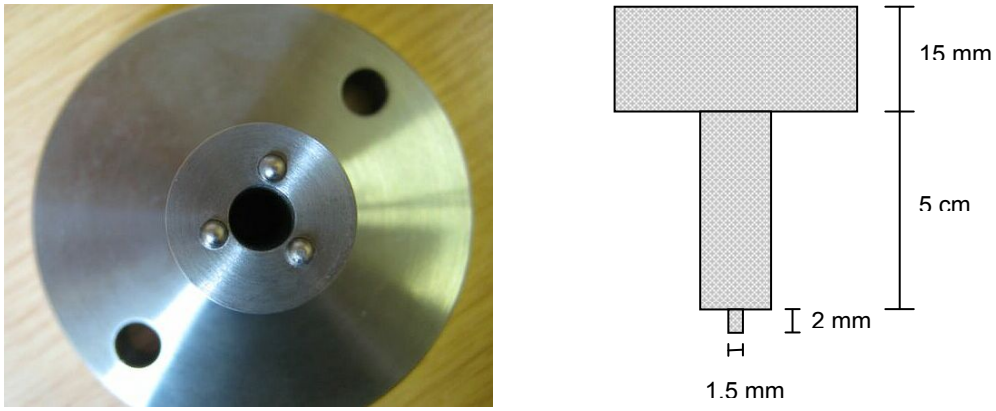

Figure 4.4. Three hardened steel balls of the support ring (left) and the loading pin (right)

The test was performed in a custom-made chamber filled with distilled water and the temperature was controlled at 37°C by a custom-made tank. Water from the chamber flowed into a reservoir tank which in turn heated and circulated warm water back into the test chamber. Water circulation was continuous throughout the experiment in order to maintain the temperature at 37°C (±1°C). The polished surface of each specimen was placed centrally on the three balls, with the polished surface face down, i.e. the tension side and the as-received surface was uppermost and loaded with a flat pin (Figure 4.5) at a cross head speed of 1 $mm.min^{-1}$ until failure occurred. Load to failure (N) of each specimen was recorded from a graph using Data manager 96 program. The biaxial flexural strength (MPa) was calculated using the following equation 4.2-4.4 according to the ISO 6872 standard (ISO 6872 1995).

$$S = -0.2387\ P(X-Y)/d^2 \qquad 4.2$$

Where S is the maximum tensile stress in Pascals, P is the total load causing fracture in Newtons, and d is the specimen thickness at fracture origin in millimetres. X and Y were determined as follows:

$$X = (1+\nu)\ln(r_2/r_3)^2 + [(1-\nu)/2](r_2/r_3) \qquad 4.3$$

$$Y = (1+\nu)[1+\ln(r_2/r_3)^2] + (1-\nu)(r_1/r_3)^2 \qquad 4.4$$

in which

v is Poisson's ratio. If the value for the ceramic concerned is not known, a Poisson's ratio = 0.25 is used (this is an average value for ceramics according to the standard ISO 6872);

r_1 is the radius of support circle, in millimetres;

r_2 is the radius of loaded area, in millimetres;

r_3 is the radius of specimen, in millimetres;

d is the specimen thickness at fracture origin, in millimetres.

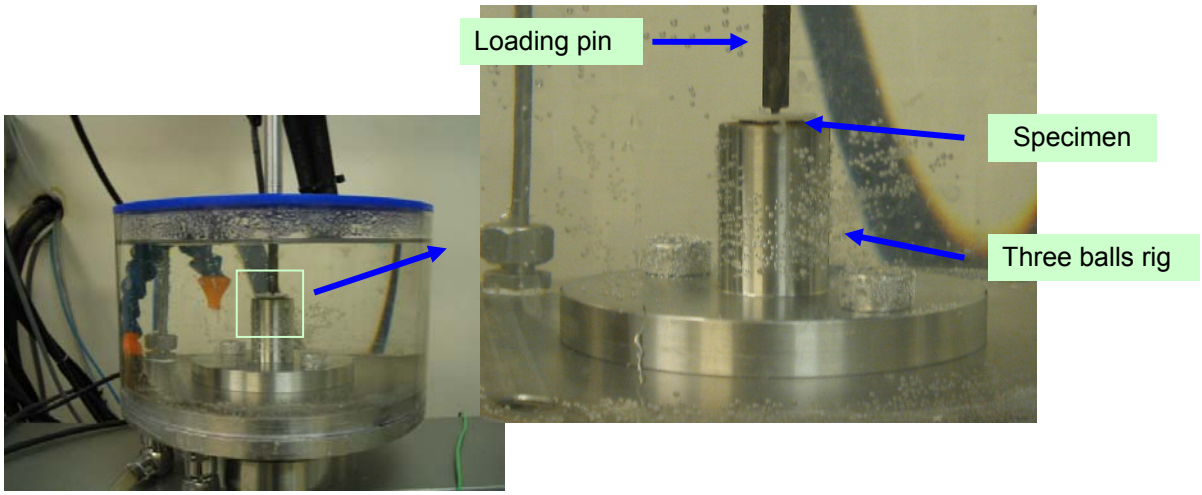

Figure 4.5. Biaxial flexural strength test

4.2.4 Weibull analysis

Weibull analysis is used to identify the reliability and probability of fracture of brittle materials. It includes plotting the data, interpreting the plot, and failure forecasting and prediction (Abernethy 2006). The horizontal scale is the age to failure (number of cycles) or stress to failure (MPa) and the vertical scale is the

cumulative distribution function (CDF) or probability of failure, describing the percentage that will fail at any age (Abernethy 2006). The complement of the CDF scale (100-CDF) is the reliability. The characteristic life or characteristic strength (σ_0) represents the 63.2 percentile of the strength distribution, which defines the age at which 63.2% of the units will have failed (Bona *et al.*, 2003).

Another significant term related to Weibull analysis is the Weibull modulus (*m*). Weibull modulus (*m*) is the slope of the Weibull plot that is used to describe the variation in the strength or asymmetric strength distribution as a result of flaws and microcracks which may develop within the microstructure (Ritter 1995). It also indicates which class of failures is present (Abernethy 2006):

- $m < 1.0$ indicates early mortality
- $m = 1$ indicates random failures (independent of age)
- $1.0 < m \leq 4.0$ implies early wear out
- $m > 4.0$ implies old age failure or rapid wear out

The lower the value of the Weibull modulus, the more flaws and defects in the material, and hence decreased reliability. Conversely, the higher the value of the Weibull, a smaller an error range, and thus the greater the structural reliability (Ritter 1995). Most ceramics are reported to have '*m*' values in the range of 5-15, whereas metals, which produce ductile failures, have '*m*' values in the range of 30-100 (Johnson 1983).

The biaxial flexural strength data was analysed statistically with the Weibull distribution using the WinSMITH™ Weibull 0.2M software program. Thirty specimens from each group (with the exception of the InVizion™ group that had only 15

specimens) were tested. The following equation 4.5 was used to calculate the Weibull modulus (Weibull 1951).

$$P_{f(\sigma c)} = 1\text{-}\exp\left[-(\sigma_c/\sigma_0)^m\right] \quad 4.5$$

Where $P_{F(\sigma c)}$ is the probability of failure, σ_c is the fracture strength, σ_0 is the characteristic strength ($P_{F(\sigma c)}$= 63.2%) and *m* is the Weibull modulus. Computer software was used to rank the mean biaxial flexural strength data in ascending order and to assign a rank over the range 1 to N, where N is the number of specimens. The probability of failure for each specimen was next calculated using the formula:

$$P_f = \frac{RANK}{(N+1)} \quad 4.6$$

The formula 4.5 in was re-arranged as follows:

$$1/(1\text{-}Pf) = 1/\exp[-(\sigma_c/\sigma_0)^m] \quad 4.7$$

Taking integral logs:

$$\ln[1/(1\text{-}Pf)]=(\sigma_c/\sigma_0)^m \quad 4.8$$

$$\ln\ln[1/(1\text{-}P_f)]=m\ln\sigma_c\text{-}m\ln\sigma_0 \quad 4.9$$

Therefore, plotting $\ln\ln[1/(1\text{-}P_f)]$ against ln σ provided a slope with the value *m* (the Weibull modulus) and an intercept $m\ln\sigma_0$. The software calculated the equations, plotted the graph and produced the results.

4.2.5 Vickers Hardness Test

This test was performed in order to examine whether the polishing process affected the surface hardness of the zirconia discs under test. Five pieces of fractured specimens of Lava™ from the uncoloured, FS4 and FS7 groups and uncoloured Cercon® and InVizion™ groups from the biaxial flexural testing were randomly selected to measure Vickers hardness using an indentation tester (Vickers-Armstrong Engineering Ltd, Kent, UK). A pilot study was carried out to find a suitable load that created a large enough indent to be visualised but without creating cracks at the corners of the indent. After the pilot study, a 1.5 kg load was selected. The specimen was placed on a flat metal plate and five indentations were placed randomly using a square-based pyramid diamond indenter on both the polished and unpolished sides within the same specimen using a loading mass of 1.5 kg. The indentation diagonal lengths (mm) were measured using Image-Pro® Plus (version 4.0) software with an optical microscope (x25) (Ceti, UK). The hardness was calculated from the following equation 4.10 using the BSI ENV 843-4:1995 standard (BSI ENV 843-4 1995) (supersede BS EN 843-3:2005).

$$HVF = 1.8544\ F/d^2 \qquad 4.10$$

Where HVF is the Vickers hardness number at an applied force F (expressed as the mass in Kg from which F is derived), and where d is the mean length of the diagonals of the indentation (mm) (BSI ENV 843-4:1995).

4.2.6 Fatigue test

4.2.6.1 Fatigue followed by biaxial flexural strength test for specimen discs

This test was performed in order to determine the effect of fatiguing on the biaxial flexural strength properties and also as a preliminary study for setting the cycle limit for fatigue tests. Ten uncoloured specimens were subjected to a fatigue regime at 10,000 (n=10) and 20,000 (n=10) cycles. Another ten specimens were subjected only to the biaxial flexural test as a control group (n=10) using a Dartec HC10 servohydraulic testing frame (Zwick Ltd., UK) and 1 kN load cell (R.D.P. Electronic Ltd, UK). The same pin and three ball rig used for the biaxial flexural test was used. A cyclic load was applied centrally to the specimen in 37°C water at 2 Hz using the load between a minimum and a maximum force from 20 to 250 N. The machine adjusted the load applied to the specimen according to the force set within ±10 N (Figure 4.6). The maximum force was set to simulate a clinical occlusal biting force in premolar and cuspid region, which was 25% of the mean biaxial flexural strength (250 N). After fatigue loading, the biaxial flexural strength measurement was performed as described in section 4.2.3 above. The parameters to control the loops of cycles, which were PID gain values (proportional, integral and differential) were fixed at 6, 10, and 0.6 respectively.

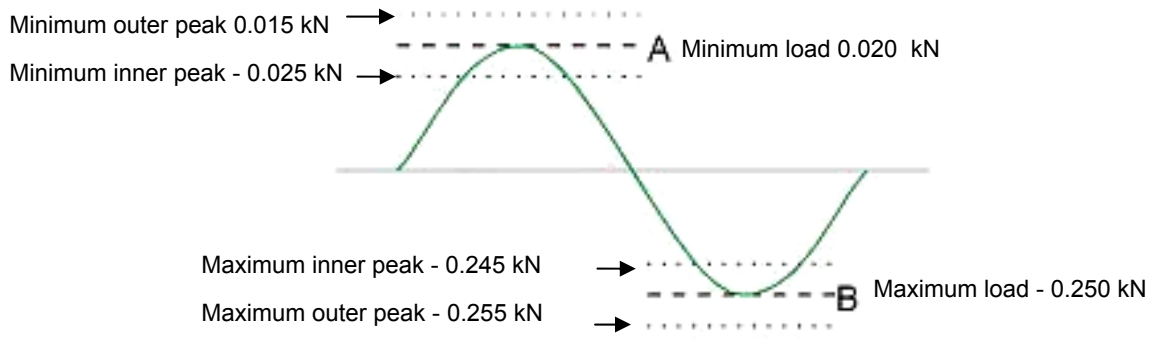

Figure 4.6. Minimum and maximum cyclic load with 10% bias

4.2.6.2 Fatigue life

Following on from the initial fatigue and failure testing, a more detailed study of the fatigue life using a classical stress-number (S-N) curve was carried out. The horizontal scale was the number of cycles (n) and the vertical scale was the stress to failure (MPa). To generate stress-number (S-N) curves, uncoloured (n=24), FS4 (n=24), FS7 (n=32) of Lava™, Cercon® (n=11), and Cerec® (n=11) zirconia discs were subjected to the fatigue testing using the same machine and equipment as the biaxial flexural strength test with a 10 kN load cell (R.D.P. Electronic Ltd, UK). The test was performed in water at 37°C at 2 Hz and a fatigue cycle limit of 500,000 was set. A sinusoidal cyclic load was applied to the centre of a specimen between a minimum of 20 N and a maximum force ranging from 50% to 90% of the mean load to failure of the specimens (N) (determined in Section 4.2.3) and 3-4 specimens were used at each load. The specific cyclic load required was applied until the failure of the specimen occurred and then the load to failure and number of cycles were recorded. The stress to failure (MPa) was calculated using the equation 4.2-4.4 and the S-N curve was plotted as the logarithmic scale of cycles to failure (x) against

stress to failure (MPa) (y). Any specimens that reached the fatigue cycle limit were recorded on the graph with an arrow.

PID gains may change if there is any violated cycle, which exceeds the set parameter. For example, if the cyclic peak exceeded the maximum force, hydraulic may shut off or premature failure of the specimen may occur. Normally, only the P (proportional) gain was adjusted higher by 1-2 units (from 6) until the cycle became normal and other parameters were left the same. Additionally, the test was started with a very low frequency, 0.25 Hz, for a few cycles and then increased slowly until reaching 2 Hz in order to avoid sudden violated cycles, which could make the specimen fail.

4.2.6.3 Fatigue followed by BFS on crown shaped specimen

Crown shaped specimens were prepared by Tsalouchou *et al* (Tsalouchou *et al.* 2007) at Queen Mary's School of Medicine and Dentistry and the materials and methods for preparing crowns are described briefly.

Fifty crown shapes were made using brass dies 7 mm (height) × 8 mm (base diameter), with a taper of 8°, giving a tip diameter of 4.2 mm (Sobrinho *et al.* 1998b). The rounded chamfer margin had a radius of 0.5 mm (Figure 4.7).

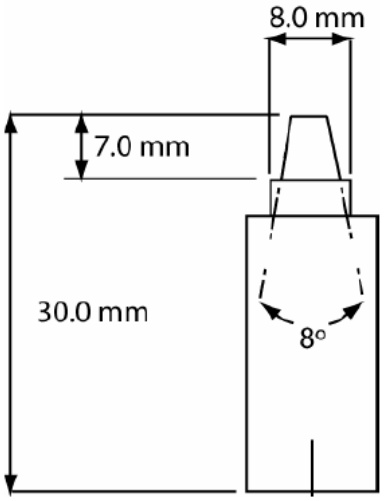

Figure 4.7. Schematic illustration of the master die

Each brass die was duplicated using reversible hydrocolloid and a stone die (GC Fujirock® EP, GC America Inc, IL) was made. The stone die was laser scanned using the Kavo Everest Scan unit (Kavo Everest® Scan 4100, Kavo, Germany). All 3D contour dimensions of the die were scanned at a ratio of 1:1 by a CCD camera and then converted into digital data. The surface of the scanned die was generated on the computer screen. The position of the finish line (preparation limit) was marked on the die using the computer software and a coping with a chamfer was constructed on the screen by the CAD module. The thickness of the coping was set at 0.5 mm and the space for set cement was set at 30 μm. There was no space left at the margins to ensure an accurate marginal fit. All data was saved by the CAM module to be used by the milling machine for the construction of the copings.

Fifty zirconia cores were machined from Kavo Everest ZS-blanks (Lot No: 100629621, Kavo, Germany) using the Kavo Everest CAD/CAM system. Each blank was mounted using a specially designed insert (Everest Insert) and a metal

positioning ring, which was filled with resin (Kavo Everest Universal Inplast). The work pieces were positioned in slots in the clamping yoke of the Kavo Everest engine (Kavo Everest® Engine 4140, Kavo, Germany) and the inner surface was milled with coarse and then fine cutting tools. Once this was completed, the inner surface of the coping was rinsed thoroughly so that any excess powder from the milling process was removed. The copings were then dried carefully and molten wax (Everest ZS Investing wax, Kavo, Germany) was applied to fill the cavity. The milling of the outer surface was next performed. Once the milling process was completed, the work pieces were removed from the clamping yoke and the copings were carefully separated by heating the wax.

All the copings (50) were placed on a firing tray and sintered in a furnace (Kavo Everest® Therm, Kavo, Germany) overnight at 1500°C. Each coping was then placed on the respective die and the margins were adjusted with a football shaped diamond bur (379-023M-HP, NTI-Kahla GmbH rotary instruments, Germany) to remove any excess. After cleaning and drying, the copings were subjected to a conditioning heat treatment, in a porcelain furnace (Multimat MCII, Dentsply, Weybridge, UK), following the manufacturer's recommended parameters (Table 4.1). Zirliner (IPS e.max® Zirliner, Lot H29042, Ivoclar Vivadent AG) was mixed with liquid (IPS e.max® Ceram Build All Around liquid, Lot H29102, Ivoclar Vivadent AG) and applied evenly on the entire coping using paint brush. The coping was vibrated, dried and fired according to Table 4.1. After firing, the thickness of the ZirLiner was measured at three points at the occlusal surface and at the margins with a caliper (Moore and Wright, Sheffield, UK). When the zirconia cores were completed, the zirconia crowns were then made by two methods: heat pressing and sintering

Table 4.1. Firing schedules for the zirconia copings, the IPS e.max® Ceram, IPS e.max® ZirPress

Firing program	Conditioning heat treatment	zirLiner firing cycle	Dentin firing of the IPS e.max® Ceram	Stain and glazing of IPS e.max® ZirPress/IPS e.max® Ceram
Start temperature (ºC)	450	403	403	403
Sintering temperature (ºC)	1056	960	750	770/725*
Temp rise (ºC/min)	60	60	50	60
Drying time (min)	2	2	2	3
Holding time (min)	10	1	1	1
Preheat (min)	2	2	2	3
Vacuum start (hPa)	Nil	450	450	450
Vacuum finish (ºC)	Nil	959	749	769/724*
* Temperature for the IPS e.max Ceram				

a. Heat-pressed group

Twenty-five zirconia cores, previously prepared and veneered with Zirliner, were placed on the brass dies and located in a specially designed split brass mould. Molten modeling wax (S-U, Schuler-Dental GmbH, Germany) was next poured into it to produce the crown shapes. The wax patterns with cores *in situ* were sprued and invested using 200 g of powder (IPS® Press Vest Speed powder, Lot HL3030, Ivoclar Vivadent AG, Schaan, Lichtenstein) with 32 ml of liquid (IPS® Press Vest

Speed liquid, Lot HL3015, Ivoclar Vivadent AG) and 22 ml of distilled water. The mixing was performed under vacuum for 2.5 minutes. After setting for 40 min, the investment ring was transferred to a preheated burnout furnace (5635 Kavo EWL, Germany) at 850°C and held for 1 hour. Cold glass-ceramic ingots (IPS e.max® ZirPress, Lot H21335, Ivoclar, Vivadent AG) were placed into the refractory muffles and an alumina plunger was inserted before transferring to a preheated optimal automatic press furnace (Jeneric Pentron, Wallington, USA). Heat pressing was carried out according to the manufacturer's recommended parameters (Table 4.2).

Table 4.2. Pressing parameters for the IPS e.max® ZirPress

Start temperature (ºC)	700
Pressing temperature (ºC)	910
Rate of climb (ºC/min)	60
Pressure (bar)	5
Hold before pressing (min)	15
Pressing time (min)	15
Vacuum start (ºC)	500
Vacuum finish (ºC)	910

After cooling, the investment was removed by sandblasting (Eurosab, Tissi, San donato Milanese, Italy) with 50 µm glass beads at 2 bar pressure. A diamond disc (006, Bracon Ltd., UK) and a sintered diamond bur (9907, Bracon Ltd., UK) were used to remove the sprue areas. The reaction layer formed during the pressing procedure was removed by immersing the crowns into an HF solution (IPS® e.max

Press Invex Liquid, Lot H31070, Ivoclar Vivadent AG) in an ultrasonic cleaner for 5 minutes. Subsequently, the crowns were cleaned under running water for 2 minutes and dried. The occlusal surface of the crown shapes was flattened and adjusted to the same height (8.0 mm diameter x 8.5 mm height) for all the specimens using diamond burs and 600 grit silicon carbide paper. Two stain firing cycles were conducted in a porcelain furnace (Multimatt MCII, Dentsply, Weybridge, UK) to simulate realistic firing cycles of the material (Table 4.1). Glaze paste (IPS e.max® Ceram Glaze paste, Lot H24056, Ivoclar Vivadent AG) was mixed with the respective liquid (IPS e.max® Ceram Glaze and Stain Liquid, Lot H25704, Ivoclar Vivadent AG) to the desired consistency and was applied evenly on the crown shapes. A glaze firing was performed with the same parameters as the stain firing (Table 4.1).

b. Sintered group

Twenty-five zirconia cores, previously prepared and veneered with Zirliner, were layered by sintering of the veneering material (group 2). Dentin powder (IPS e.max® Ceram Dentin/Body powder, Lot H29178, Ivoclar Vivadent AG) was mixed with liquid (IPS e.max® Ceram Build up Liquid, Lot H29102, Ivoclar Vivadent AG) in a ratio 0.91 g to 0.33 ml to produce a slurry. The material was applied with a paint brush to the zirconia coping and compacted with the split brass mould used in group 1. Condensation was achieved by applying a tissue for 30 seconds and brushing to remove excess liquid. A dentine firing cycle according to the manufacturer's recommended parameters was next carried out (Table 4.1). Following sintering, the space left by the shrinkage was filled with a second layer of

veneering material applied and condensed by applying a tissue for another 30 seconds. Each specimen was placed in the mould to ensure correct dimensions of the crown shape (8 mm in diameter×8.5 mm in height) and then subjected to a second dentin firing cycle. The occlusal surface of the crown shapes was flattened and adjusted to the same height (8.0 mm diameter x 8.5 mm height) for all the specimens using diamond burs and 600 grit silicon carbide paper. Two stain firing cycles were conducted to simulate realistic firing cycles of the material (Table 4.1). Glaze paste (IPS e.max® Ceram Glaze paste, Lot H24056, Ivoclar Vivadent AG) was mixed with the liquid (IPS e.max® Ceram Glaze and Stain Liquid, Lot H25704, Ivoclar Vivadent AG) to the creamy consistency and applied with paint brush on the entire surface of each specimen evenly. A glaze firing was performed with the same parameters as the stain firing (Table 4.1).

c. Cementation

The inner surface of the zirconia copings was cleaned with 50 μm aluminium oxide at 2 bar pressure, rinsed and dried. All the specimens were cemented to the brass dies using zinc phosphate cement (PhosphaCEM® IC, Lot H30756, Ivoclar Vivadent AG) at room temperature. The cement came in the form of injection capsules that had a specific amount of powder and liquid in the different chambers. The injection capsules were activated by wetting the powder with the liquid and securing in the mixing fork of a mixer (Satelec, SDS Kerr 4000, Italy, S /No 23219). The mixing time was set to 5 seconds. After mixing, the capsule injector was used to apply the cement to the inner surface of the crowns. These were seated with firm finger pressure to allow excess cement to flow. Crown samples were immediately

placed in an alignment rig and subjected to a constant static load of 500 g for 5 minutes. Once the cement was set the excess was removed. All the samples were stored in distilled water for 24 hours at 37°C prior to fatigue and fracture testing.

d. Fatigue test

Fifty cylindrical crowns, (8.0 mm diameter x 8.5 mm height), were subjected to cyclic fatigue and fracture testing using a Dartec HC10 Servohydraulic testing machine (Zwick Ltd, UK). Each specimen was positioned in a custom made testing rig (Figure 4.8), which was used in previous studies (Sobrinho *et al.* 1998a; Sobrinho *et al.* 1998b), and it was placed in a chamber with distilled water at 37°C (Figure 4.8).

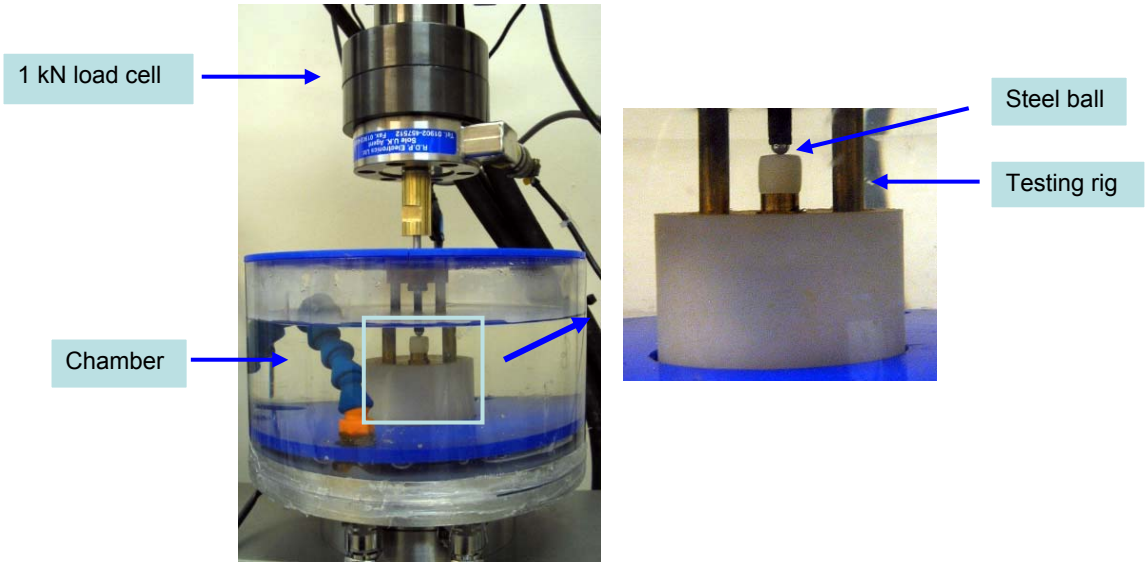

Figure 4.8. Fatigue test of crown shaped specimen

The crowns were subjected to sinusoidal cyclic loading between a minimum and a maximum force from 20 to 200 N by means of a steel ball (4 mm diameter),

applied perpendicular to the middle of the occlusal surface of the crowns, at a frequency of 1 Hz. The maximum force was set to simulate a clinical posterior occlusal biting force and the rate was used as equivalent to the average masticatory cycle of 0.8 to 1.0 second (Anderson 1956). Both groups were subjected to 50,000 cycles of loading based on the preliminary study of the fatigue followed by biaxial flexural strength, which indicated that 20,000 cycles did not reduce the flexural strength.

Fatigue testing was followed by dynamic testing, at a crosshead speed of 1mm.min^{-1}, until failure. The fragments of each specimen were retrieved according to a specific protocol (Thompson *et al.* 1994) to avoid contamination of the fracture surfaces.

4.2.7 Subcritical crack growth resistance test

Subcritical crack growth testing was carried out in order to study the crack growth parameters and also to predict the life time of the material. Forty zirconia discs of each Lava™ groups (uncoloured, FS1-FS7) were loaded at four stressing rates; 10^{-1}, 1, 10, and 100 N.s^{-1} and 10 discs were tested at each rate in the following manner. The testing was performed in water at 37°C using a Dartec HC10 Servohydraulic testing machine (Zwick Ltd, UK). They were placed centrally on three hardened steel balls rig and loaded with a metal pin (the same equipment as biaxial flexural test and detailed elsewhere) until failure. The load to failure (N) was recorded and converted to fracture stress (MPa) using equation 4.2-4.4. The fracture stress (MPa) and stressing rates (N.s^{-1}) were plotted as a graph of log fracture stress versus log stressing rate using SigmaPlot software and the slope S was calculated from the

graph. The subcritical crack growth parameter *n* was calculated following the standard DD ENV 843-3 (1997) (supersede BS EN 843-3:2005) equation 4.11.

$$n = \frac{1}{S} - 1 \qquad 4.11$$

Where *n* is a crack growth exponent, *S* is a slope of the plot. B_0 (or *A*) is a constant, which is calculated from the intercept log B_0 at log σ = *0* using a least squares fit.

4.2.8 Failure analysis using Scanning electron microscope

Scanning electron microscopy (SEM) was employed to examine the fractured surface of zirconia specimens. Representative samples of fractured uncoloured, FS4 and FS7 of Lava™, uncoloured Cercon® and InVizion™ specimens after biaxial flexural and fatigue tests, and from the Lava™ group after subcritical crack growth testing were selected. The specimens were mounted onto a 0.5" aluminium stubs (Agar scientific, Cambridge, UK) for SEM using conductive carbon cement (Leit-C, Neubauer, Münster, Germany). The solvent was allowed to evaporate overnight. The specimens were coated with carbon on the surfaces for elemental analysis and coated with gold-palladium for imaging using the sputter coating machine (Polaron E5000, UK) for 90 seconds at 20 mA. They were then analysed by SEM (Cambridge Stereoscan S90B, Cambridge Instruments; Crawley, UK) in combination with the Oxford instruments INCA software. The INCA software facilitated the rapid analysis

of chemical elements presented in the area of the SEM sample and the elements were displayed on a spectrum.

4.2.9 Microstructure analysis using atomic force microscopy

Uncoloured, FS4 and FS7 of Lava™, Cercon® and InviZion™ specimens were selected for microstructural analysis. The specimens were ultrasonically cleaned for 3 minutes to remove any dust that may affect the scanned image. The specimens were then placed in a furnace (Lenton Thermal Designs Ltd, UK) and heated to 1400°C for 30 minutes to thermally etch and reveal the microstructure (Kosmac *et al.* 1999). The surfaces of the specimens were then analysed using atomic force microscopy (AFM) in conjunction with XEP software program (PSIA Inc). The AFM (XE-100, PSIA Inc, CA, USA) was used in non-contact mode with an oxide sharpened silicon nitride cantilever (NSC 15) (MicroMash, Portland, USA) exhibiting a tip radius of curvature of less than 10 nm. The surface scan was performed with an average scanning speed of 1 Hz using XE scanner. The grain sizes were measured using Image-Pro® Plus software (version 5.1). The measurement was performed using mean grain diameters. This is an average diameter measured at 2 degree intervals passing through an object's centroid. The grains were measured in a 2x2 μm area (a whole area got from AFM image). The average size and standard deviation were calculated from the software.

4.2.10 X-ray Diffraction Analysis (XRD)

4.2.10.1 Disc specimens

X-ray diffraction (XRD) was used to analyse the as-received and polished specimens to determine the effects of the polishing (for specimen preparation) on the phases present in the surface of the samples. Representative specimens of uncoloured, FS4 and FS7 of Lava™, Cercon® and InVizion™ specimens were selected for XRD analysis. XRD was performed using a Brüker D8 Advance diffractometer. Data was collected in flat plate geometry, with Ni filtered CuKα radiation (wavelength = 1.5406 Å). The data was collected from a 2θ range of 10 to 100°, with a step size of 0.02° and a count time of 12 seconds. Refinement of the data was carried out using Topas (Coelho 2004). A standard model for each of the three phases was used for the refinement of the samples and they were determined from the Daresbury Crystal Structure Database. A starting model for the tetragonal zirconia phase was based on Teufer *et al* (Teufer 1962) with a P42/nmc space group and lattice parameters of a=3.64Å and c=5.27Å. A starting model for the cubic phase was based on Katz *et al* (Katz 1971) with a space group of Fm3m and lattice parameters of a=5.14Å (note these are adjusted from those values quoted in the paper). The second cubic phase also used a starting model from Katz *et al* (Katz 1971) but again the starting lattice parameters were adjusted to 5.19Å. The peak shapes for the refinement were modelled on a pseudo Voigt distribution. Background parameters, a scale factor, four peak shape variables, an asymmetry factor, cell parameters, and a zero point correction were all refined.

Additionally, uncoloured Lava™, Cercon® and InVizion™ specimens were sequentially ground with 80, 320, 500, and 1000 grit silicon carbide paper (Struers,

UK) using the Struers RotoPol-11 machine. These different ground surface specimens were analysed by XRD to investigate any phase transformation in the different commercial zirconia specimens.

4.2.10.2 Crown shaped specimens

Samples of IPS e.max® Ceram (Ivoclar Vivadent AG, Schaan Liechtenstein), IPS e.max® ZirPress (Ivoclar Vivadent AG) and zirconium oxide powder (Kavo Everest ZS-blanks, Kavo, Germany) before and after sintering, were selected for XRD analysis. The specimens were placed in the holder of a Brüker D8 Advance diffractometer and using flat plate geometry, data were collected from 10 to 100° 2θ, with a step size of 0.02° and a count time of 12 seconds. Ni filtered Cu Kα radiation was used (wavelength=1.5406 Å) and data were collected using a scintillation counter.

4.2.11 Raman spectroscopic analysis

Stress-induced transformation toughening of zirconia was studied using Raman microscopy. The uncoloured Lava™, Cercon® and InVizion™ specimens were subjected to the Vickers hardness test, which was used to generate indentations with cracks (without surface damages) on the polished surface of specimens using loads of 20, 30, 40 and 50 kg. Images of the indentations were then obtained using a microscope at 10 x objectives with the Raman spectrometer (LabRam 5, Horiba Jobin Yvon Ltd, Stanmore, Middlesex, UK). For each load, the Raman laser (He/Ne 633 nm) was focussed on the indentation centre. For the 30 kg indentation, spectra

were obtained over the full and surrounding indentation region (250 micron square) at 2 micron intervals. These were then modelled by comparison with the full spectra of samples of pure tetragonal (t), cubic (c) (Whitfield and son limited, Newcastle) and monoclinic (m) zirconia phases using LabRam software. From this modelling, images indicating regions of high versus lower levels of the three phases within and outside the indentation region were obtained. Additionally, spectra were generated at 2 micron intervals along two lines passing through the centre of the indentation. The first was through the groove produced by the sharp edge of the Vickers diamond and the second at 45 degrees to this groove (Figure 4.9).

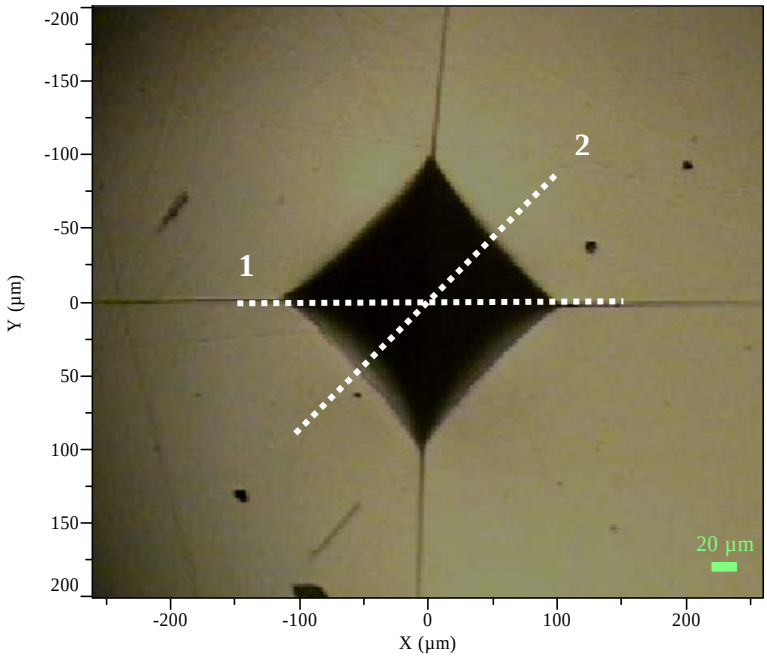

Figure 4.9. Raman microscopic images of an indentation produced using a force of 30 kg. The two lines indicate the regions examined.

The Raman intensity as a function of wavenumber will, at a given distance d from the centre of the indentation, be given by an expression of the form

$$I_d(\upsilon) = tI_t(\upsilon)+cI_c(\upsilon)+mI_m(\upsilon) \quad 4.12$$

$I_d(\upsilon) = tI_t(\upsilon)+cI_c(\upsilon)+mI_m(\upsilon)$ are the Raman intensity at wavenumber υ of the specimen, and pure tetragonal (t), cubic (c) and monoclinic (m) phases respectively. Using LabRam software, values for tetragonal, cubic and monoclinic phases are calculated that give the least mean square deviation between the measured specimens' Raman intensity at all wavenumbers and equation 4.12. Values of tetragonal, cubic and monoclinic phases as a function of distance from the indentation centre will be proportional to any changes in the concentration of a particular phase.

With all sample loads, spectra were also generated every 5 microns along five equally spaced lines within a rectangle of height 20 microns and length 150 microns (Figure 4.10). This rectangle was placed with the centre of its left short side positioned at the indentation centre and its long side parallel to the groove in the indentation generated by the sharp edge of the Vickers diamond. Values of t, c and m in equation 4.12 at each point were determined again using the LabRam software and the spectra of the pure phases. Mean values and their standard deviation (n=5) as a function of distance from the indentation centre were then calculated.

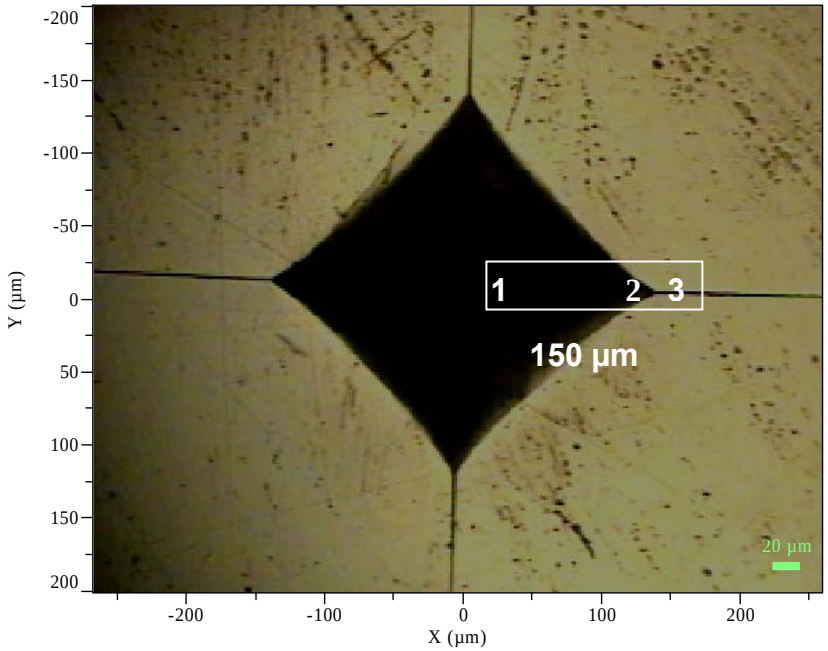

Figure 4.10. Raman microscopic image of an indentation produced using a force of 50 kg. The rectangle shows the scanned area studied at all loads and used to generate fractions of each phase as a function of distance from the indentation centre

Finally, the fracture surfaces of representative specimens used in the biaxial flexural and subcritical crack growth tests were scanned at the fracture origin area. LabRam software was again used to obtain and interpret images indicating relative levels of the three phases within the fracture origin area.

4.3 Titanium phosphate glass reinforced 3Y-TZP

The reaction of engineering ceramics such as zirconia and alumina with additives is not a predictive science and the use of phosphate based glasses as a sintering aid was investigated. The potential benefits may be a material with good strength that sinters at much lower temperatures than zirconia; and also it will be

more susceptible to etching than zirconia, which may allow adhesive cementation. Titanium dioxide was added to the glass in order to reduce the solubility by increasing the cross linking or covalent character of the bonds in the glass structure (Abou Neel *et al.* 2008). This is an interesting route to pursue and may not achieve significant improvements, but it may give an insight into how phosphate glasses react with zirconia. The titanium phosphate glass selected in this study consisted of $0.3CaO\text{-}0.15Na_2O\text{-}0.05TiO_2\text{-}0.5P_2O_5$. This pilot study investigated the effect of titanium phosphate glass on the strength and bonding properties of zirconia. The sintering temperature required for titanium phosphate glass zirconia and the phases produced were also studied.

4.3.1 Specimen preparation

4.3.1.1 Chemical equation and composition calculations:

In order to obtain $0.3CaO\text{-}0.15Na_2O\text{-}0.05TiO_2\text{-}0.5P_2O_5$, the glass compositions and chemical reactions and were calculated as follows:

Calculations for composition with glass code $0.3CaO\text{-}0.15Na_2O\text{-}0.05TiO_2\text{-}0.5P_2O_5$ (i.e. 50 mol% P_2O_5, 30 mol% CaO, 15 mol% Na_2O, and 5 mol%TiO_2) were made by using

$2NaH_2PO_4$	⟶	Na_2O +	P_2O_5 +	$2H_2O$	
RMM=240 $gmol^{-1}$		62	142	36	$gmol^{-1}$

Where RMM is a relative molecular mass, which is calculated from an atomic mass of each atom.

Total amount of Na_2O (15 mol%) required is 0.15x62= 9.3 g

Therefore, NaH_2PO_4 would be used for 15 mol% Na_2O [(240/62)x9.3] = 36 g However, using 36 g of NaH_2PO_4 would yield P_2O_5 [(142/240)x36] =21.3 g

Total amount of P_2O_5 required is (50 mol%) 0.5x142= 71 g, therefore, 71-21.3=49.7 g would have to be added (This is added last due to its hygroscopic nature).

$$CaCO_3 \longrightarrow CaO + CO_2$$

RMM=100 $gmol^{-1}$ 56 44 $gmol^{-1}$

Total $CaCO_3$ required to be added to give 30 mol% CaO is 0.3x56=16.8 g. Therefore, $CaCO_3$ (100/56)x16.8=30 g would be used for 30 mol% CaO.

$$TiO_2 \longrightarrow TiO_2$$

Total TiO_2 required is 79.9x0.05= 3.995 g

Therefore, 36g of NaH_2PO_4, 49.7g of P_2O_5, 30g of $CaCO_3$ and 4g of TiO_2 are required to give $0.3CaO\text{-}0.15Na_2O\text{-}0.05TiO_2\text{-}0.5P_2O_5$ glass. However, only half of the quantity of each powder was placed in the crucible to allow space for degassing during melting.

4.3.1.2 Glass preparation

The powder of 18g of NaH_2PO_4, 24.85g of P_2O_5, 15g of $CaCO_3$ and 2g of TiO_2 was weighed on an analytical balance (Mettler Toledo, UK) and thoroughly mixed together using a blender (Stomacher 400 Circulator, Seward, UK) at 230 rpm for 30s. The mixed powder was put into a platinum crucible type 71040 (Johnson

Matthey, Royston, UK), which was then placed in a Carbolite furnace and melted at 700°C for 15 minutes, then 1300°C for 3 hours. The liquid glass was poured onto a steel plate and allowed to cool. The resulting glass was then ground to a fine powder using an agate ball grinder (Retsch®, UK) at 12 Hz for 2-3 minutes.

4.3.1.3 Milling of glass 3Y-TZP

A steatite mill pot can contain a maximum powder of 200 g; therefore, in order to obtain compositions with 1 wt%, 2 wt%, 5 wt%, 10 wt% and 20 wt% of titanium phosphate glass reinforced 3Y-TZP ceramic, 2, 4, 10, 20 and 40 g of glass powder and 198, 196, 190, 180 and 160 g of 3Y-TZP powder containing binder (YZ01B, Saint-Gobain Industrial Ceramic Ltd, St. Helens, UK) were used respectively. Firstly, the glass powder was placed in the porcelain mill pot (Pascall Engineering Co. Ltd, UK) and milled dry for 24 hours. 3Y-TZP powder was then added to the mill pot depending on the pre-determined weight. 300ml of methanol GPR (BDH Laboratory Supplied, UK) 300 ml was also added and the mixture was then wet-milled for a further 24 hours.

4.3.1.4 Preparation of 3Y-TZP (control) and 3Y-TZP containing glass discs

The slip (liquid mixture) obtained from the milling pot was then dried at 70°C for 24 hours. The dry powder was then sieved through Endecotts sieves (Christisons, Newcastle, UK) of size 1 mm, 200 μm, 150 μm, 75 μm using a vibratory sieve shaker (Fritsch, Germany) in order to get homogenous and fine, free flowing powder.

Figure 4.11. Stainless steel die

2.5 g of glass zirconia powder was weighed on an analytical balance (Mettler Toledo, UK) and placed into a stainless steel die (20 mm diameter) (Specac Ltd, Kent, UK) (Figure 4.11) and uni-axially pressed at 6.5 tons using a hydraulic press to give approximately 2.6 mm thickness discs. The discs were fired in a furnace (Lenton Thermal Designs Ltd, UK) following the manufacturers' instructions (Figure 4.12). First, temperature was raised to 300°C using 1 °C/min rate and held for 3 hours. Then it was raised to 800°C using 1 °C/min rate and held for 2 hours. The final temperature was 1400°C, which was held for 2 hours using the rate of 2 °C/min. The temperature was cooled down using the rate of 6 °C/min. A pilot study was carried out to investigate the flexural strength and the sintering temperature required for 5 wt%, 10 wt%, and 20 wt% titanium phosphate glass reinforced zirconia. Therefore, the final sintering temperature was modified and examined from 1200-1400°C.

For the control group (non-glass zirconia), 2.5 g zirconia powder, which was 3YTZP containing a binder (polyvinylic alcohol and polyethylene glycol) (YZ01B,

Saint-Gobain Industrial Ceramic Ltd, St. Helens, UK), was placed into the metal die (20 mm diameter) (Specac Ltd, Kent, UK) directly without any milling process and it was uni-axially pressed at 6.5 tons using a hydraulic press to give approximately 2.6 mm thickness discs. They were then sintered following the manufacturer's instruction (Figure 4.12) with no variation from the stipulated temperatures.

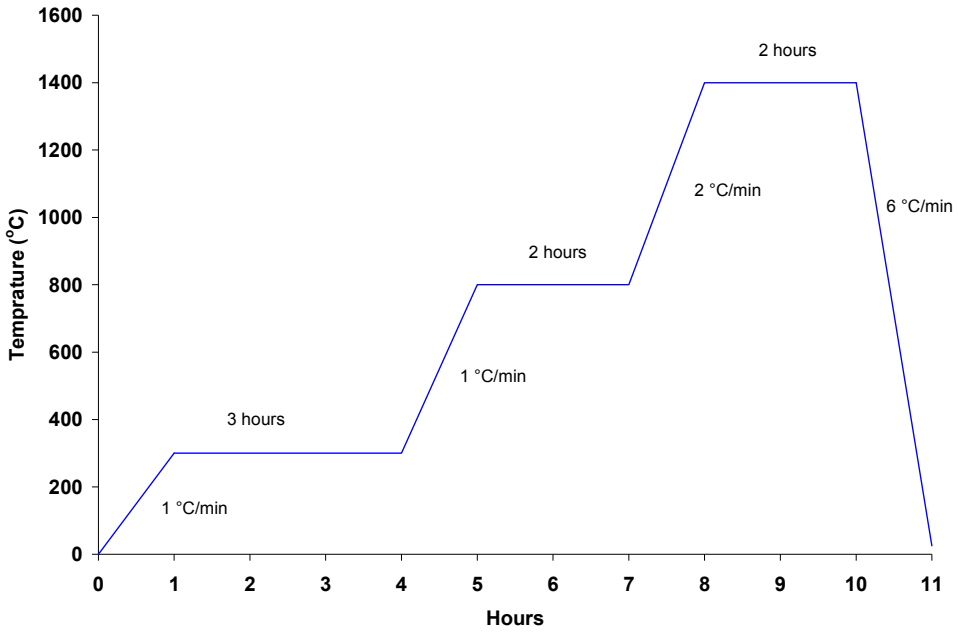

Figure 4.12. The firing schedule

The specimens obtained after firing were approximately 16 mm in diameter and 2 mm in thickness. They were polished using the same technique as commercial 3Y-TZP groups (See Section 4.2.1) and ultrasonically cleaned for 3 minutes before testing.

4.3.2 Density and Shrinkage measurement

Density measurements were performed on each sintered specimen using the Archimedes principle and using the same equipment as for the commercial 3Y-TZP (See Section 4.2.2).

The determination of linear shrinkage before and after firing was performed by measuring the change in diameter of the specimen disc before (l_0-initial diameter) and after sintering (l) and dividing by the initial diameter:

$$Shrinkage = \frac{l_0 - l}{l} x100 \qquad 4.13$$

4.3.3 Biaxial flexural strength test

A pilot study investigated the flexural strength of 5 wt%, 10 wt% and 20 wt% of titanium phosphate glass reinforced zirconia, which was sintered at different temperature (1200-1400°C) compared with control (1400°C) group. Five discs of each group were subjected to the biaxial flexural test. The specimens were tested in water at 37°C using a Dartec HC10 Servohydraulic testing machine (Zwick Ltd, UK) with 10 kN load cell (R.D.P. Electronic Ltd, UK). They were placed centrally on a three hardened steel balls rig and loaded with metal pin (the same equipment as biaxial flexural test) until failure at a cross head speed of 1mm/min. The load to failure (N) was recorded and converted to fracture stress (MPa) using equations 4.2-4.4.

From the initial results, the study continued to examine the flexural strength of 1 wt% and 2 wt% of titanium phosphate glass reinforced zirconia and control groups

sintered at 1400°C in more detail. Twenty five discs of each group were submitted to the biaxial flexural test using the same conditions as described above and this would allow a more detailed statistical analysis.

4.3.4 Weibull analysis

The biaxial flexural strength data was analysed statistically with the Weibull distribution using the WinSMITH™ Weibull 0.2M software program. Twenty five specimens of 1 wt% and 2 wt% of titanium phosphate glass reinforced zirconia and control groups were tested. The following equations 4.5-4.9 were used to calculate the Weibull modulus (Weibull 1951). The software calculated the equations, plotted the graph and reported the results automatically.

4.3.5 Vickers Hardness test

This test was performed in order to examine the hardness of titanium phosphate glass reinforced zirconia compared with control groups. Five pieces of broken specimens of 1 wt% and 2 wt% of titanium phosphate glass reinforced zirconia and control groups from the biaxial flexural testing were randomly selected to measure Vickers hardness using an indentation tester (Vickers-Armstrongs Engineering Ltd, Kent, UK). Five indentations were placed on both polished and unpolished sides within the same specimen using a loading mass of 1.5 kg. The indentation diagonal lengths (nm) were measured using Image-Pro® Plus (version 4.0) software with an optical microscope (x25) (Ceti, UK). The hardness was calculated from the following equation 4.10 using the BS ENV 843-4:1994 standard (BSI ENV 843-4 1995).

4.3.6 Shear bond strength test

Shear bond testing was carried out by using a composite cylindrical block cemented with phosphate monomer containing resin cement to an etched glass reinforced zirconia disc. The materials used are shown in Table 4.3 and the method is described as follows:

Table 4.3. Materials used for shear test

Materials	Components	Composition
Panavia® 21 (opaque shade)	Catalyst Paste	MDP, co-monomers, filler, BPO
	Universal Paste	Co-monomers, filler, amine, initiator
	Oxyguard II	
Vita Ceramic Etch		<5% Hydrofluoric acid (HF) <10% Sulfuric acid (H_2SO_4)
ED Primer	Liquid A	HEMA, MDP, 5-NMSA, Accelerator, water
	Liquid B	5-NMSA, Accelerator, water
Clearfil Porcelain Bond Activator (Silane coupling agent)		Bis-PEDMA, MPS
Clearfil™ SE Bond	Self-etching primer	MDP, HEMA, hydrophilic dimethacrylate, di-camphorquinon, *N*,*N*-diethanol-*p*-toluidine, water
	Bonding agent	MDP, Bis-GMA, HEMA, hydrophobic dimethacrylate, di-camphorquinon, *N*,*N*-diethanol-*p*-toluidine, silanated colloidal silica
Filtek P60 (A3 shade)	Posterior restorative	Bis-GMA, TEGDMA, UDMA, Bis-EMA

4.3.6.1 Preparation of composite cylindrical block

The custom-made metal mould, 6 mm in height and 4 mm in diameter, was filled with an A3 shaded posterior composite resin (Filtek P60, 3M ESPE, Seefeld, Germany) and a glass slide was placed on the top of the mould to create a flat and smooth composite resin surface (Figure 4.13). The composite resin was then polymerised by a visible-light curing unit (L.E. Demetron I, Kerr, UK) positioned immediately above and below the specimens for 40 seconds on each side, for a total of 80 seconds (Atsu *et al.* 2006). The smooth composite surface was applied with Panavia A&B primer in order to activate the setting of Panavia® 21 resin cement according to the manufacturers' instruction.

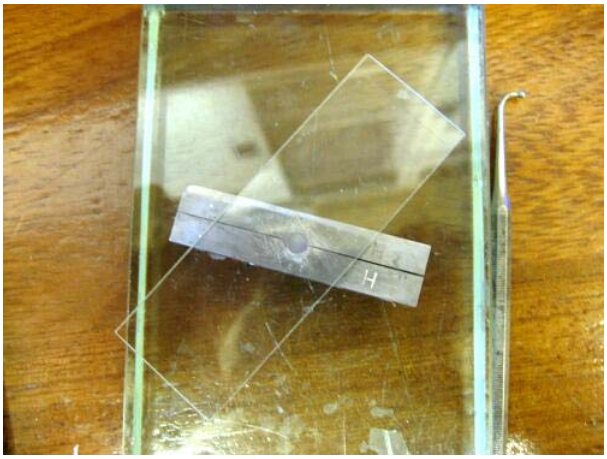

Figure 4.13. Equipment making the composite blocks

4.3.6.2 Preparation of ceramic surface

Fifty discs of each three glass zirconia groups containing 1 wt%, 2 wt%, 5 wt% titanium phosphate glass and non-glass zirconia group (control) were divided into two subgroups according to etching time (2 and 5 minutes). Twenty five discs of

each group were etched with 5% HF (Vita Ceramic Etch, UK) for 2 minutes on the polished surfaces and twenty five discs were etched for 5 minutes. After etching, the specimens were neutralised with neutralising agent (alkaline salts) for 2 minutes and then washed in tap water for 30 seconds in a container (Awliya *et al.* 1998). They were ultrasonically cleaned for 3 minutes in order to remove any remaining acid, and then air-dried using compressed aerosol air spray (Dust off, Falcon Safety Product Inc, USA) (Chen *et al.* 1998).

4.3.6.3 Bonding procedure on ceramic surface

The bonding procedures were carried out in accordance with the manufacturers' instructions. The areas for bonding were isolated by placing a one-sided adhesive tape with a pre-punched circular hole (5 mm) onto the bonded area to prevent excess flash adhering to the surrounding core material (Awliya *et al.* 1998). The zirconia surface was coated with a silane coupling agent (Clearfil Porcelain Bond activator, Kuraray Medical Inc, Okayama, Japan). This was mixed with Clearfil SE Bond Primer using a brush according to the manufacturers' recommendation and applied to the ceramic, left for 20 seconds, and dried with mild compressed air flow (Dust off, Falcon Safety Product Inc, USA) (manufacturer recommendation). Adhesive resin, Clearfil SE Bond, was then applied as a thin layer. It was light polymerised using a light curing unit for 10 seconds (manufacturer's recommendation) which was held at a distance of 1 cm from the specimen's surface.

4.3.6.4 Cementation with composite resin

The cementation process and time was performed according to the manufacturers' recommendation (Table 4.4).

Table 4.4. Processing time for cementation of Panavia® 21

Procedures	Time
Mixing time	20-30 sec
Working time	4 min
Setting time	1 min
Complete setting	3 min
Total time 8 minutes 30 seconds	

Panavia® 21 (opaque shade), which is a chemical cured MDP modified resin composite, was dispensed in equal amounts of catalyst and universal pastes. It was mixed for 30 seconds until a smooth and uniform paste was obtained. All resin cement was applied to the composite surface using a flat plastic hand instrument which was then placed onto the ceramic surface. The composite-ceramic specimen was placed under a load of 750 g in a custom made pressing machine. Excess composite resin was removed with a brush and oxygen blocking gel (Oxyguard) was then applied over the cement in order to facilitate cement setting. After 10 minutes, the load was removed and the oxyguard was washed using tap water until it was all clearly removed. All specimens were stored in distilled water at 37°C for 3 days (Della Bona and van Noort 1995; Kern and Wegner 1998).

4.3.6.5 Shear test

Each specimen was mounted onto the resin block (room temperature curing epoxy system, Specifix-20 kit, Struers, UK) using cyanoacrylic adhesive (Northants, UK) (Figure 4.14a). The specimen was then mounted in a rig (Instron, UK) for a shear test (Figure 4.14b). Each sample was subjected to a shear load using a universal testing machine (Instron 4505, UK) with 1kN static load cell (Instron, UK) at a cross head speed of 1 $mm.min^{-1}$. The force was applied parallel to the ceramic surface at the composite-ceramic bonded area until failure occurred. The bonding failure (N) was recorded and the bond strength value (MPa) was calculated using the following equation 4.14.

$$\sigma = L/A \qquad 4.14$$

Where L is the load at failure (N) and A is the adhesive area (mm^2)

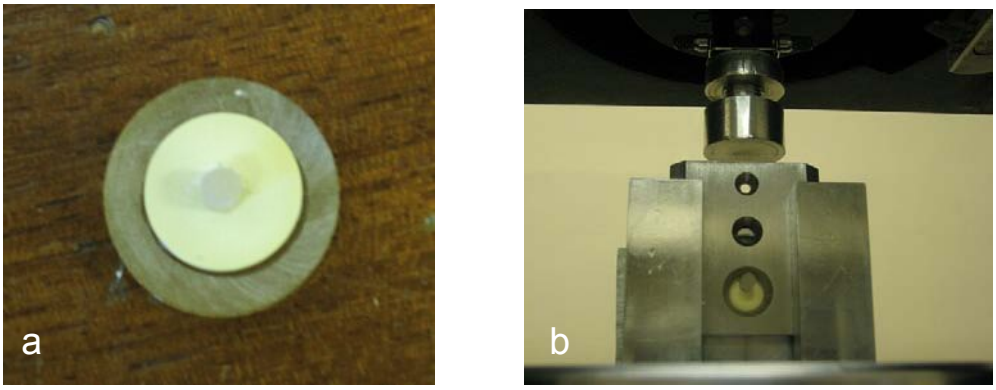

Figure 4.14. Image *a* shows the mounted specimen and *b* is the specimen after mounting in the rig and prepared for shear testing.

4.3.7 Scanning electron microscopy analysis

4.3.7.1 Fractured surface of BFS specimens

A scanning electron microscope (SEM) was employed to examine the fractured surface of 1 wt% and 2 wt% of titanium phosphate glass reinforced zirconia and control groups. Representative samples from each group, which fractured at high and low forces, were selected after biaxial flexural tests. The specimens were mounted onto 0.5" aluminium stubs (Agar scientific, Cambridge, UK) for SEM using conductive carbon cement (Leit-C, Neubauer, Münster, Germany). The cement was allowed to set over night. The specimens were coated with gold-palladium for imaging using the SEM coating machine (Polaron E5000, UK) for 1 minute 30 seconds at 20 mA. They were then analysed by SEM (Cambridge Stereoscan S90B, Cambridge Instruments; Crawley, UK) in combination with the INCA software.

4.3.7.2 Etched surface and Bonding failure

After etching with 5% HF for 2 and 5 minutes, two specimens from control 1 wt%, 2 wt% and 5 wt% glass zirconia groups were examined with a scanning electron microscope (SEM) for determination of a surface morphology. After shear tests, all specimens were examined by an optical microscope (x 4 and x10 magnification) (Olympus BX50, Best Scientific, Wiltshire, UK) in order to study the mode to failure. Adhesive and cohesive failure of bonding could occur in 3 locations: (1) adhesive failure at the interface between the ceramic and resin luting agent or between the resin luting agent and the composite resin interface; (2) cohesive failure within the ceramic, within the resin luting agent, or within the composite resin only;

and (3) adhesive and cohesive failure at the same site, or a mixed failure (Rosenstiel *et al.* 2000).

4.3.8 X-ray Diffraction analysis (XRD)

X-ray diffraction (XRD) was used to analyse the phases present in the glass zirconia compared with non-glass zirconia samples using a Brüker D8 Advance diffractometer. The procedure used was the same as detailed in 4.2.10.

CHAPTER 5

Results

5.1 Commercial 3YTZP

5.1.1 Biaxial flexural strength, hardness and reliability of zirconia specimens

The mean biaxial flexural strength and the results from Weibull analysis of eight-shaded Lava™ (uncoloured, FS1-FS7), Cercon® and Invizion™ discs are presented in Table 5.1. Multiple comparisons performed using a one-way analysis of variance (ANOVA) and paired Bonferroni test at the 5% significance level identified no significant difference in the mean biaxial flexural strength values among all groups (P>0.05) except Cercon® (823±115 MPa) and Invizion™ (828±87 MPa) groups, which had significantly lower flexural strength than Lava™ groups (≈1100 MPa) (P<0.001). Cercon® and Invizion™ had similar flexural strengths, which were not significantly different (P>0.05).

The survival probability distributions were plotted against the ranked biaxial flexural strengths in ascending order. All groups exhibited a similar distribution except Cercon® and Invizion™, which showed lower strength distribution values (Figure 5.1). The Weibull modulus represents the slope of the plot and the strength at 63.2% probability of survival was the characteristic strength. These results were shown in Table 5.1.

Table 5.1. The biaxial flexural strength (MPa), probability of failure, Weibull moduli (*m*), confidence interval, R^2-values and Vickers hardness of Lava™ (n = 30), Cercon® (n = 30), Invizion™ (n=15) and as-received FS5 (n=25) specimens.

Group	Mean strength (MPa) (±SD)	Characteristic strength (σ) (MPa)	95% Confidence intervals for characteristic strength (σ)	Weibull modulus (*m*)	95% Confidence intervals for Weibull modulus	R^2-value	Vickers hardness (HV) (±SD)	
							unpolished	polished
Uncolour	1152 (±138)	1209	1171-1248	9.94	7.92-12.49	0.97	1368 (±58)	1339 (±64)
FS1	1164 (±143)	1226	1185-1268	9.34	7.36-11.84	0.97	*1395 (±74)	*1375 (±79)
FS2	1136 (±133)	1194	1156-1233	9.83	7.71-12.53	0.97	1379 (±68)	1353 (±63)
FS3	1105 (±124)	1160	1123-1197	10.06	7.74-13.08	0.89	1362 (±51)	1338 (±48)
FS4	1086 (±108)	1134	*1102-1166	11.48	8.89-14.82	0.97	1344 (±75)	1319 (±70)
FS5	1147 (±107)	1192	1164-1222	12.9	10.31-16.15	0.96	*1393 (±49)	*1381 (±51)
FS6	1156 (±129)	1222	1175-1250	10.22	8.06-12.95	0.98	1374 (±43)	1332 (±55)
FS7	1087 (±123)	1141	*1105-1177	10.09	7.92-12.86	0.97	1343 (±63)	1319 (±48)
Cercon	*823 (±115)	871	*839-905	8.3	6.62-10.46	0.98	1379(±52)	1354 (±51)
Invizion	*828 (±87)	864	*831-900	11.18	7.97-15.69	0.95	1365 (±63)	1352 (±72)
FS5 as-received	*1275 (±84)	1313	*1287-1339	17.6	13.37-23.16	0.94	-	-

** groups which had significant difference from other groups*

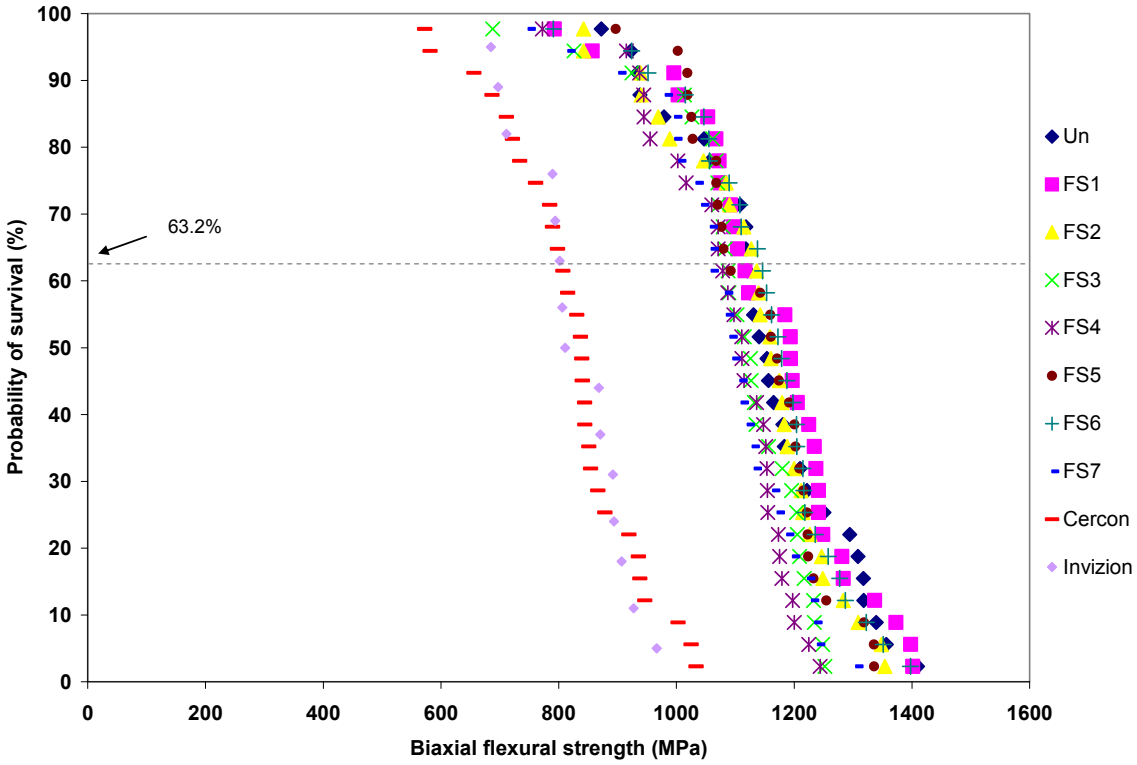

Figure 5.1. Survival probabilities of uncoloured and coloured (FS1-FS7) Lava™, uncoloured Cercon® and Invizion™ specimens.

When comparing between Lava™ groups, the characteristic strength (σ) of FS1 had the highest value (1226 MPa), which means 63.2% of the units will have failed at or below 1226 MPa, while the FS4 group had the lowest value (1141 MPa). The 95% confidence intervals of the characteristic strength identified no significant differences in the characteristic strength between groups. However, there was only a significant difference between FS4 and uncoloured; FS1; FS6 and between FS1 and FS7 (Table 5.1). The characteristic strengths of Cercon® and Invizion™ groups were statistically different from the Lava™ groups and also showed the lowest values

which were 871 and 864, respectively (Table 5.1). Cercon® and Invizion™ groups had similar characteristic strengths.

Additionally, all groups had similar Weibull moduli with FS5 and Cercon® representing the highest (12.9) and the lowest (8.3) values, respectively. However, there was no significant difference in Weibull modulus or strength reliability between groups (Table 5.1).

The "as-received" FS5 discs were subjected to biaxial flexural test in order to investigate whether polishing affected the biaxial flexural strength and Weibull modulus of specimens. The results showed that the biaxial flexural strength of "as-received" was significantly higher than all polished specimens (P<0.05 with FS1 and FS6; P<0.01 with FS2 and uncoloured; P<0.0001 with FS3-5, FS7, Cercon® and Invizion™). The characteristic strength and Weibull modulus of as-received FS5 was also significantly higher than all groups except Invizion™, FS4 and FS5 where there was no significant difference in the Weibull modulus.

Table 5.1 shows that all groups had similar hardness values except FS4 and FS7 which had lower hardness values compared with other groups. Hierarchical two-way ANOVA analysis showed no significant differences in hardness values between groups except FS1 and FS5 which had significantly higher hardness values than FS4 and FS7 (P<0.001), and FS5 also had significantly higher hardness values than FS3 (P<0.05). In addition, polished specimens had lower hardness values than as received specimens; however, there was no statistically significant difference between polished and "as received" (P>0.05) except FS6 and FS7 whose "as received" side had significantly higher hardness values than the polished side (P<0.05).

5.1.2 SEM analysis of Lava™, Cercon® and Invizion™ specimens after biaxial flexural test

5.1.2.1 Elemental analysis of Lava™, Cercon® and Invizion™ specimens

The results from elemental analysis identified that the uncoloured and coloured Lava™ and Cercon® specimens contained Zr, O, Y and Hf while only Zr, O and Y was detected in Invizion™. Uncoloured Lava™ consisted of Zr, O, Y, and Hf by % weight (wt%): 64.5, 29.7, 2.9, and 2.9 respectively. Coloured Lava™ contained slightly lower Zr and Hf, which was approximately 60 wt% and 1.5 wt% respectively compared with uncoloured and Cercon® while it contained higher O approximately 35 wt%. The coloured element could not be detected in the coloured Lava™. Cercon® had the highest Zr (~68.05 wt%) and slightly low O (~25.90 wt%) compared with others. There were lower amounts of Zr and higher O detected in the Invizion™, which was approximately 50 and 40 wt%, respectively, compared with other groups. Additionally, Invizion™ had the lowest wt% of Y compared with Lava™ and Cercon® and Hf could not be detected in Invizion™.

Therefore, it can be concluded that the amount of elemental components of uncoloured and coloured Lava™ and Cercon® were slightly different. The amount of elemental components of Invizion™ clearly differs from the others.

Table 5.2. Elemental analysis of uncoloured and coloured Lava, Cercon® and Invizion™.

Elements	Uncolour (wt%)(±SD)	FS4 (wt%)(±SD)	FS7 (wt%)(±SD)	Cercon® (wt%)(±SD)	Invizion™ (wt%)(±SD)
Zr	64.5±0.6	59.7±0.7	61.4±0.65	68.05±0.91	50.50 ±2.45
O	29.7±0.9	36.2±0.7	34.7±0.61	25.90±0.85	39.50± 2.45
Y	2.9±0.6	2.6±0.5	2.7±0.43	3.67±0.60	1.5±2.5
Hf	2.9±0.4	1.5±0.3	1.3±0.26	2.37±0.43	_

5.1.2.1 Fracture analysis of Lava™, Cercon® and Invizion™ specimens

Figure 5.2-5.17 shows that the fracture initiation site was located on the polished side which was opposite to the loading point (tension side) as expected. No obvious porosity or flaws were detected in the fracture areas; however, small porosities or voids were seen around the fracture origins at higher magnification. The area of the fracture origin presents as a classic smooth almost mirror-like region called the 'fracture mirror'. When the crack reaches a critical speed, it can deviate from the original plane and may change direction forming the small ridges called 'mist' before transforming into larger ridges called hackle lines. However, not all the fracture surfaces of specimens appear as the classic mirror like region.

The uncoloured Lava™specimens that failed at 934 MPa and 1401 MPa were selected to compare the fracture pattern and surface defects. The fracture surfaces of both low and high strength specimens did not show the classic smooth surfaces like other Lava™ groups. For the low strength uncoloured specimen (Figure 5.2), no obvious porosities or voids were found and several crack lines appeared at the fracture origin area (Figure 5.3). The high strength uncoloured specimen (Figure 5.4)

showed a smoother surface compared with the low strength specimens. Some voids were found at the fracture origin area (Figure 5.5).

The FS6 Lava™ specimens that failed at 790.72 MPa and 1397.57 MPa were selected to compare the fracture pattern and surface defects. The fracture surfaces of both specimens had smooth surfaces at the fracture origin, which was the fracture mirror (Figure 5.6 and 5.8). The mist and hackle was located in the area outside the fracture origin. When using the higher magnification, several porosities were found at the fracture origin area of the low failure strength specimen (Figure 5.7). These porosities were larger and more frequent than the porosities found at the fracture surface of high strength FS6 Lava™ specimens (Figure 5.9).

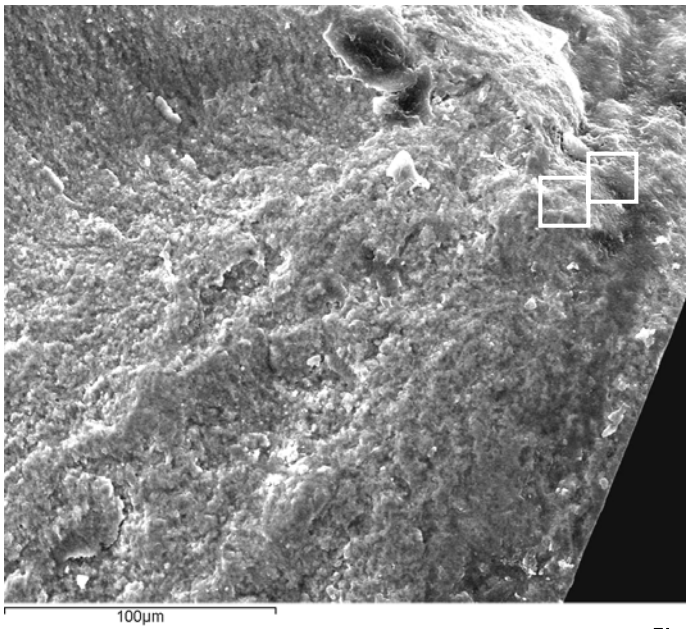

Figure 5.2. Fractured surface of low strength uncoloured Lava™ specimen after BFS. The area within the square was investigated by using SEM at higher magnification (Figure 5.3).

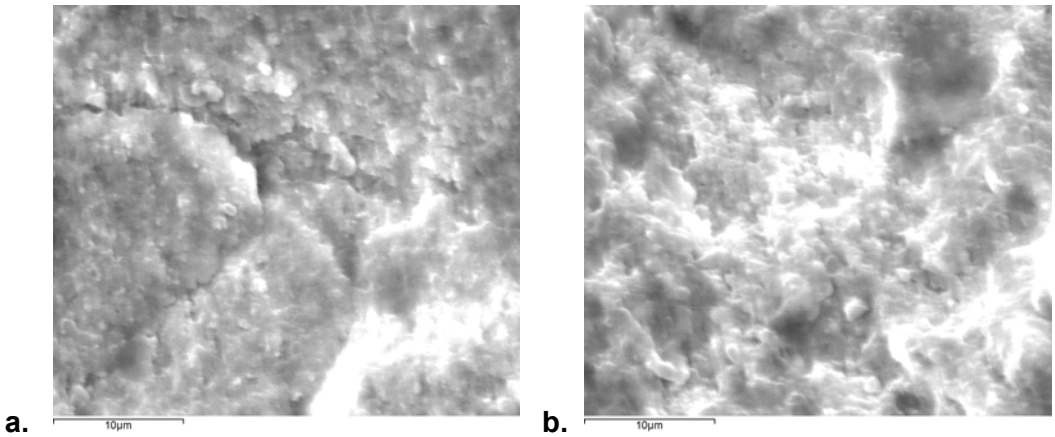

Figure 5.3. Fractured surface of low strength uncoloured Lava™ specimen after BFS. Some crack lines were found at the fracture origin (a); however, no any obvious voids were found when other fracture origin areas were investigated (b).

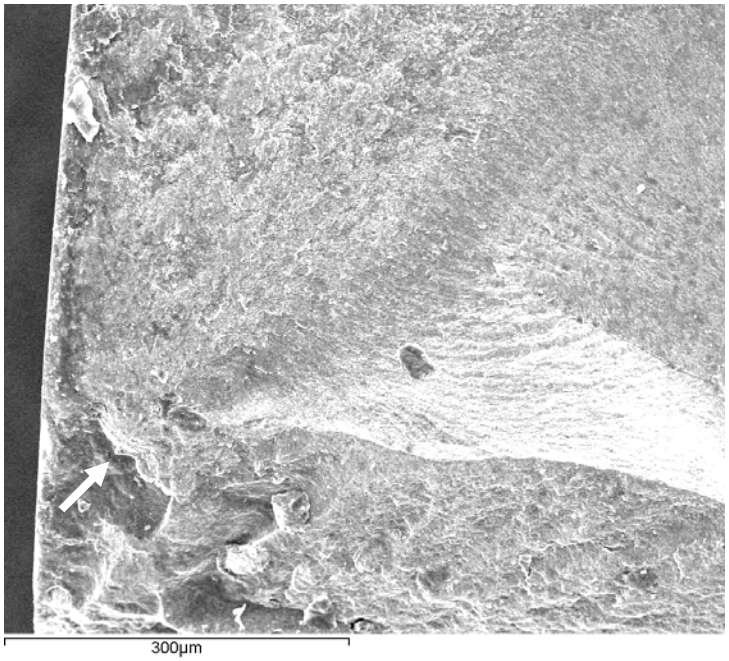

Figure 5.4. Fractured surface of high strength uncoloured Lava™ specimen after BFS. Arrow showed the area which was investigated by using SEM at higher magnification (Figure 5.5).

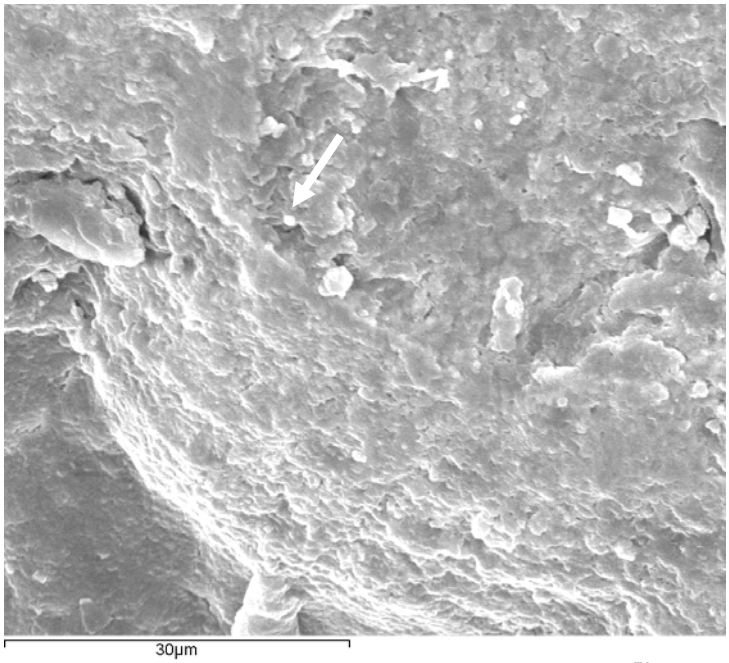

Figure 5.5. Fractured surface of high strength uncoloured Lava™ specimen after BFS. The arrows points out the voids which appeared around the fracture origin.

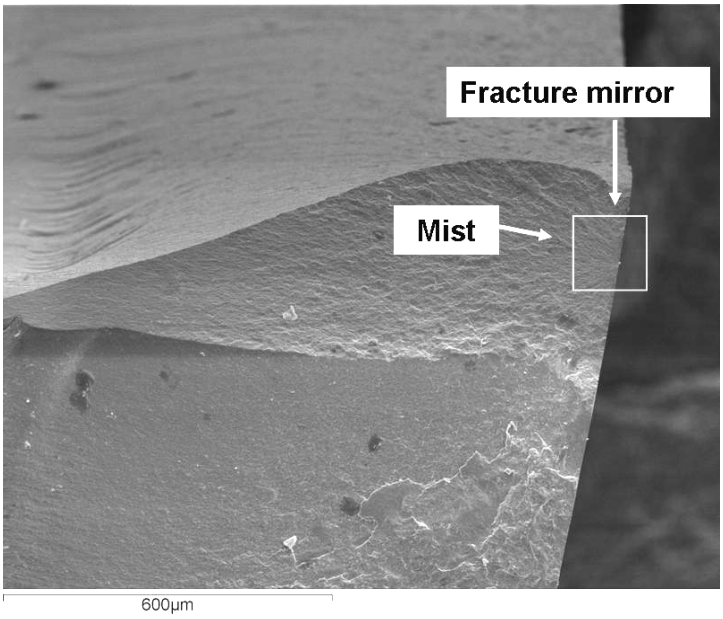

Figure 5.6. Fractured surface of low strength FS6 Lava™specimen after BFS. The area within the square was investigated by using SEM at higher magnification (Figure 5.7).

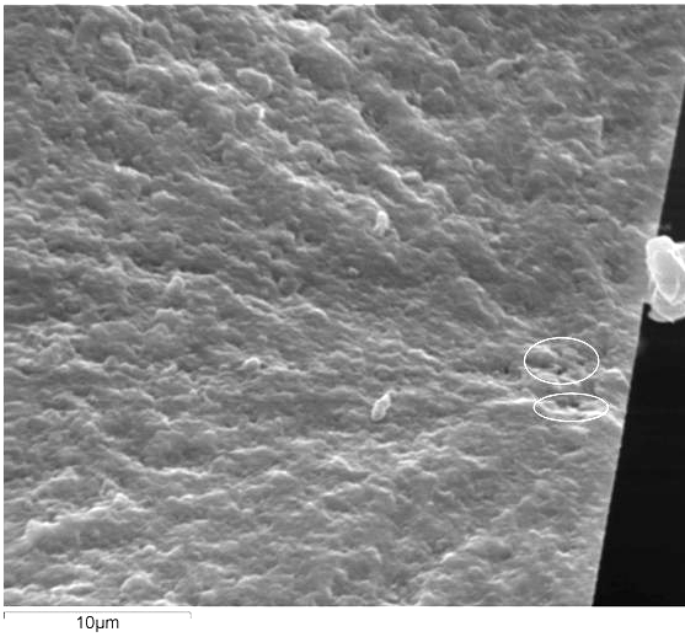

Figure 5.7. Fractured surface of low strength FS6 Lava™ specimen after BFS. Porosities are circled to aid identification.

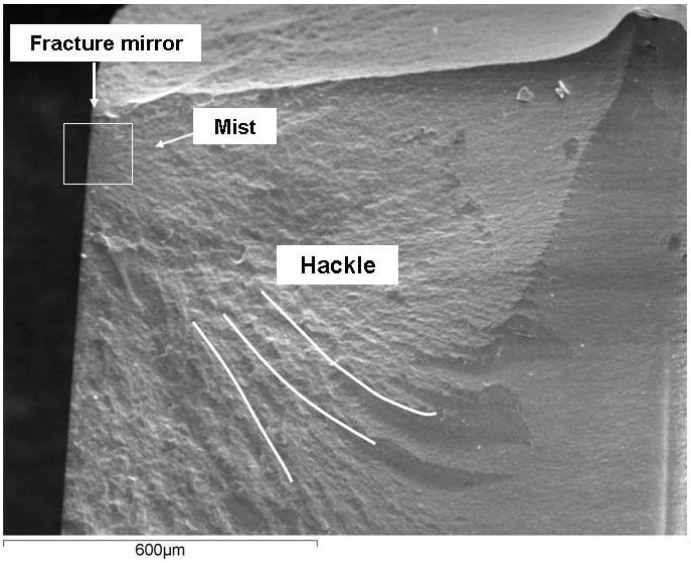

Figure 5.8. Fractured surface of a high strength FS6 Lava™specimen after BFS. The area within the square was investigated by using SEM at higher magnification (Figure 5.9)

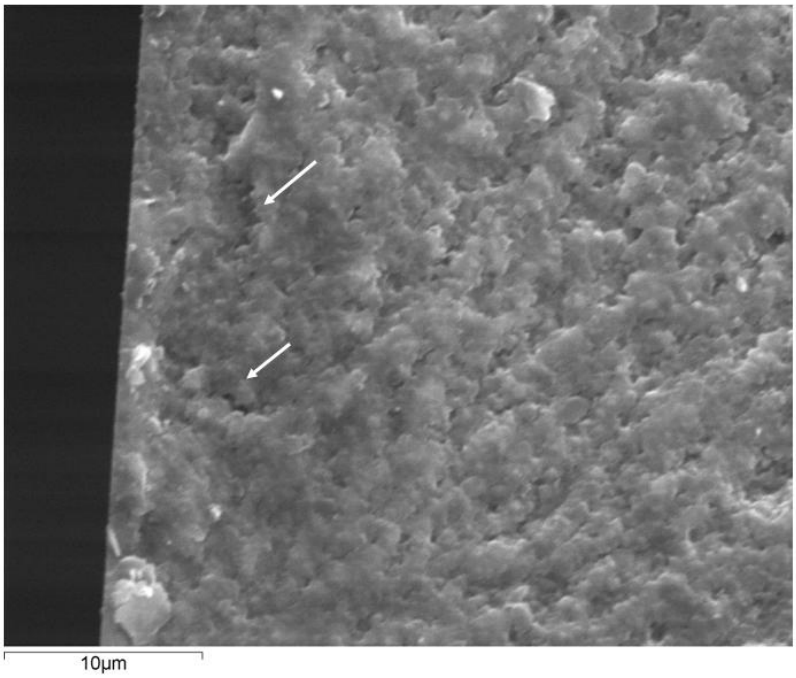

Figure 5.9. Fractured surface of a high strength FS6 Lava™ specimen after BFS. Arrows points out the small voids near the tension side

Figure 5.10-5.13 show the fractured surface of Cercon® failed at high and low stresses, which were 572.33 and 1022.59 MPa respectively. The fracture mirror was not found at the fracture origin of low strength Cercon® (Figure 5.10) and several large porosities were detected when using higher magnification (Figure 5.11). The fracture area was rougher than Cercon® specimens that failed at a high strength and Lava™ specimens.

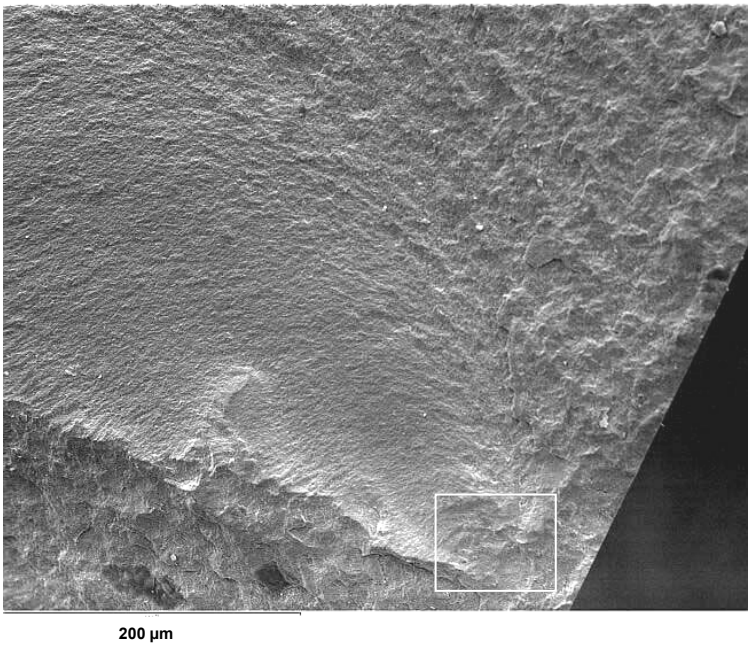

Figure 5.10. Fractured surface of low strength Cercon® specimen after BFS. The area within the square was investigated by using SEM at higher magnification (Figure 5.11)

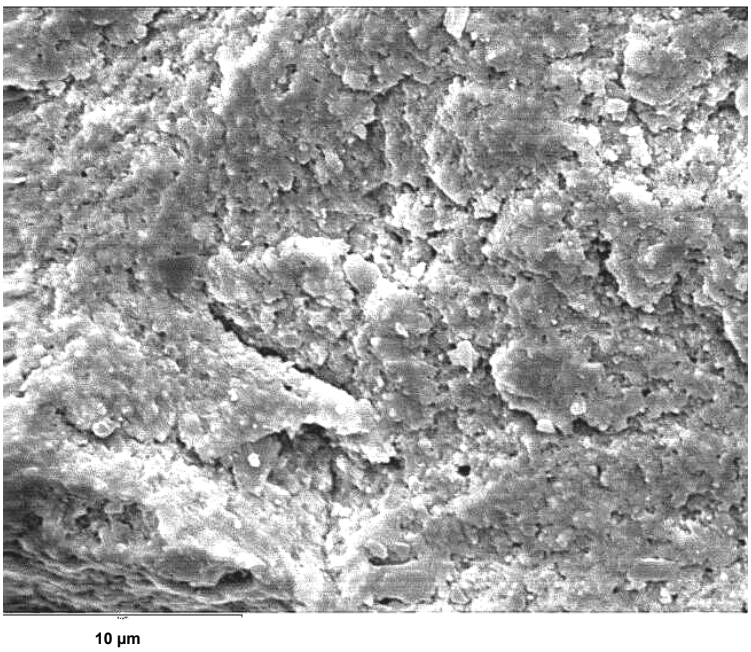

Figure 5.11. Fractured surface of low strength Cercon® specimen after BFS.

The fracture surface of high strength Cercon® had a smooth surface at the fracture origin which was the fracture mirror (Figure 5.12). The mist and hackle zones were located at the outer edges of the fracture mirror region. The high strength Cercon® had a similar fracture pattern to Lava™ specimens. No obvious porosity was found at the fracture origin area (Figure 5.13).

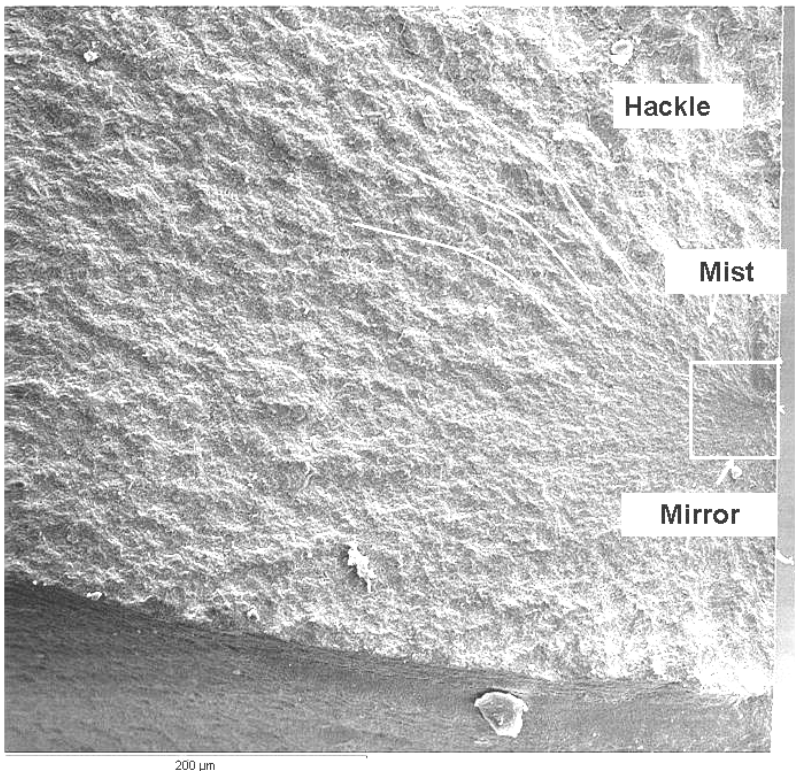

Figure 5.12. Fractured surface of high strength Cercon® specimen after BFS. The area within the square was investigated by using SEM at higher magnification (Figure 5.13).

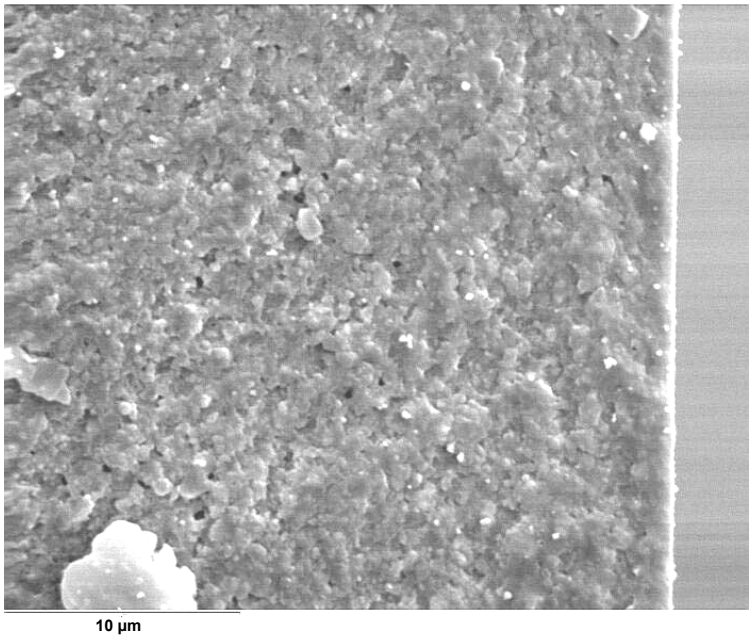

Figure 5.13. Fractured surface of high strength Cercon® specimen after BFS.

Figure 5.14-5.17 show the fractured surface of Invizion™ specimens that have failed at low and high forces. The low strength Invizion™ specimens fractured into two pieces while the high strength Invizion™ fractured into four pieces. The fractured surface of Invizion™ specimen failing at low strength differed from those that failed at high strength (Figure 5.14), Lava™ and Cercon® specimens. Several irregular crack lines were found on the surface. At higher magnification, large porosities were seen and this contrasted with specimens that failed at high strength, which had very small porosities (Figure 5.15).

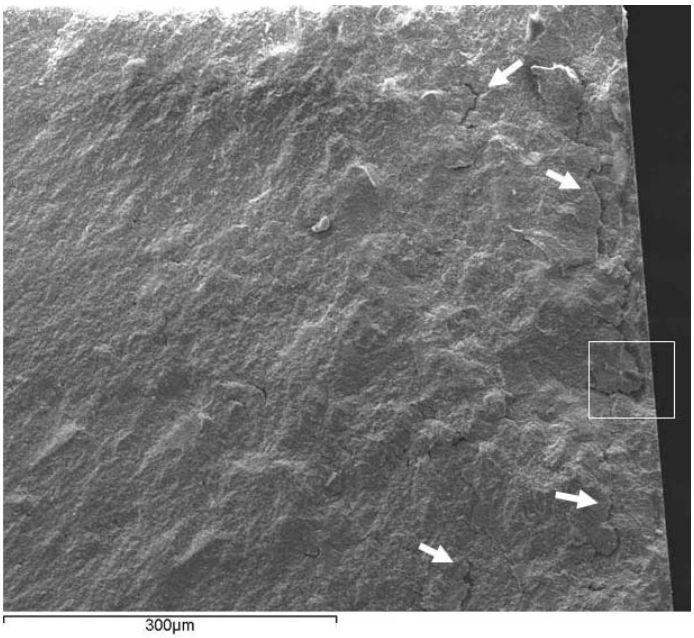

Figure 5.14. Fractured surface of low strength Invizion™ specimen after BFS. The area within the square was investigated by using SEM at higher magnification (Figure 5.15). The arrows pointed the crack lines on the surface.

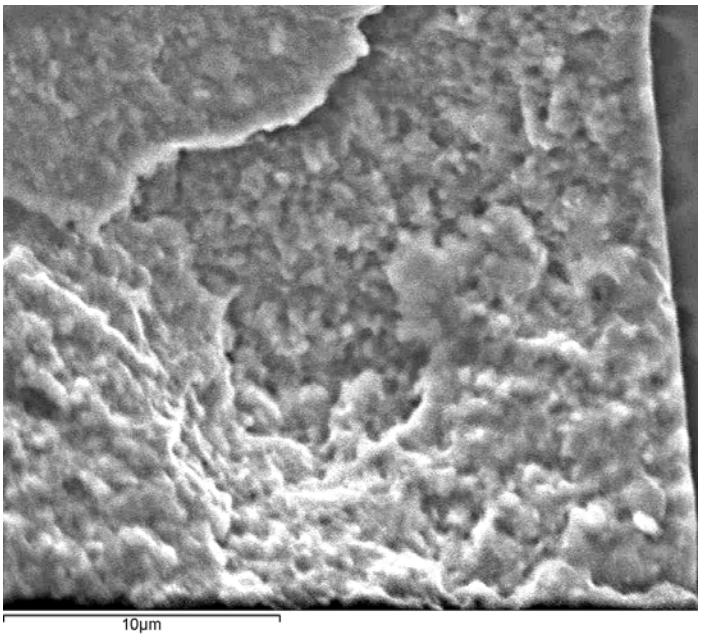

Figure 5.15. Fractured surface of low strength Invizion™ specimen after BFS.

The fracture pattern of Invizion™ specimens that had failed at high forces was different to Lava™ specimens failed at high forces in that the fracture mirror was not found in the centre of fracture origin (Figure 5.16). The centre of fracture origin was rough and there were several pores that occurred around that area (Figure 5.17).

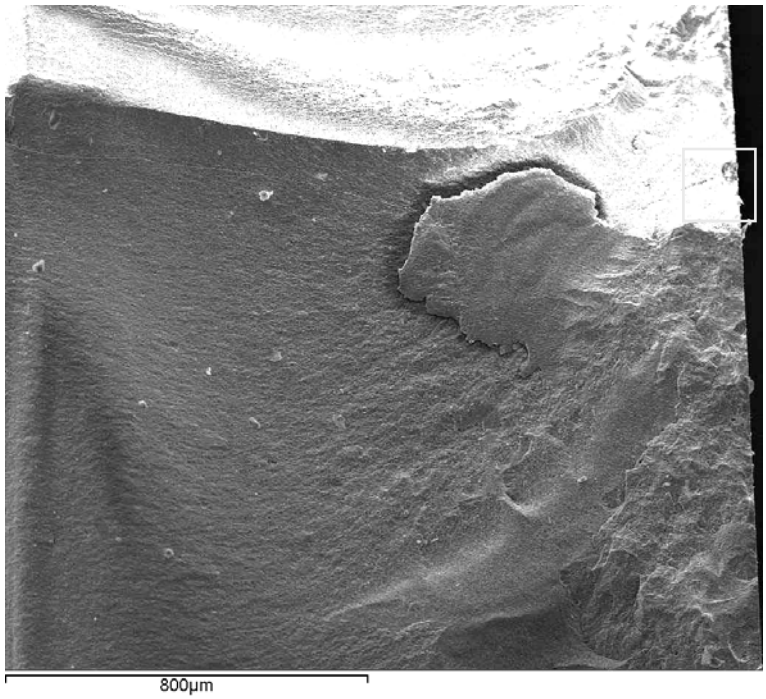

Figure 5.16. Fractured surface of high strength Invizion™ specimen after BFS. The square was the area that was investigated at higher magnification (10 µm).

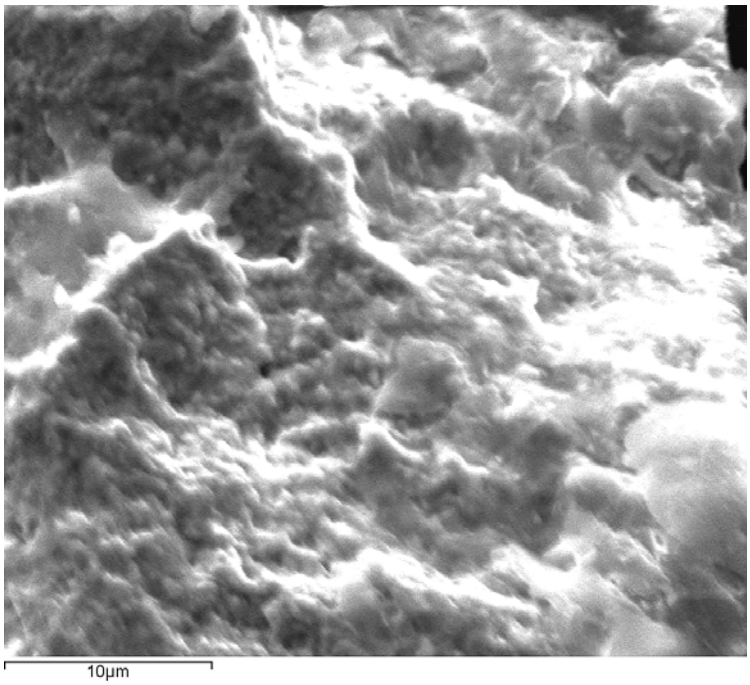

Figure 5.17. Fractured surface of high strength Invizion™ specimen after BFS.

The results from SEM analysis can be concluded that most of the specimens failed at the high force had a smooth surface or fracture mirror at the centre of fracture origin while the specimens failed at the low force had rough surfaces and more frequent porosities. Lava™ and Cercon® had similar fracture pattern while Invizion™ had more rough fracture surfaces and porosities compared with the other materials.

5.1.3 Fatigue properties

5.1.3.1 Fatigue followed by BFS on disc shaped specimen

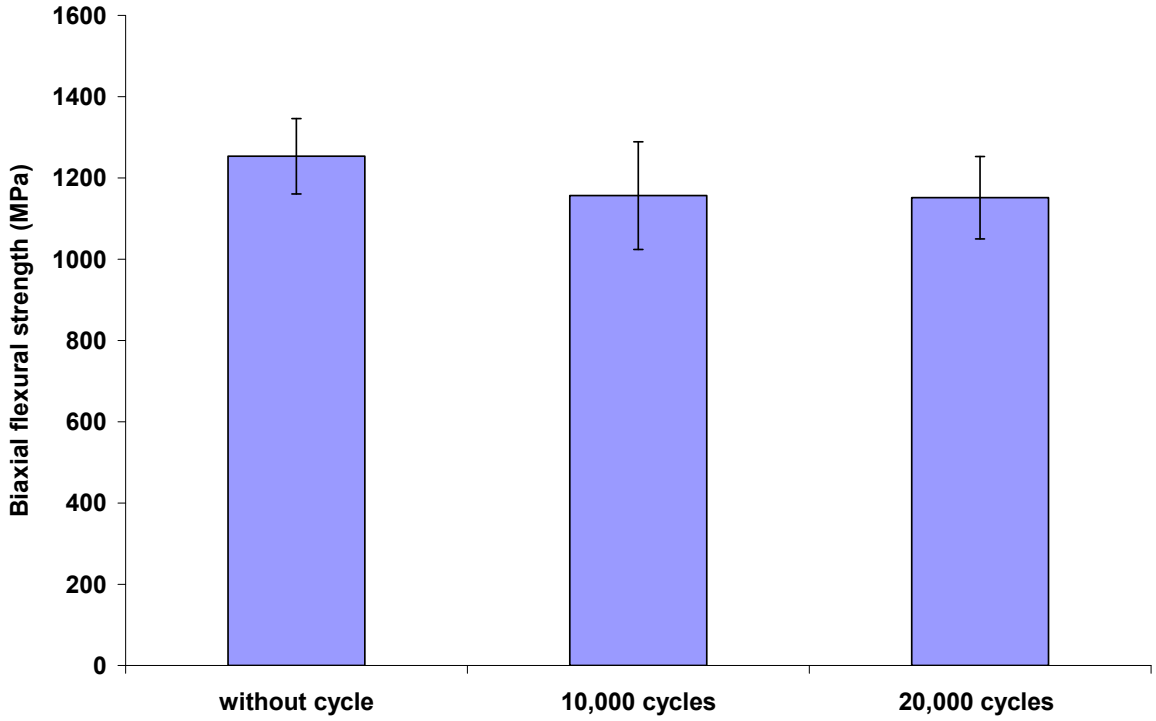

Figure 5.18. The mean biaxial flexural strength of uncoloured Lava™ specimens without and after fatigue test at 10,000 and 20,000 cycles.

Figure 5.18 shows the mean biaxial flexural strength of uncoloured Lava™ specimens without and after 10,000 and 20,000 load cycles, which were 1253 ± 93, 1156 ± 132, 1151 ± 101 MPa, respectively. The dynamic cycles at 10,000 and 20,000 cycles at a force of 25% of the mean biaxial flexural strength of uncoloured (~250 N), slightly decreased flexural strength values. However, one-way analysis of variance (ANOVA) showed no significant difference between groups (P>0.05). Therefore, it may be concluded that samples subjected to fatigue for 10,000 or

20,000 cycles at an applied force of 25% of the mean biaxial flexural strength showed no change in the biaxial flexural strength. These experiment values were used to guide the determination of force to be used in the fatigue (classical stress-number experiments) experiments to ≥ 50% of mean biaxial flexural strength and up to 500,000 cycles.

5.1.3.2 Fatigue life

a. Uncoloured

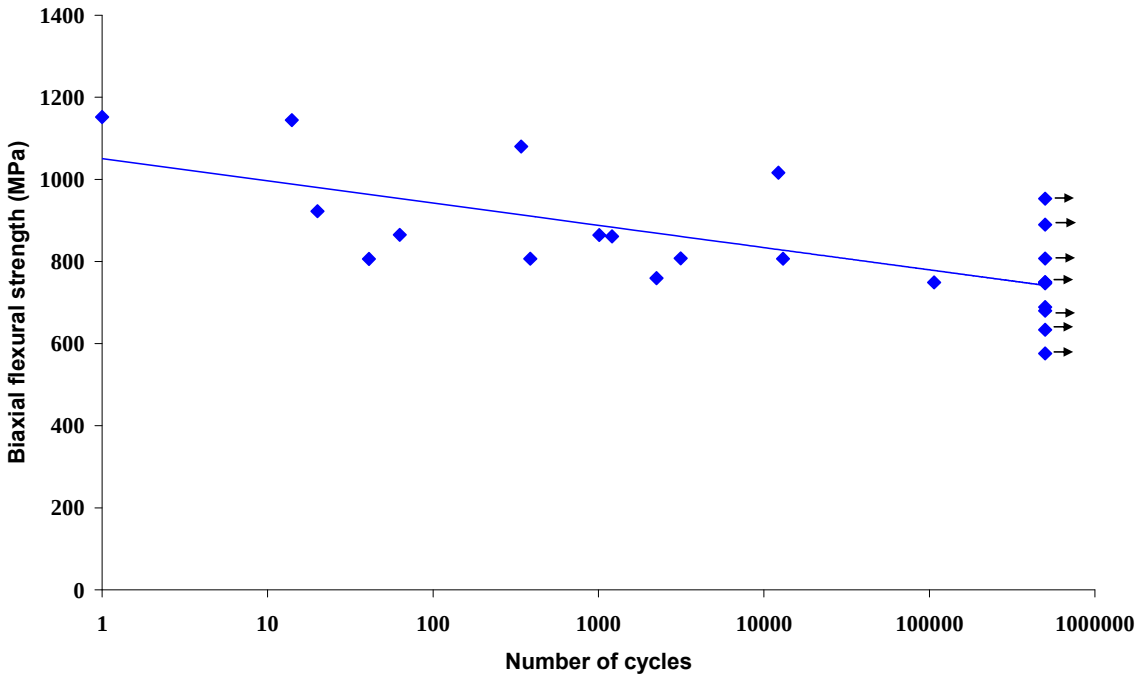

Figure 5.19. Fatigue of uncoloured Lava™ discs at a force of 50-90% mean biaxial flexural strength. Arrows indicate specimens that survived to the fatigue limit of 500,000 cycles.

In general, for all specimens (Figures 5.19-5.23), the data had a wide scatter as expected with brittle materials. Figure 5.19 shows that when using a fatigue force

of 65% of the mean biaxial flexural strength (~685 MPa) or lower, most specimens survived to 500,000 cycles. Conversely, when using a force above 65% of mean biaxial flexural strength, the failure of specimens occurred as seen in Figure 5.19 at a range of cycle numbers depending on the fatigue load. However, three specimens did not fail when using a higher force at 75% (953 MPa) and 70% (890 and 807 MPa), respectively. In addition, when the force was increased, the number of cycles needed to cause failure tended to be reduced, as expected.

b. FS4

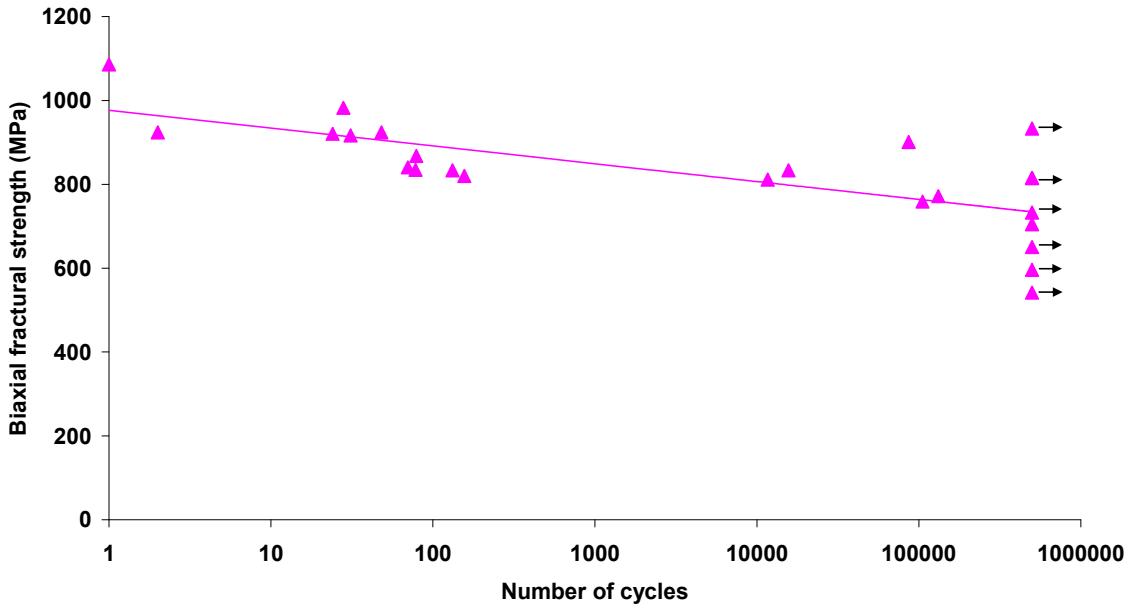

Figure 5.20. Fatigue of FS4 Lava™ discs at forces of 50-90% mean biaxial flexural strength.

Figure 5.20 shows that when using 65% of the mean biaxial flexural strength (~705 MPa) or lower, specimens survived to 500,000 cycles. Conversely, when using a force above 65% of mean biaxial strength, the fracture of specimens

occurred as seen in Figure 5.20. Only a few specimens survived to 500,000 cycles when using a high force above 800 MPa. The trend of the fatigue graph in general is that when the force was increased, the number of cycles needed to cause failure tended to be reduced.

c. FS 7

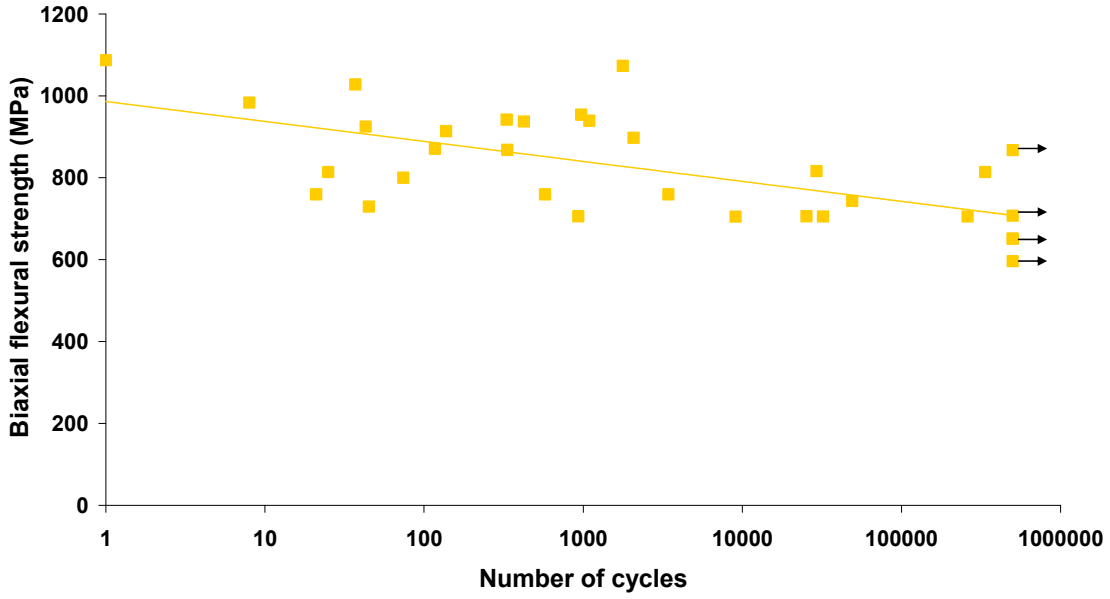

Figure 5.21 Fatigue of FS7 Lava™ discs at forces of 50-90% mean biaxial flexural strength.

Figure 5.21 shows that when using 60% of the mean biaxial flexural strength (~651 MPa) specimens survived to 500,000 cycles. Conversely, when using a force above 60% of the mean biaxial strength, fracture of specimens occurred as seen in Figure 5.21. Only two specimens did not fail at 65% and 75% of mean biaxial flexural strength.

d. Cercon®

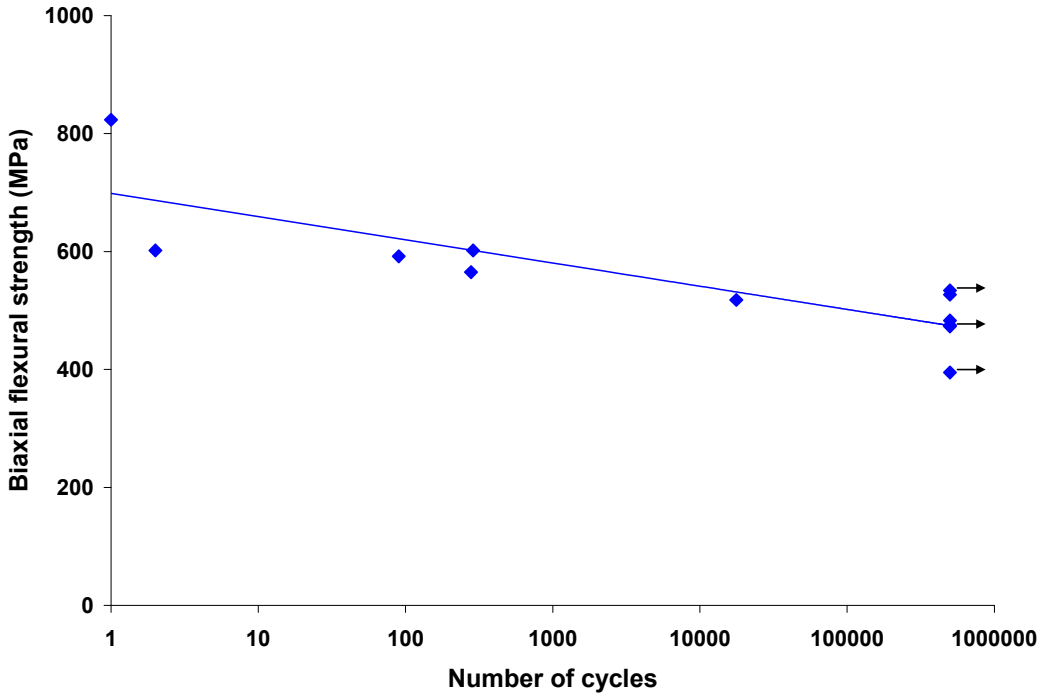

Figure 5.22. Fatigue of Cercon® discs at forces of 60-90% mean biaxial flexural strength.

Figure 5.22 shows that when using a force of 70% mean biaxial flexural strength (~575 MPa) or lower, Cercon® specimens survived to 500,000 cycles. Conversely, when using a force above 70% of mean biaxial strength, the fracture of specimens occurred as seen in Figure 5.22. Only one specimen survived at 500,000 cycles when using a force at 75% of mean biaxial flexural strength (~617 MPa). It should be noted (and can clearly be seen) that a reduced number of specimens were available for this test.

e. Invizion™

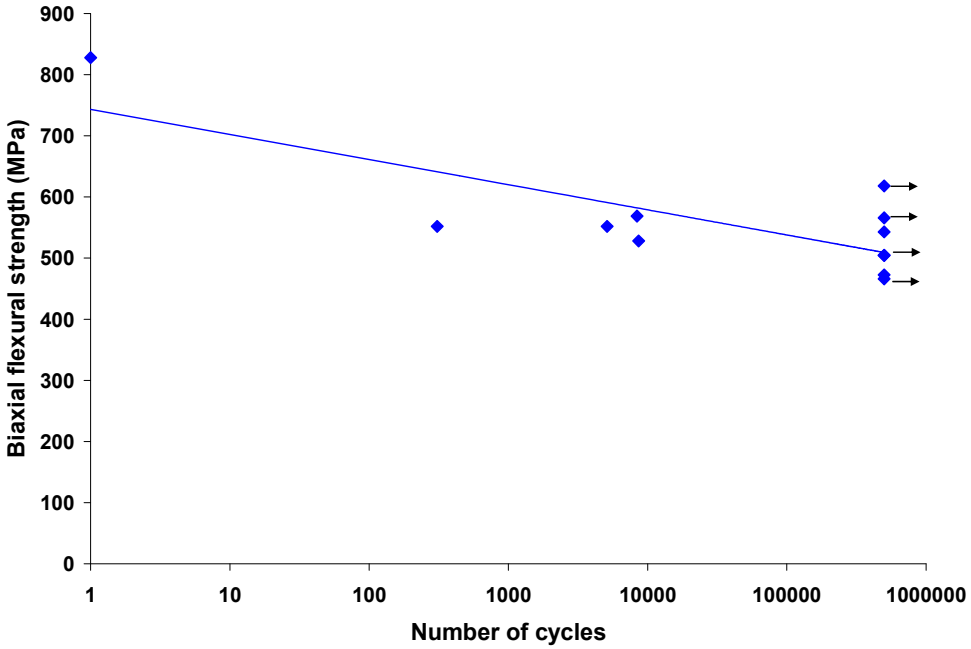

Figure 5.23. Fatigue of Invizion™ discs at forces of 60-80% mean biaxial flexural strength.

Figure 5.23 shows that when using 65% of the mean of the biaxial flexural strength (~526 MPa) or lower, Invizion™ specimens survived to 500,000 cycles. Conversely, when using a force above 65% of mean biaxial strength, the fracture of specimens occurred as seen in Figure 5.23. Only a few specimens survived at 500,000 cycles when using a force at 70% of mean biaxial flexural strength.

From these fatigue results, it can be concluded that zirconia specimens survived to the 500,000 cycle limit when using a force of 60-65% of the mean biaxial flexural strength. Lava™ specimens had higher fatigue life values at 500,000 cycles (~650-700 MPa) than Cercon® (575 MPa) and Invizion™ (526 MPa) and Invizion™ specimens had the lowest fatigue life value at 500,000 cycles.

5.1.3.3 Fracture analysis of Lava™, Cercon® and Invizion™specimens after fatiguing

a. Uncoloured specimen fatigued at a force of 75% of the mean biaxial flexural strength

The fracture surface of specimens that failed during fatigue had a rough surface and there were several crack lines present. (Figure 5.24 at higher magnification) Hackle lines were deeper compared with the fracture surface failed from biaxial flexural strength testing. The fracture pattern did not showed any evidence of fatigue lines.

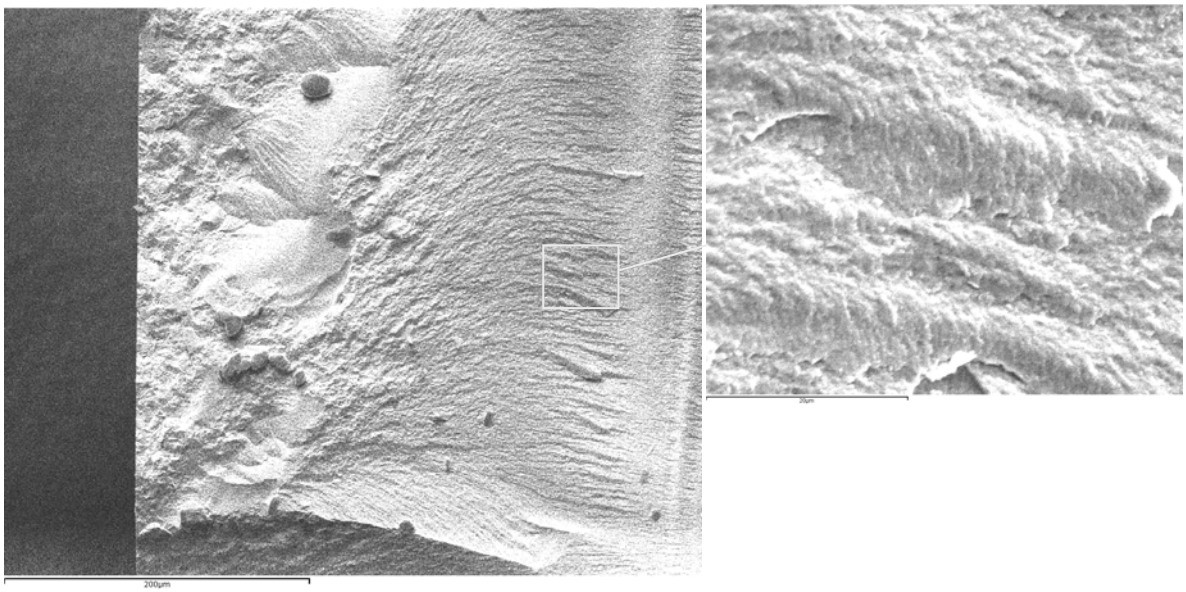

Figure 5.24. The fractured surface of uncoloured Lava™ failed from fatigue test using 75% of mean biaxial flexural strength.

b. FS7 specimen fatigued using a force of 70% of the mean biaxial flexural strength

The fracture pattern of a representative FS7 specimen seen in figure 5.25 was different from other specimens failed from fatigue in that the crack lines were deep on the surface (Figure 5.25). The fracture surface was not flat and therefore, it was difficult to investigate at higher magnifications.

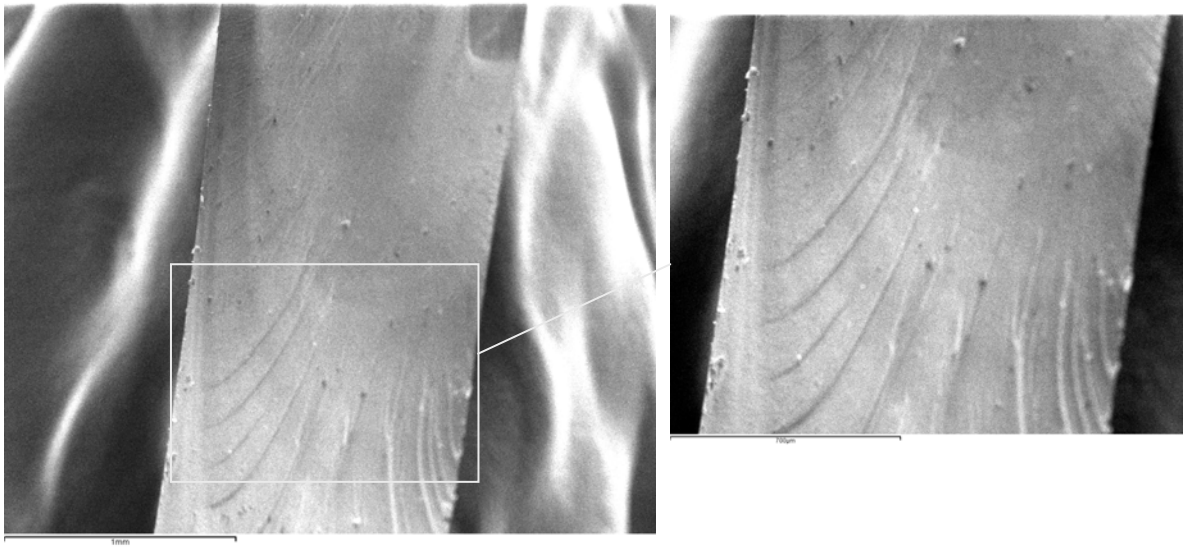

Figure 5.25. The fractured surface of FS7 Lava™ failed during fatigue testing at a force of 70% of mean biaxial flexural strength.

c. Cercon® specimen using a force 70% of mean biaxial flexural strength

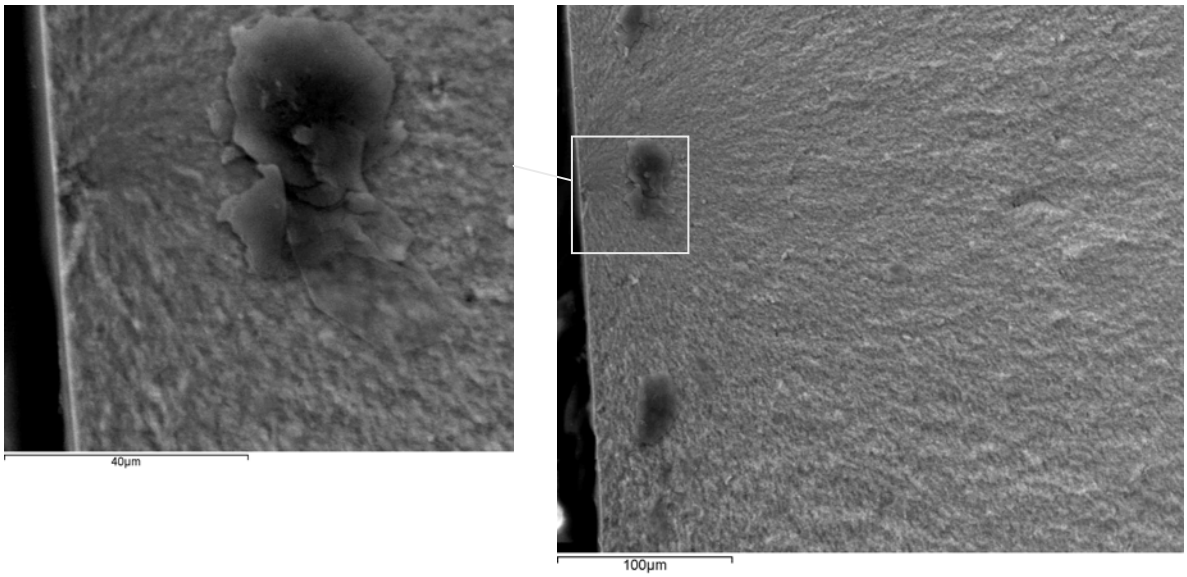

Figure 5.26. The fractured surface of Cercon® during fatigue testing using a force of 70% of the mean biaxial flexural strength. The image on the left presented voids at the fracture origin.

All Cercon® specimens fractured into two pieces. The representative SEM image presents the fracture origin and surrounding area (Figure 5.26). The fracture origin has a mirror-like region in the centre and the surface is smooth. The higher magnification image (on the left) showed the defect located at the load surface. The fracture pattern of the specimens failed from the fatigue was not different from those failed from the biaxial flexural strength testing.

d. Invizion™ specimen fatigued using a force of 70% of the mean biaxial flexural strength

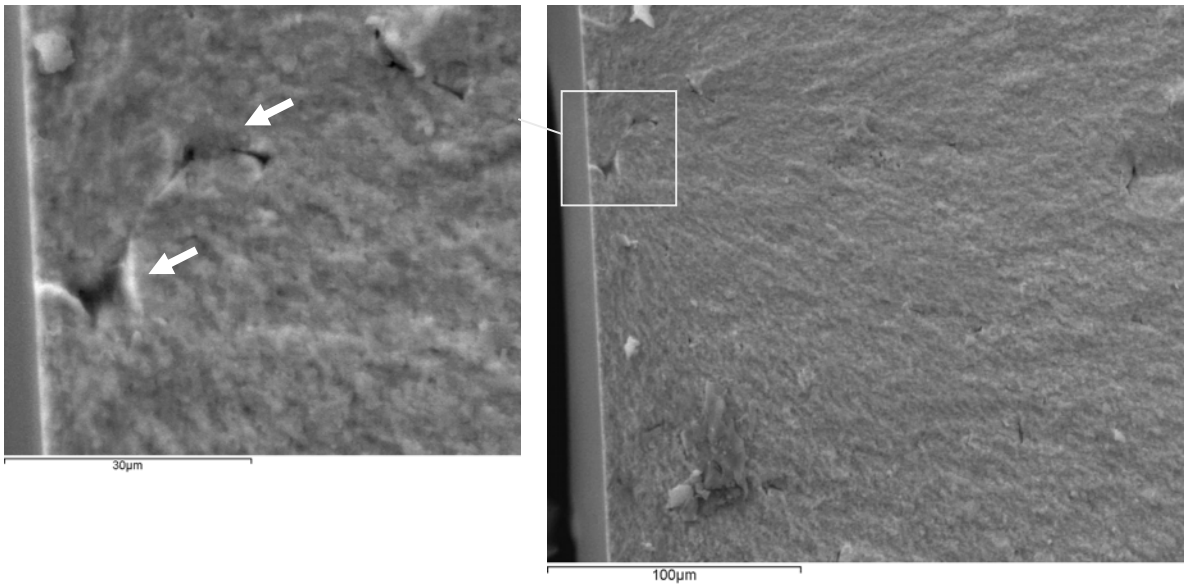

Figure 5.27. The fractured surface of Invizion™ failed during fatigue testing at a force of 70% of the mean biaxial flexural strength.

All Invizion™ specimens fractured into two pieces. The representative SEM image presents the fracture origin and the surrounding area (Figure 5.27). The large porosity was seen at the fracture origin area, which can be seen at the image on the left. The fracture pattern of the specimens failed from fatigue was not different from those fractured from the biaxial flexural strength test.

Therefore, the fracture pattern of the specimens that failed during fatigue testing was not different from those having undergone biaxial flexural strength testing. However, the fracture pattern of Lava™ groups had rougher surfaces and deeper crack lines, which was slightly different from others. The fracture pattern of

Cercon® and Invizion™ differed from Lava because they usually fractured into two pieces during fatigue testing, whilst Lava™ fractured into three or more pieces. The porosities and flaws may influence the premature failure of the Cercon® and Invizion™ specimens.

5.1.3.4 Fatigue followed by BFS on crown shaped specimens

Data from fatigue and fracture strength testing showed a normal distribution (P=0.095). The results from the fracture testing are listed in Table 5.3. There was no statistically significant difference in the mean failure load between heat pressed and sintered groups, using the Bonferrroni t-test (P>0.05).

Table 5.3. The fatigue and fracture testing results

Group Name	Number of specimen	Mean (N)	SD (N)
Group 1 (Heat pressed)	25	2135.6	330.1
Group 2 (Sintered)	25	2189.9	317.6

The results of the Weibull regression analysis are listed in Table 5.4. Both the specimen groups were good fits to the regression used, according to the difference between the coefficient of determination (r^2) values and the comparison with the 90% critical correlation coefficient (CCC). No statistically significant difference was identified in the Weibull modulus and characteristic failure load values between the two groups according to the overlap of their confidence intervals (C.I.) at the 95% level. The distribution of values was very similar between the two groups.

The two types of processing techniques, hot pressed and sintered methods, did not affect the biaxial flexural strength after fatigue of zirconia.

Table 5.4. Results of the Weibull regression analysis

Group	*m* Value	σ 0.01	σ 0.05	σ 0.10	r^2	σ_o	C.I. (95%) for σ_o	C.I. (95%) for m
Group 1	7.1	1193	1500	1660	0.94	2276.7	2167-2390	5.3-9.4
Group 2	7.7	1280	1582	1737	0.98	2325.9	2223-2433	5.8-10.1

Where m Value= Weibull modulus, σ 0.01, σ 0.05, σ 0.10= stress levels at 1%, 5% and 10% probability of failure, r^2= regression coefficient, σ_o=characteristic failure load, C.I.= Confidence Intervals.

5.1.3.5 Secondary electron imaging of the fractured specimens

Ninety two percent of the fractured heat pressed specimens (Group 1) demonstrated cohesive failure within the veneering material, while there was no fracture in the zirconia core. The crack origin was located at the centre of the occlusal surface, at the point of loading by the indenter (Figure 5.28) as expected. The fracture surface had a scalloped appearance, presenting mirror, mist and hackle regions. Secondary Wallner lines were formed in most of the crown shapes as the crack front propagated along their long axes to the margin. In addition, two specimens exhibited delamination of the veneering material and exposure of the zirconium core at the margin (Figure 5.29). Sixty percent of the crown shapes fractured in five or more pieces (5-6) while forty percent fractured in four or less (2-4).

The sintered specimens (Group 2) demonstrated similar failure patterns to the heat pressed ones. Observation of the fracture surfaces showed no signs of major interfacial failure between the core and the veneer material. The zirconia core did not fracture under the applied stress (Figure 5.30). In most of the crown shapes the crack originated from the centre of the occlusal surface and propagated evenly along their long axes involving most of the axial walls and the margins (Figure 5.30). Wake hackle markings were formed as the crack front passed small spherical voids present in the bulk of the material, indicating the direction of the crack growth (Figure 5.31). Forty percent of the specimens fractured in six or more pieces (6-9) while sixty per cent fractured in five or less (2-5).

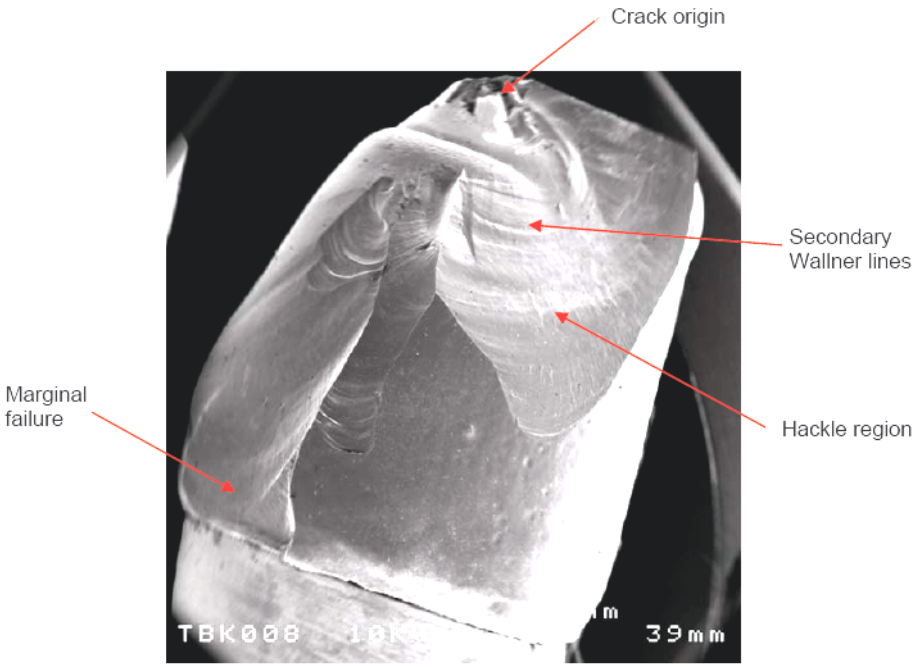

Figure 5.28. SEM photomicrograph of a fractured heat pressed crown shape.

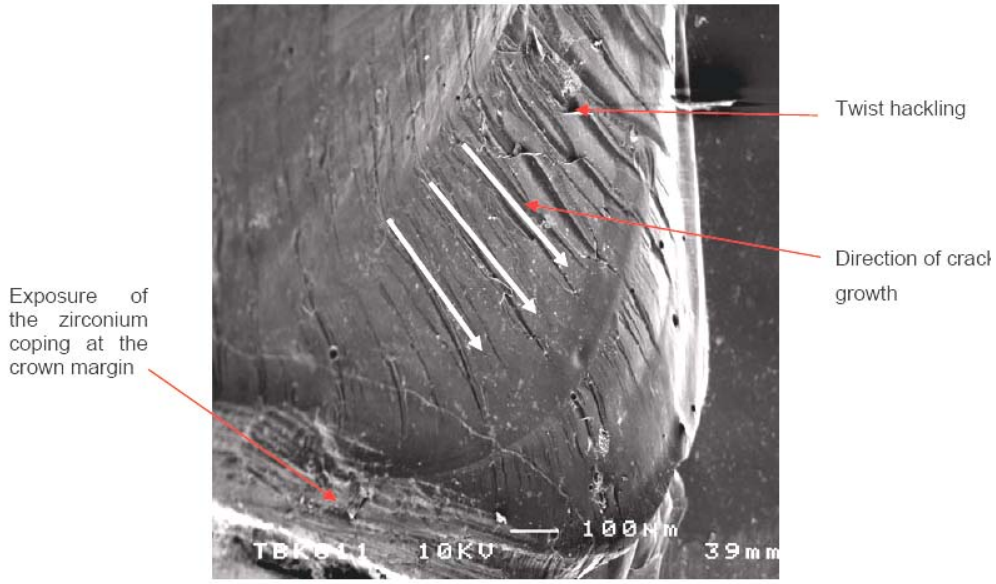

Figure 5.29. SEM photomicrograph of a heat pressed specimen showing marginal failure and major hackling.

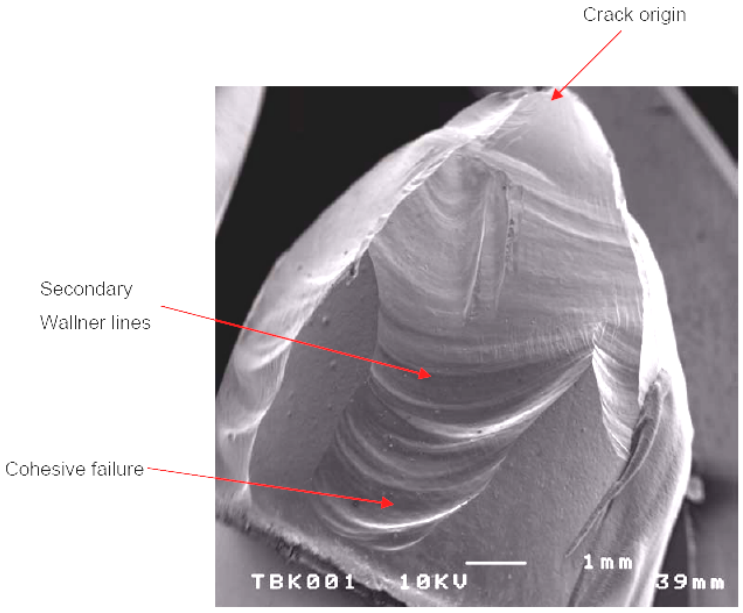

Figure 5.30. SEM photomicrograph of a sintered specimen showing cohesive failure limited to the veneering material.

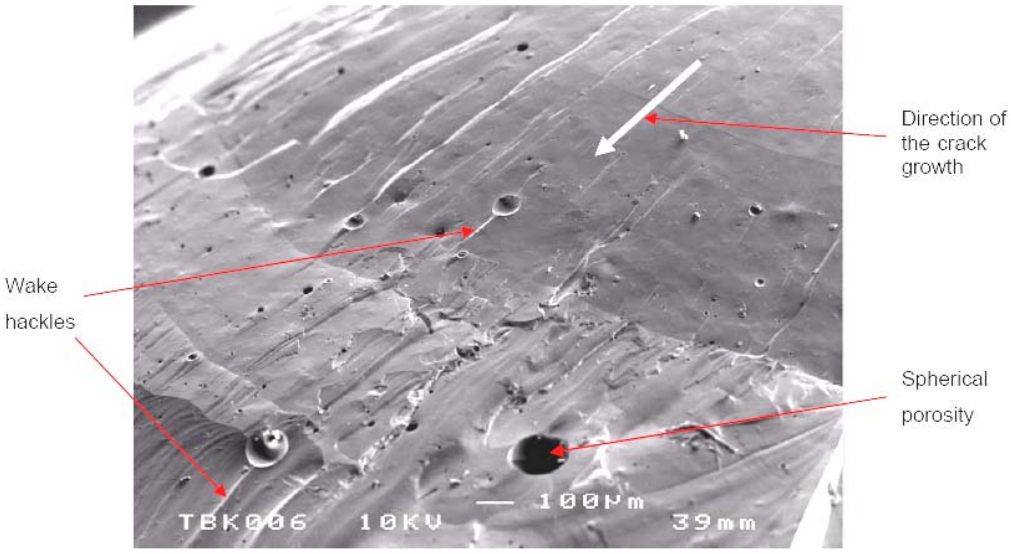

Figure 5.31. SEM photomicrograph of wake hackles in a sintered specimen, indicating the direction of the crack growth (white arrow).

5.1.3.6 Secondary electron imaging of the microstructures

The SEM photomicrographs of sintered, polished and thermally etched Y-TZP coping are shown in Figure 5.32, illustrating a dense dispersal of zirconium grains (mean ± SD) 0.16 ± 0.14 μm^2 present. The fractional area of these grains exceeded the 95% of the total area measured.

The microstructure of the IPS e.max® Ceram veneering material revealed the presence of angular fibre containing particles (mean ± SD) 555.9 ± 758.3 μm^2, with a particle range of 125.5-3414.4 μm^2, within the glassy matrix and some spherical porosities (Figure 5.33). The fractional area of these particles was 8.5%. Domains of

fine fibres in the nanometre range were also distributed within the particles and the glassy matrix.

Secondary electron imaging of the IPS e.max® ZirPress veneering material, revealed the presence of areas with higher density interspersed within the glassy matrix that did not have a definitive outline and also some spherical porosities. These areas displayed a high density of larger fibres than the sintered veneering material that have been found along longitudinal axis (mean ± SD) 0.19 ± 0.08 μm^2 and fine fibres (Figure 5.34). These larger fibres have been measured to be (mean ± SD) 1.18 ± 0.55 μm in length. In the higher magnification, a dense dispersal of randomly oriented fine fibres (mean ± SD) 73.70 ± 24.40 nm in length can also be identified (Figure 5.35).

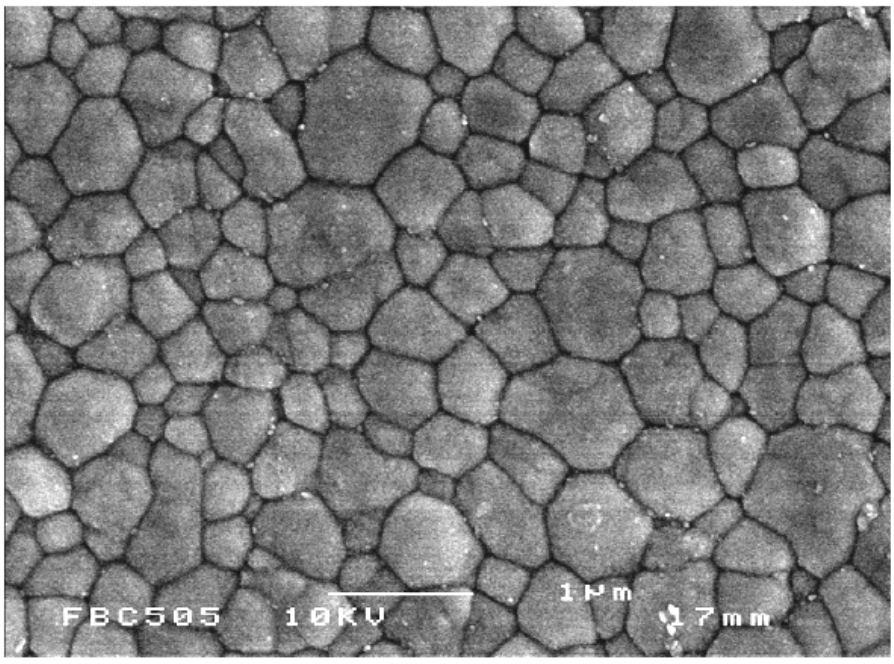

Figure 5.32. SEM photomicrograph of the Y-TZP core at a higher magnification showing zirconia grains (mean ± S.D) 0.16 ± 0.14 μm^2 present.

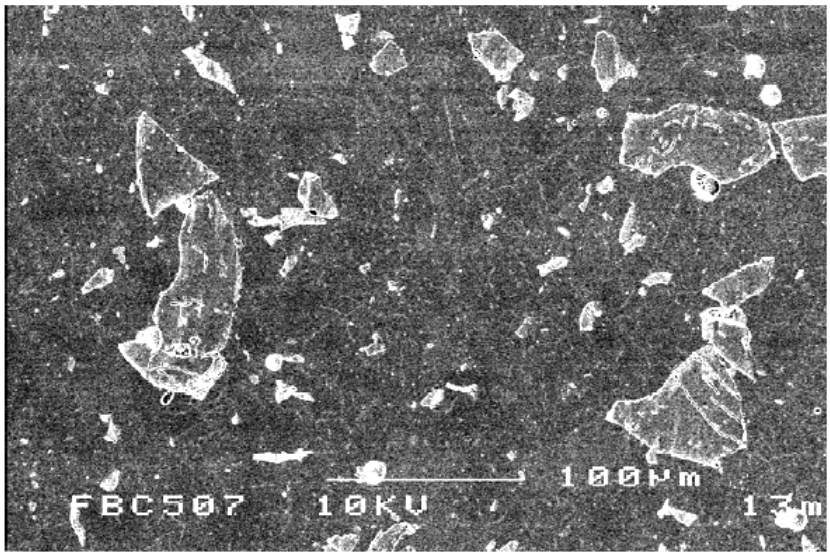

Figure 5.33. SEM photomicrograph of the IPS e.max® Ceram veneering material showing particles (mean ± SD) 555.9 ± 758.27 µm^2 and some spherical porosity.

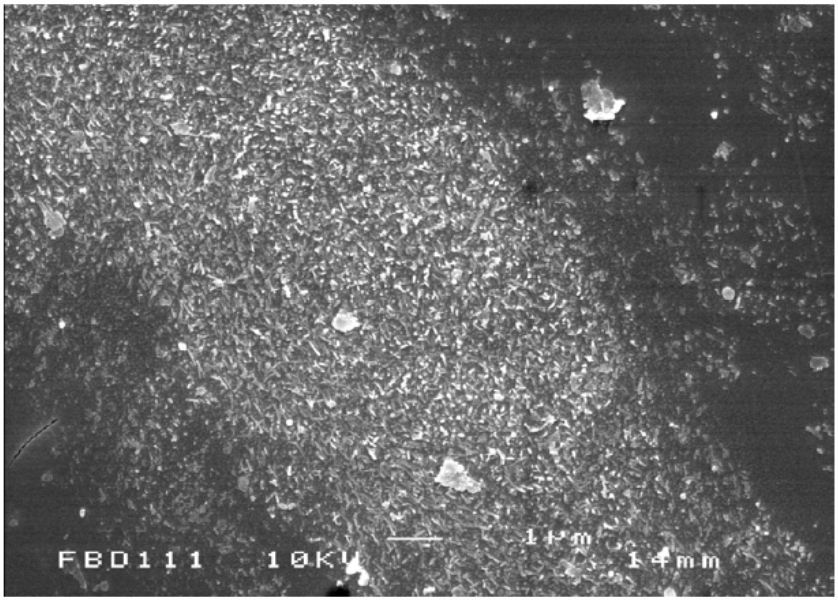

Figure 5.34. Higher magnification of a dense area showing the high content of randomly oriented fibres of different sizes present in the IPS e.max® ZirPress veneering material.

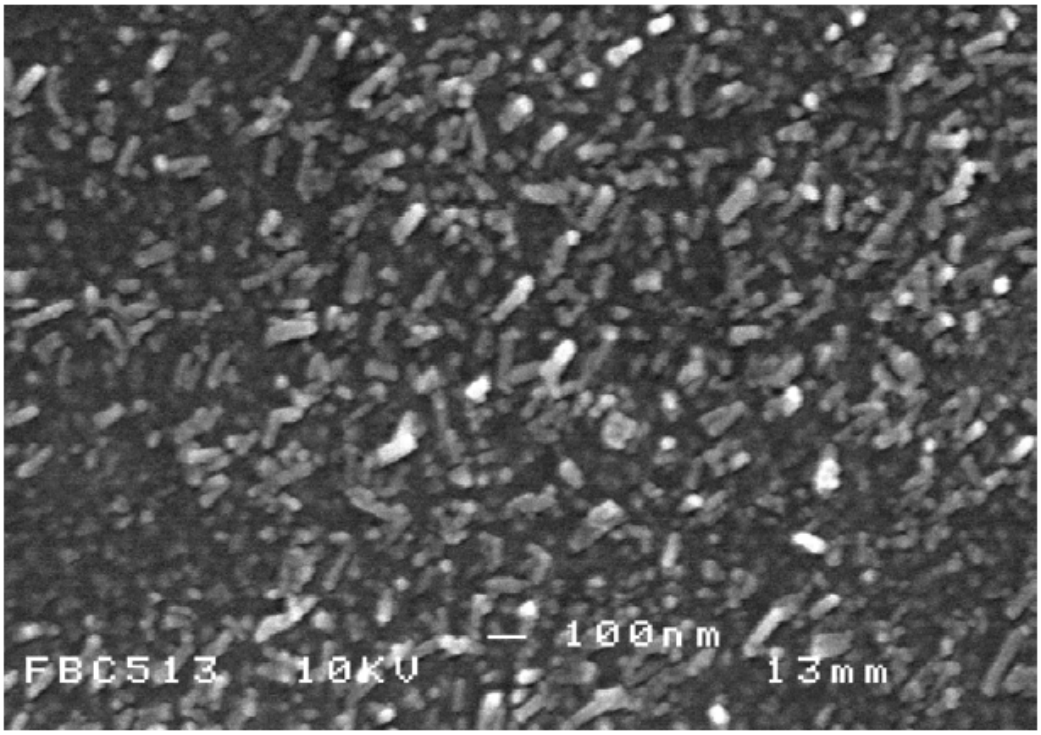

Figure 5.35. SEM photomicrograph of the IPS e.max® ZirPress veneering material, showing a dense distribution of fibres (mean ± SD) 73.70 ± 24.40 nm in length within the glassy matrix.

5.1.4 Subcritical crack growth

5.1.4.1 Uncoloured specimens

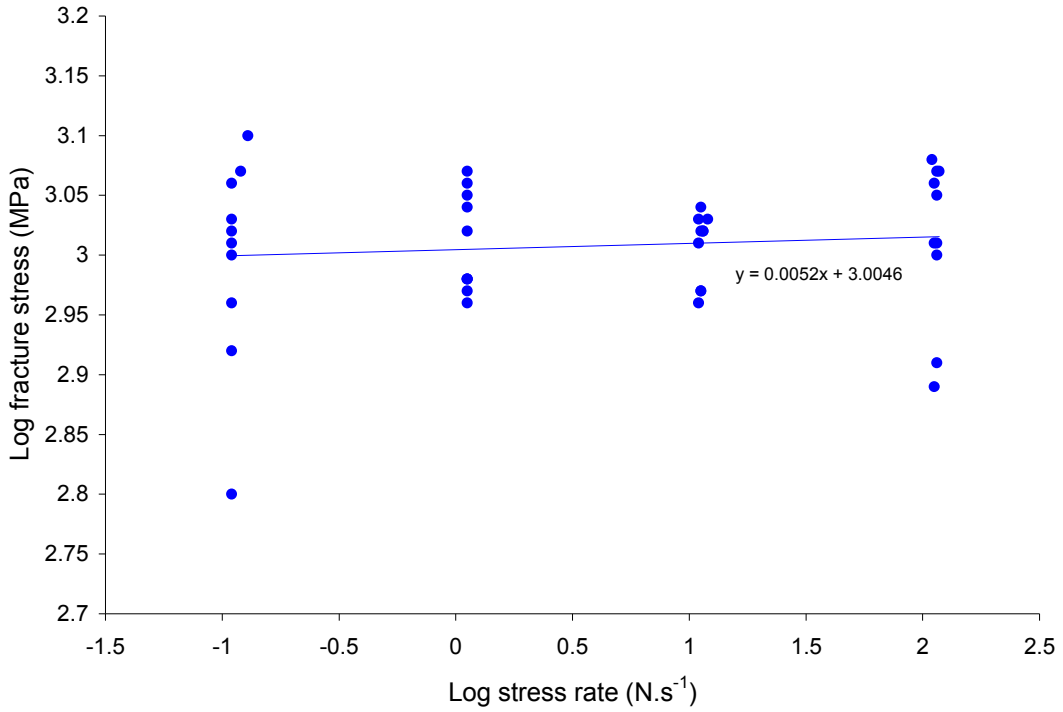

Figure 5.36. The stress-rate-flexural strength curve with the best-fit regression line for uncoloured specimens

Subcritical crack growth was performed to characterise the susceptibility of the material to subcritical crack growth and its ability to support spontaneous mechanical loading. In addition, susceptibility to loss of strength under load in particular environments can be compared using subcritical crack growth parameters.

In general, when the stress rate ($N.s^{-1}$) was decreased, the fracture stress (MPa) tended to be reduced. Figure 5.36 shows the slope of graph for uncoloured specimens, which was 0.0052. Therefore, subcritical crack growth parameter n calculated from n=1/(S-1) was 197 and constant B_0 which was intercept log B_0 at log=0 was 3.0046 $m.s^{-1}$.

5.1.4.2 FS1

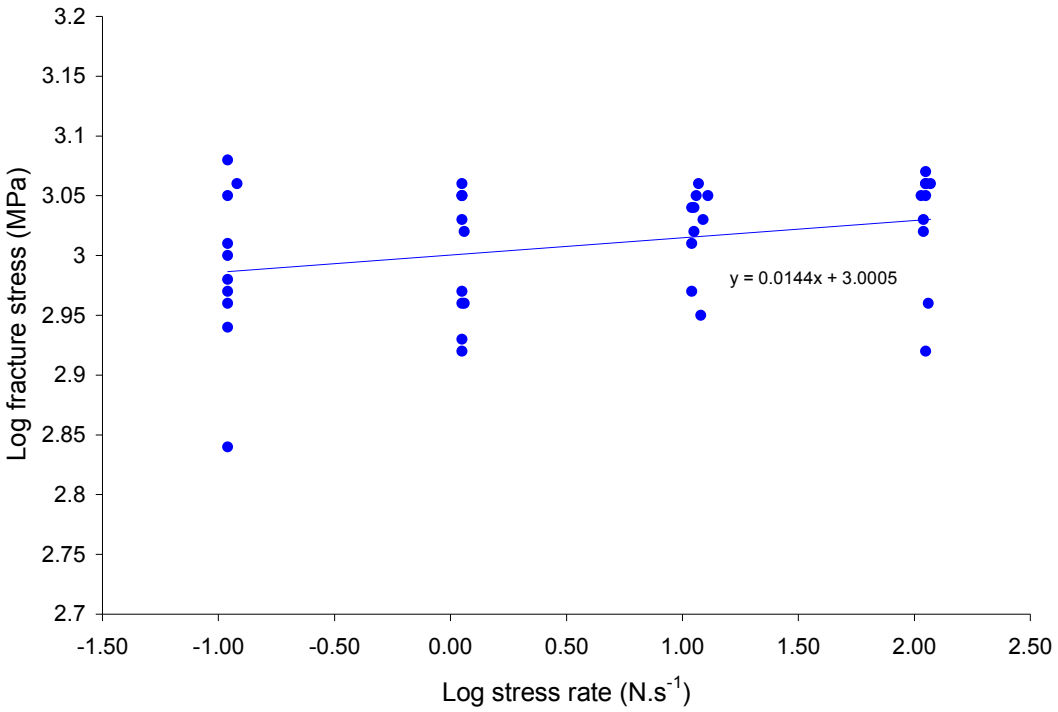

Figure 5.37. The stress-rate-flexural strength curve with the best-fit regression line of FS1 specimens

Figure 5.37 shows the slope of FS1 graph which was 0.0144. Therefore, subcritical crack growth parameter n was 68.44 and constant B_0 was 3.0005 $m.s^{-1}$.

5.1.4.3 FS2

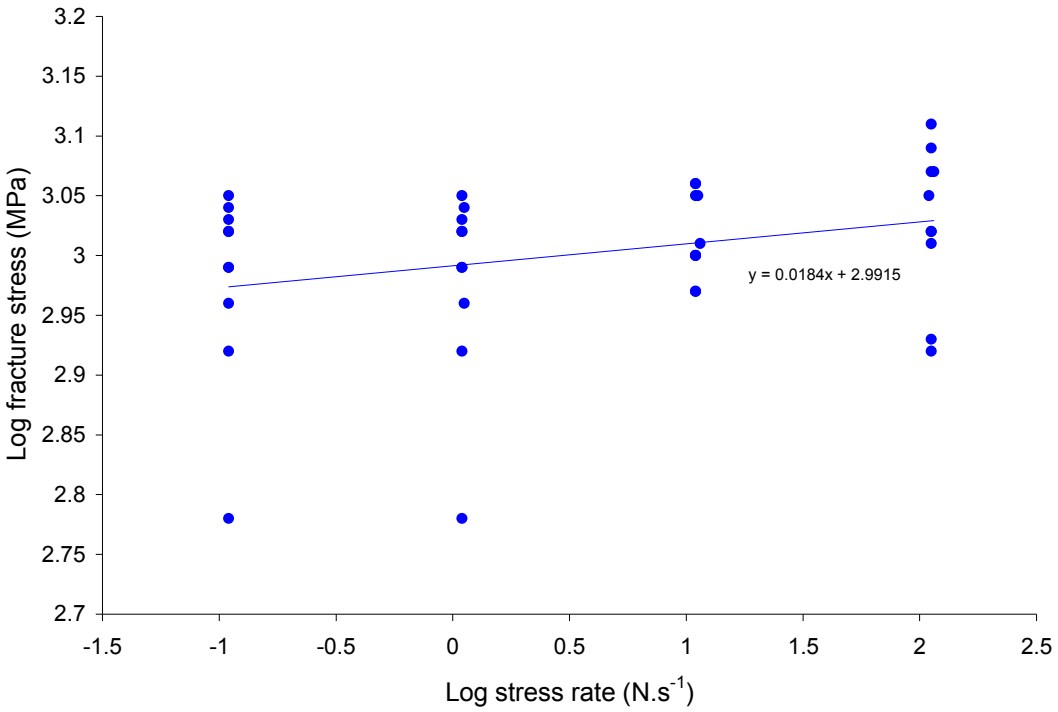

Figure 5.38. The stress-rate-flexural strength curve with the best-fit regression line of FS2 specimens

Figure 5.38 shows the slope of FS2 graph which was 0.0184. Therefore, subcritical crack growth parameter n was 53.35 and constant B_0 was 2.9915 $m.s^{-1}$.

5.1.4.4 FS3

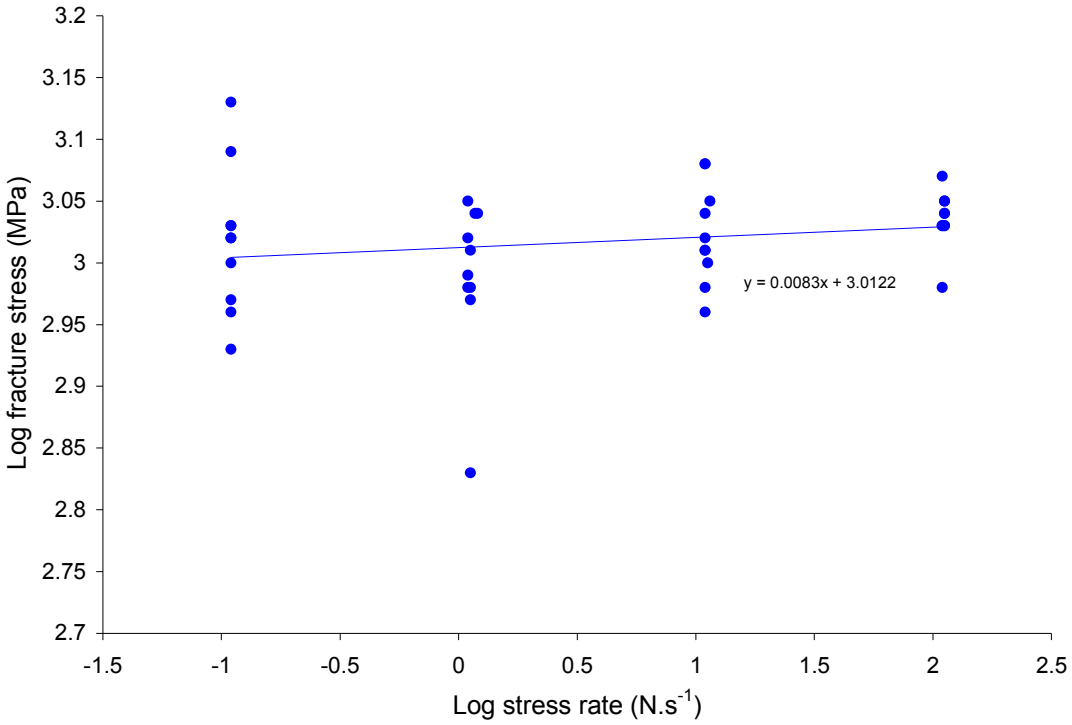

Figure 5.39. The stress-rate-flexural strength curve with the best-fit regression line of FS3 specimens

Figure 5.39 shows the slope of FS3 graph which was 0.0083. Therefore, subcritical crack growth parameter n was 119.48 and constant B_0 was 3.0122 $m.s^{-1}$.

5.1.4.5 FS4

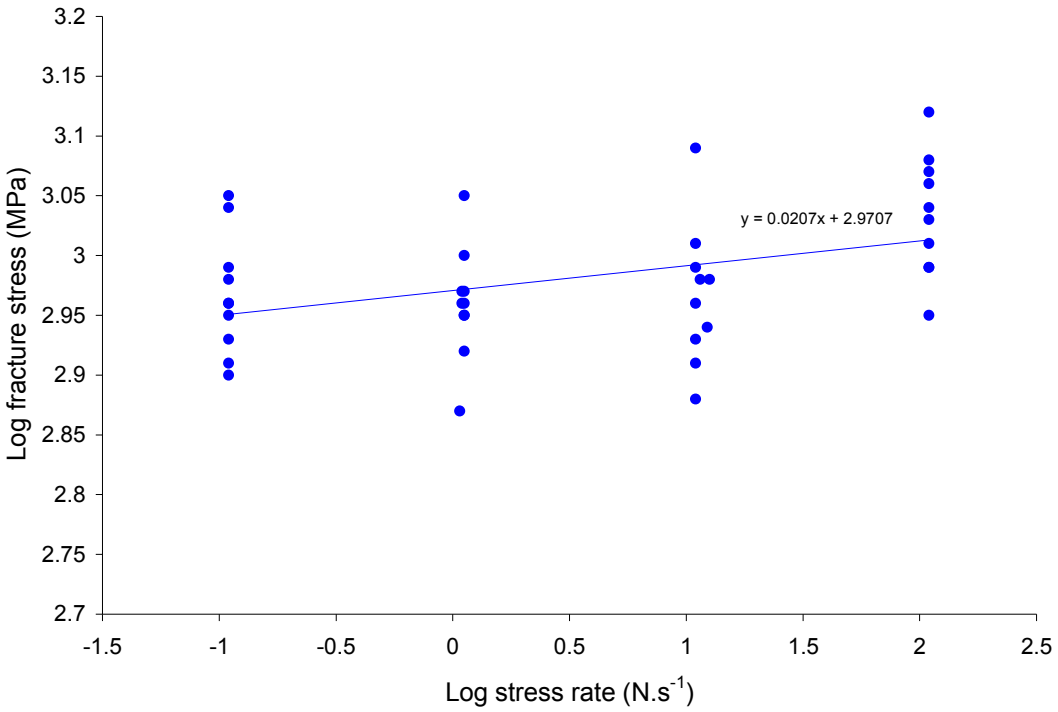

Figure 5.40. The stress-rate-flexural strength curve with the best-fit regression line of FS4 specimens

Figure 5.40 shows the slope of FS4 graph which was 0.0207. Therefore, subcritical crack growth parameter n was 47.31 and constant B_0 was 2.9707 $m.s^{-1}$.

5.1.4.6 FS5

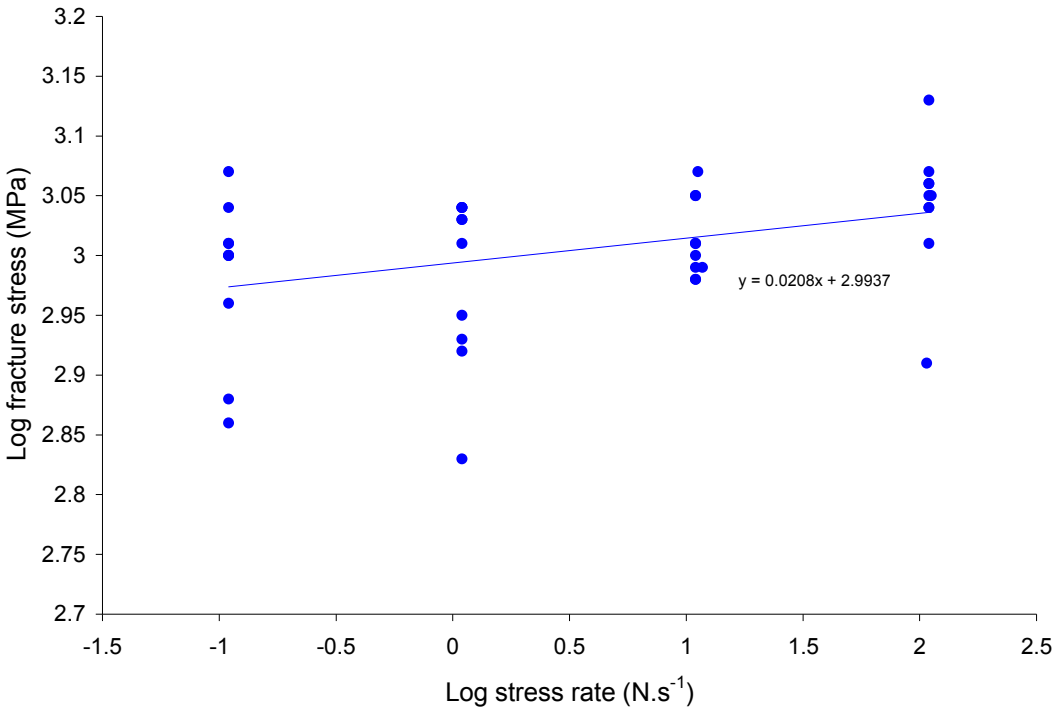

Figure 5.41. The stress-rate-flexural strength curve with the best-fit regression line of FS5 specimens

Figure 5.41 shows the slope of FS5 graph which was 0.0208. Therefore, subcritical crack growth parameter n was 47.08 and constant B_0 was 2.9937 $m.s^{-1}$.

5.1.4.7 FS6

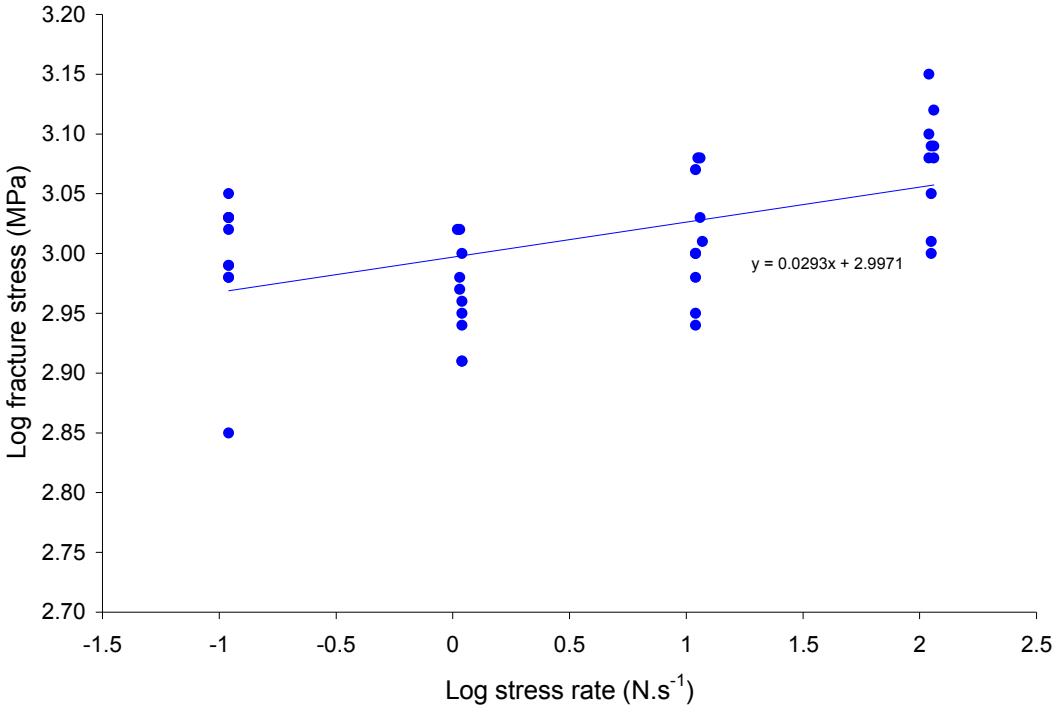

Figure 5.42. The stress-rate-flexural strength curve with the best-fit regression line of FS6 specimens

Figure 5.42 shows the slope of FS6 graph which was 0.0293. Therefore, subcritical crack growth parameter n was 33.13 and constant B_0 was 2.9971 $m.s^{-1}$.

5.1.4.8 FS7

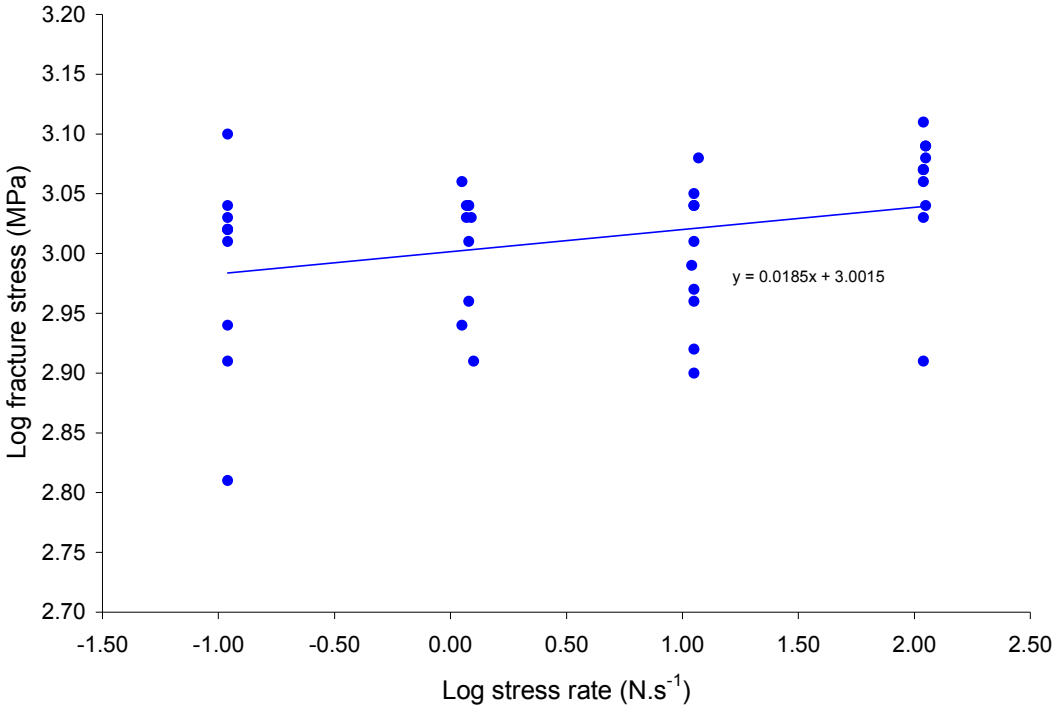

Figure 5.43. The stress-rate-flexural strength curve with the best-fit regression line of FS7 specimens

Figure 5.43 shows the slope of FS7 graph which was 0.0185. Therefore, subcritical crack growth parameter n was 53.05 and constant B_0 was 3.0015 $m.s^{-1}$.

Table 5.5. Summary of the parameters n and B_0 of Lava™ specimens

Groups	n	B_0 ($m.s^{-1}$)
Uncoloured	197	3.0046
FS1	68.44	3.005
FS2	53.35	2.9915
FS3	119.48	3.0122
FS4	47.31	2.9707
FS5	47.08	2.9937
FS6	33.13	2.9971
FS7	53.05	3.0015

Table 5.5 shows the values of parameter n and B_0 of Lava™ specimens. The uncoloured group had the highest parameter n compared with others which means it has a very high resistance to subcritical crack growth. Other groups had similar n parameters except FS3 which had very high n value. All groups had similar B_0 constant. The constant B_0 related to A_0 which is the constant in meters per second and co responses with crack growth velocity (v) as the equation follow:

$$v = A_0\left(\frac{K_I}{K_{IC}}\right) \qquad 5.1$$

where

v is the velocity of the growing crack in metres per second;

A_0 is a constant in metres per second;

K_I is the critical stress intensity factor developed at the crack tip by the applied stress in Megapascals metres1/2;

K_{IC} = critical stress intensity factor at the crack tip required to cause instantaneous crack propagatio.

5.1.4.9 Fracture analysis of uncoloured and FS6 Lava™ specimens failed after subcritical crack growth test using SEM

a. Uncoloured

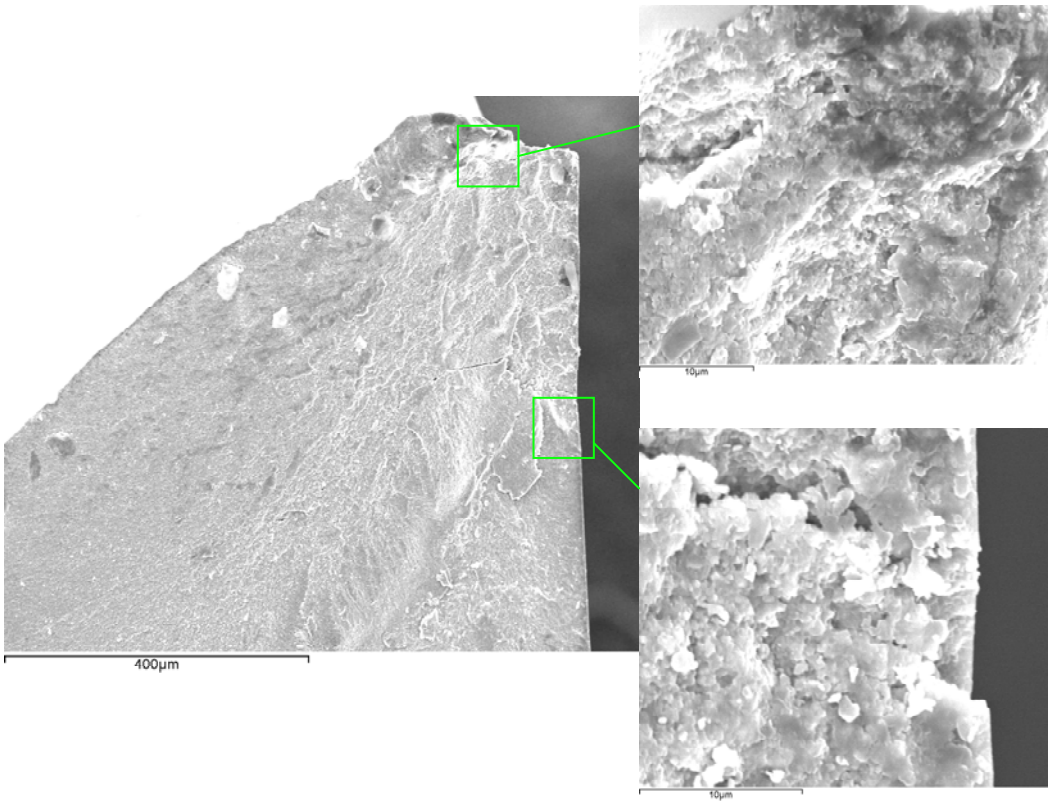

Figure 5.44. SEM image of fractured uncoloured Lava™ specimen after subcritical crack growth test using loading rate of 0.1 $N.s^{-1}$.

SEM image (Figure 5.44) of a fractured uncoloured Lava™ specimen failed in a subcritical crack growth test using 0.1 $N.s^{-1}$ loading rate showed that the surface was slightly rough. There were irregular crack lines on the fractured surfaces, which initiated at the fracture origin and also on the tension side as expected. No mirror-like area occurred in the central of the fractured origin.

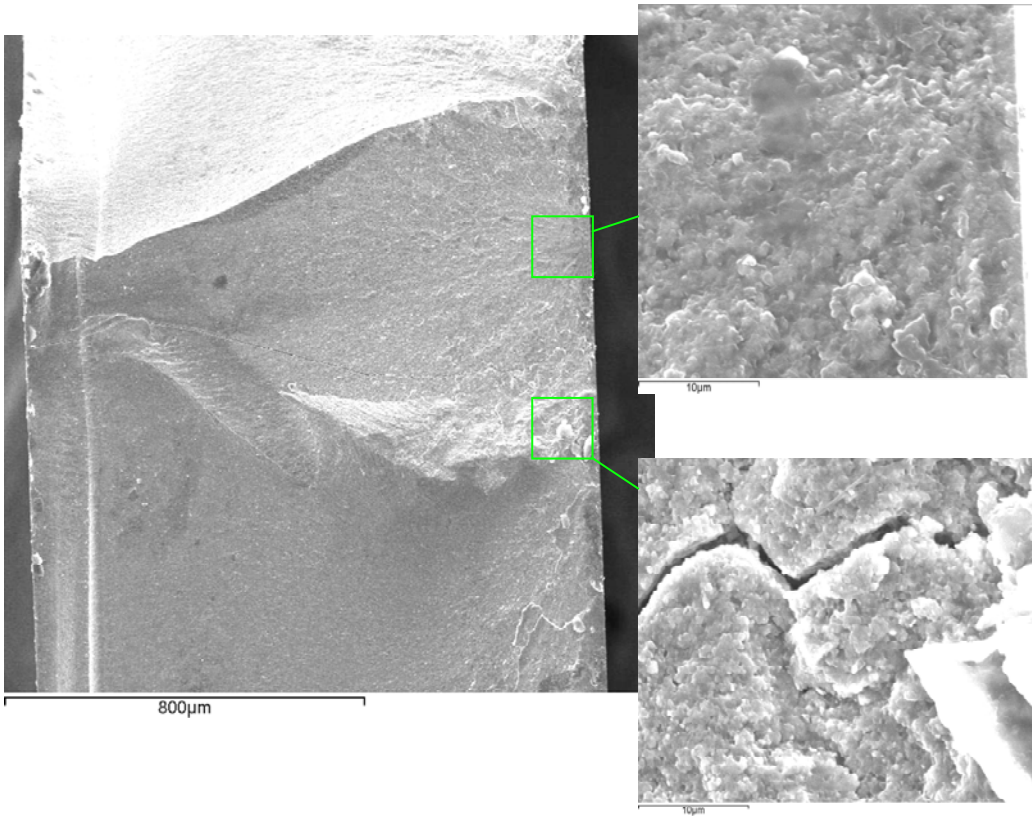

Figure 5.45. SEM image of fractured uncoloured Lava™ specimen after subcritical crack growth test using a loading rate of 100 $N.s^{-1}$.

The specimens fractured in the subcritical crack growth test using high loading rate (100 $N.S^{-1}$) had sharp crack lines compared with the specimen failed using 0.1 $N.s^{-1}$ loading rate. The mirror-like region was appeared in the centre of the fracture origin (Figure 5.45 on the left). There were also some major cracks that occurred at

the tension side which initiated at a distance away from the fracture origin area (Figure 5.45 on the right). The fracture pattern of other specimens using loading rate 1 and 10 $N.s^{-1}$ was similar to 0.1 $N.s^{-1}$ which had irregular crack lines and had rough surfaces (shown in appendix).

b. FS6

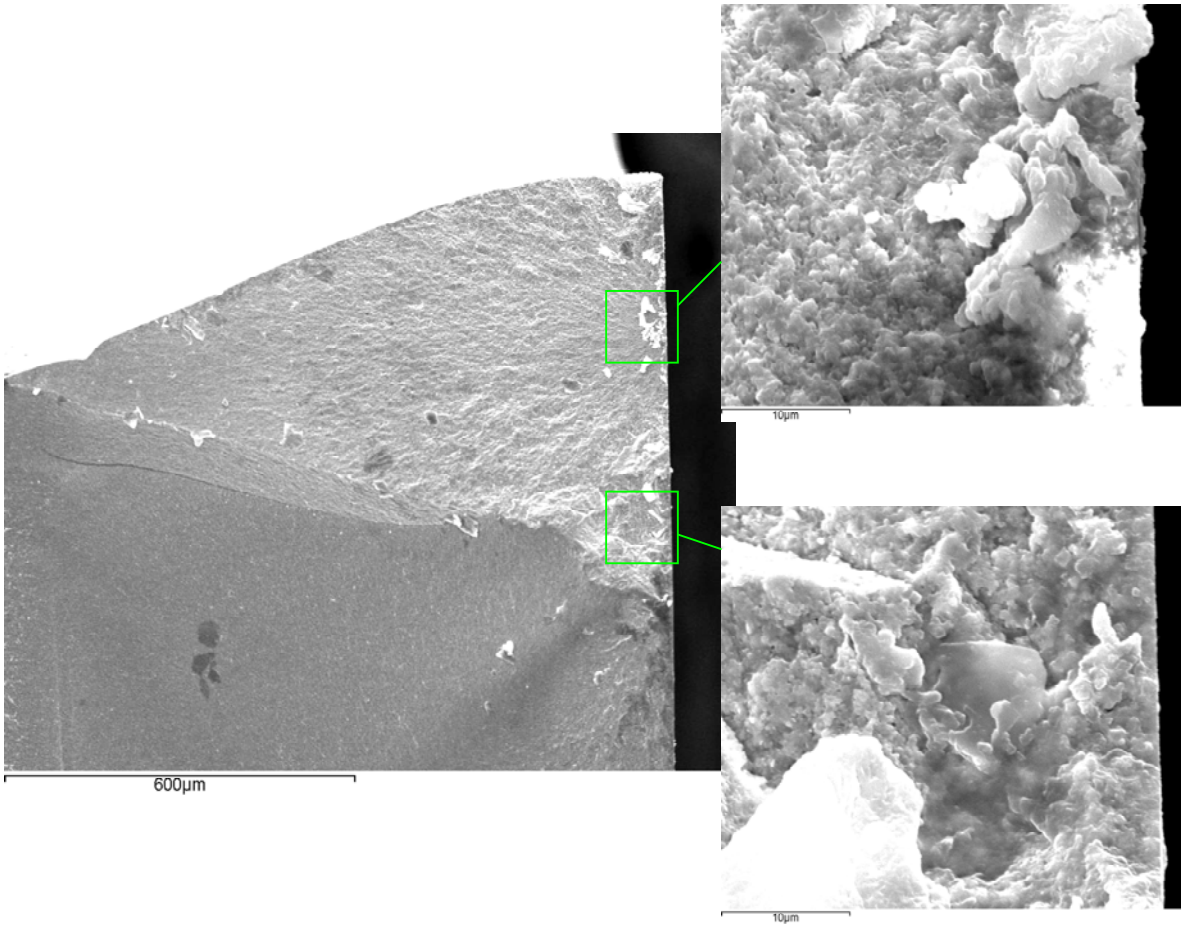

Figure 5.46. SEM image of fractured FS6 Lava™ specimen after subcritical crack growth test using loading rate of 0.1 $N.s^{-1}$.

The fractured surface of FS6 failed during subcritical crack growth testing using a loading rate of 0.1 $N.s^{-1}$ had a mirror-like region, which was different to the uncoloured specimens that presented with a more irregular crack pattern (Figure 5.46). Some cracks initiated at the tension surface at some distance away from the fracture origin.

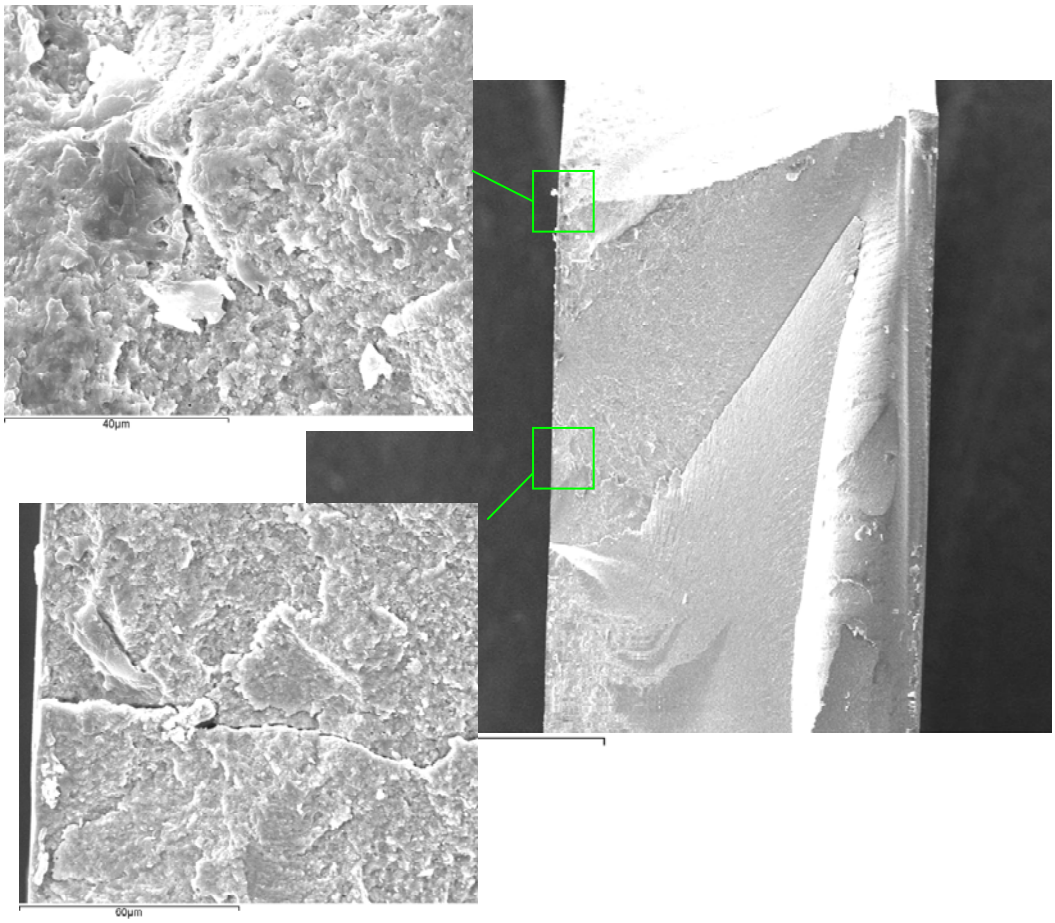

Figure 5.47. SEM image of fractured FS6 Lava™ specimen after subcritical crack growth test using loading rate of 100 $N.s^{-1}$.

The fractured surface of FS6 specimens that failed during subcritical crack growth using a loading rate of 100 $N.s^{-1}$ showed a smooth surface (Figure 5.47 on

the right). The fracture origin did not appear mirror- like and a few major cracks occurred on the tension side, which were sharper than those seen in specimens fractured using 0.1 $N.s^{-1}$ loading rate. The fracture patterns of other specimens using loading rates of 1 and 10 $N.s^{-1}$ had the same pattern as 0.1 and 100 $N.s^{-1}$ and are presented in the appendix. However, the fracture from higher loading rates tended to create sharper cracks.

Therefore, the fracture pattern of the uncoloured specimens which had a higher n value using a low loading rate was slightly different from FS6 which had a lower n value. The surface was rougher with more irregular crack lines on the surfaces of the uncoloured specimens.

5.1.5 Atomic force microscopy images of polished Lava™, Cercon®, and Invizion™ specimens

5.1.5.1 Lava™

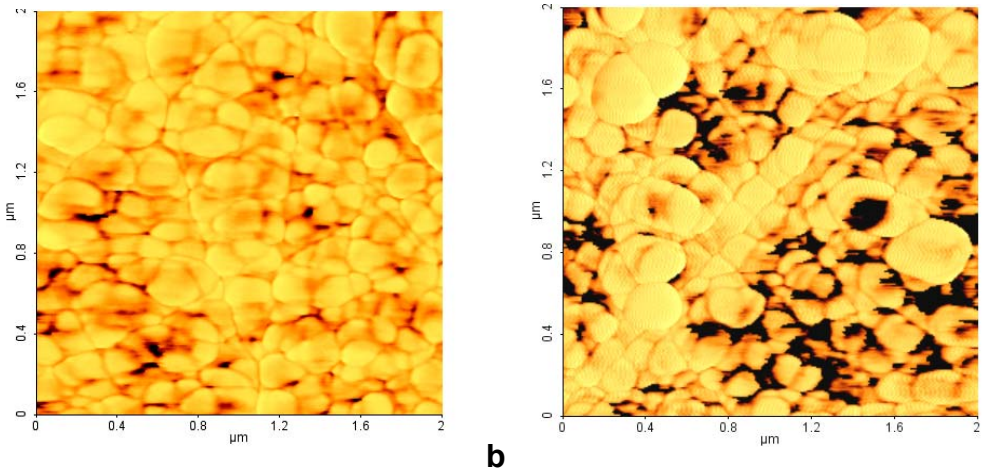

a b

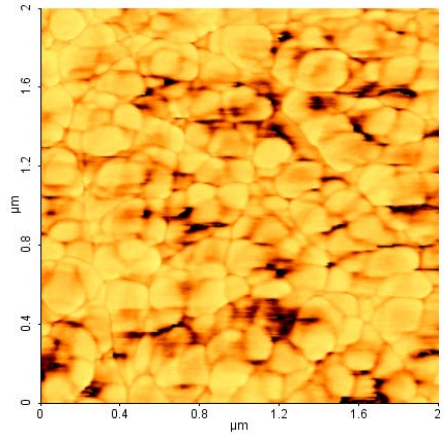

c

Figure 5.48. AFM imaging of the microstructure of uncoloured (a), FS4 (b) and FS7 (c) Lava™ specimens.

Figure 5.48 shows the very fine microstructures of polished uncoloured, FS4, FS7 Lava™ specimens. The microstructure of Lava™ discs contained predominantly fine grains with some larger grains. The grain appearance was rounded. After measurement, the mean grain size of uncoloured was 0.11±0.042 μm; whereas the large grains were about 0.2 μm. FS4 had the mean grain size 0.11±0.05 μm, while the large grains were ranged from 0.2-0.3 μm. The mean grain size of FS7 was 0.10±0.04 μm, while the large grains were approximately 0.2 μm.

5.1.5.2 Cercon

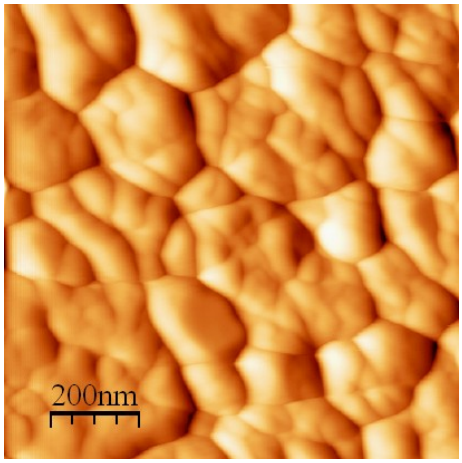

Figure 5.49 AFM image of microstructure of Cercon® specimen

Microstructure of Cercon® discs contained fine grains with some larger grains (Figure 5.49). After measurement, the mean grain size was 0.11±0.04 μm, while large grains were approximately 0.2-0.3 μm. The grains in Cercon® specimens appeared to have a coalesced pattern.

5.1.5.3 Invizion

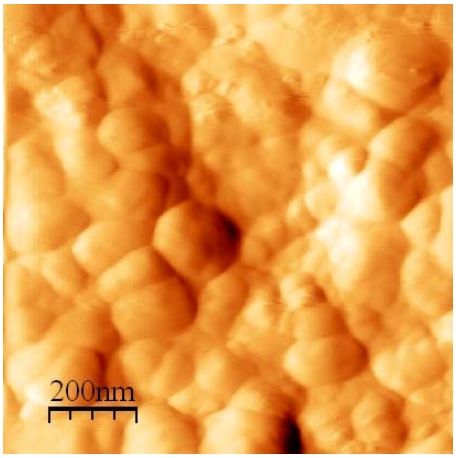

Figure 5.50. AFM image of the microstructure of Invizion™ specimen

Microstructure of Invizion™ disc contained larger grains with some finer grains (Figure 5.50). After measurement, the mean grain size was 0.11±0.13 μm, while some large grains were approximately 0.2 μm.

Therefore, the results from grain measurement showed that Lava™ and Cercon® zirconia based ceramic had similar grain size of approximately 0.1 μm. Invizion™ had slightly larger grain size. Additionally, Lava™, Cercon® and Invizion™ had different surface appearances. Lava™ grains appeared more rounded and separated compared with others while Cercon® had what appeared to be fused grains.

5.1.6 X-ray diffraction analysis

5.1.6.1 Phase analysis of polished and as-received surfaces

For the as-received uncoloured and coloured (FS4 and FS7) Lava™, Cercon® and Invizion™ specimens, the results from X-ray diffraction analysis identified three distinct phases present within the ceramics. The dominant phase was tetragonal

zirconia and was identified as having lattice parameters (*a*≈3.606Å and *c*≈5.179Å) and the phase was present at levels of about 60 to 70 wt% of the total (Table 5.6). The second phase was identified as cubic zirconia (denoted cubic 1) with lattice parameters of *a*≈5.138 Å which was present in quantities ranging from 6 to 19 wt%. Intriguingly, a third phase was identified as cubic (denoted cubic 2), but with slightly larger lattice parameters of a≈5.20 Å compared to the first cubic phase (Table 5.6) and was present in the as-received specimens at levels of 20-29 wt%. Interestingly, in polished specimens, the second cubic phase virtually disappeared and there was a two to four-fold increase in the amount of the first cubic phase. Only a slight change occurred in the amount of tetragonal phase. The XRD graph (Figure 5.51 and 5.52) also confirmed that polished specimens had only tetragonal and cubic 1 whereas as-received had tetragonal, cubic 1 and cubic 2. This can be seen from the graph for the as-received specimen where the as-received had a broader shoulder on certain peaks compared to the polished specimens. This identified that there was another phase within the as-received specimens. In addition, there was no difference in the amount of tetragonal, cubic 1 and cubic 2 phases within uncoloured, FS4 and FS7 Lava™, Cercon® and Invizion specimens as seen in Table 5.6 and Figure 5.51 and 5.52.

Table 5.6. Phase composition of "as-received" and polished specimens of uncoloured, FS4 and FS7 of Lava™, Cercon® and Invizion™ specimens.

Sample	Tetragonal phase		Cubic 1		Cubic 2	
	a (A°)(±SD) *c* (A°)(±SD)	Wt% (±SD)	*a* (A°)(±SD)	Wt% (±SD)	*a* (A°)(±SD)	Wt% (±SD)
Uncoloured as received	3.6066 (±0.0001), 5.1789 (±0.0003)	67 (±1)	5.1403 (±0.0004)	6 (±1)	5.2009 (±0.0019)	27 (±1)
Uncoloured polished	3.6067 (±0.0009), 5.1796 (±0.0002)	70 (±1)	5.1388 (±0.0004)	30 (±1)	-	-
FS4 as received	3.6070 (±0.0002), 5.1772 (±0.0003)	60 (±1)	5.1378 (±0.0004)	11 (±1)	5.2074 (±0.0018)	29 (±2)
FS4 polished	3.6061 (±0.0001), 5.1789 (±0.0002)	60 (±1)	5.1330 (±0.0003)	40 (±1)	-	-
FS7 as received	3.6064 (±0.0001), 5.1790 (±0.0003)	64 (±1)	5.1389 (±0.0004)	8 (±1)	5.2088 (±0.0002)	28 (±1)
FS7 polished	3.6075 (±0.0009), 5.1808 (±0.0002)	66 (±1)	5.1360 (±0.0003)	33 (±1)	-	-
Cercon as received	3.6607 (±0.0001), 5.1808 (±0.0003)	61 (±1)	5.1525 (±0.0008)	19 (±1)	5.3300 (±0.0001)	20 (±1)
Cercon polished	3.6054 (±0.0001), 5.1802 (±0.0001)	68 (±1)	5.1346 (±0.0003)	32 (±1)	-	-
Invizion as received	3.6055 (±0.0001), 5.1794 (±0.0001)	67 (±1)	5.1290 (±0.0003)	15 (±1)	5.1354 (±0.0003)	18 (±1)
Invizion polished	3.6053 (±0.0001), 5.1784 (±0.0001)	61 (±1)	5.1277 (±0.0002)	11 (±1)	5.1277 (±0.0002)	28 (±1)

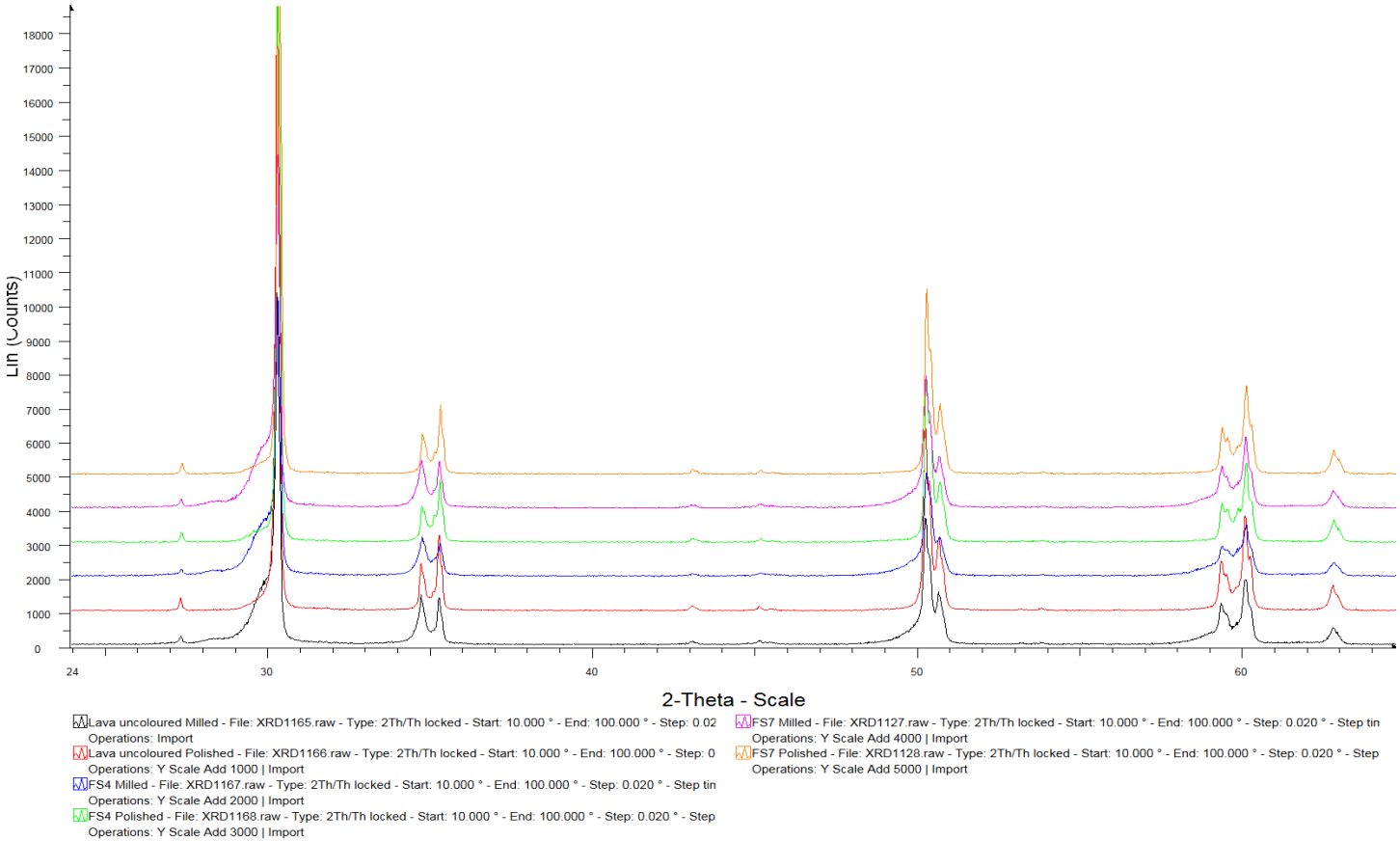

Figure 5.51. X-ray diffraction patterns for the "as received" and polished for uncoloured, FS4, and FS7 specimens.

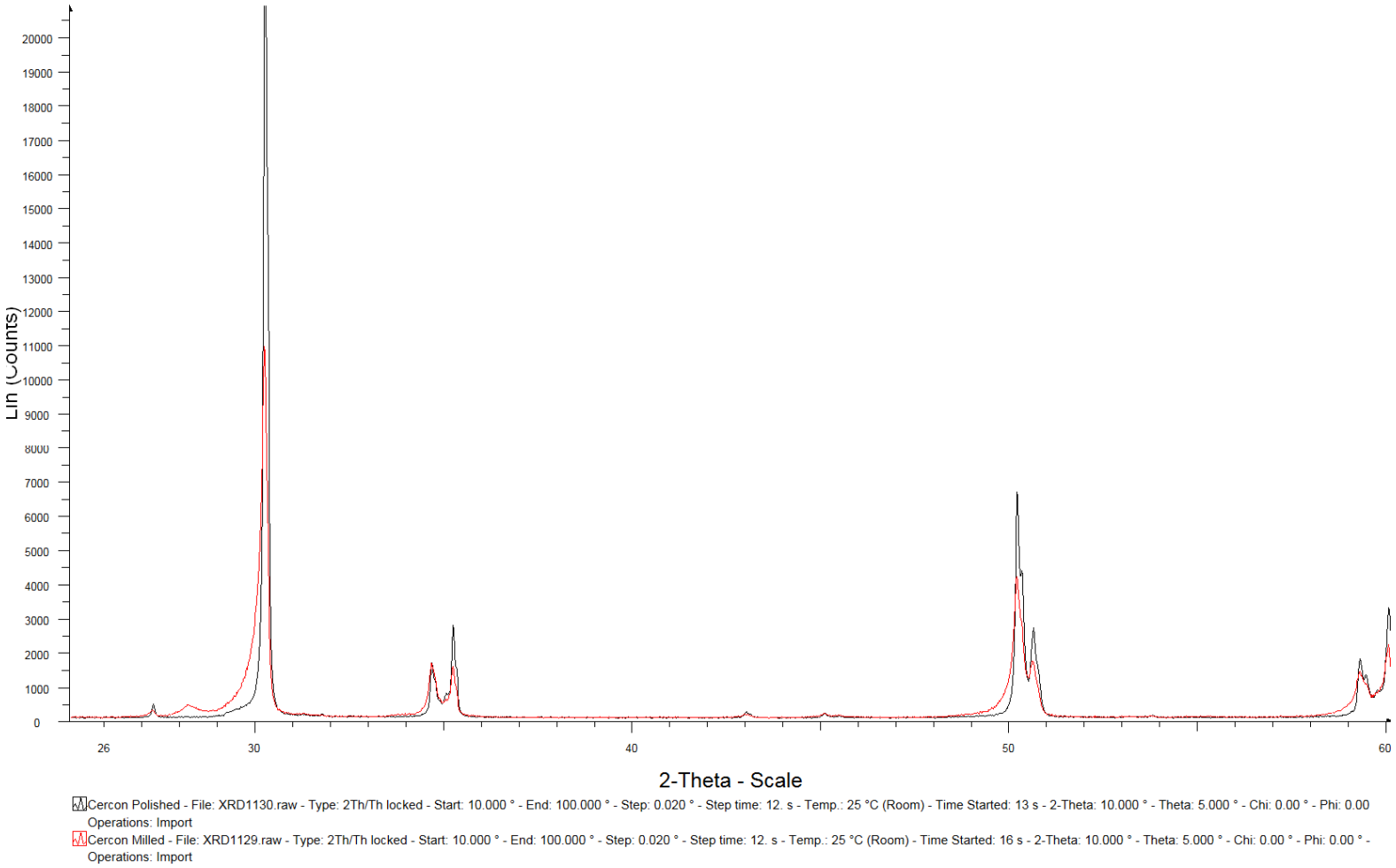

Figure 5.52. X-ray diffraction patterns for the "as received" and polished Cercon® specimens.

In general, after grinding uncoloured Lava™ and Cercon® with 1000, 500, 320, and 80 grit carbon carbide papers for 5 min, there was a decrease in the amount of tetragonal and cubic 1 phases when using 320 and 80 grits while cubic 2 phase increased. Zirconia ground with 1000 and 500 grits has similar phases as in the as-received specimens. Additionally, there was no significant difference in the amount of tetragonal, cubic 1, and cubic 2 phases either using wet or dry grinding between Lava™ and Cercon® zirconia. However, there was the difference between wet and dry grinding in Invizion™ specimens.

XRD results (Table 5.7) showed that uncoloured Lava™ zirconia ground with 500 and 1000 grit papers had a similar amount of tetragonal, cubic 1 and cubic 2 phases as the “as-received” uncoloured and coloured Lava™ zirconia. The amount of tetragonal, cubic 1 and cubic 2 phases of those two groups ranged from 67-72 wt%, 11-17 wt%, and 16-20 wt%, respectively. In zirconia ground with 320 grit paper, tetragonal and cubic 1 phases were slightly decreased while cubic 2 phase was increased. However, tetragonal and cubic 1 were decreased by approximately 45% while cubic 2 increased approximately 50% compared with the as-received specimen after grinding with 80 grit paper.

Table 5.7. Effect of surface preparation on the phase composition of uncoloured Lava™

Grits	Tetragonal phase		Cubic 1		Cubic 2	
	a (Å)(±SD) *c* (Å)(±SD)	Wt% (±SD)	*a* (Å)(±SD)	Wt% (±SD)	*a* (Å)(±SD)	Wt% (±SD)
as-received	3.6066 (±0.0001), 5.1789 (±0.0003)	67 (±1)	5.1403 (±0.0004)	6 (±1)	5.2009 (±0.0019)	27 (±1)
polished	3.6067 (±0.0009), 5.1796 (±0.0002)	70 (±1)	5.1388 (±0.0004)	30 (±1)	-	-
1000, wet	3.6066 (±0.0001), 5.1796 (±0.0002)	68 (±1)	5.1370 (±0.0004)	11 (±1)	5.1970 (±0.0002)	21 (±1)
1000, dry	3.6071 (±0.0001), 5.1800 (±0.0002)	67 (±1)	5.1387 (±0.0004)	13 (±1)	5.1960 (±0.0003)	20 (±1)
500, wet	3.6081 (±0.0001), 5.1774 (±0.0003)	67 (±4)	4.99 (±0.0005)	17 (±5)	5.2010(±0.0002)	16 (±1)
500, dry	3.6078 (±0.0001), 5.1775 (±0.0003)	72 (±1)	5.16 (±0.0002)	13 (±1)	5.2043 (±0.0009)	16 (±1)
320, wet	3.6064 (±0.0001), 5.1781 (±0.0003)	64 (±1)	5.1381 (±0.0001)	8 (±1)	5.1940 (±0.0002)	28 (±1)
320, dry	3.6070 (±0.0001), 5.1795 (±0.0002)	62 (±1)	5.1385 (±0.0005)	8 (±1)	5.2006 (±0.0007)	30 (±1)
80, wet	3.6060 (±0.0002), 5.1763 (±0.0004)	48 (±1)	5.1383 (±0.0009)	8 (±1)	5.1723 (±0.0008)	44 (±1)
80, dry	3.6039 (±0.0003), 5.1732 (±0.0006)	41 (±1)	5.139 (±0.0002)	6 (±2)	5.1860 (±0.0009)	54 (±1)

XRD results for Cercon® ground with 1000, 500 and 320 grits wet and dry (Table 5.8) showed that it had a similar amount of the tetragonal phase as the “as-received” Cercon® ranging from 66-70 wt%. However, cubic 1 was slightly decreased and cubic 2 was increased, ranging from 3-11 wt% and 22-29 wt%, respectively. The specimen ground with 80 grit

paper had the lowest amount of tetragonal and cubic 1 compared to other grit sizes by approximately 50 wt% and 5 wt% respectively while cubic 2 was increased twofold.

Table 5.8. Effect of surface preparation on the phase composition of Cercon® specimens.

Grits	Tetragonal phase		Cubic1		Cubic2	
	a (Å)(±SD) *c* (Å)(±SD)	Wt% (±SD)	*a* (Å)(±SD)	Wt% (±SD)	*a* (Å)(±SD)	Wt% (±SD)
as-received	3.6607 (±0.0001), 5.1808 (±0.0003)	61 (±1)	5.1525 (±0.0008)	19 (±1)	5.3300 (±0.0001)	20
polished	3.6054 (±0.0001), 5.1802 (±0.0001)	68 (±1)	5.1346 (±0.0003)	32 (±1)	-	-
1000, wet	3.6067 (±0.0001), 5.1796 (±0.0002)	70 (±1)	5.1370 (±0.0004)	11 (±1)	5.200 (±0.0001)	19 (±1)
1000, dry	3.6087 (±0.0001), 5.1794 (±0.0002)	73 (±1)	5.1412 (±0.0004)	5 (±1)	5.203 (±0.0001)	22 (±1)
500, wet	3.6086 (±0.0001), 5.1794 (±0.0003)	74 (±1)	5.1404 (±0.0006)	4 (±1)	5.196 (±0.0002)	22 (±1)
500, dry	3.6071 (±0.0001), 5.1798 (±0.0002)	66 (±1)	5.1380 (±0.0005)	8 (±1)	5.200 (±0.0001)	26 (±1)
320, wet	3.6079 (±0.0001), 5.1782 (±0.0002)	69 (±1)	5.1400 (±0.0006)	3 (±1)	5.195 (±0.0001)	28 (±1)
320, dry	3.6081 (±0.0001), 5.1782 (±0.0003)	68 (±1)	5.1419 (±0.0005)	3 (±1)	5.197 (±0.0001)	29 (±1)
80, wet	3.6062 (±0.0002), 5.1751 (±0.0004)	55 (±2)	5.147 (±0.0004)	5 (±2)	5.192 (±0.0001)	40 (±2)
80, dry	3.6045 (±0.0003), 5.1732 (±0.0007)	43 (±2)	5.149 (±0.0005)	4 (±3)	5.185 (±0.0001)	53 (±2)

Table 5.9. Effect of surface preparation on the phase composition of Invizion™ specimens.

Grits	Tetragonal phase		Cubic1		Cubic2	
	a (Å)(±SD) *c* (Å)(±SD)	Wt% (±SD)	*a* (Å)(±SD)	Wt% (±SD)	*a* (Å)(±SD)	Wt% (±SD)
as-received	3.6055 (±0.0001), 5.1794 (±0.0001)	67 (±1)	5.1290 (±0.0003)	15 (±1)	5.1354 (±0.0003)	18 (±1)
polished	3.6053 (±0.0001), 5.1784 (±0.0001)	61(±1)	5.1277 (±0.0002)	11 (±1)	5.1277 (±0.0002)	28 (±1)
1000 wet	3.6074 (±0.0001), 5.1793 (±0.0003)	66 (±1)	5.1434 (±0.0003)	14 (±1)	5.192 (±0.0002)	20 (±1)
1000 dry	3.6059 (±0.0001), 5.1791 (±0.0002)	55 (±1)	5.1354 (±0.0003)	11 (±1)	5.2003 (±0.0009)	34 (±1)
500 wet	3.6066 (±0.0001), 5.1776 (±0.0003)	73 (±1)	5.1411 (±0.0004)	8 (±1)	5.1930 (±0.0001)	19 (±1)
500 dry	3.6065 (±0.0001), 5.1765 (±0.0002)	65 (±1)	5.1890 (±0.0003)	30 (±1)	5.2064 (±0.0003)	6 (±1)
320 wet	3.6064 (±0.0002), 5.1777 (±0.0003)	82 (±1)	5.1402 (±0.0007)	3 (±1)	5.1870 (±0.0002)	15 (±1)
320 dry	3.6061 (±0.0001), 5.1761 (±0.0002)	58 (±1)	5.1753 (±0.0003)	28 (±1)	5.2062 (±0.0008)	14 (±1)
80 wet	3.6054 (±0.0002), 5.1749 (±0.0003)	74 (±1)	5.1394 (±0.0009)	1 (±1)	5.1941 (±0.0007)	24 (±1)
80 dry	3.6059 (±0.0002), 5.1744 (±0.0003)	40 (±1)	5.1860 (±0.0003)	6 (±1)	5.229 (±0.0007)	54 (±1)

The phase percentages of as-received and ground/polished Invizion™ specimens are shown in Table 5.9. The result of Invizion differ from Lava™ and Cercon® that all the three phases of as-received, polished and wet ground specimens were not different. However, 1000, 500, 320 and 80 grits dry ground specimens result in the reduction of the tetragonal phase and the cubic 1 phase was increased.

Therefore, the XRD results may be concluded that as-received zirconia specimens of Lava™ and Cercon® had three phases which were tetragonal, cubic 1 and cubic 2. The polishing process led to a change of the cubic 2 (the strained cubic phase) to cubic 1 while the grinding process created more cubic 2, but did not induce the transformation toughening *(t → m)*. After grinding with coarse grits, tetragonal and cubic 1 phases were reduced and cubic 2 was increased. There was no significant change in the three phases between wet and dry grinding and also between Lava™ and Cercon® zirconia specimens. On the other hand, the polishing process did not affect the amounts of cubic 2 of Invizion™ specimens and there was a difference in three phases between wet and dry ground specimens.

5.1.6.2 X-ray diffraction crown fatigue

X-ray diffraction traces for zirconia powder before and after sintering (Kavo Everest ZS-blanks, Kavo, Germany), IPS e.max® Ceram, and IPS e.max® ZirPress specimens were analysed and the results were showed in Table 5.10 and Figure 5.53-5.56. The zirconia powder before sintering contained tetragonal as well as monoclinic phases while after sintering contained only tetragonal zirconia (Figure 5.53 and 5.54). There were no changes in the unit cell dimensions of the tetragonal phase before and after sintering (Table 5.10). The IPS e.max® Ceram and IPS e.max® ZirPress specimens revealed an amorphous glass with some small peaks that were difficult to unambiguously identify (Figure 5.55 and 5.56). There was no difference in the x-ray diffraction patterns of the veneering materials before and after sintering or heat pressing.

Table 5.10. The mean unit cell dimensions and the mean unit cell volume for zirconia specimens (Kavo Everest ZS-blanks) before and after sintering

Specimen	Phase	Mean α-axis unit cell (Å) (±SD)	Mean b-axis unit cell (Å) (±SD)	Mean c-axis unit cell (Å) (±SD)	Mean alpha (Å) (±SD)	Mean beta (Å) (±SD)	Mean gamma (Å) (±SD)	Mean unit cell volume (Å) (±SD)
Zirconia before sintering	Tetragonal	3.6030 (±0.0007)	-	5.1992 (± 0.001)	-	-	-	67.516 (±0.036)
	Monoclinic	5.1550 (±0.0010)	5.2090 (±0.0011)	5.3162 (±0.0011)	90.0 (± 0.0)	99.199 (±0.011)	90.0 (± 0.0)	140.908 (±0.062)
Zirconia after sintering	Tetragonal	3.6020 (±0.0010)	-	5.172 (±0.002)	-	-	-	67.080 (±0.070)

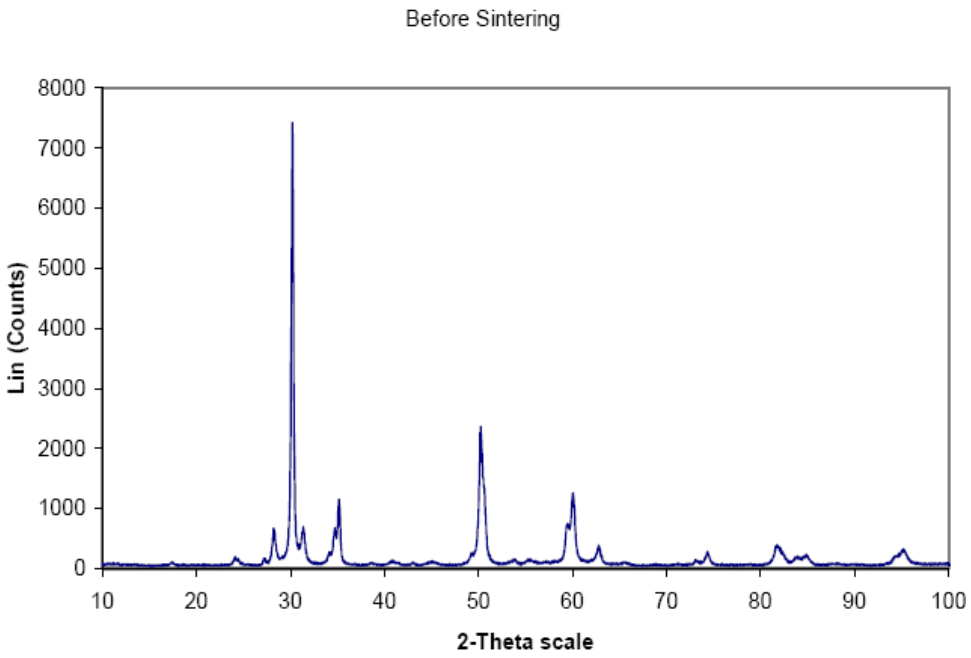

Figure 5.53. X-ray diffraction trace of the zirconia powder before sintering

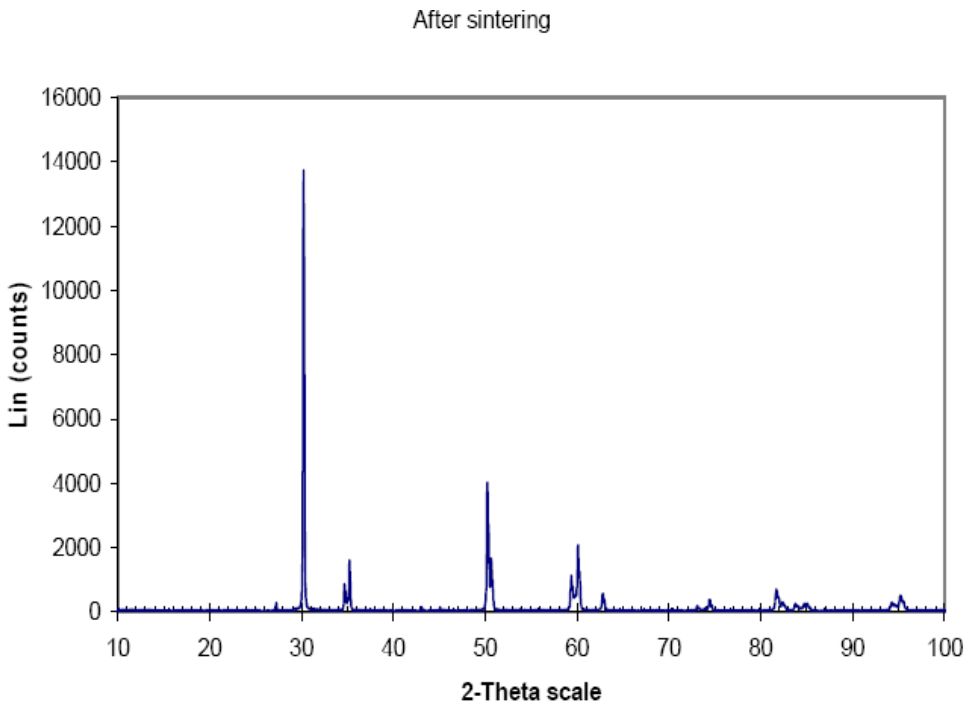

Figure 5.54. X-ray diffraction trace of the zirconia powder after sintering.

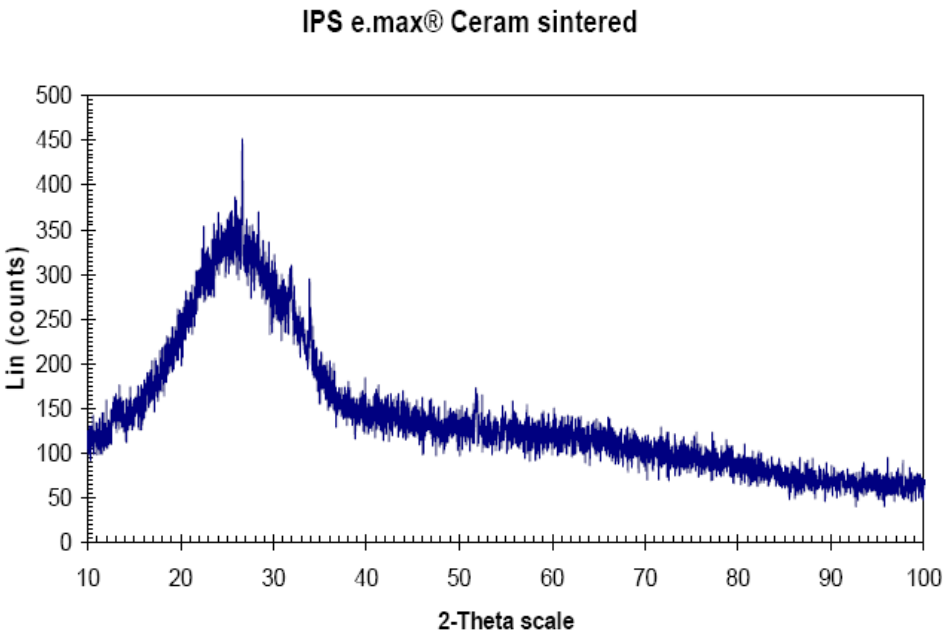

Figure 5.55. X-ray diffraction trace of the IPS e.max Ceram bar specimen after sintering, staining and glazing.

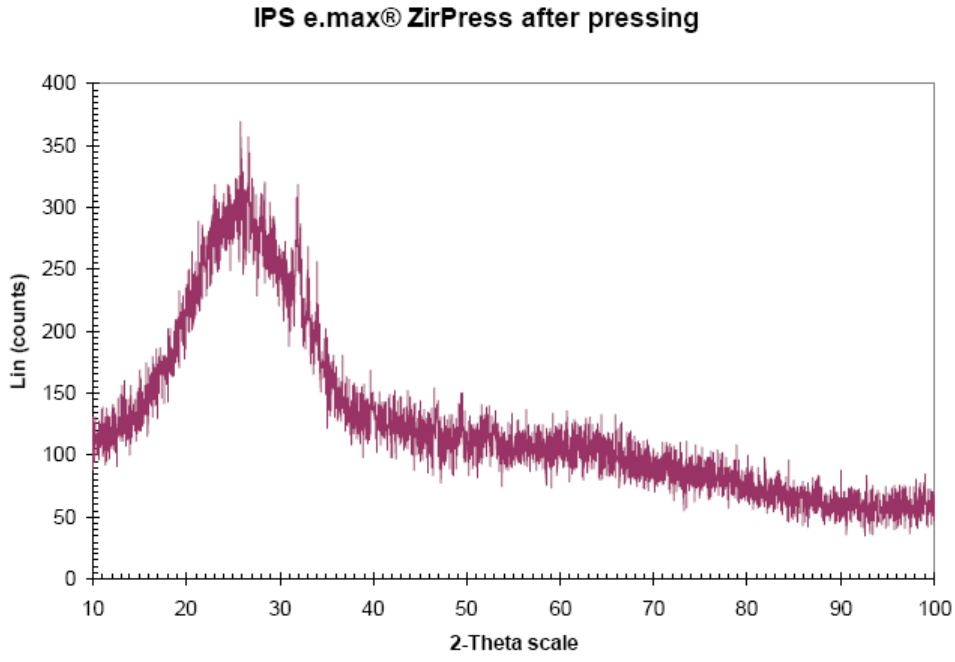

Figure 5.56. X-ray diffraction trace of the IPS e.max® ZirPress disc specimen after heat pressing, staining and glazing.

5.1.7 Raman spectroscopy

Raman spectroscopy allows the mapping and quantification of phases and thus this was used to map phase distributions and in particular around indentations made in the surface. Raman spectra of pure phases used in modelling of raman spectra from specimens are given in Figure 5.11. That of tetragonal zirconia was observed to have broad bands at approximately 256, 320, 466 and 637 cm^{-1}. The spectrum of cubic zirconia was similar to that of tetragonal although some differences in relative peak heights particularly of the 630 and 256 bands were noted. These results are in agreement with Witke *et al* (2001) (Witke *et al.* 2001) and Li *et al* (2003) (Li *et al.* 2003). Conversely, the monoclinic phase had sharp strong Raman peaks at 177, 185 and 382 cm^{-1} (Figure 5.57) as previously observed by Sekulic *et al* (1997) and Witke *et al* (2001) (Witke *et al.* 2001; Sekulic *et al.* 1997).

Table 5.11 Showed the peak spectra of three phases (Sekulic *et al.* 1997; Witke *et al.* 2001)

Raman Shift (cm^{-1})		
Tetragonal	**Cubic**	**Monoclinic**
256	256	176
320	466	188
466	630	219
637		303
		331
		345
		379
		474
		500
		534
		559
		615
		638

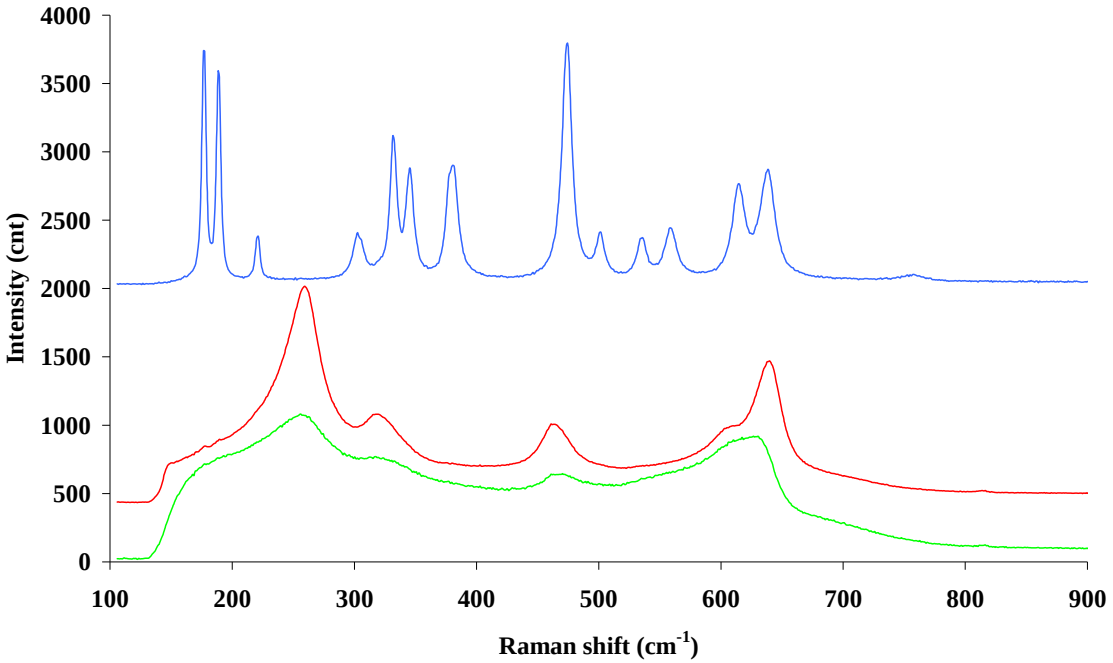

Figure 5.57. Raman spectra and tabulated peaks of pure monoclinic (blue), tetragonal (red), and cubic (green) phases obtained from pure powder

5.1.7.1 Study to determine the effect of indentation on phase transformation

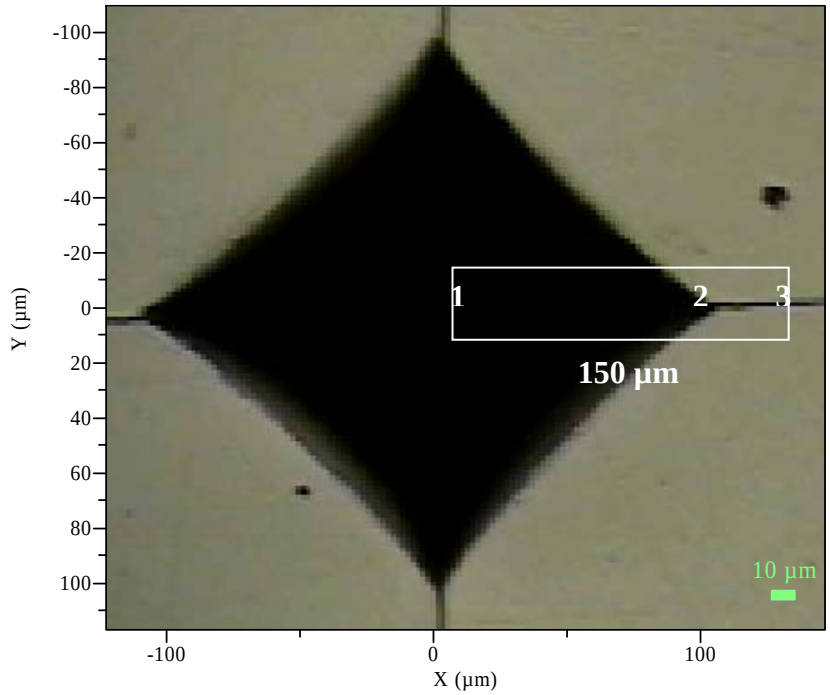

Figure 5.58 Visual image obtained with the Raman microscope camera of an indentation produced using a load of 50 kg. The numbers indicate the approximate areas studied to generate spectra.

A typical indentation image is provided in Figure 5.58. The centre is labelled 1, edge 2 and outer region 3. Example spectra at these points are shown in Figure 5.59. In all three regions broad bands due to tetragonal or cubic phases are observed. The peak at 637 cm^{-1} shows only marginal variation but that at 256 cm^{-1} is greatest in the outer region and least at the centre. Comparison with the spectra of pure tetragonal and cubic phases (Figure 5.57) suggests there is more cubic phase at the centre but more tetragonal phase outside the indentation. No monoclinic peaks were detected in the Raman spectra obtained from the regions outside the

indentation zone. At the edge and to a lesser extent the indentation centre, however, peaks at 177, 185 and 382 cm^{-1} due to this phase are clearly evident.

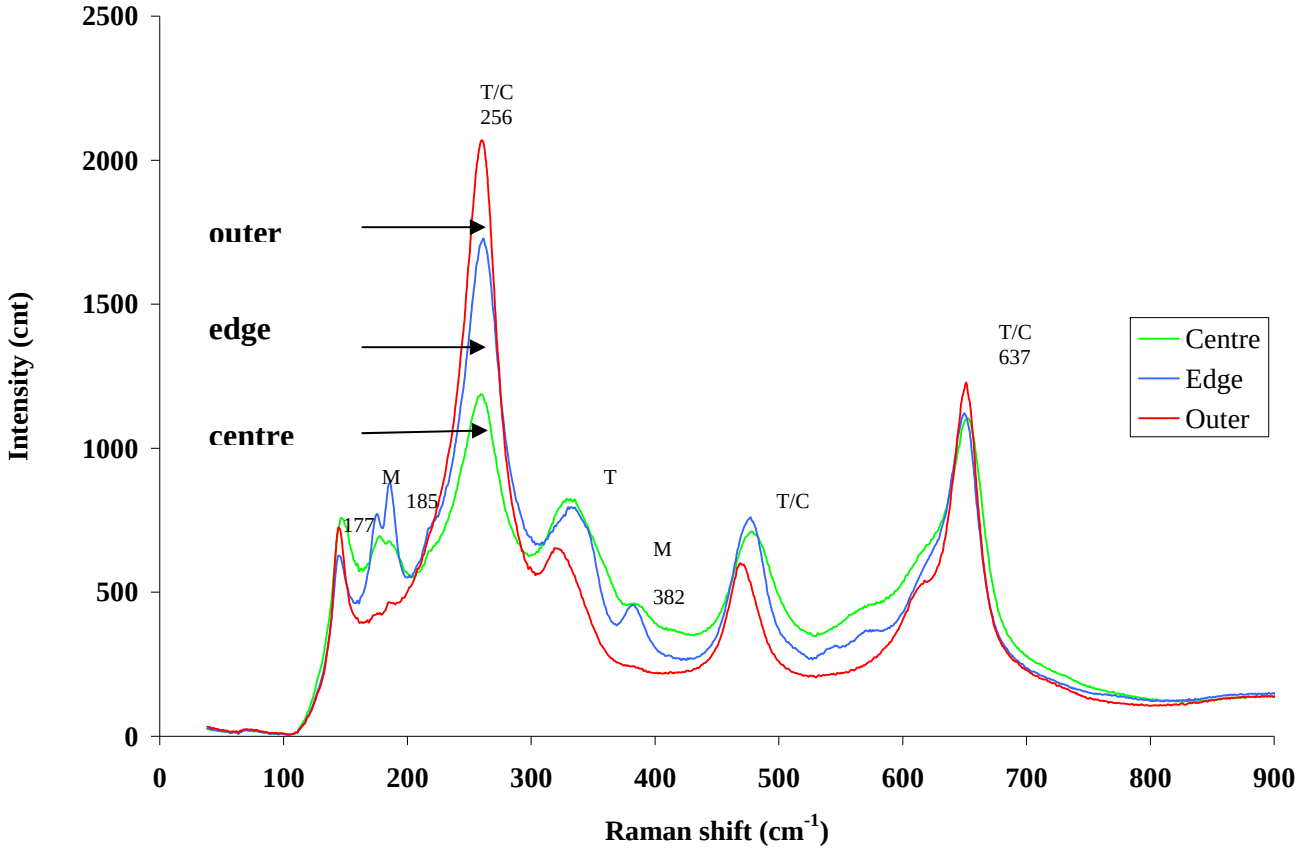

Figure 5.59. Example Raman spectra (from the 50 kg loaded specimen) at the centre (green), edge (blue) and outer (red) regions of an indentation (see numbers 1, 2 and 3 respectively in figure 5). The letters t, c and m indicate peaks associated with the tetragonal, cubic and monoclinic phases respectively.

When spectra were compared with the full spectra of tetragonal (red), cubic (green) and monoclinic (blue) phases, modelling indicated there was some cubic phase outside the indentation region but its level was higher within, especially along the grooves generated by the sharp edges of the indenter (Figure 5.60b). In these grooves, the relative calculated contributions of tetragonal and monoclinic phases to the total Raman scattering was reduced causing them to be observed as black lines in images 5.60a and 5.60c. The monoclinic phase was only detected within and around the indentation area and had the highest intensity around the edge of the indentation (Figure 5.60c) whereas calculated intensity due to the tetragonal phase was greatest outside. When comparing the Raman images between Lava™ (Figure 5.60), Cercon® (Figure 5.61) and Invizion™ (Figure 5.62), the location of the tetragonal cubic and monoclinic was similar except for Invizion™, which had lower intensity of the tetragonal phase within the indentation compared to the others.

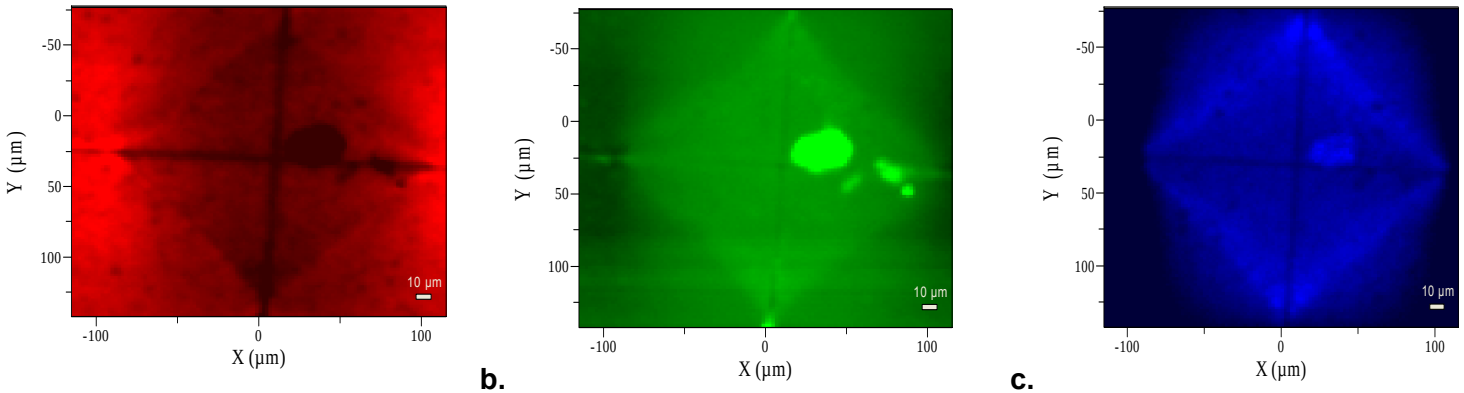

a. **b.** **c.**

Figure 5.60. Images indicating the relative intensities of tetragonal (a), cubic (b) and monoclinic (c) phases of uncoloured Lava™ within and around the indentation produced using a 30 kg load. In all images the black areas indicate lower levels of a given phase.

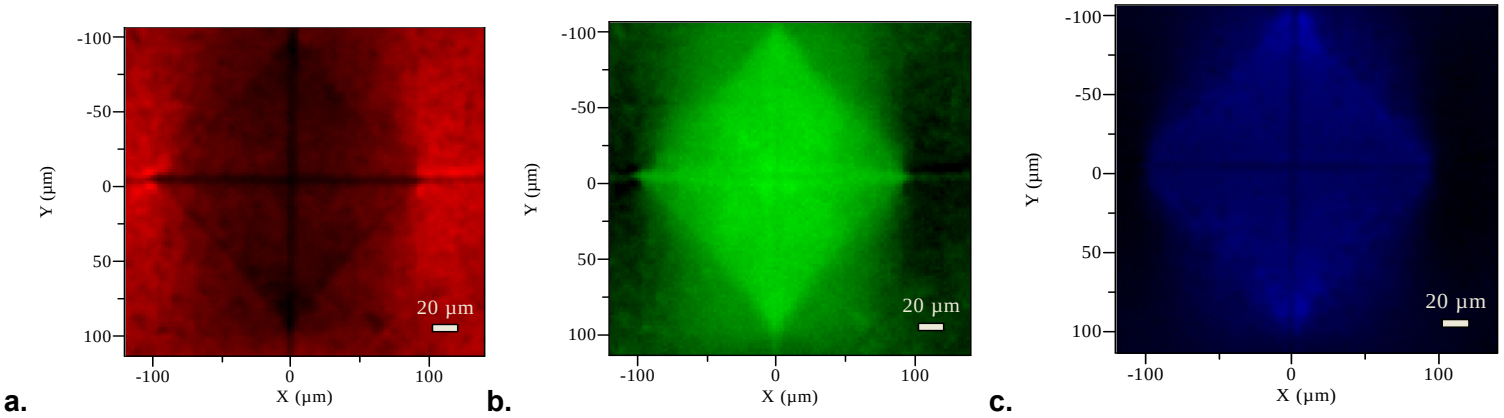

Figure 5.61. Images indicating the relative intensities of tetragonal (red), cubic (green) and monoclinic (blue) phases of Cercon® specimen within and around the indentation produced using a 30 kg load. In all images, the black areas indicate lower levels of a given phase.

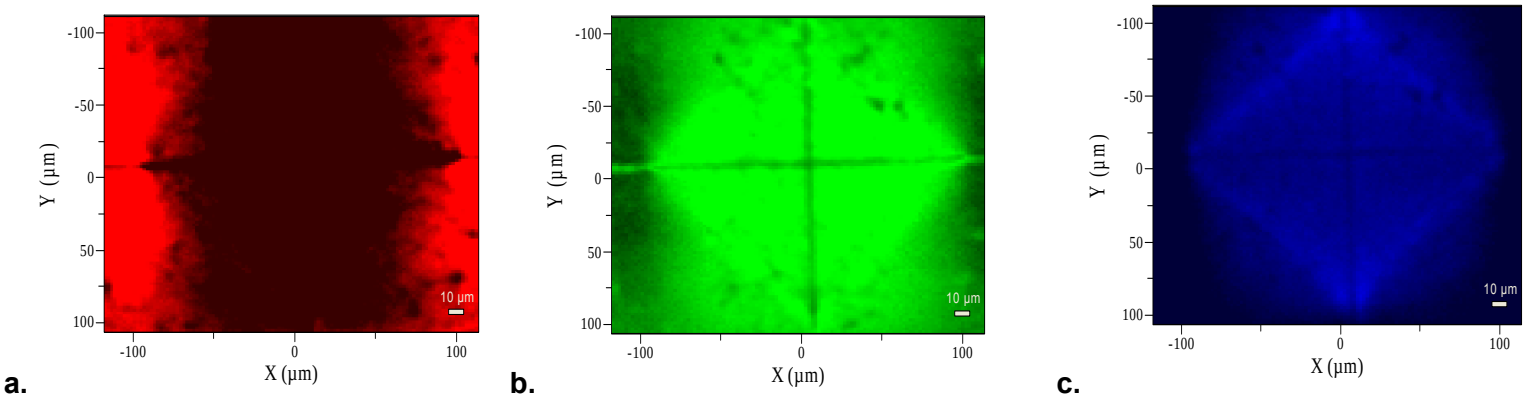

Figure 5.62. Images indicating the relative intensities of tetragonal (a), cubic (b) and monoclinic (c) phases of Cerec® within and around the indentation produced using a 30 kg load. In all images, the black areas indicate lower levels of a given phase.

Intensities of tetragonal, cubic, and monoclinic phases on two lines along and 45° to the grooves in the Lava™, Cercon® and Invizion™ zirconia had similar patterns. Intensity parameters tetragonal, cubic and monoclinic (see equation 6) associated with changes in tetragonal, cubic and monoclinic phase levels respectively as a function of distance from the centre along and at 45° to the indentation groove are given in Figure 5.63. Along the groove, tetragonal phase increased slightly upon moving away from the centre towards the edge but cubic phase declined (Figure 5.63). Intensity of monoclinic phase is stable from the centre to the edge of the indentation; however, monoclinic of Cercon® specimen (Figure 5.63b) had a slight increase from the centre toward the edge. At the edge (100 μm from the centre), there was an abrupt decrease in cubic whilst tetragonal increased sharply and monoclinic reduced to zero.

Along the line at 45° to the groove, t exhibited an abrupt increase in the first 20 μm away from the centre groove (Figure 5.64). It then remained approximately constant until 40 to 50 μm from the centre. At this point, it began to increase again until the edge at approximately 70 microns for Lava™ (Figure 5.64b) and Invizion™ (Figure 5.64c) and 65 μm for Cercon® (Figure 5.64a) from the centre. Monoclinic was approximately constant up to 50 μm from the centre, but it slightly increased at the edge (70 μm for Lava™ and Invizion™ and 65 μm for Cercon®) and then declined towards zero outside the indentation. Conversely, cubic declined slowly upon moving to 60 μm for Lava™ and Invizion™ and 50 μm for Cercon® from the centre and then more abruptly down to the outer region level. These results suggested that the tetragonal phase may convert to cubic and monoclinic phases within the indentation

region but additionally that greater conversion to the cubic phase occurred along the grooves. Overall near the edge of the indentation, there was an abrupt change in the relative levels of the different phases when traversing the groove, whereas along the 45° line, changes were more gradual.

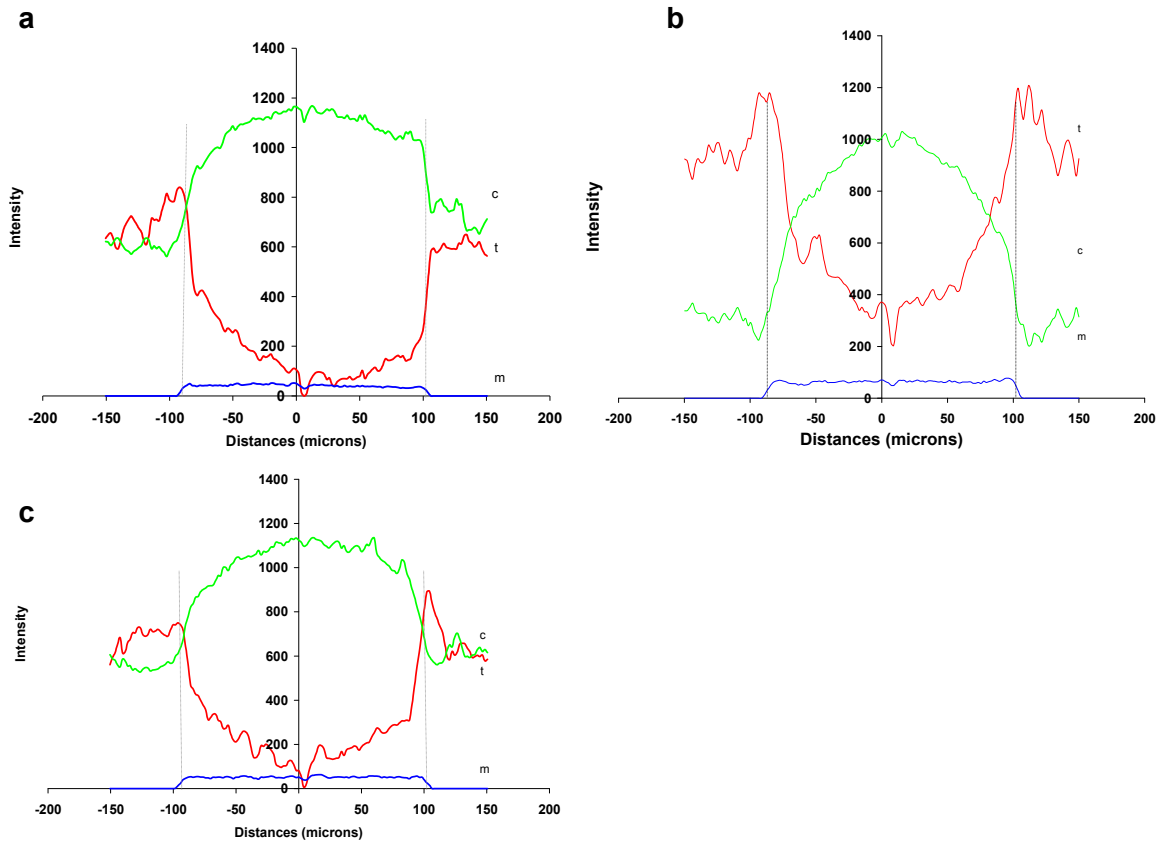

Figure 5.63 Relative Raman intensity of Lava™ (a), Cercon® (b) and Invizion™ (c) due to tetragonal (t), cubic (c) and monoclinic (m) phases as a function of distance from the centre of the indentation produced using a 30 kg load. Data were obtained along a horizontal crack line.

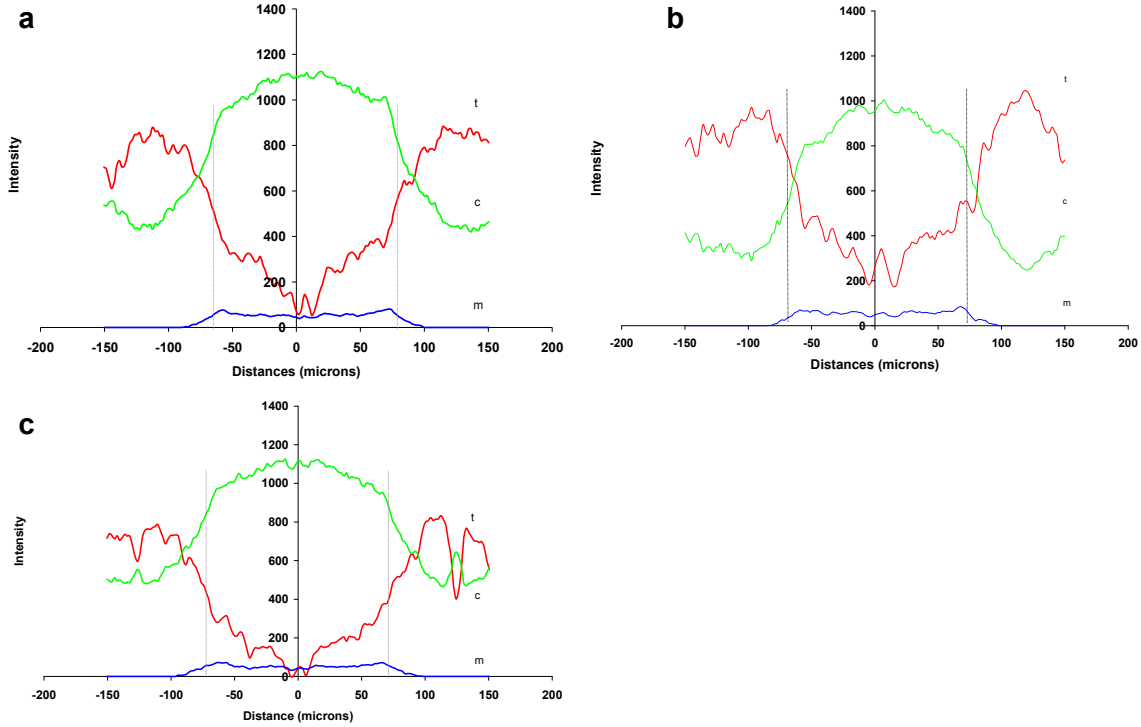

Figure 5.64 Relative Raman intensity of Lava™ (a), Cercon® (b) and Invizion™ (c) due to tetragonal (t), cubic (c) and monoclinic (m) phases as a function of distance from the centre of the indentation produced using a 30 kg load. Data were obtained along a diagonal line (45º to the groove).

Upon increasing the load there was an increase in the size of the indentation areas as expected. Mean values of tetragonal, cubic and monoclinic phases of Lava™, Cercon® and Invizion™ obtained within the rectangle shown in Figure 5.65-5.67 and within the indentation region, however, exhibited no experimentally significant variation with increasing the load from 20 to 50 kg. This would indicate that the level of transformation was largely determined by the indentation area. Assuming tetragonal, cubic and monoclinic were proportional to the fractions of each phase, it can be presumed that the fraction of tetragonal and cubic phases at a distance d from the centre x_d and y_d respectively are given by

$$x_d = \frac{t_d}{t_o} x_o$$

And

$$y_d = \frac{c_d}{c_o} y_o$$

where the subscript O indicates values for a polished surface. x_o and y_o are then the fractions of tetragonal and cubic phases in a polished surface which from XRD and Table 5.6 are equal to 0.68 and 0.32 respectively. The fraction of monoclinic phase in the indentation region will then be given by

$$z_d = 1 - x_d - y_d$$

Fractions of each phase as a function of distance from the indentation centre for the 50kg load are shown in Figure 5.65-5.67. There was a difference in the fractions of the three phases between Lava™ Cercon® and Invizion™ from the centre of the indentation to outside the indentation area. Figure 5.65 presents the data for the fractions of the three phases in Lava™ specimens. The monoclinic phase was higher at the centre by approximately 25%, but slightly declined to 13% and stayed at the same level along the indentation. It slightly decreased after the edge area and increased again along the crack line. The cubic phase was higher at the centre area then gradually decreased along the indentation. In contrast, the tetragonal phase increased from the centre (20%) to the outside (70%) area. The result for the Cercon® specimens (Figure 5.66) indicated that in the centre of the indentation, the level of tetragonal phase declined to approximately 25%, whereas the cubic and monoclinic phases increased to around 43 % and 32% respectively. The difference in the phase fractions between the three phases of Cercon® specimens was not large compared to Lava™ and Invizion™. The results for the Invizion™ specimens (Figure 5.67) showed that the monoclinic was higher by approximately 28% at the centre but slightly decreased along the indentation. The cubic phase slightly decreased from the centre and dropped dramatically outside the indentation area while the tetragonal phase increased along the indentation. The monoclinic phase along the indentation of Lava™ and Invizion™ was slightly lower at approximately 10% compared to Cercon® (20%).

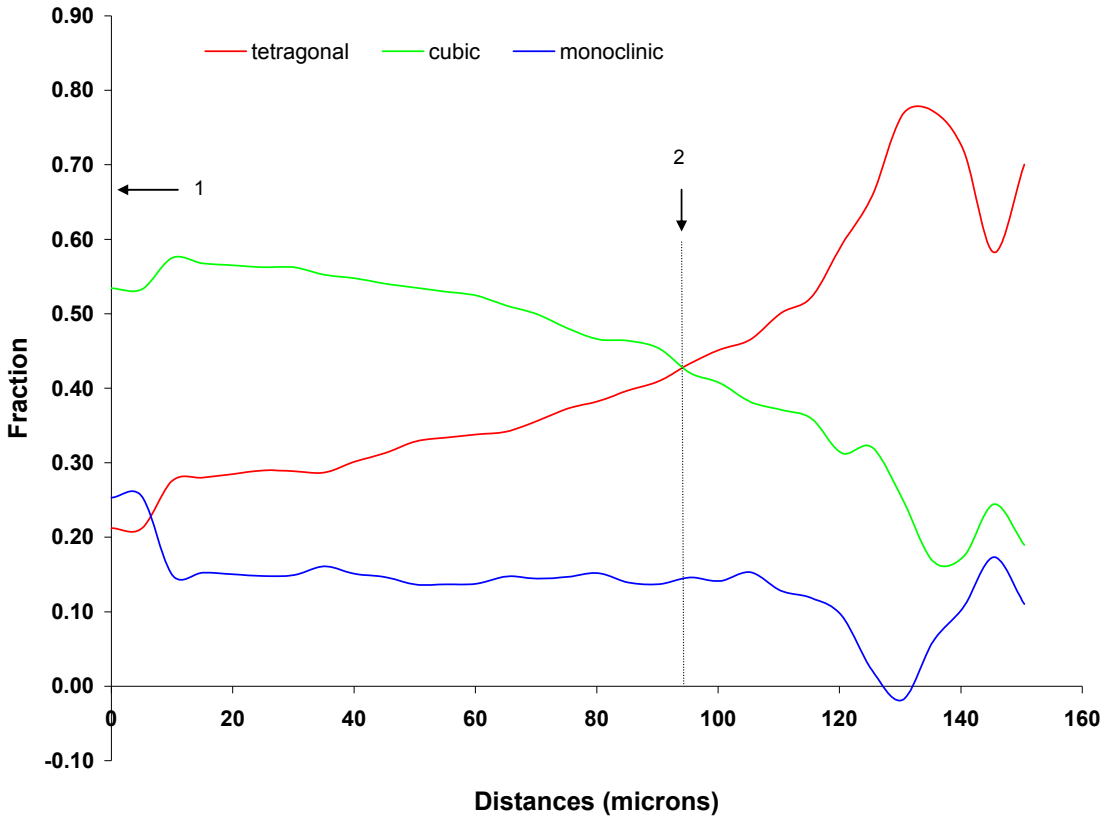

Figure 5.65. Example of the variation in average tetragonal (red), cubic (green) and monoclinic (blue) phase fractions of Lava™ specimens obtained within the rectangle shown in Figure 5a as a function of distance from the centre (1) (Data shown are for the 50 kg loaded specimen).

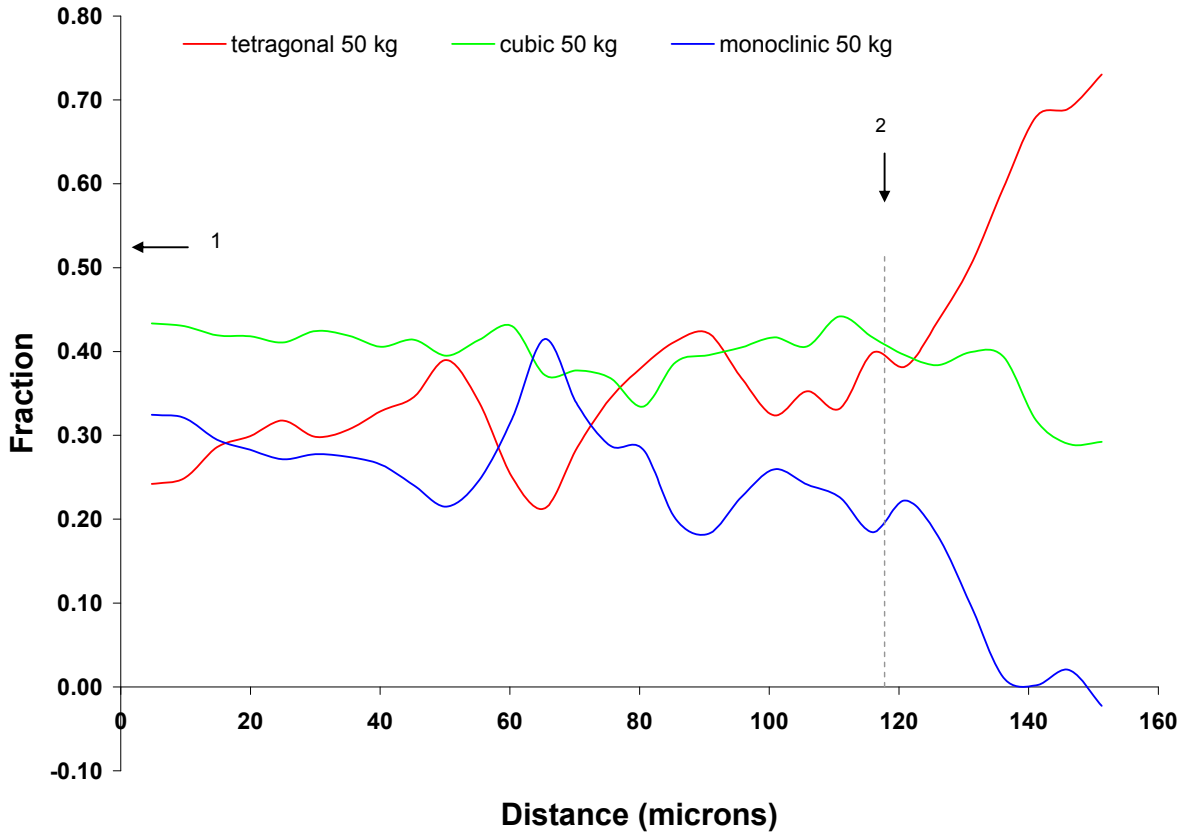

Figure 5.66. Example of the variation in average tetragonal (red), cubic (green) and monoclinic (blue) phase fractions of Cercon® specimens obtained within the rectangle shown in Figure 5a as a function of distance from the centre (1) (Data shown are for the 50 kg loaded specimen).

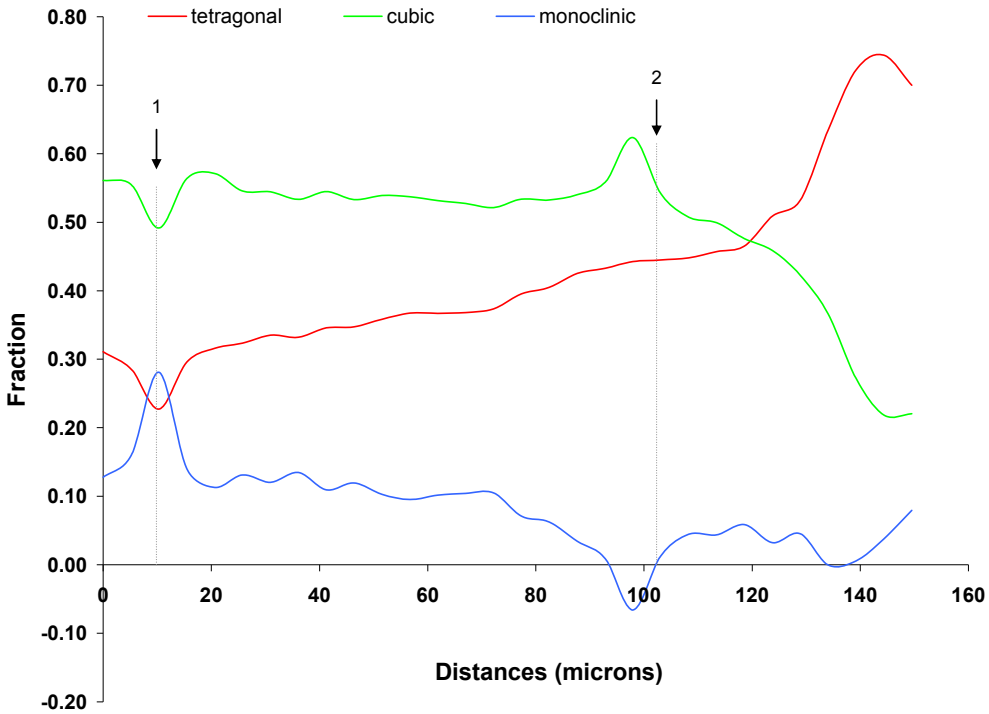

Figure 5.67. Example of the variation in average tetragonal (red), cubic (green) and monoclinic (blue) phase fractions of Invizon® specimens obtained within the rectangle shown in Figure 5a as a function of distance from the centre (1) (Data shown are for the 50 kg loaded specimen).

5.1.7.2 Study of phase transformation of fractured specimen surface from biaxial flexural strength

Figure 5.68 shows that the fracture surface has all three phases (tetragonal, Figure 5.68b; cubic, Figure 5.68c; and monoclinic, Figure 5.68d). Higher levels of monoclinic phase were found in the area near the fracture origin compared to other areas (Figure 5.68d). The cubic phase was also found to be of greater intensity at the fracture origin and the tensile side, whilst the tetragonal intensity slightly decreased at the fracture origin area.

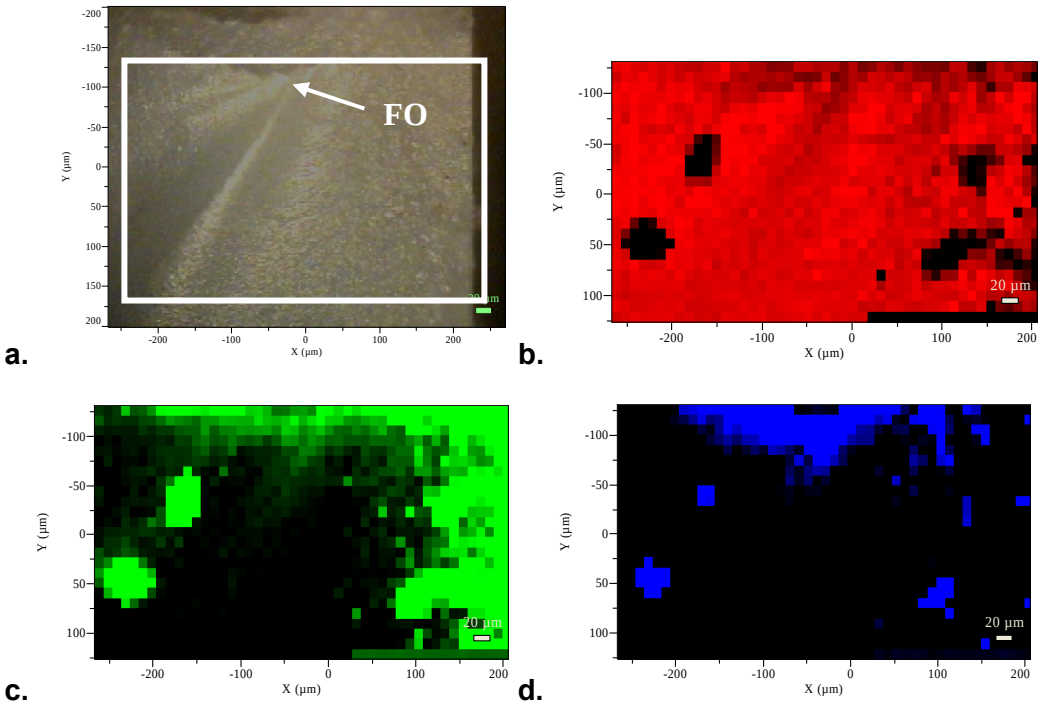

Figure 5.68. Visual image of one part of fracture surfaces obtained using the Raman microscope camera. The white square showed the area which was scanned. FO is the fracture origin and T is the tensile side. Figures 5.68 b, c and d indicate the relative levels of tetragonal (b), cubic (c), and monoclinic (d) phases within the rectangle shown in figure 10a. Black regions indicate lower levels of each given phase.

5.1.7.3 Measurement of phase transformation of fracture surface of specimens from subcritical crack growth test

Raman images of the tension side of the fractured surfaces of specimens (Figure 5.69-5.70) after subcritical crack growth testing using different loading rates from 100 to 0.1 $N.s^{-1}$ showed that the fractured specimen had all three phases (tetragonal, b; cubic, c; and monoclinic, d). The tetragonal phase was found throughout the specimen surface; however, it slightly decreased at the fracture origin area. The cubic phase was also found to be greater intensity at the fracture origin and at the edge under tensile stress whilst higher levels of monoclinic phase were located in the area near the fracture origin, at the edge under tensile stress and appeared along with some crack lines. Raman images showed no difference in the intensity of the three phases when using different loading rates. Therefore, the Raman images of the specimens using a loading rate of 100 and 0.1 $N.s^{-1}$ were compared and others are presented in the appendix.

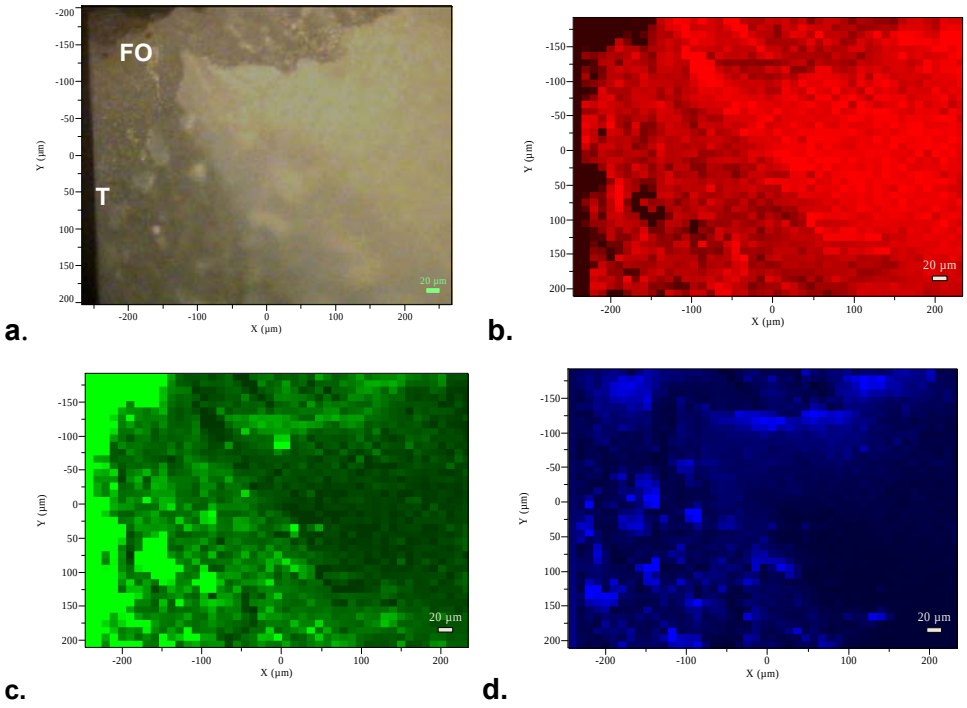

Figure 5.69. Visual image of one part of fracture surfaces at tension side after subcritical crack growth test using 100 $N.s^{-1}$ obtained using the Raman microscope camera. FO is the fracture origin and T is the tensile side. Figures 10 b, c and d indicate the relative levels of tetragonal (b), cubic (c), and monoclinic (d) phases. Black regions indicate lower levels of each given phase.

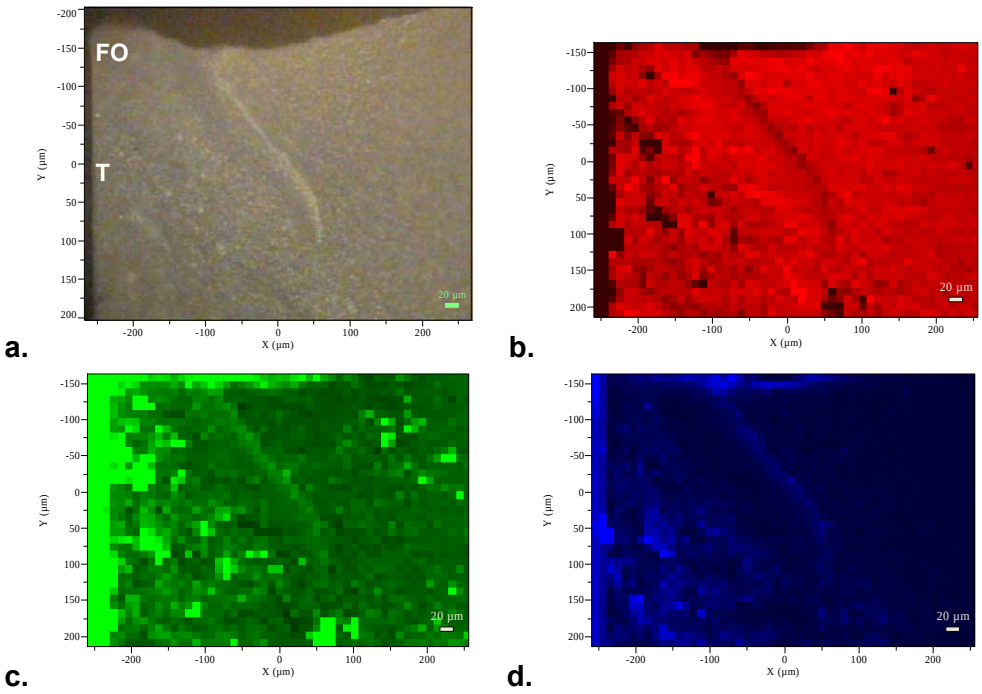

Figure 5.70. Visual image of one part of fracture surfaces at tension side after subcritical crack growth test using 0.1 $N.s^{-1}$ obtained using the Raman microscope camera. FO is the fracture origin and T is the tensile side. Figures 5.70 b, c and d indicate the relative levels of tetragonal (b), cubic (c), and monoclinic (d) phases. Black regions indicate lower levels of each given phase.

Raman images of fractured surfaces of specimens on the compression side (Figure 5.71-5.72) after subcritical crack growth testing using different loading rates from 100 to 0.1 $N.s^{-1}$ showed that the fractured specimen had all three phases (tetragonal, b; cubic, c; and monoclinic, d). The tetragonal phase was found throughout the whole specimen surface; however, it slightly decreased at the edge under compression stress and along the crack lines. The cubic phase was found to be greater at the area under compression stress and along the crack lines. The higher intensity of the monoclinic phase was found only at the edge under compression stress and the crack line. Raman images showed no difference in the intensity of the three phases on the compression side when using different loading rates. The Figure 5.71 and 5.72 showed the intensity of three phases using the loading rate of 100 and 0.1 $N.s^{-1}$. Other images are shown in the appendix.

Raman images of tetragonal and cubic phases on the compression side had a similar pattern compared to the tension side; however, the monoclinic phase on the compression side had a lower intensity compared with the tension side.

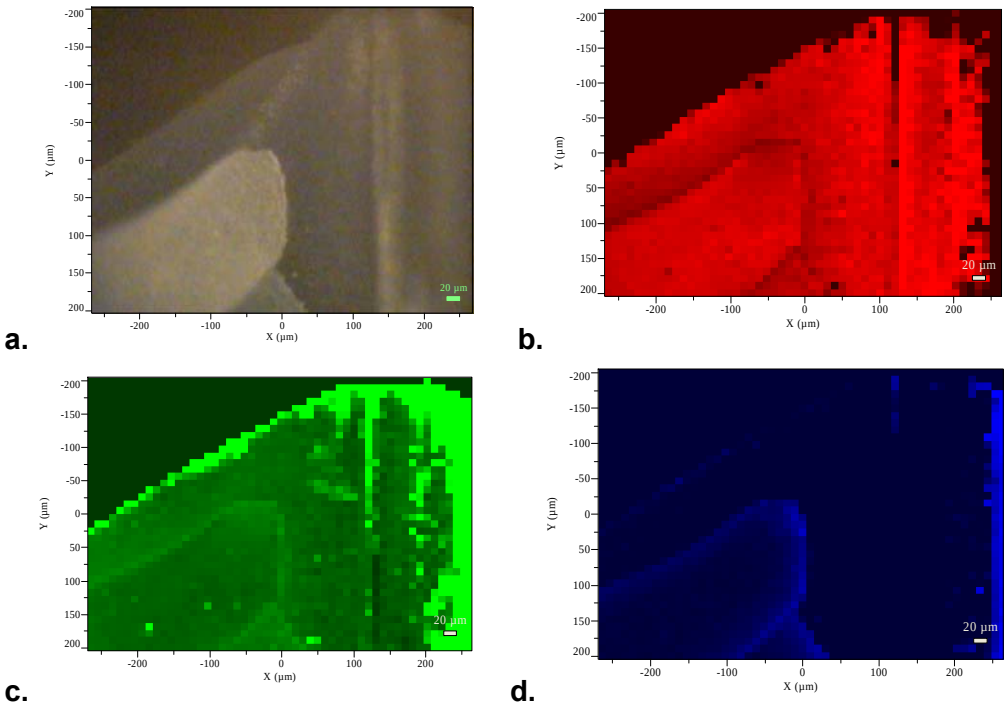

Figure 5.71. Visual image of one part of fracture surfaces at compression side after a subcritical crack growth test using 100 $N.s^{-1}$ obtained using the Raman microscope camera. Figures 5.71 b, c and d indicate the relative levels of tetragonal (b), cubic (c), and monoclinic (d) phases. Black regions indicate lower levels of each given phase.

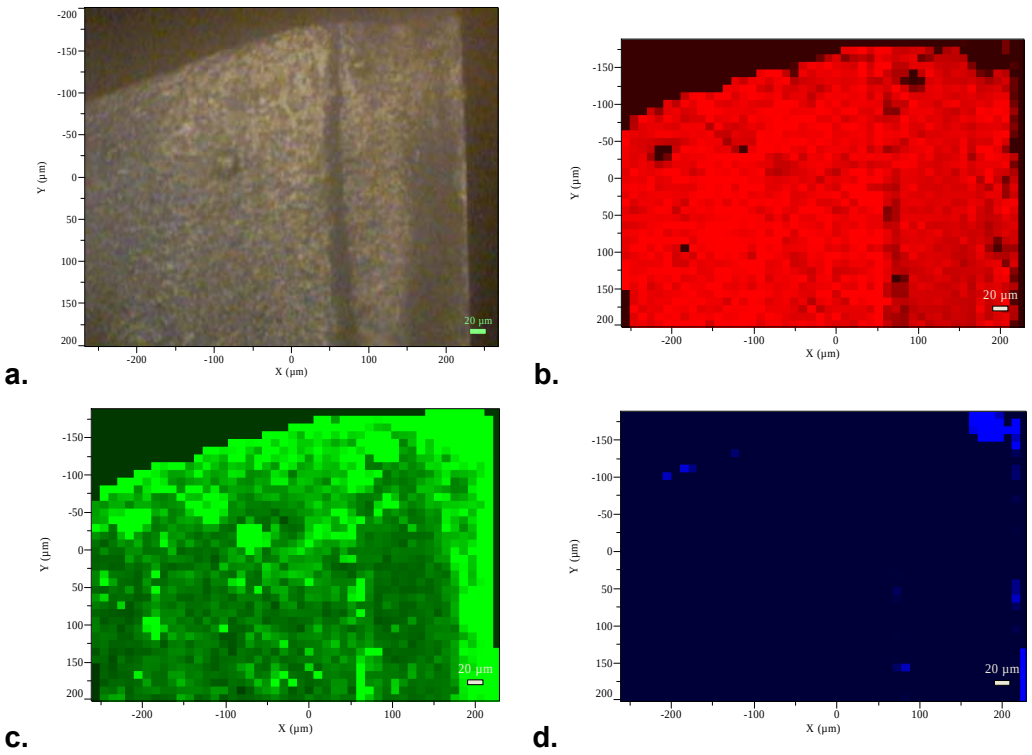

Figure 5.72. Visual image of one part of fracture surfaces at compression side after subcritical crack growth test using 0.1 $N.s^{-1}$ obtained using the Raman microscope camera. Figures 5.72 b, c and d indicate the relative levels of tetragonal (b), cubic (c), and monoclinic (d) phases. Black regions indicate lower levels of each given phase.

In general, the Raman intensity of the three phases as a function of distance from the fractured areas, comparing between tension and compression sides identified that the cubic phase had the highest intensity at the fracture origin areas and had an abrupt decrease while moving away from the fracture areas. In addition, it had higher intensity at the edge of the specimen, which under the stress. The tetragonal phase was slightly low at the fracture origin area, but slightly increased when moving away from the fracture. The higher level intensity of the monoclinic phase was found at the fracture area and it became zero when moving away from the fracture. The monoclinic phase also had very low intensity when compared with tetragonal and cubic intensity.

Figure 5.73 shows that the Raman intensity of fractured specimens on the tension and compression sides after subcritical crack growth testing using a loading rate 100 $N.S^{-1}$ had higher intensity of the cubic and monoclinic phases at the fractured area while the tetragonal phase had a lower intensity compared with the other phases. The tension and compression sides had the highest intensity of the cubic phase approximately 100 μm from the fracture area. The tetragonal phase had a low intensity at the fracture area and an abrupt increase at 50 μm on the tension and 30 μm on the compression side and then slightly increased while moving away from the fracture sites. The monoclinic phase occurred at the fracture area until 438 μm on the tension side and 20 μm on the compression side.

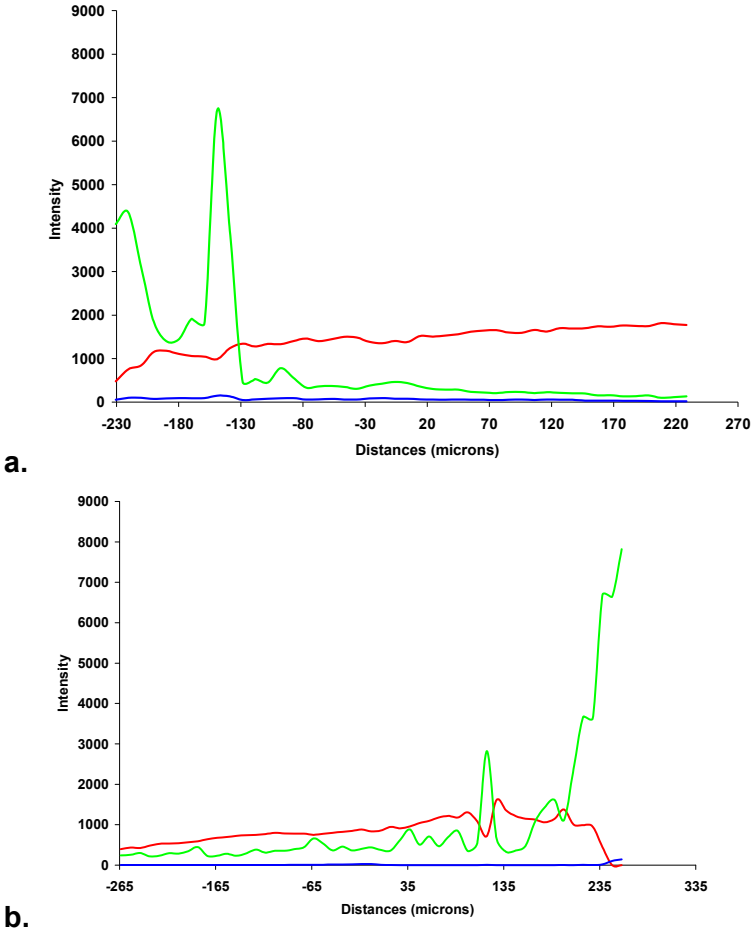

Figure 5.73. Raman intensity of tetragonal (red), cubic (green) and monoclinic phases (blue) at the tension (a) and compression (b) sides of fractured Lava™ specimens after subcritical test using 100 $N.s^{-1}$ loading rate as a function of a distance from the fractured area.

Figure 5.74 shows that the Raman intensity of fractured specimens on the tension and compression sides after subcritical crack growth testing using a loading rate at 0.1 $N.s^{-1}$ had a high intensity of the cubic and monoclinic phases at the fractured area while the tetragonal phase had a lower intensity compared with the other phases. The cubic phase was found to have a high intensity approximately 100

μm from the fracture area on the tension and compression sides. Tetragonal phase had low intensity at the fracture area and an abrupt increase until 20 μm from the fracture at the tension and the compression side and then only slightly increased when moving away from the fracture. The monoclinic phase on the tension side was found to have a high intensity at the fracture origin area until 11 μm and had very low intensity up to 400 μm, whilst on the compression side was found to have high intensity until 61 μm from the fracture area.

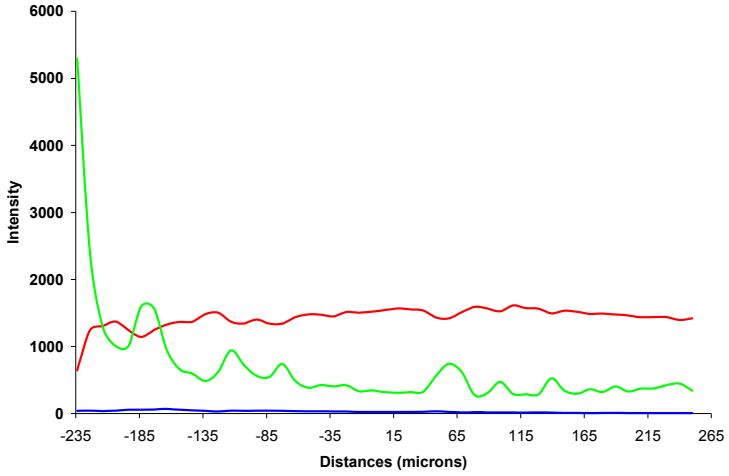

a.

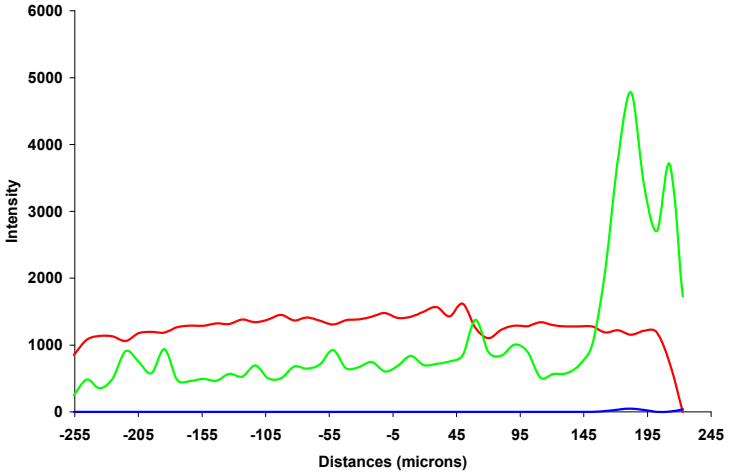

b.

Figure 5.74. Raman intensity of tetragonal (red), cubic (green) and monoclinic phases (blue) at the tension (a) and compression (b) sides of fractured Lava™ specimens after subcritical test using 0.1 $N.s^{-1}$ loading rate as a function of distance from the fractured area.

Therefore, it may be concluded that the variation in the indentation load between 20 and 50kg has little effect on the level of transformation toughening per unit area. The transformation toughening occurred mainly in the indentation. Within experimental error no transformation toughening was detectable along the crack line outside the indentation even using the highest load. In fractured samples from biaxial flexural strength, phase transformation was found only near the fracture origin.

The different loading rates ranging from 100 to 0.1 $N.s^{-1}$ used in the subcritical crack growth test did not affect the intensity of the three phases; however, a higher level of the phase transformation was found at the fracture origin area of the tension side compared with the compression side.

5.2 3Y-TZP containing titanium phosphate glass

5.2.1 Density and Shrinkage

Lava specimens had a density of 6.1 g/cm^3 which was higher than experimental non-glass zirconia and phosphate glass contained zirconia density. The experimental zirconia had a density ranging from 4.4 to 5.7 g/cm^3 dependant on the percentage of glass contained and the sintering temperature. Although, experimental non-glass zirconia had a density of 5.62 g/cm^3 which was lower than the commercial zirconia density, it had similar value to 1 and 2% glass reinforced zirconia sintered at 1400°C (Table 5.12). 5% phosphate glass zirconia had a slightly lower density compared with other zirconia specimens sintered at 1400°C. 1, 2 and 5% titanium phosphate glass zirconia sintered at 1400°C had a higher density than 5% and 20% titanium phosphate glass zirconia sintered at 1300°C (Table 5.12).

Non-glass zirconia and titanium phosphate glass zirconia sintered at 1400°C had similar linear shrinkage values ranging from 21-23%. This was higher than zirconia groups sintered at 1300°C (10-13%) (Table 5.12). However, they had a similar shrinkage percentage to commercial zirconia that ranged from 20-25% (Piwowarczk *et al.* 2005).

Table 5.12. Densities of Lava and titanium phosphate glass reinforced zirconia with different glass percentages and firing temperatures.

Groups	Density (±SD)(g/cm^3)	Shrinkage (%)
Lava discs	6.1 (±0.06)	20-25% (Piwowarczk *et al.* 2005)
Control 1400 ºC	5.62 (±0.03)	21.25
1 wt% 1400 ºC	5.77 (±0.05)	23.81
2 wt% 1400 ºC	5.73 (±0.28)	23.23
5 wt% 1400 ºC	5.05 (±0.07)	17.99
5 wt% 1300 ºC	4.90 (±0.35)	10.59
20 wt%1300 ºC	4.41 (±0.04)	13.75

5.2.2 Biaxial flexural strength (BFS), hardness and reliability

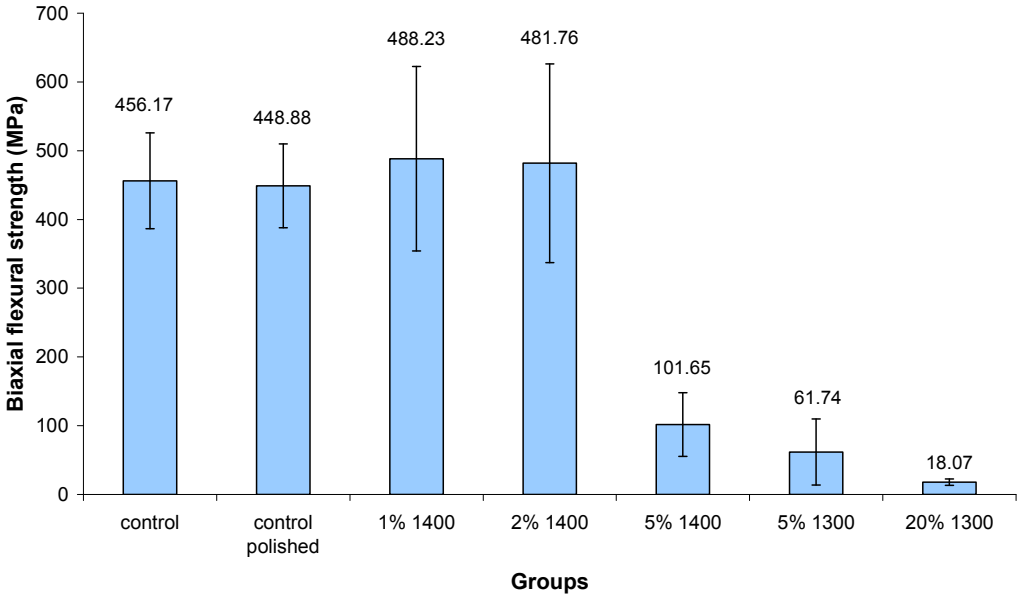

Figure 5.75. Biaxial flexural strength of control and phosphate glass reinforced zirconia groups containing 1-20 wt% titanium phosphate glass at different firing temperature

Non-glass zirconia groups had mean biaxial flexural strengths of approximately 450 MPa (Figure 5.75), which was lower compared to commercial zirconia groups (800-1100). There was no significant difference in biaxial flexural strength between the as-received and polished control specimens. Additionally, two control groups had a mean biaxial flexural strength slightly lower than 1 wt% and 2 wt% glass zirconia. However, there was no statistically significant difference in the mean biaxial flexural strength among the groups ($P>0.05$) except the 5 wt% and 20 wt%, which had significantly lower biaxial flexural strength compared with other groups ($P<0.001$).

Table 5.13. The biaxial flexural strength (MPa), characteristic strength(σ), Weibull moduli (*m*), confidence interval, R^2-values and Vickers hardness of control as-received control, polished control, 1%, 2%, and 5% phosphate glass discs (n = 30) sintered at 1400°C

Group	Mean strength (MPa) (±SD)	Characteristic strength (σ) (MPa)	95% Confidence intervals for characteristic strength (σ)	Weibull modulus (*m*)	95% Confidence intervals for Weibull modulus	R^2-value	Hardness (HV)
Control as-received	458.40 (±69.26)	486.96	465.34-509.58	7.6	5.8-10.1	0.95	1015.98 (±47.08)
Control polished	448.88 (±60.92)	475.13	445.46-495.65	8.2	6.3-10.8	0.95	1010.24 (±50.35)
1%	488.23 (±134.23)	536.59	493.23-583.75	4.1	3.2-5.3	0.96	1158.02 (±44.16)
2%	481.76 (±144.61)	530.48	485.19-579.99	3.9	3.0-5.0	0.96	1139.51 (±89.15)
5%	101.65 (±46.22)	111.19	99.52-126.47	3	2.4-3.6	0.96	519.98 (±28.26)

The highest characteristic strength (σ) of titanium phosphate glass-containing zirconia was found in the groups containing 1 wt% and 2 wt% glass with a value of approximately 530 MPa, while 5 wt% titanium phosphate glass-zirconia specimens had the lowest value (111.19 MPa). The 95% confidence intervals of the characteristic strength identified no significant difference in the characteristic strength among control groups and 1 and 2 wt% titanium phosphate glass-zirconia groups except 5% titanium phosphate glass-zirconia group. The latter group had a significantly lower characteristic strength. The Weibull modulus of the as-received and polished control groups were 7.6 and 8.2, respectively. Titanium phosphate glass-zirconia groups had significantly lower Weibull modulus of approximately 3. The 95% confidence intervals of Weibull modulus of glass zirconia failed to overlap with control groups (Table 5.13).

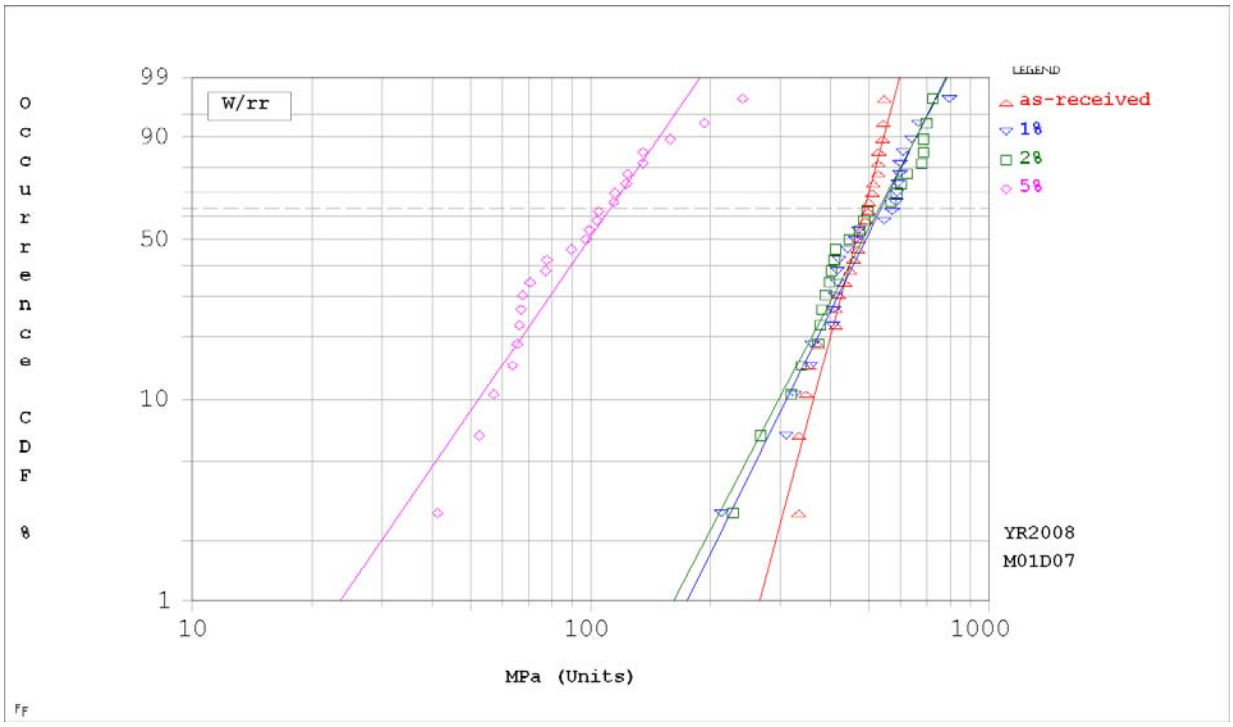

Figure 5.76. Weibull plot of as-received non-glass zirconia and glass-zirconia groups (1, 2 and 5 wt%).

The Weibull plot (Figure 5.76) showed that 5 wt% titanium phosphate glass-zirconia had a significantly different data distribution compared with the other groups. Additionally, 1, 2 and 5 wt% titanium phosphate glass-zirconia had a different slope compared with the as-received non-glass zirconia group, which means the titanium phosphate glass-zirconia had a different strength reliability compared with the as-received non-glass zirconia group.

5.2.3 Fracture analysis of surfaces of specimens failed from biaxial flexural test using SEM

Figure 5.77 shows the fracture surfaces of non-glass and titanium phosphate glass reinforced zirconia following biaxial flexural strength testing. The specimens showed different failure mechanisms. Some specimens failed by forming two pieces and some failed by delamination. Only a few failed by forming 3-4 pieces. Representative samples of non-glass zirconia fractured into two pieces (Figure 5.77). Significant porosity was seen at the fracture origin. The fracture pattern was not the classic mirror like region; however, the crack was initiated at the tension side.

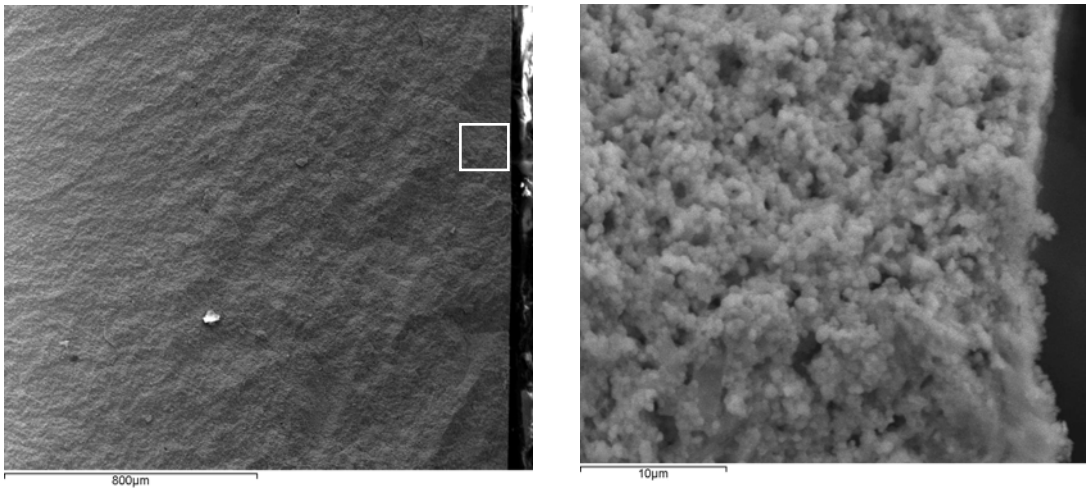

Figure 5.77. Fracture surface of non-glass zirconia failed in biaxial flexural test.

A representative sample of 1 wt% titanium phosphate glass zirconia failed by forming four pieces showed that there was no mirror-like region at the fracture origin. The fracture origin area was slightly rough and there were several irregular cracks which had occurred.

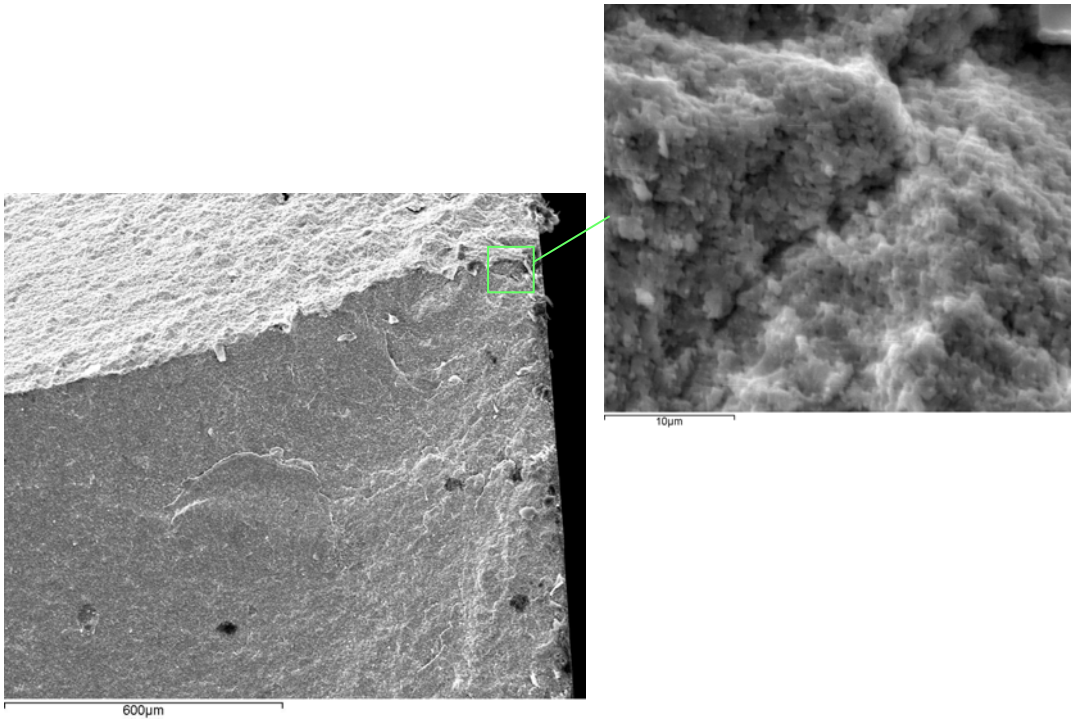

Figure 5.78. Fracture surface of 1 wt% glass zirconia failed in biaxial flexural test.

A representative sample of 2 wt% titanium phosphate glass zirconia failed by forming two pieces and it showed a rough surface with the crack lines initiated from the tension side and no mirror like region was found. Significant porosity was identified when using higher magnification.

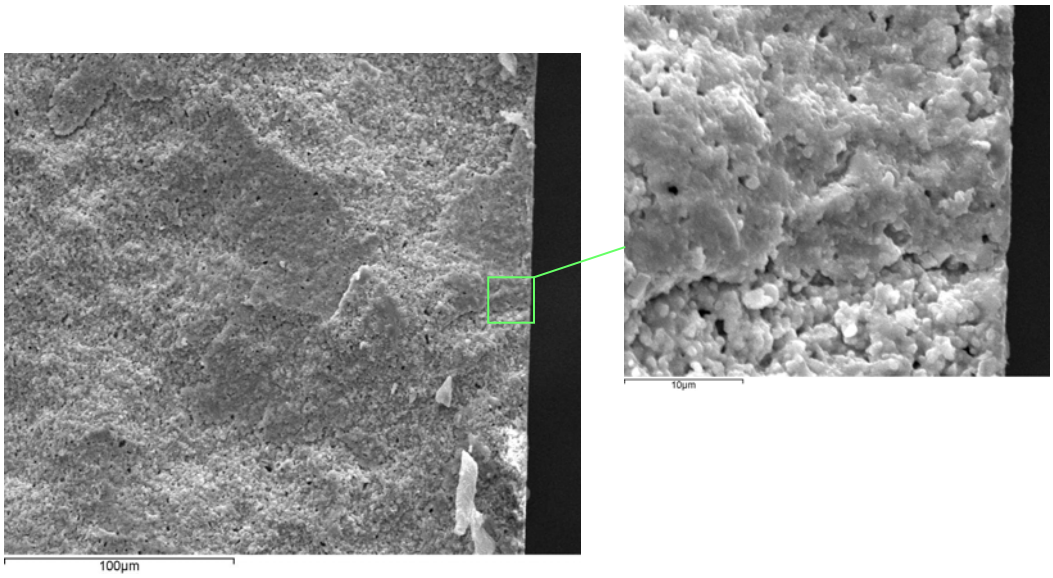

Figure 5.79. Fracture surface of 2 wt% glass zirconia failed in biaxial flexural test.

A representative sample of 5 wt% glass zirconia showed larger and more widespread porosity compared with the other groups. The surface was rough with several irregular crack lines.

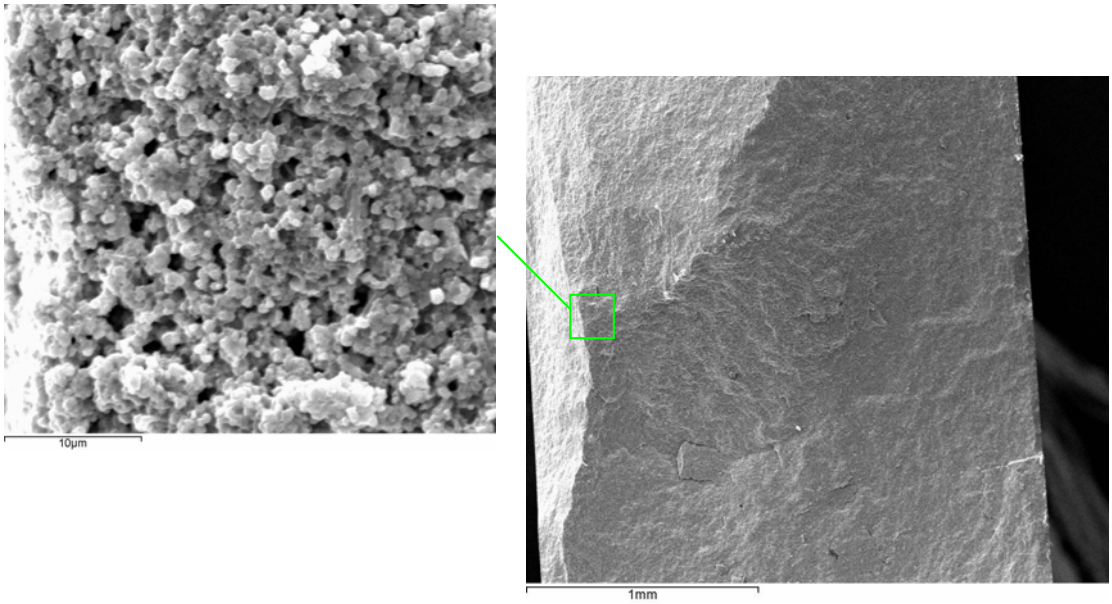

Figure 5.80. Fracture surface of 5 wt% glass zirconia failed in biaxial flexural test.

5.2.4 Shear bond strength

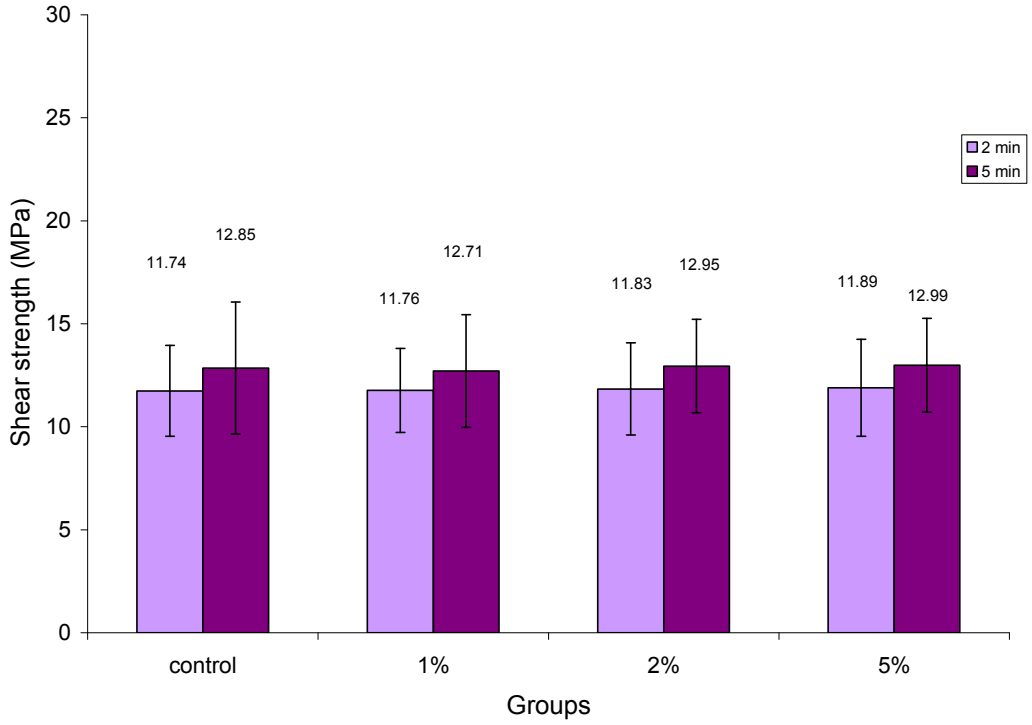

Figure 5.81. Shear bond strengths of experimental non-glass and glass zirconia groups and unetched composite resin blocks.

Figure 5.81 presents shear bond strength of etched experimental zirconia with unetched composite blocks. A five minute HF etching provided slightly higher (12.9 MPa) shear bond strength compared with two minute etching (11.8 MPa), however, one-way ANOVA showed no significant difference between the two groups (P>0.05). The shear bond strength values of control and 1, 2, and 5 wt% titanium phosphate glass containing zirconia were also not statistically different (P>0.05).

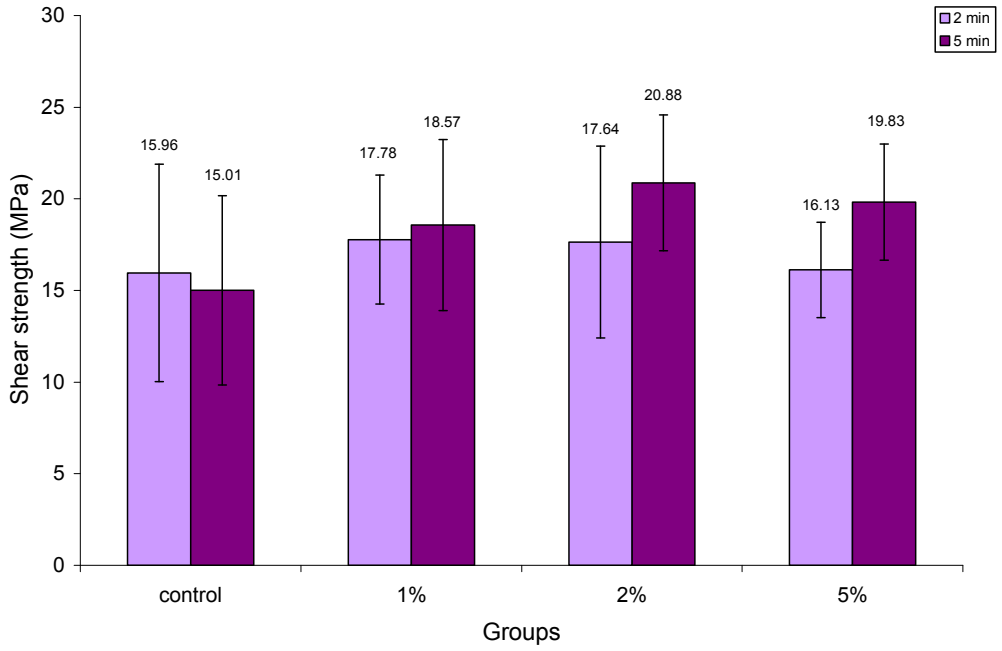

Figure 5.82. Shear bond strengths of experimental non-glass and glass zirconia groups and etched composite resin blocks.

Figure 5.82 shows the shear bond strength of etched experimental zirconia with etched composite blocks. Etching for 5 minutes provided slightly higher shear bond strength compared with 2 minute etching groups except the control group which had a shear bond strength after 5 minutes etching slightly lower than the two minutes etching group. However, one-way ANOVA showed there was no significant difference in shear bond strength between 2 and 5 minutes and also control and the 1, 2 and 5 wt% titanium phosphate glass containing zirconia.

In addition, zirconia groups with unetched composite resin blocks had lower shear bond strength than zirconia groups with etched composite resin blocks.

5.2.5 SEM analysis of etched titanium glass reinforced zirconia surface

5.2.5.1 Control

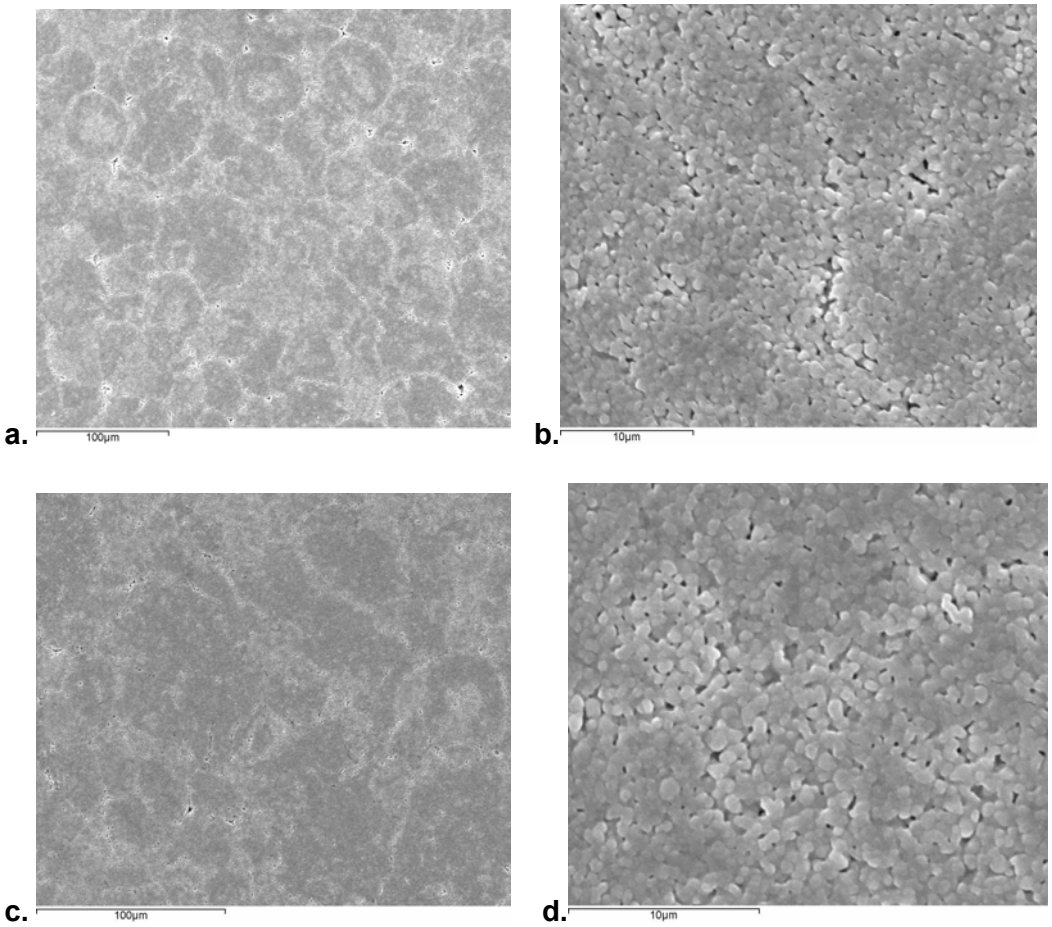

Figure 5.83. SEM images of non-glass zirconia specimen surfaces etched for 2 minutes (a, b) and 5 minutes (c, d) at 100 and 10 µm magnification.

SEM images (Figure 5.83) shows that the control or non-glass zirconia groups etched for 2 and 5 minutes had similar etched surfaces. Some porosity was seen on the surface.

5.2.5.2 zirconia containing 1 wt% titanium phosphate glass

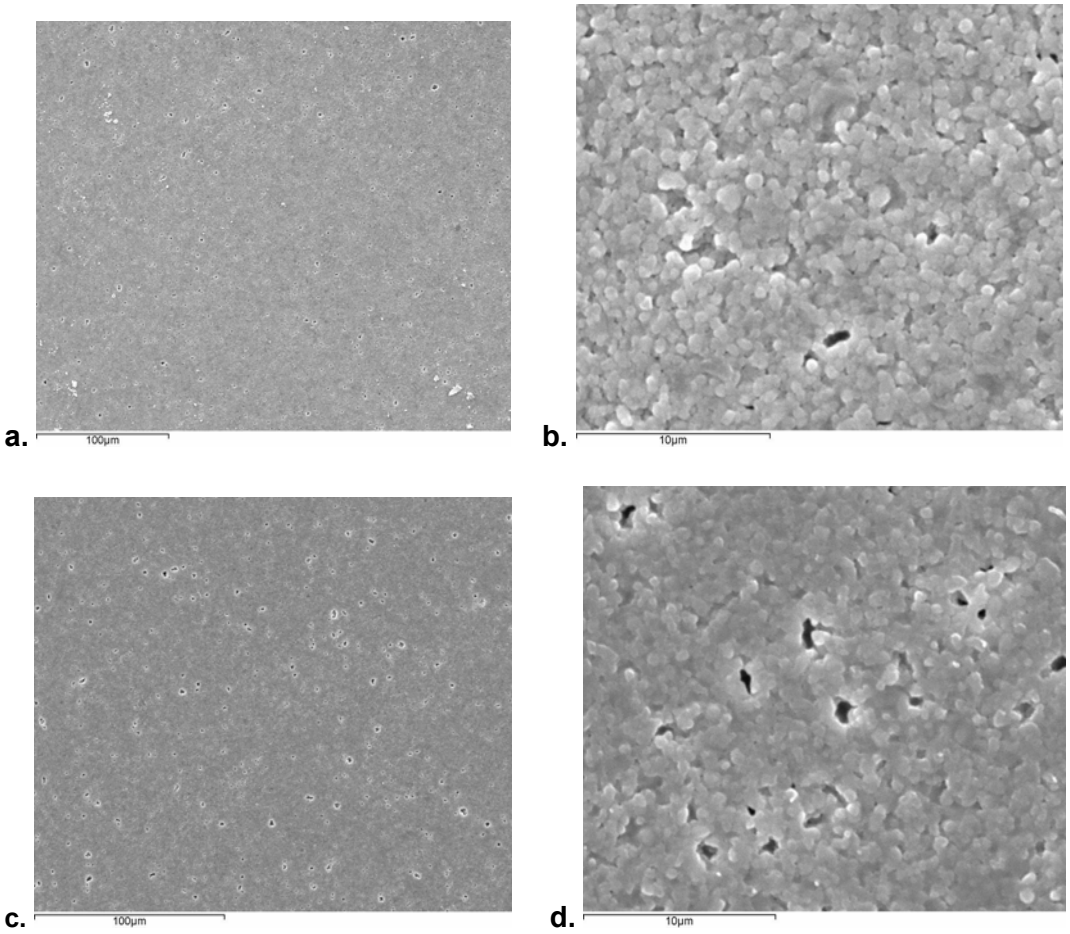

Figure 5.84. SEM images of zirconia containing 1 wt% titanium phosphate glass specimen surfaces etched for 2 minutes (a, b) and 5 minutes (c, d) at 100 and 10 µm magnification.

SEM images (Figure 5.84) shows that zirconia containing 1 wt% titanium phosphate glass etched for 2 and 5 minutes had slight differences in etch patterns. 1 wt% glass zirconia etched for 5 minutes had more numerous pores compared with 1 wt% glass zirconia etched for 2 minutes. Zirconia containing 1 wt% glass tended to have larger porosity than the control groups.

5.2.5.3 zirconia containing 2 wt% titanium phosphate glass

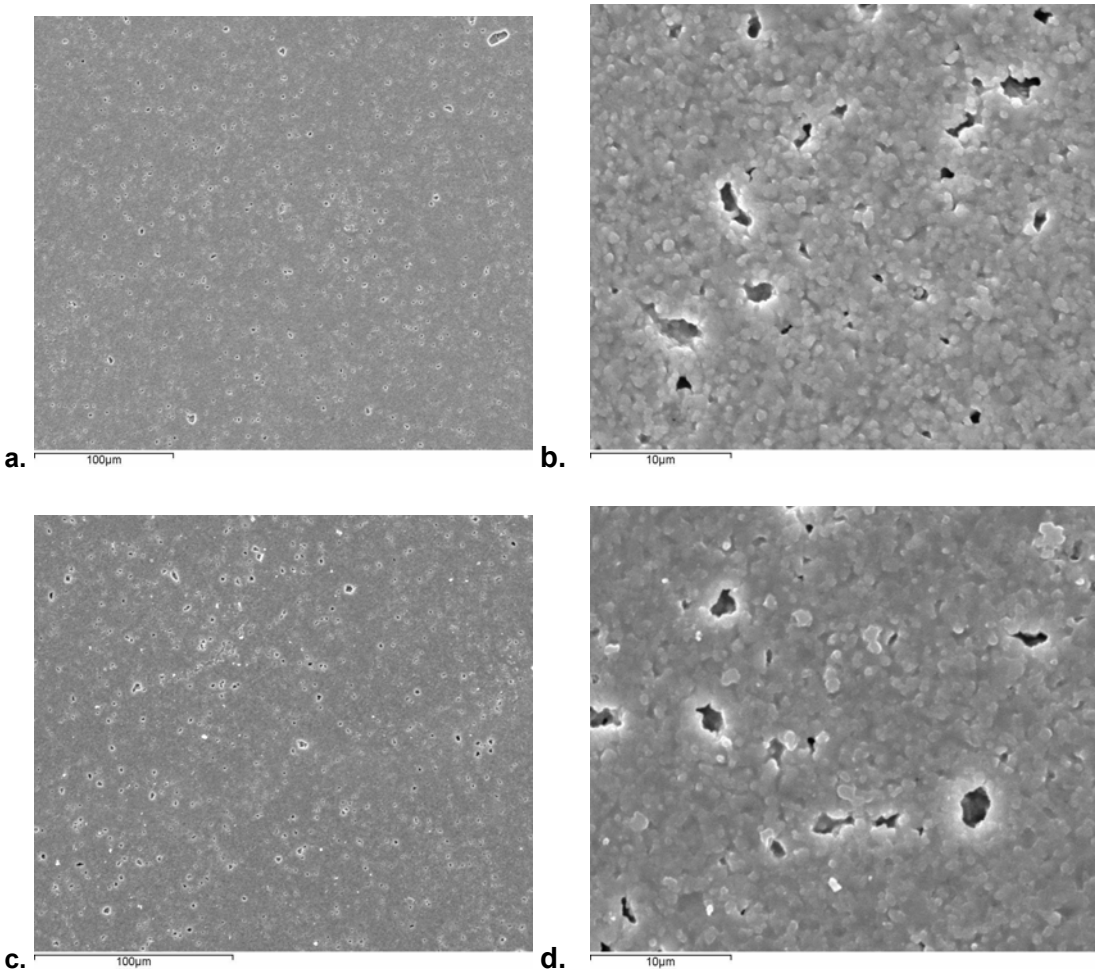

Figure 5.85. SEM images of zirconia containing 2 wt% titanium phosphate glass specimen surfaces etched for 2 minutes (a, b) and 5 minutes (c, d) at 100 and 10 µm magnification.

SEM images (Figure 5.85) shows that zirconia containing 2 wt% titanium phosphate glass etched for 2 and 5 minutes showed differences in etch patterns. 2 wt% glass zirconia etched for 5 minutes had larger pores compared with 2 wt% glass zirconia etched for 2 minutes. Additionally, they had larger pores compared with the control and 1 wt% glass zirconia.

5.2.5.4 zirconia containing 5 wt% titanium phosphate glass

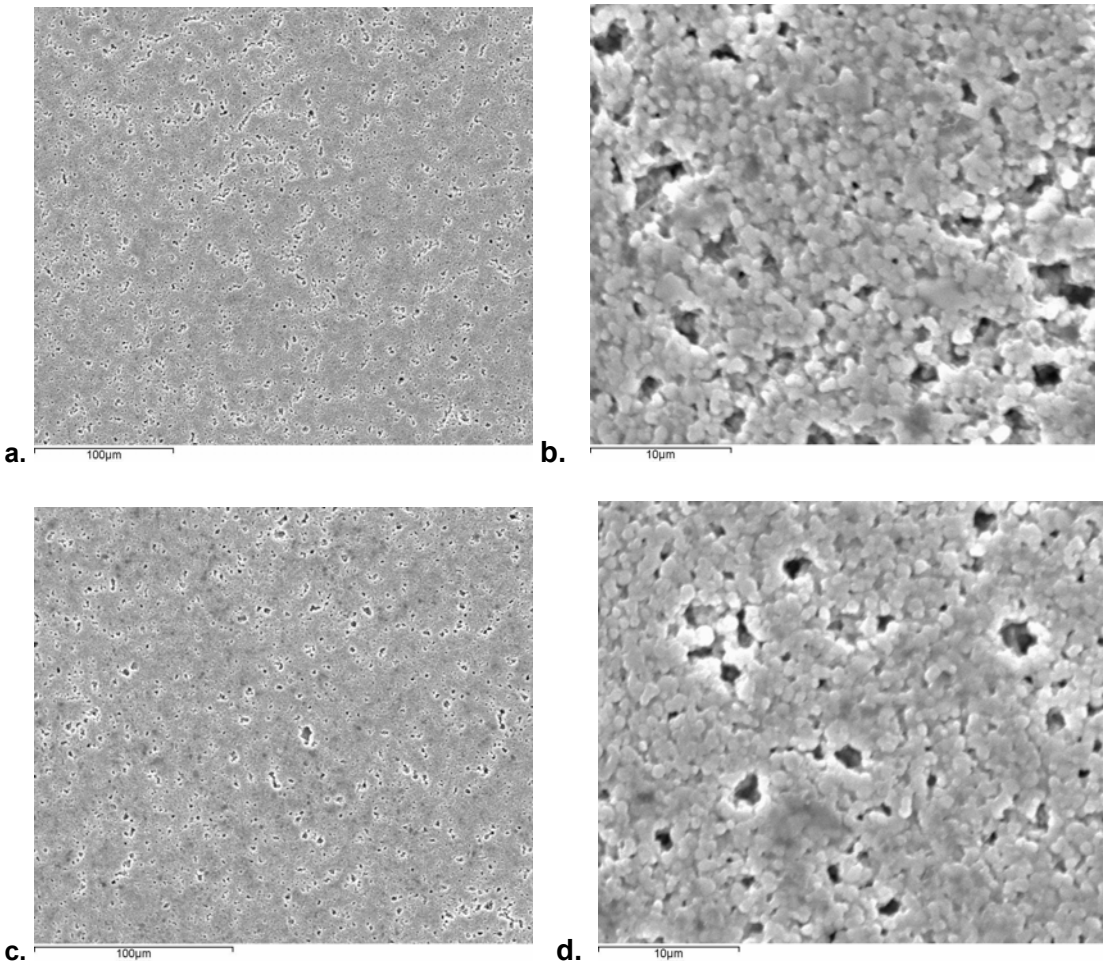

Figure 5.86. SEM images of zirconia containing 5 wt% titanium phosphate glass specimen surfaces etched for 2 minutes (a, b) and 5 minutes (c, d) at 100 and 10 µm magnification.

SEM images (Figure 5.86) shows that 5 wt% glass zirconia etched for 2 and 5 minutes had similar etch patterns. However, they have larger and more pores compared with the control, 1 wt% and 2 wt% glass zirconia groups.

5.2.6 Bonding failure

Bonding failure of etched composites occurred in three categories which were adhesive, cohesive and mixed types (Figure 5.87). The majority of the specimens had an adhesive failure and only a few failed by cohesive and mixed type. The types of failure of the specimens etched for 2 and 5 minutes was not significantly different. However, adhesive failure occurred in all specimens when the composite block was not etched.

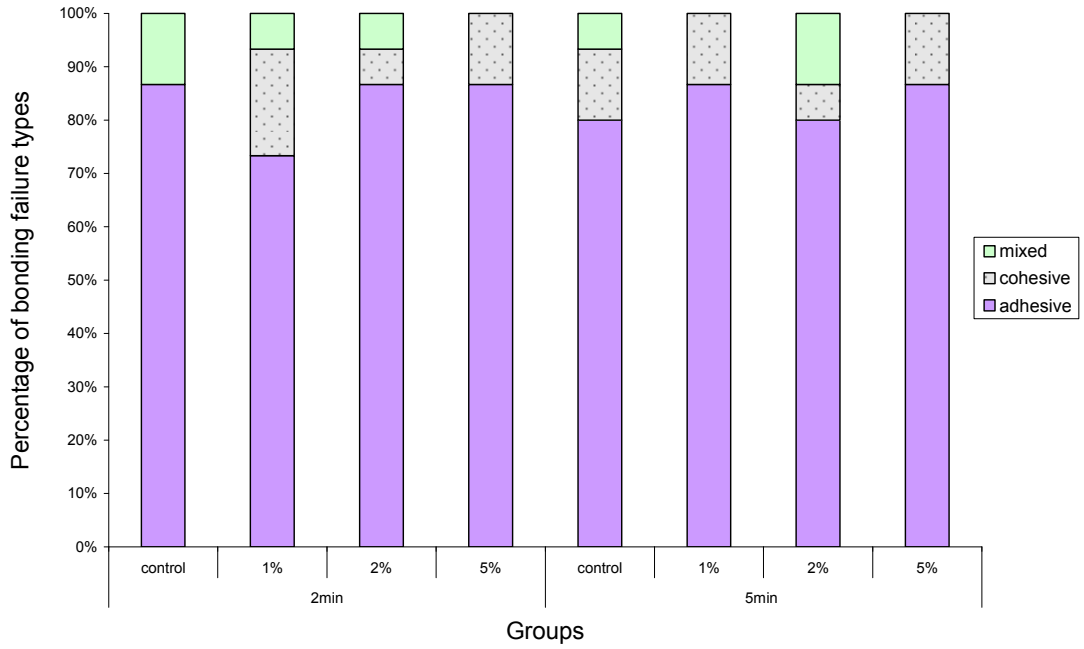

Figure 5.87. Bonding failure between etched composite block and non-glass and glass-zirconia (1 wt%, 2 wt% and 5 wt%) ceramics etched for 2 and 5 minutes.

Most of the specimens etched for 2 and 5 minutes had cement left on the surfaces of both composite blocks and ceramics. However, a few 2 and 5 minute etching specimens had all cement left either on the composite or ceramic surfaces while there were higher numbers of specimens which had all cement left on the

ceramic surfaces when etched for 5 minutes. Some pores were found on the cement layer.

Figure 5.88 shows the bonding failure of control groups when etched for 2 and 5 minutes. The 2 minute etching specimens had all cement left on the ceramic surface while 5 minute etching specimens had more cement on the composite block.

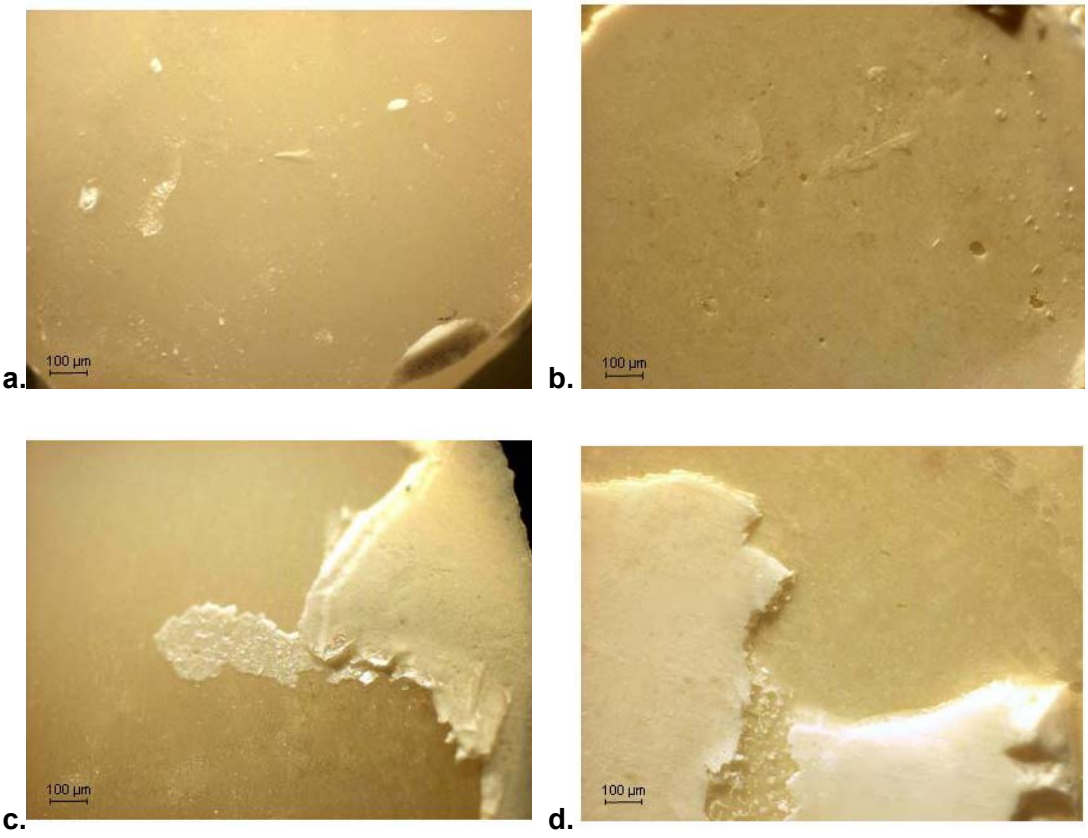

Figure 5.88. Images (x10 magnification) of bonding failure of unetched composite (left) and ceramic (right) non-glass zirconia specimen etched for 2 (a,b) and 5 minutes (c,d).

Figure 5.89 shows the bonding failure of 1 wt% glass zirconia which etched for 2 and 5 minutes. The 2 minute etching specimens had the cement left on both composite and ceramic surfaces, which were similar to the 5 minute etching

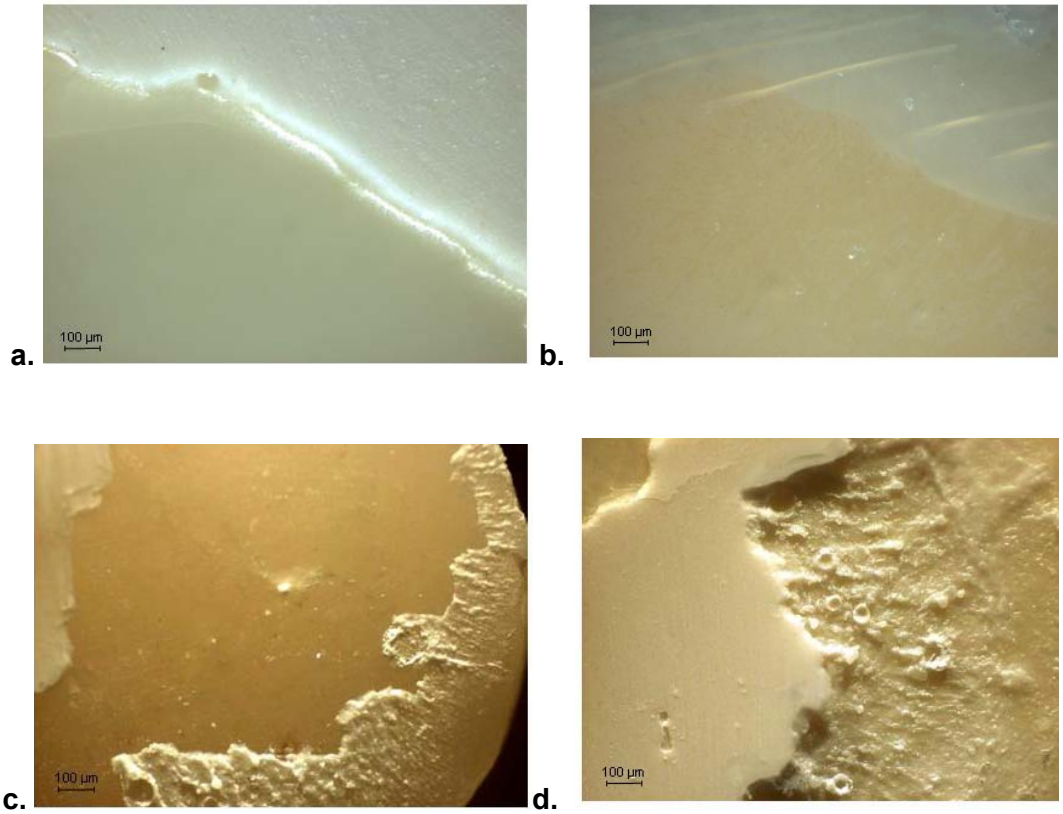

Figure 5.89. Images (x10 magnification) of bonding failure of unetched composite (left) and ceramic (right) 1 wt% glass zirconia specimen etched for 2 (a,b) and 5 minutes (c,d).

Figure 5.90 shows the bonding failure of 2 wt% glass zirconia which was etched for 2 and 5 minutes. The 2 and 5 minute etching specimens had the cement left mainly on the ceramic and some on the composite surfaces. The representative specimen of the 5 minute etching (Figure 5.90c, d) showed most of the cement left on the ceramic surface.

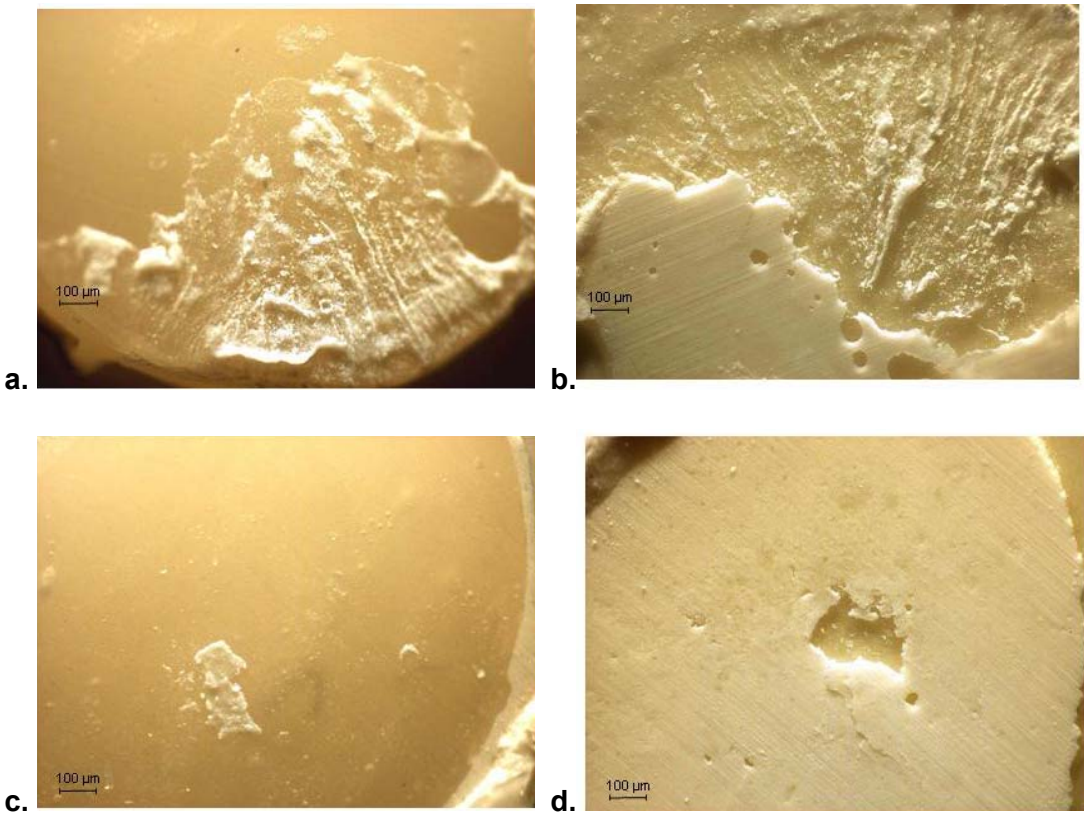

Figure 5.90. Images (x10 magnification) of bonding failure of unetched composite (left) and ceramic (right) 2 wt% glass-zirconia specimen etched for 2 (a,b) and 5 minutes (c,d).

Figure 5.91 shows the bonding failure of 5 wt% glass zirconia, after etching for 2 and 5 minutes. Both 2 and 5 minute etching specimens had the cement left mainly on ceramic and some on the composite surfaces

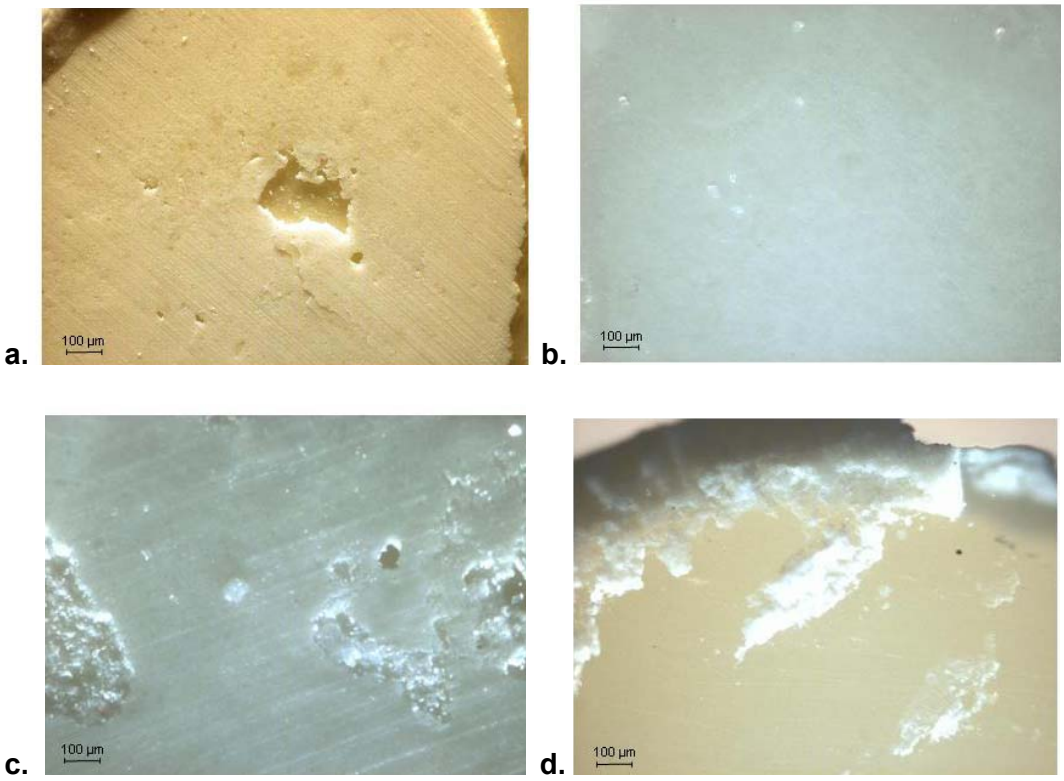

Figure 5.91. Images (x10 magnification) of bonding failure of unetched composite (left) and ceramic (right) 5 wt% glass-zirconia specimen etched for 2 (a,b) and 5 minutes (c,d).

5.2.5 Phase configurations

Table 5.14. Phase configuration of as-received non-glass and titanium phosphate glass contained zirconia specimens sintered at different temperatures.

Ti glass (wt%) / (°C)	Phase	Wt%	a(Å)	b(Å)	c(Å)	α(°)	Phase	Wt%	a(Å)	c(Å)
0% (1400 °C)	-	-	-	-	-	-	Tetragonal	100 (±0)	3.6081 (0.000±1)	5.1773 (±2)
1% (1400 °C)	-	-	-	-	-	-	Tetragonal	100 (±0)	3.60712 (0.000±9)	5.1790 (±2)
2%(1400 °C)	-	-	-	-	-	-	Tetragonal	100 (±0)	3.6371 (0.000±3)	5.1040 (±6)
5% (1400 °C)	Monoclinic	85 (±0)	5.1645 (±0.0004)	5.2145 (±0.0005)	5.3212 (0.000±4)	99.136 (±0.0003)	Tetragonal	15 (±0)	3.6182 (0.000±9)	5.1740 (±3)
5% (1300 °C)	Monoclinic	86 (±0)	5.1580 (±0.0004)	5.2091 (±0.0005)	5.3168 (±0.0004)	99.181 (0.000±3)	Tetragonal	14 (±0)	3.607 (0.000±1)	5.1680 (±3)
20%(1300 °C)	Monoclinic	89 (±0)	5.1472 (±0.0003)	5.2024 (0.000±4)	5.3160 (±0.0004)	99.200 (0.000±3)	Tetragonal	11 (±0)	3.630 (0.000±6)	5.200 (±2)

Table 5.14 shows that as-received non-glass zirconia and zirconia containing 1-2 wt% titanium phosphate glass specimens sintered at 1400°C had only tetragonal phase. However, adding ≥ 5 wt% glass activates the phase transformation; therefore, the specimens contained predominantly monoclinic phase approximately 85-89 wt% and tetragonal phase 11-15 wt%.

CHAPTER 6

Discussion

6.1 Commercial yttria stabilised tetragonal zirconia polycrystal ceramic

6.1.1 Biaxial flexural strength and reliability

Lava™ zirconia ceramics have high flexural strength and the addition of colour did not have a statistically significant effect on its flexural strength. This contrasts with one study (Ardlin 2002). Ardlin (Ardlin 2002) examined two colours of yttria stabilised tetragonal zirconia polycrystal (Y-TZP) specimens of Denzir™ and found that the flexural strength of white shade specimens was lower than yellow shade specimens. This may be attributed to components such as CeO_2, Fe_2O_3 and Bi_2O_3 that were added to obtain the different shades and also to the different manufacturing processes. Shah *et al* (2008) also reported the decrease in flexural strength at higher concentration of cerium and bismuth colouring salts, which led to an increase in porosity in the zirconia specimens (Shah *et al.* 2008). However, according to the manufacturer, both the processing procedure and sintering process of the uncoloured and coloured discs in this study are similar. In addition, the colour was added to the specimen by dipping the specimens into coloured liquid for 2 minutes and a this small amount may not affect the strength of the materials.

Zirconia specimens made by different companies differ in their biaxial flexural strength in this study. The zirconia based ceramic Lava™ specimen had flexural strength and Weibull modulus of approximately 1100 MPa and 10 respectively, which is similar to other studies (Curtis *et al.* 2005; Guazzato *et al.* 2005a; Kosmac *et al.* 1999). Guazzato *et al* (2005a) found DC-Zirkon (5 mol% Y_2O_3-TZP) had a flexural strength and Weibull modulus of 1150 (±150) MPa and 7.5 respectively. Another study (Curtis *et al.* 2005) found that as-received Lava™ specimens tested in a wet environment had a flexural strength 1308 (±188) MPa with Weibull modulus

7.1 (±1.32). Conversely, Cercon® and Invizion™ had a flexural strength of approximately 823 (±115) MPa and 828 (±87) MPa respectively, which are lower than the flexural strength of Lava™ specimen and Y-TZP ceramics in other studies (Curtis *et al.* 2005; Guazzato *et al.* 2005a; Kosmac *et al.* 1999). However, Denry and Holloway (2005) found the biaxial flexural strength of the as-sintered Cercon® was 944 (±156) MPa, which was a similar value to the results found in this project. The lower flexural strength of two groups may have been due to differing specimen preparation methods or surface preparations, which led to the variation of the flexural strength. In this study, grinding and polishing of the as-received specimens in all groups (tension side) was performed in order to standardize the specimens. The result in this project revealed that as-received FS5 had a higher flexural strength (1275±84) and Weibull modulus (*m*) (17.6) compared with FS5 polished specimens (1147±107, *m*=12.9). Additionally, the XRD also identified that the strained cubic phase disappeared after polishing; however, this detail will be discussed in further section.

Another factor which affects zirconia strength is the exact sintering process. The sintering temperature and the duration of the sintering process are well known to affect grain size and phase content, which influence the strength of zirconia (Casellas *et al.* 2001; Ruiz and Readey 1996). Ruiz and Ready proposed that the grain size increased with increasing sintering temperature, which led to an increase in fracture toughness, owing to larger transformation zones. However, no significant difference in biaxial flexural strength of various grain size zirconia ceramics was reported in that study (the grain sizes produced by different sintering temperatures),

which contrast with the results of Casellas *et al* (2001) who found that a decrease in grain size gave a slight increase in flexural strength.

In this study, Lava™ and Cercon® zirconia based ceramic had similar mean grain sizes of approximately 0.1 μm while Invizion™ had a slightly larger grain size. These three groups also had a different appearance in microstructure. Lava™ grains appeared more rounded and separated compared with others while Cercon® had more fused grains. The difference in microstructure between Lava™, Cercon® and Invizion™ may explain the difference in the flexural strength. However, the grain size values found in this study were slightly smaller than the results of previous studies. Guazzato *et al* (2005b) reported that 3 % Y-TZP grain size was 0.2 μm while Denry and Holloway (2005) found as-sintered Cercon® had an average particle size of 0.33 (±0.12) μm. In addition, a few large grains (0.2-0.3 μm) were found in all groups which may have occurred during the sintering process.

Variation in the strength may also have been due to differing amounts of elemental components. Lava™, Cercon® and Invizion™ were slightly different in composition (Zr, O, Y, and Hf). Cercon® had the highest Zr (~68.05 wt%) and slightly low O (~25.90 wt%) compared with others while the Invizion™ had the lowest amount of Zr and highest amount of O which were 50 and 40 wt% respectively.

Weibull modulus (*m*) is used to describe the variation of the strength or asymmetrical strength distribution as a result of flaws and microcracks which may develop within the microstructure (Ritter 1995). The lower the value of the Weibull modulus indicates more flaws and defects in the material, and hence decreased reliability. Conversely, the higher values of Weibull modulus indicates a smaller error range, and thus greater structural reliability (Ritter 1995). Most ceramics are reported

to have '*m*' values in the range of 5-15, whereas metals, which usually fail in a ductile manner, have '*m*' values in the range of 30-100 (Johnson 1983). In this study, the Weibull modulus of Lava™, Cercon® and Invizion™ were approximately 10, 8 and 11 respectively which is in the range usually quoted for dental ceramics (Curtis *et al.* 2005; Guazzato *et al.* 2005a).

Most of the fractographic images of the failed specimens from biaxial flexural strength testing showed the classic fracture pattern, which presented a smooth mirror-like surface at the fracture origin. Lava™ and Cercon® showed no obvious differences in the fracture surface. However, Invizion™ showed evidence for large porosities and rough surfaces located in the area near the tensile surface. These internal defects may be one of the factors contributing to Invizion™'s lower flexural strength compared with Lava™ specimens.

6.1.2 Fatigue properties

The presence of water in association with the repetitive loads generated during chewing cycles can lead to the fatigue and degradation of the materials. The reduction of the mechanical strength due to fatigue is caused by the propagation of natural cracks initially present in the component's microstructure (Studart *et al.* 2007a). The dental restoration is usually exposed to the aqueous environment and to the cyclic loading; therefore, fatigue is one of the major factors that can predict the success of the restorations. Additionally, the evaluation of the fatigue behaviour of dental ceramics under water is designed to correspond as closely as possible to physiological conditions. Fatiguing veneer/zirconia bilayered specimens is more

related to the clinical situation; however, this project would like to focus on fatigue property of the zirconia framework.

In a preliminary study, the effect of fatigue on the flexural strength of zirconia was evaluated. Initial fatigue tests were performed at 10,000 and 20,000 cycles using a force of 25% of mean biaxial flexural strength (~250 N) as used by Sobrinho *et al* (Sobrinho *et al.* 1998b). They found that fatigue in a wet environment significantly reduced the strength of IPS Empress and In Ceram when using a force between 20 and 300 N at 10,000 cycles. However, the force used in this study (250 N) was lower than the biting force in a molar region, which is quoted as ranging from 400-800 N (Anusavice 2003b; Craig and Ward 1997). However, this test was only a preliminary study and investigated the fatigue on the flexural strength of zirconia specimens; therefore, in order to try and drive crack propagation without failure of the specimens, a low force was used.

The results in this present study showed the cyclic loading at 10,000 and 20,000 cycles in water, using a force of 250 N, did not significantly (P>0.05) affect the flexural strength of zirconia ceramic. Similarly, a recent study (Itinoche *et al.* 2006) investigated the flexural strength of In-Ceram Zirconia and Procera (high alumina oxide) after fatigue, which used a 50 N force for 20,000 cycles. There was no significant difference between before and after cycling for both materials. Although the materials are different from the present study, they showed higher fatigue resistance than glass ceramics from Sobrinho *et al* (1998) because In-Ceram Zirconia contains 35% zirconium oxide and Procera is a polycrystalline ceramic, which would have high fatigue resistance. Another study (Curtis *et al.* 2006) examined the effect of fatigue on the biaxial flexural strength of a zirconia ceramic.

They reported that using forces of 500, 700 and 800 N for 2000 cycles did not affect the biaxial flexural strength of the specimens in either dry or wet conditions. Although the specimens were tested to 100,000 cycles using an 80 N force, the biaxial flexural strength was still no different (Curtis *et al.* 2006). However, when extending the fatigue to 100,000 cycles, the mean Weibull modulus was reduced from 7.5 (control specimen) to 5.3. They suggested that there was an accumulation of subcritical cracks within the materials (Curtis *et al.* 2006).

Therefore, using 25% of the mean biaxial flexural strength, which was approximately 250 N force, did not affect the strength of the Lava™ zirconia specimen, the force application in the range of 50-90% of the mean biaxial flexural strength was performed in the fatigue study. The maximum number of fatigue cycles was set at 500,000. When using a low force, it took several days to reach the cycle limit. A maximum cycle of 500,000 simulates a service time of 2 years according to clinical studies that have calculated that a human has an average of 250,000 masticatory cycles per years (Delong and Douglas 1980, Sakaguchi *et al*, 1986). The frequency of the force applied at 2 Hz was slightly higher than the length of the masticatory cycle reported in the literature (DeLong *et al.* 1984). They indicated that the average masticatory cycle was between 0.8 and 1.0 second. However, Hulm and Evans (2000) found that a cyclic frequency ranging from 1 to 5 Hz did not affect the fatigue life of 3Y-TZP (Hulm and Evans 2000).

The fatigue test was performed using a pin on three balls, which was the same geometry as the biaxial flexural strength test. An indenter with a flattened tip as described by ISO 6872 may induce stress concentrations or damage on the surface which could in turn generate microcracks within the damage zone (Ohyama *et al.*

1999a; Zhang *et al.* 2004). Furthermore, White *et al* (White *et al.* 1997) also found circular cracks on specimen surfaces loaded by the pin. However, this study found no evidence of any surface damage on specimens, which were subjected to fatigue testing. This may be due to the high hardness or fracture toughness of Y-TZP ceramic in this study. The latter is also a property that indicates the ability of a material to resist rapid crack propagation (Albakry *et al.* 2003a).

In this present study, the fatigue life of Lava™, Cercon® and Invizion™ at 500,000 cycles was in the range of 60-70% (530-700 MPa). Cercon® and Invizion™ had lower survival fatigue values (575 and 526 MPa respectively) compared with Lava™ (650-700). Kosmac and Dakskobler (2007) investigated the survival strength of the zirconia ceramic using a maximum force of 60% of the mean strength (850 N or 650 MPa). They found that after 1,000,000 cycles, the survival strength of as-received zirconia specimens tested in air and artificial saliva was 1,070 and 890 MPa, respectively (Kosmac and Dakskobler 2007). Dry ground (150 μm) reduced the survival rate whereas sandblasted and sandblasted with annealing increased the survival rate of the zirconia specimens (Kosmac and Dakskobler 2007). Studart *et al* (2007) investigated the fatigue of zirconia 3-unit bridges and found that if the maximum stress applied to the prosthesis is 346 MPa, the lifetimes could be longer than 20 years with 5% failure probability (Studart *et al.* 2007a). In this study, all specimens survived over 500,000 cycles when using a force that was 60-70% of the mean biaxial flexural strength (530-700 MPa).

An average force on the premolar and cuspid has been reported to be approximately 300 and 200 N, respectively (Anusavice 2003b; Craig and Ward 1997). The biting force in the molar region varies from 400-800 N (Anusavice 2003b;

Craig and Ward 1997). Additionally, several studies showed that the maximal bite forces in posterior teeth was approximately 700 N or higher in healthy people (Ferrario *et al.* 2004; Okiyama *et al.* 2003; Anusavice 2003b). Therefore, Y-TZP ceramics in this study might be strong enough to withstand the high load in posterior areas. However, long-term clinical studies need to be carried out in order to confirm the endurance of 3Y-TZP in high loading areas.

Fractographic images of the fractured surfaces of specimens failed from fatigue testing showed the same pattern as the biaxial flexural test. No fatigue striations were found which was similar to one study (Hulm and Evans 2000). However, Liu and Chen suggested that when crack growth is entirely in the fatigue regime, no striation should appear (Liu and Chen 1991). The fatigue striations form when overload fracture and fatigue fracture alternate successively during cyclic loading, but this may refer to the overload on the small scale.

6.1.3 Fatigue of crown shapes

There are several factors that may affect the fatigue and fracture behaviour of materials used in all-ceramic crowns. The zirconia core and veneer thickness ratio is very important to the strength of the composite system (Guazzato *et al.* 2004a). In the present study, brass dies rather than natural teeth were selected to accurately control and duplicate preparation parameters, such as taper and finish line. In this way, all the crown shapes had an identical core/veneer material thickness ratio (0.5/1.0 mm) and geometry. However, they did not match the mechanical properties such as elastic modulus and fracture toughness of natural tooth structure (Sano *et al.* 1994). Additionally, the adhesion of the cement was different to that of natural

tooth structure. However, as a conventional cement was recommended by the manufacturer, adhesion was not as issue. Furthermore, there were no cementation failures of any of the specimens in contrast to other studies that used resin dies in combination with resin cements (Pallis *et al.* 2004). Crown forms were fabricated with a flat occlusal morphology and cylindrical shape to achieve precision and reproducibility.

Heat pressing is expected to introduce significantly fewer flaws than sintering, resulting in better strength properties, as it is a more controlled procedure. In contrast, the sintering process is more technique sensitive and subject to variability due to the individual building and firing techniques. However, there was no significant difference in the compressive strength between heat pressed (2135.6±330.1 N) and sintered specimens (2189.9±317.6 N). These results may be related to the microstructural nature of the veneering material and they were supported by a zirconium oxide core. In addition, the Weibull modulus and characteristic strength of the heat pressed group (m=7.1, σ_o=2276.7) was not different from the sintered group (m=7.7, σ_o=2325.9). The homogeneity and the distribution of flaws may be similar between test groups.

In this study, the specimens displayed predominantly cohesive failure limited within the veneer material. This type of failure indicates a good interfacial bond between the core and the veneer materials that is critical for the success of this composite structure (Kelly *et al.* 1995). The crack initiated at the point of load applied by the indentor. On the other hand, previous studies reported that other all ceramic crown systems had a failure origin located at the interface of the veneer and the core materials and at the interface of the luting agent layer with the core (Curtis *et al.*

2006; Pallis *et al.* 2004; Quinn *et al.* 2005). No failure of the zirconia framework was reported under the applied stress (Kim *et al.* 2007).

6.1.4 Subcritical crack growth

Brittle materials are susceptible to time-dependent failure under static loads, caused by the subcritical growth of cracks to critical lengths (Reese and Cox, 1992). The subcritical crack growth refers to environmentally enhanced crack propagation at subcritical stress levels. The propagation of the pre-existing natural defects occurs at low rates (slow crack growth), and causes delayed failure of ceramics when the flaw size reaches a critical value (Benaqqa *et al.* 2005). It is very important to understand the mechanisms that are involved and to determine with precision the crack propagation laws in order to predict the lifetime of these materials for a given application.

The subcritical parameter *A and n* are usually examined for estimating crack growth resistance and lifetime of materials. Where *A* is a constant and *n* is an exponent, which in most ceramics has a value >10 (Reese and Cox 1992). The higher the subcritical crack growth (SCG) resistance means slower strength degradation and higher remaining strength, thus longer life time.

Common methods used to test subcritical crack growth of materials are the double torsion method and dynamic fatigue test. In this present study, the subcritical crack growth test was performed using dynamic fatigue test which used similar equipment to the fatigue and biaxial flexural test. The specimens and equipment were easier to prepare compared to the double torsion method. However, previous studies reported that these two methods provide a difference in subcritical *n* values

of zirconia ceramics (Chevalier *et al.* 1995; Li and Pabst 1980). Li and Pabst (1980) reported that the *n* value of as-received ZrO_2 specimens tested using the double torsion test (*n*=80) was higher than the flexural test (*n*=51) because of a different reaction of the specimen surface on the subcritical crack extension. The crack extension of the flexural test specimen started after the external load stress at the surface exceeded the surface compressive stress while the crack of the double torsion specimen moved through the compressive stress and did not start at the compressive surface. In contrast, Chevalier *et al* (1995) found that the *n* value obtained from the double torsion method (*n*=19) was lower than the *n* value obtained from the dynamic fatigue test (*n*=100). They suggested that dynamic fatigue investigates the surface flaws while the double torsion examines both surface and bulk defects (Chevalier *et al.* 1995). Although these two studies have reported different results, they both found that the *n* value is strongly affected by surface compression (Chevalier *et al.* 1995; Li and Pabst 1980). Higher surface compressive stress led to higher *n* values (Chevalier *et al.* 1995). On the other hand, the *n* value is reduced when the specimen is annealed. Transformation toughening was not found to influence the *n* value as Li and Pabst found no difference in *n* values between tetragonal and monoclinic specimens (Li and Pabst 1980).

The *n* exponent value of the specimens tested in water in this study showed a large variation ranging from 33 to 197 although the fracture strength was only slightly different. The variation of the *n* value of the zirconia specimens in this present study may be attributed to the difference in defects within the zirconia materials in each group. The surface compressive stress may not affect the variation of *n* values in this study as all the specimens were ground and polished in a standardised way. The *n*

value of zirconia ceramics from several studies varied from 20-100 (Chevalier *et al.* 1995; Chevalier *et al.* 1999; Studart *et al.* 2007b). The difference in the *n* value between this study and other studies (Chevalier *et al.* 1995; Chevalier *et al.* 1999; Studart *et al.* 2007b) may be attributed to the test methods and specimen preparation. The *n* value of glass ceramics was slightly lower than the *n* value of zirconia ceramics. Feldspathic and aluminous porcelain had lower n values, which were 14.6 (±1.4) and 28.9 (±5.8), respectively (Morena *et al.* 1986). High density aluminium oxide ceramic had a high *n* value ranging from 30-100 (Pletka and Weiderhorn 1982). Another study calculated the *n* and *A* values of 3Y-TZP, In-Ceram Zirconia and Empress 2 ceramic from Weibull distribution and subcritical crack growth curves (Studart *et al.* 2007b); however, the results were not significantly different. From the Weibull distribution, the constant *A* for 3Y-TZP, In-Ceram Zirconia and Empress 2 ceramic were $3.15x10^{-24}$, $2.61x10^{-25}$ and $1.69x10^{-21}$ $m.s^{-1}$ and *n* values were 28.9, 26.3 and 38.0, respectively (Studart *et al.* 2007b). Therefore, according to the results in this study and the literature, *n* values for zirconia ceramics can vary and tend to be higher than the *n* value for conventional glass ceramics. However, high density aluminium oxide seems to have an *n* value in the same range as zirconia ceramics.

In this present study, the results showed that the strength of zirconia was slightly reduced when using the low stress rate ($N.s^{-1}$). This might be because the low stress rate created several small cracks before the specimens failed while the high stress caused immediate specimen failure. Additionally, the specimens subjected to the low stress rate had longer contact with the aqueous environment. Several studies (Chevalier 1999; Deville *et al.* 2005; Deville *et al.* 2006) reported that

water assisted crack growth in zirconia ceramics; therefore, the longer the specimens were in contact with water, the more gradual the increase in the subcritical crack and the decrease in the specimen strength.

Fractographic analysis in this study showed that lower stress rate created more crack lines than higher stress rate. The high *n* value specimens had slightly more crack lines and rougher fractured surfaces compared with low n value specimens. It may be because the low *n* value specimens failed early before they could create the small cracks.

6.1.5 Transformation toughening and hardness of the specimen

The x-ray diffraction analysis was performed in order to study whether the polishing and grinding processes affected the phase present in the samples. X-ray diffraction analysis of the Y-TZP specimens in this study identified that as-received Lava™, Cercon® and Invizion™ specimens contained two phases, predominantly consisting of a tetragonal phase with two cubic phases (denoted cubic 1 and cubic 2) (Table 5.6). This result agrees with the phase diagram of a previous study (Scott 1975) that 3% Y-TZP at sintering temperature 1400-1550°C should present two phases which are tetragonal and cubic phases.

After polishing Lava™ and Cercon® specimens, cubic 2 phase disappeared (Table 5.6) and wt% of cubic 1 phase was increased. There was only a slight change in wt% of tetragonal phase. However, major changes occurred between the cubic 1 and cubic 2 (within the cubic phase itself). Therefore, this work indicated that the cubic 2 represented a proportion of the cubic phase that was “strained” and hence an increase its unit cell size. The cubic 2 phase is always present when an

aggressive grinding step is used and reduces as the grain size of the preparation medium reduces. After polishing, the cubic 2 phase (strained cubic) transformed back to cubic 1 phase (Table 5.6) by a four or fivefold increase in the wt% of cubic 1 within the polished specimen when compared with the as-received specimen. It could be concluded that the polishing process relieved the strain that was constraining a portion of the cubic phase. This may lead to reduced compressive stresses within the surface of specimens. This study agrees with Garvie *et al* (Garvie *et al.* 1975) who first found that polishing reduced the surface strain and failure stress without transformation of the tetragonal phase to the monoclinic phase. However they reported that the surface strain was reduced because polishing removed some of the transformed monoclinic phase, therefore, the wt% of the monoclinic phase was reduced whereas the wt% of the tetragonal phase was increased. In contrast, this current study found polishing did not remove the cubic 2 (strained cubic) phase because the wt% of both tetragonal and cubic (cubic1+cubic2) phases was very similar compared to the as-received and polished specimens. Additionally, it was interesting to note that no detectable amounts of the monoclinic phase within either as-sintered or polished specimens were found. This may be because of the manufacturer's polishing process, although it can induce the strained cubic, but it is not strong enough to trigger transformation toughening ($t \rightarrow m$ *or* $t \rightarrow c$).

The results for the ground Lava™ and Cercon® using silicon carbide paper of 1000, 500, 320 and 80 grits showed no significant difference in the phase content between the two groups. Additionally, using 1000, 500, 320 grits showed no difference in the phase content compared with the as-received specimens. On the

other hand, the tetragonal and cubic 1 phases decreased dramatically and cubic 2 increased twofold when using 80 grit size. Thus it may be concluded that the phase transformation *t→c* and the strained cubic phase occurred when using aggressive coarse grinding; however, no monoclinic phase was detected on the surface. These results are similar to Curtis *et al* (2005) who found tetragonal and cubic phases within the Lava™ specimens. However, they reported that only the tetragonal and cubic 1 phase was found in the as-received materials, and tetragonal, cubic 1 and cubic 2 phases were found after a grinding process. Difference in findings in as-received specimens may be attributed to the difference in methods for preparing the specimens by the manufacturer such as grinding and polishing. In this study, the specimens were finely ground by the manufacturer using 10 μm diamond paper before sending. This may create some stresses within the specimens and cause some cubic to increase its unit cell size. In contrast, one study (Kosmac *et al.* 2000) found the monoclinic phase of 3Y-TZP after grinding with a diamond bur of 150 μm and 50 μm grits and sandblasting; however, tetragonal and cubic phases were not mentioned in this study. They also reported the highest amount of the monoclinic phase found after sandblasting regardless of whether the samples were ground prior to sandblasting. These results were similar to Guazzato et al (2005a) who reported that the amount of monoclinic phase was highest after sandblasting (9.5%) then grinding (8.3%). The transformation between cubic to tetragonal was presented by Reed and Lejus (1977) who found a reduction of the cubic phase and increased amount of the tetragonal and monoclinic phases after wet and dry grinding using 4-SiC paper (Reed and Lejus 1977). The results in this study differ to other studies in that the tetragonal increased after grinding; however, they used zirconia containing

4.5 mol% Y_2O_3, which may lead to a difference in the transformation behaviour compared with other studies (Curtis *et al.* 2005; Guazzato *et al.* 2005a; Kosmac *et al.* 2000). They also found zirconia containing 7% Y_2O_3 was completely cubic with no detectable change in phase after grinding. Furthermore, grinding conditions either wet or dry, did not affect the phase content in this study, which agrees with the other studies (Curtis *et al.* 2005; Kosmac *et al.* 2000); however, the critical defect size obtained from surface grinding is smaller when using wet grinding (Kosmac *et al.* 2000).

On the other hand, the cubic 2 in Invizion™ did not disappear after polishing and the amounts of three phases before and after polishing were similar. In addition, the result of Invizion™ specimens after wet grinding with 1000, 500, 320 and 80 grits were different from the Lava™ and Cercon® specimens and also other studies (Curtis *et al.* 2005; Kosmac *et al.* 2000) that either fine or coarse wet grinding did not affect the amounts of three phases. However, dry grinding provided the similar results as Lava™ and Cercon®. The polishing or wet grinding processes did not create or remove stress in the Invizion™ specimen; however, stress occurred after dry grinding. The difference in the susceptibility of the transformation of Invizion™ may contribute to the difference in the amounts of stabilising agent and the elemental compositions within Invizion™ compared to Lava™ and Cercon®.

Therefore, according to previous work (Curtis *et al.* 2005; Guazzato *et al.* 2005a; Kosmac *et al.* 2000; Reed and Lejus 1977) and this study, the transformation after grinding can be either $t \rightarrow m$ or $t \rightarrow c$ or no phase change. The difference in the phase content in the as-received specimens and the phase transformation between this study and others (Curtis *et al.* 2005; Guazzato *et al.* 2005a; Kosmac *et al.* 2000;

Reed and Lejus 1977) may be influenced by the percentage of the stabilising agent and the final sintering temperature according to the phase diagram by Scott (Scott 1975). The specimen preparation leads to the difference in phase contents. The type, degree and duration of the surface treatment such as grinding, sandblasting or polishing and heat created during the preparation affect the phase contents and phase transformation. The heat that may occur during grinding can lead to the reverse transformation from the monoclinic to the tetragonal phase if the locally developed temperature exceeds *m→t* transformation (700ºC) (Kosmac *et al.* 1999; Swain and Hannink 1989). The dry grinding can also create larger defects on the specimen surface compared with wet grinding (Kosmac *et al.* 2000).

When the Vickers hardness test was conducted within the same specimen, the as-received side had slightly higher mean hardness values than the polished side because there was cubic 2 occurred on the as-received surfaces. Unit cell of cubic 2 is bigger than cubic 1, which may lead to create the compressive stresses and result to increase the hardness. Although all groups showed no statistically significant difference between both sides, FS6 and FS7 showed a reduction in hardness of zirconia after polishing. Regarding the XRD results, the polishing reduced the stress on the surface and hence the strained cubic transformed back to the normal cubic, and so reduced the hardness of the zirconia specimen. The biaxial flexural strength and Weibull modulus of the materials in this study were also decreased after the polishing process, which may be due to the reduction of the stress on the surface. Curtis *et al* (2005) demonstrated that sandblasting (alumina abrasion) and fine grinding gave no difference in hardness and biaxial flexural strength of Lava™ specimens; however, the biaxial flexural strength was significantly reduced when

specimens were coarse ground (120-150 μm). Some studies (Kosmac *et al.* 1999; Kosmac *et al.* 2000) found that sandblasting significantly increased the biaxial flexural strength. Additionally, fine grinding did not alter the strength while coarse grinding also reduced the strength of zirconia and is the more expected result. Coarse grinding may introduce surface flaws that in turn may cause strength degradation (Kosmac *et al.* 1999). Furthermore, it has been shown that Y-TZP ceramic presents the slow transformation at the sample surface in humid environments with time, the so-called ageing phenomenon (Chevalier 1999). The transformation rate is related to factors such as temperature, grain size, concentration of stabilising agent (Chevalier 1999) and surface finish (Deville *et al.* 2006). Extensive transformations can degrade the ceramic and strength decreases. However, some studies found ageing did not affect the flexural strength of zirconia. Ardlin (Ardlin 2002) investigated the chemical stability and effect of low-temperature ageing (4% acetic acid) at 80°C for 168 hours on flexural strength of Y-TZP ceramic for crowns and bridges. They found that transformation was low and did not cause a reduction of the flexural strength of specimens. Another study (Cales *et al.* 1994) found that zirconia aged at 37°C for 1 year did not change the flexural strength of Y-TZP ceramic. Dental zirconia frameworks have a porcelain veneer surface and ageing in the oral environment may be limited; however, they are exposed on the internal surface to the cement lute and dentine. In addition, 37°C is a relatively low temperature and may not trigger transformation for an extended period of time. However, long-term ageing at 37°C in the oral environment should be tested.

6.1.6 Stress-induced phase transformation

The stress-induced phase transformation and phase compositions can be analysed using X-ray diffraction (XRD) or Raman microspectroscopy. However, XRD tends to be used for bulk or large area surface analysis. Even the new focussing systems have relatively large incident spot sizes. Raman microspectroscopy; however, has the ability to analyse very small and specific areas on a sample surface without any sample preparation (Kailer *et al.* 1999) and it can discern the phases present (Casellas *et al.* 2001). Hardness indentation has been used to induce phase transformation when the material is subjected to highly localised stresses during loading. The stresses can not only cause crack formation by dislocation gliding, but can cause a complete change of the crystal structure and the formation of amorphous phases (Kailer *et al.* 1999). Raman spectroscopy combined with the hardness indentation testing has been used in some studies (Casellas *et al.* 2001; Colomban and Havel 2002; Kailer *et al.* 1999; Behrens *et al.* 1993) in order to examine pressure-induced phase transformations.

The present study investigated the phase transformation of Lava™, Cercon® and Invizion™ within and around the indentation using different loads ranged from 20-50 Kg. Additionally, the phase transformation of fractured surfaces of the materials failed from biaxial flexural strength and subcritical crack growth were also examined. The results of this study showed that the tetragonal phase can be converted to both cubic and monoclinic phases upon the application of localised high stress. Lava™ and Invizion™ showed similarities in the relative fractions of three phases within the indentation grooves while Cercon® presented a different pattern compared with others. In the grooves generated by the edges of the indenter of the

Cercon® specimen, the variation in the relative levels of transformation with distance from the centre was only small. Also no significant variation in the relative fractions of each phase within the indentation grooves could be detected upon increasing the load from 20 to 50 kg. However, the variation of the relative fractions of tetragonal and cubic phases with the distance from the centre was found in Lava™ and Invizion™ specimens. The fraction of the cubic phase was much higher in the centre while the tetragonal phase was lower compared with the surrounding region. There was also a difference in the relative fractions of the cubic and tetragonal phases within the indentation grooves of Lava™ and Invizion™ specimens upon increasing the load from 20 to 50 Kg. The cubic phase was higher when using the higher load compared with the lower load while for the monoclinic phase there was no significant difference. Although Lava™, Cercon® and Invizion™ showed a difference in the relative fractions of the three phases within the indentation grooves, the level of transformation of the three groups declined rapidly outside the indentation region despite being along a crack in the surface. Since, however, higher loads produce larger indents, greater absolute amounts of transformation are obtained with higher loads.

Along the diagonal line, the monoclinic fraction varied little from the centre to the edge. The cubic phase had the highest level at the centre compared with the outer region. The tetragonal level, however, was reduced at the centre. This may be because there is much higher compressive stress in the groove compared with other areas, which induced high cubic and some monoclinic phase formation. More abrupt changes of the three phases occur at the indentation edge along the groove line

compared with the line at 45°. This may be due to greater stress at these corner edges which then generates a crack.

Figure 5.65-5.67 (page 213-215) indicates a higher level of the cubic phase in the indentation especially at the centre compared to the outside. An increase in the cubic phase with high stress was previously reported (Curtis *et al.* 2005). Curtis *et al* found aggressive grinding resulted in an increased amount of strained cubic phase while the tetragonal phase was reduced; however, no monoclinic phase was detected. The level of monoclinic phase exhibited only limited variation within the indentation except within the grooves. This study found the monoclinic phase decreased with the distance from the indent centre which is similar to another study (Clarke and Adar 1982). They reported that 3.5 mol% Y_2O_3 stabilised zirconia indented using 20 kg load had the highest monoclinic concentration in the centre and decreased with distance from the crack. Reese *et al* (Reese *et al.* 1992) also found that Y-TZP showed a linear decrease with distance from the indent centre; however, transformation ($t \rightarrow m$) of Ce-TZP was greatest near the edge of an indentation. One study (Behrens *et al.* 1993) also found that the monoclinic fraction of 3YTZP ceramic showed the highest amount at the edge of the indent which was approximately 48%. They reported that it is because the tetragonal to monoclinic transformation is more easily induced by tensile and shear stresses which exhibited the highest level at the edge than by the compressive stresses in the centre due to the transformation dilatation of about 4% (Behrens *et al.* 1993). Zhang and Kelly (Zhang and Kelly 2002) found the transformation of Fe-Ni-C alloy formed in tension less than compression which contrasted to previous studies (Behrens *et al.* 1993). They concluded that the types of stresses do not really affect the transformation, however,

the amount of transformation depends on the amount of plastic deformation in the materials.

In this present study, the monoclinic phase could be detected on the fractured surface of the specimen after biaxial testing. This was previously also observed by Ruiz and Readey using XRD (Ruiz and Readey 1996). Exactly which area had high monoclinic content, however, was not determined in their work. Leach (Leach 1989) examined the transformation of 9 mol% MgO-PSZ specimens after fracture in three-point bending using a Raman microprobe. The monoclinic phase was reported to have the highest amount on the tension side. This present study also found the monoclinic phase to only be at the fracture origin area and not the whole fracture surface. It additionally demonstrated, however, an increased concentration of cubic phase was around the fracture origin and on the tensile side. Furthermore, XRD analysis could not be used to detect the phase content at the fracture surface in this study. The fracture surface is not flat and also the area investigated is too small to investigate by XRD. This can lead to misinterpretation of the results and therefore, Raman spectroscopy is more appropriate to use in this case.

Phase transformation at the fracture surface of specimens failed after subcritical crack growth testing was not influenced by the loading rate from 0.1-100 $N.s^{-1}$. The low loading rate leads to the slow fracture which could create more accumulation of crack growth within the materials compared with high loading rate. However, this did not affect the intensity of the monoclinic phase on the fracture specimen surface. In addition, the monoclinic phase was detected on the specimen surfaces at the tension and compression side. However, the tension side tended to

have more of the monoclinic phase than the compression side. This may be because the tension side is the side form which the crack originates.

6.2 Titanium phosphate glass reinforced 3YTZP

6.1.1 Effect of glasses on the properties

The biaxial flexural strength of experimental zirconia is lower than commercial zirconia mainly due to the difference in preparation method and final sintering temperature and equipment. The steps in the specimen's preparation included sieving (or screening), powder compaction, final sintering temperature, which together with the percentage of the titanium phosphate glass added to zirconia affect the properties of the specimens.

Before powder compaction, the powder would be made as homogenous as possible in order to press the powder conveniently. An efficient method of separating a powder's particle size is running the powder through a specific sized mesh screen, called *sieving or screening*. In this study, a problem that was encountered during screening was powder agglomeration. This behaviour normally took place below a sieve opening of 44 μm and involves groups of fine particles acting as a single particle this clogging the screen and preventing further screening. This can reduce the effectiveness of particle sizing (Richerson 1992). Additionally, moisture can cause powder agglomeration and make powder difficult to pass through the screen; this can be reduced by placing the mesh into an oven for an hour at 37°C and then continue sieving.

Other factors that may affect a specimen's strength are powder compaction methods and final sintering temperature. In this study, the specimens were made by

using uni-axial pressure using a load of 6.5 tons. The final sintering temperature was 1400°C, which was the highest temperature achievable in the furnace. Uni-axial pressing involves the application of pressure along a single axis upon a powder that is placed into a rigid die to produce a compact (Richerson 1992). Even though it is a simple technique and the process is inexpensive, problems with using uni-axial pressing can occur, which are cracks on the surface of the specimens. After the pressure is released from the upper punch, the material rebounds and simultaneously causes drag between the material and the die wall (Richerson 1992). This can cause cracks from the tensile stress concentrated at the upper edge of the green compact. Ejection from the die can cause a series of laminar cracks to occur as a result of further rebounding. Rebounding to a larger cross section usually takes place as the materials passes above the top of the die. The effect of rebounding can be minimised by the addition of a suitable binder (Richerson 1992). In this study, the zirconia powder as-received from the manufacturer, already contained a binder in order to make it ready to press and also reduce lamination. However, an inappropriate load applied can induce lamination and cracking. Therefore, a pilot study was carried out in this study in order to find a suitable pressing load. The homogeneity of powder also influences powder compaction. No cracked or laminated specimens were found during the pilot study. Titanium phosphate glass mixed zirconia specimens tend to have more cracks and laminations after compaction compared with the pure zirconia powder. This is because the homogeneity of the titanium phosphate glass reinforced zirconia powder was lower than the pure zirconia powder.

Density variation in the green compact is another problem associated with uni-axial pressing and causes distortion or cracking during firing (Richerson 1992). One source of density variation is the friction between the powder and the die wall and between powder particles (Richerson 1992). A uni-axial pressure applied from one end of a die full of powder will be dissipated by friction so that a substantial portion of the powder will experience much lower than the applied pressure. These areas will compact to a lower density than the areas exposed to higher pressure (Richerson 1992). During firing, the lower-density areas will either not densify completely or will shrink more than surrounding areas. Both will result in flaws that can cause rejection of the part. Use of suitable binders and lubricants can reduce both die wall and particle friction and thus reduce density variation in the compact (Richerson 1992). The application of pressure in all directions is an effective way of avoiding cracks and non uniform density. This method is often referred to as isostatic pressing either hot or cold and is and effective means of achieving greater uniformity of compaction a uniform green density (Richerson 1992). However, isostatic pressing is an expensive and time consuming method compared to uni-axial pressing (Callister 2005) but may account for the difference between our experimental material and commercial materials.

Adding titanium phosphate glass of 1-2 wt% did not affect the flexural strength of zirconia, however, glass at 5 wt% or greater led to lower flexural strength of zirconia. This may be attributed to the homogeneity of the powder after mixing zirconia and glass powder. The higher the concentration of the glass powder, the more inhomogeneous the mixed powder and this could have lead to the cracking of the specimens after pressing or create porosity within the material. SEM images also

confirmed that there were more porosities on the 5 wt% glass compared to control and 1, 2 wt% glass. Additionally, the phases in the non-glass zirconia, 1 and 2 wt% titanium phosphate glass zirconia was mainly the tetragonal phase, while 5 wt% glass zirconia had predominantly monoclinic and some tetragonal phase. The presence of the monoclinic or the combined effect of monoclinic and tetragonal phases accounts for to the difference in flexural strength of the experimental zirconia specimens. However, the phases will be discussed in more detail later.

6.1.2 Effect of glasses on the bond strength

Successful adhesion between a ceramic and tooth is one of the major factors for long-term clinical success of ceramic restorations. To achieve high bond strength of luting cement to the ceramic, a micromechanical interlocking and chemical bonding to the ceramic surface are required (Blatz *et al.* 2003). Etching porcelain surfaces with hydrofluoric acid is a well known method to increase bond strength (Stangel *et al.* 1987). However, it is difficult to achieve good bond strength between zirconia ceramics and composite resin by etching due to the extreme durability of zirconia ceramics, which make them resistant to acid etching (Derand and Derand 2000). Therefore, other surface treatment methods are required to achieve an adequate bond strength such as sandblasting and tribochemical silica coating. Additionally, the sintering temperature of zirconia ceramics is very high at approximately 1500°C. Phosphate base glass was added to the zirconia powder as a sintering aid in order to study whether zirconia could be sintered at a lower temperature but also to measure the susceptibility to etching prior to cementation as well as the mechanical strength. There is a requirement to ensure that the glass is

very low solubility and this was achieved by the addition of titanium dioxide to the glass.

Although hydrofluoric acid (HF) is the commonly used acid to etch ceramic (Stangel *et al.* 1987), HF is hazardous and has extremely caustic effects to all tissues (Brentel *et al.* 2007). Some studies have supported the use of acidulated phosphate fluoride (APF) rather than HF (Tylka and Stewart 1994; Kukiattrakoon and Thammasitboon 2007). However, HF was used in this study as it is a stronger acid than APF (Kukiattrakoon and Thammasitboon 2007), and more suitable for use with the zirconia ceramic which has a low etchability. Additionally, the etch time of APF is longer than HF in order to achieve the same bond strength (Kukiattrakoon and Thammasitboon 2007). Although HF is a hazardous acid, proper and cautious handling following the manufacturers recommendation can limit the danger posed by this acid (Chen *et al.* 1998).

The application of a silica coating, silanisation and a resin cement is suggested for generating a good bond strength between resin cement and ceramic (Atsu *et al.* 2006) However, this study used only HF etching with silanisation because the main objective was to examine whether the percentage of the glass contained in the zirconia specimens affected etchability and the sintering temperature.

The results in this study showed that the shear bond strength was not affected by the addition of titanium phosphate glass and there was no significant difference in the shear bond strength between 1, 2, 5 wt % titanium phosphate glass. However, a longer duration of hydrofluoric etching (5 minuets) increased the shear bond strength. Chen *et al* (1998) found the extension of the etching time period more than 30 seconds did not significantly increase the bond strength between composite resin

and feldspathic porcelain as the etched pattern of the ceramic surface was not different (Chen *et al.* 1998). However, higher concentrations of HF etchant generated greater bond strength than that etched with lower concentration HF etchant (Chen *et al.* 1998). They suggested that if the porcelain was over-etched, the bond strength would be reduced due to the difficulty in removing the etchant from the surface, the wettability of the intermittent resin and postcuring stress concentration due to the complicated adhesive interface structure (Chen *et al.* 1998).

In this present study, the shear bond strengths of Panavia 21 resin cement to the zirconia ceramics were approximately 12 and 13 MPa when etching for 2 and 5 minutes, respectively with a completely adhesive failure mode. However, it is difficult to compare the bond strength value with other studies due to the difference in surface treatment, storage condition and type of resin cement (Van Noort *et al*, 1989). Additionally, no universal agreement on the minimal bond strength required for successful bonding has been established (Anusavice 2003a). However, Thurmond *et al* (1994) suggested that a minimum shear bond strength required for porcelain repairs is approximately 13 MPa for a good clinical service (Thurmond *et al.* 1994) while Anusavice (2003) reported a value of 20 MPa is a reasonable goal for the successful bonding. Derand and Derand investigated the bond strength of luting cement to the zirconia ceramics (Denzir) (Derand and Derand 2000) and found that Superbond C&B possessed higher mean bond strength (19.5 MPa) than Twinlock (8.9 MPa) and Panavia 21 (8.9 MPa). However, they used HF acid with other surface treatment methods unlike this study where HF was used solely. They reported that Superbond provided higher bond strength because it contains 4-META/MMA-TBB resin, which is a crosslinked and very strong adhesive agent regardless of the types

of ceramic surfaces used. Panavia and Twinlock had a stronger bond if the ceramic surface was primarily coated with Rocatec. Conversely, Lüthy *et al* (2006) examined the shear bond strength between sandblasted zirconia surface with resin cements and found that Panavia possessed the highest mean shear bond strength (63.4 MPa) compared with other cements (Lüthy *et al.* 2006) which is also similar to one study (Kern and Wegner 1998). The phosphate ester group of the monomer within the Panavia resin cement is reported to bond directly to metal oxides, which promotes a water-resistant chemical bond to zirconia ceramic (Lüthy *et al.* 2006). Some studies have shown that the bond strength of composite resins with a phosphate ester monomer was increased after thermocycling (14 days) (Lüthy *et al.* 2006) or slightly decreased but not statistically significantly different after longer ageing time (150 days) (Kern and Wegner 1998). However, the failure mode in this study presents completely adhesive type even though Panavia 21 was used. The use of an additional surface treatment such as silica coating or sandblasting may still be required in order to achieve high bond strengths.

6.1.3 Effect of glasses on phase configurations

The results in this study showed that the zirconia containing titanium phosphate glass had different phases that this was dependant on the percentages of the glass added. Low percentages (1-2 wt%) of titanium phosphate glass zirconia showed only the tetragonal phase while more than 5 wt% titanium phosphate glass zirconia contained two phases, which were mainly the monoclinic phase (89-85 wt%) and the tetragonal phase (11-15 wt%). The result of the 5 wt% group contrasts with the theory that the tetragonal phase should be the major phase at room temperature.

It was assumed that the glass in the zirconia activated the phase transformation which induced the tetragonal phase transformation to the monoclinic phase. One study examined the characterization of InCeram alumina, InCeram zirconia, InCeram-glass powder and InCeram zirconia-glass powder identified by x-ray diffraction (Diego *et al.* 2007). They found that InCeram alumina was composed of only the Al_2O_3 crystalline phase while InCeram zirconia powder had Al_2O_3, tetragonal ZrO_2, and monoclinic ZrO_2 (Diego *et al.* 2007). However, they did not mention the reason why the monoclinic phase was found in the powders. Several researchers (Balakrishnan *et al.* 2007; Sheng *et al.* 2004) studied glass infiltrated zirconia which is the strengthening process that allows the molten glass to infiltrate through the surface of porous sintered zirconia. The results showed that there was no monoclinic phase detected before glass infiltration; however, the monoclinic phase at the surface of glass infiltrated zirconia was found. The phase transformation that occurred during infiltration may have been due to the thermal expansion mismatch between glass and ceramic matrix inevitably causing interior stress in the composites, which induced the phase transformation of zirconia from tetragonal to a monoclinic phase (Sheng *et al.* 2004). In addition, Balakrishnan *et al* (2007) reported that the phase transformation after glass infiltration could be attributed to yttria that is responsible for stabilising the tetragonal phase. Yttria may be partially dissolved in the molten glass at high temperature causing an uncontrolled grain growth and destabilising the tetragonal phase (Balakrishnan *et al.* 2007). The larger grain size due to the presence of the glassy phase within the zirconia composites may provide favourable conditions for the monoclinic phase transformation and the lattice oxygen

ion valancy decrease in the presence of the glass (which contains various glass oxides) could also be a factor in the phase transformation (Balakrishnan *et al.* 2007).

The flexural strength was reduced when the experimental glass zirconia was added at more than 5 wt% titanium phosphate glass. This was related to the higher amount of the monoclinic phase formed in the specimens. The large percentage of monoclinic formed at room temperature led to a significant volume expansion, which generated small cracks within the specimen; hence the flexural strength of the specimens was reduced. One study also reported the formation of micro and macro cracks, loss of strength and the deterioration of mechanical properties of the zirconia ceramics in a humid environment due to the tetragonal to monoclinic transformation (Li and Watanabe 1998). This study found that addition of larger amounts of glass caused a reduction in the strength of the zirconia and triggered the phase transformation. However, within the limitation of this present study, the 1, 2, 5 wt% of zirconia containing titanium phosphate glass was investigated. Therefore, it may be beneficial to examine the phase configurations of 3 and 4 wt% titanium phosphate glass and/or adding different types of glasses in the future in order to understand more about the phase transformation of glass zirconia.

CHAPTER 7

Conclusions

Overall, the present study has shown that

1. There was a difference in the mechanical properties of different zirconia ceramic systems (Lava™, Cercon®, and Invizion™). Lava™ specimens had a flexural strength, hardness, and Weibull modulus approximately 1100 MPa, 1300 HV and 9-12.9 respectively. Additionally, specimen colouring and dynamic fatigue (at 10,000 and 20,000 cycles) did not have an effect on the flexural strength of Lava™ groups. Cercon® (823±115 MPa) and Invizion™ (828±87 MPa) groups had significantly lower flexural strength than Lava™ groups. Overall, there was no significant difference in Weibull modulus and hardness values between the groups; however, two groups in Lava™ specimens (FS4 and FS7) had different hardness values compared to others. The three groups had different elemental components and grain appearances. Lava™ and Cercon® had similar grain sizes (approximately 0.1 μm) diameter whereas Invizion™ had a slightly larger grain size. Additionally, Lava™ grains appeared rounded and separated whilst Cercon® had fused grains.

2. The fatigue test at 10,000 and 20,000 cycles did not affect the biaxial flexural strength of zirconia specimens. All zirconia specimens survived when using a force at 60-65% of mean biaxial flexural strength at a 500,000 cycle limit (simulates a service time of 2 years). However, Lava™ specimens had higher fatigue life values at 500,000 cycles (~650-700 MPa) than Cercon® (575 MPa) and Invizion™ (526 MPa). When fatiguing the crown shaped specimens (Kavo Everest ZS-blanks with IPS e.max® Ceram and IPS e.max® Zirpress), the types of sintering processes (heat pressed and sintered methods) did not influence the flexural strength of crown shaped specimens after fatigue for 50,000 cycles.

3. The *n* exponent value, which represents the resistance to the subcritical crack growth of the specimens tested in water, showed a large variation ranging from 33 to 197 for the Lava™ system. Conversely, the fracture strength was only slightly different.

4. As-sintered Lava™, Cercon® and Invizion™ specimens contained predominantly a tetragonal phase with two cubic phases (cubic 1 and a strained cubic 2). Following polishing, the strained phase changed in unit cell size back to the cubic 1 size and appeared to reduce the hardness of the material. However, polishing did not relieve the strained in Invizion™ specimens. There was a decrease in the amount of tetragonal and cubic 1 phases while the cubic 2 phase was increased when grinding using 320 and 80 grits. Zirconia ground with 1000 and 500 grits had similar phases as in the as-received specimens. Additionally, wet and dry grinding did not influence the phase changes except Invizion™. There were also no changes in the unit cell dimensions of the tetragonal phase before and after sintering zirconia.

5. The degree of transformation toughening was not dependent either on the indentation loads or the distance within the indentation. Monoclinic and high amounts of cubic phase were found at the fracture origin and tension side when compared to compression side on the fracture surface of specimens after biaxial flexural and subcritical crack growth tests. It could be concluded that transformation toughening ($t \rightarrow m$) occurred only at the area, which received the highest forces during indentation of the surface. There was also an increased amount of cubic phase at the high impact area compared with other areas. However, there were differences in

the amount of monoclinic and cubic phases within the indentation for Lava™, Cercon® and Invizion™ systems.

6. Experimental zirconia specimens had a density ranging from 4.4 to 5.7 g/cm^3. Higher percentages of titanium phosphate glass zirconia and lower sintering temperature provided slightly lower density compared with other groups. 5% wt glass contents specimens also had higher porosities compared with the control and 1 and 2 wt% glasses. Non-glass zirconia and glass zirconia sintered at 1400 ºC had similar linear shrinkage values ranging from 21-23%. Additionally, 1 wt% and 2 wt% glass showed no difference in the mean biaxial flexural strength compared with the control group; however, 5 wt% or more glasses reduced the biaxial flexural strength of the specimens. Zirconia containing 5 wt% or more glasses had a high level of the monoclinic phase (85-89 wt%) when compared to the control and lower glass contents, which had predominantly the tetragonal phase. Glass addition did not affect the sintering temperature, and the final sintering temperature according to the manufacturer's recommendation is still required to achieve the higher strength. High glass content induced phase transformations that led to the reduction of the strength of zirconia.

7. HF Etching for 2 and 5 minutes and the percentage of glass contained within the zirconia did not affect the shear bond strength of resin cement and zirconia ceramic. However, the shear bond strength of etched composite resin blocks to zirconia was slightly higher when compared to unetched composite blocks.

8. Hypotheses in this study were rejected because there were the differences in the properties between three commercial zirconia systems and there were also the difference between experimental non-glass and titanium phosphate glass zirconia. In addition, the phase transformation is influenced by the level of load applied as the larger load creates bigger areas and the transformation is also varied by the distance from the centre of the indentation.

Future work

The fatigue test was set at a 500,000 cycle limit. Therefore, to understand the nature of the fatigue, the cycle limit can be set to a longer period. In addition, an effect of different surface treatments on the fatigue of zirconia frameworks can be studied in the future. Because of the susceptibility of zirconia ceramic to the low-temperature ageing, the relationship between ageing of the zirconia framework and the strength after long term loading can also be evaluated. The long-term clinical evaluation of the zirconia restoration should also be studied especially for long span bridges. Additionally, due to the problem of chipped veneer in clinical studies, the development of the high strength veneer ceramic should be carried out and the bond strength between the veneer and zirconia framework should be investigated.

Glass-reinforced zirconia ceramic is also an interesting issue to pursue in order to improve the mechanical properties of the zirconia ceramics by using different types of glasses. Additionally, the development of glass-reinforced zirconia ceramics may lead to an etchable zirconia ceramic framework, which will allow an adhesive cementation to the underlying substrate.

CHAPTER 8

References

Abernethy RB (2006). An overview of Weibull analysis. In 'The new Weibull handbook'. pp. 1-12. North Palm Beach, Florida

Abou Neel E, Chrzanowski W, Knowles J (2008). Effect of increasing titanium dioxide content on bulk and surface properties of phosphate-based glasses. *Acta Biomaterialia* 4, 523-534.

Aboushelib MN, Kleverlaan CJ, Feilzer AJ (2007). Effect of zirconia type on its bond strength with different veneer ceramics. *Journal of Prosthodontics* 17, 401-408.

Ahmad I (2006) 'Protocols for predictable aesthetic dental restorations.' Blackwell Publishing Company, Oxford, UK

Al-Dohan HM, Yaman P, Dennison JB, Razzoog ME, Lang BR (2004). Shear strength of core-veneer interface in bi-layered ceramics. *The Journal of Prosthetic Dentistry* 91, 349-355.

Albakry M, Guazzato M, Swain MV (2004). Biaxial flexural strength and microstructure changes of two recycled pressable glass ceramics. *Journal of Prosthodontics* 13, 141-149.

Albakry M, Guazzato M, Swain MV (2003a). Fracture toughness and hardness evaluation of three pressable all-ceramic dental materials. *Journal of Dentistry* 31, 181-188.

Albakry M, Guazzato M, Swain MV (2003b). Biaxial flexural strength, elastic moduli, and x-ray diffraction characterization of three pressable all-ceramic materials. *The Journal of Prosthetic Dentistry* 89, 374-380.

Anderson DJ (1956). Measurement of stress in mastication: I Journal of *Dental Research* 35, 664-671.

Anderson JC, Leaver KD, Rawlings RD, Alexander JM (1990). 'Material Science', Chapman and Hall, London.

Anderson M, Odén A (1993). A new all-ceramic crown. A dense-sintered, high-purity alumina coping with porcelain. *Acta Odontologica Scandinavica* 51, 59-64.

Anusavice KJ (1996). Dental Ceramics. In 'Phillips' science of dental materials'. p. 583, W.B. Sounders Company, Philadephia, Pennsylvania.

Anusavice KJ (2003a). 'Dental materials', Saunders, St. Louis, Missouri.

Anusavice KJ (2003b). Mechanical properties of dental materials. In 'Phillips' science of dental materials'. (Ed. KJ Anusavice) p. 93, Saunders, Philadelphia, PA

Anusavice KJ (2003c). Dental ceramics. In 'Phillips' Science of dental materials'. (Ed. KJ Anusavice) pp. 655-719. Saunders, Missouri, USA.

Apholt W, Bindl A, Lüthy H, Mörmann WH (2001). Flexural strength of Cerec 2 machined and jointed InCeram-Alumina and InCeram-Zirconia bars. *Dental Materials* 17, 260-267.

Ardlin BI (2002). Transformation-toughened zirconia for dental inlays, crowns and bridges: chemical stability and effect of low-temperature aging on flexural strength and surface structure. *Dental Materials* 18, 590-595.

Atsu SS, Kilicarslan MA, Kucukesmen HC, Aka PS (2006). Effect of zirconium-oxide ceramic surface treatments on the bond strength to adhesive resin. *The Journal of Prosthetic Dentistry* 95, 430-436.

Attia A, Kern M (2004). Influence of cyclic loading and luting agents on the fracture load of two all-ceramic crown systems. *The Journal of Prosthetic Dentistry* 92, 551-556.

Awliya W, Odén A, Yaman P, Dennison JB, Razzoog ME (1998). Shear bond strength of a resin cement to densely sintered high-purity alumina with various surface conditions. *Acta Odontologica Scandinavica* 56, 9-13.

Balakrishnan A, Panigrahi BB, Chu MC, Kim TN, Yoon KJ, Cho SJ (2007). Improvement in mechanical properties of sintered zirconia (3% yttria stabilized) by glass infiltration. *Journal of Materials Research* 22, 2550-2557.

Ban S, Anusavice KJ (1990). Influence of test method on failure stress of brittle dental materials. *Journal of Dental Research* 69, 1791-1799.

Behrens A, Reusch B, Hauptmann H (2004). Fracture strength of colored versus uncolored zirconia specimens. *International Association for Dental Research* 0243.

Behrens G, Dransmann GW, Heuer AH (1993). On the isothermal martensitic transformation in 3Y-TZP. *Journal of the American Ceramic Society* 76, 1025-1030.

Benaqqa C, Chevalier J, Saädaoui M, Fantozzi G (2005). Slow crack growth behaviour of hydroxyapatite ceramics. *Biomaterials* 26, 6106-6112.

Beuer F, Edelhoff D, Garnet W, Naumann M (2008). Effect of preparation angles on the precision of zirconia crown copings fabricated by CAD/CAM system. *Dental Materials Journal* 27, 814-820.

Binnig G, Quate CF (1986). Atomic force microscope. *Physical Review Letters* 56, 930-933.

Blatz MB, Sadan A, Kern M (2003). Resin-ceramic bonding: a review of the literature. *The Journal of Prosthetic Dentistry* 89, 268-274.

Brentel AS, Özcan M, Valandro LF, Alarca LG, Amaral R, Bottino MA (2007). Microtensile bond strength of a resin cement to feldspathic ceramic after different etching and silanization regimens in dry and aged conditions. *Dental Materials* 23, 1323-1331.

BSI ENV 843-4 (1995) 'Advanced technical ceramics. Monolithic ceramics. Mechanical properties at room temperatures. Vickers, Knoop and Rockwell superficial hardness tests.'

Calamia JR, SImonsen RJ (1984). Effect of coupling agents on bond strength of etched porcelain. *Journal of Dental Research* 63 (Abstr.79), 179.

Cales B, Stefani Y, Lilley E (1994). Long-term in vivo and in vitro aging of a zirconia ceramic in orthopaedy. *Journal of Biomedical Materials Research* 28, 619-624.

Callister WDJ (2005). 'Materials science and engineering: An integrated approch.' John Wiley&Sons, Inc, USA.

Casellas D, Cumbrera FL, Sánchez-Bajo F, Forsling W, Llanes L, Anglada M (2001). On the transformation toughening of Y-ZrO_2 ceramics with mixed Y-TZP/PSZ microstructures. *Journal of the European Ceramic Society* 21, 765-777.

Cattell MJ, Knowles JC, Clarke RL, Lynch E (1999). The biaxial flexural strength of two pressable ceramic systems. *Journal of Dentistry* 27, 183-196.

Cattell MJ, Palumbo RP, Knowles JC, Clarke RL, Samarawickrama DYD (2002). The effect of veneering and heat treatment on the flexural strength of Empress 2 ceramics. *Journal of Dentistry* 30, 161-169.

Cesar PF, Miranda junior WG, Braga RR (2001). Influence of shade and storage time on the flexural strength, flexural modulus, and hardness of composites used for indirect restorations. The *Journal of Prosthetic Dentistry* 86, 289-296.

Chen HY, Hickel R, Setcos JC, Kunzelmann KH (1999). Effects of surface finish and fatigue testing on the fracture strength of CAD-CAM and pressed-ceramic crowns. *The Journal of Prosthetic Dentistry* 82, 468-475.

Chen JH, Matsumura H, Atsuta M (1998). Effect of etchant, etching period, and silane priming on bond strength to porcelain of composite resin. *Operative Dentistry* 23, 250-257.

Chen SY, Lu HY (1988). Sintering of 3 mol% Y_2O_3 -TZP and its fracture after ageing treatment. *Journal of Materials Science* 23, 1195-1200.

Chevalier J (1999). Low-temperature aging of Y-TZP ceramics. *Journal of the American Ceramic Society* 82, 2150-2154.

Chevalier J (2006). What future for zirconia as a biomaterial? *Biomaterials* 27, 535-543.

Chevalier J, Olagnon C, Fantozzi G (1996). Study of the residual stress field around Vickers indentations in a 3Y-TZP. *Journal of Medical and Dental Sciences* 31, 2711-2717.

Chevalier J, Olagnon C, Fantozzi G (1999). Subcritical crack propagation in 3Y-TZP ceramics: static and cyclic fatigue. *Journal of the American Ceramic Society* 82, 3129-3138.

Chevalier J, Olagnon C, Fantozzi G, Calés B (1995). Crack propagation behaviour of Y-TZP ceramics. *Journal of the American Ceramic Society* 78, 1889-1894.

Christel P, Meunier A, Heller M, Torre JP, Peille CN (1989). Mechanical properties and short-term *in vivo* evaluation of yttria-oxide-partially-stabilized zirconia. *Journal of Biomedical Materials Research* 23, 45-61.

Christensen GJ (1971). Clinical and research advancements in cast-gold restorations. *The Journal of Prosthetic Dentistry* 25, 62-68.

Christie T, Brathwaite B (1999). 'Mineral commodity report 19: Beryllium, Gallium, Lithium, Magnesium, Iranium and Zirconium.' Institute of geological and nuclear sciences Ltd,No. 19, New Zealand Mining

Clarke DR, Adar F (1982). Measurement of the crystallographically transformed zone produced by fracture in ceramic containing tetragonal zirconia. *Journal of the American Ceramic Society* 65, 284-288.

Clarke IC, Manaka M, Green DD, Williams P, Pezzotti G, Kim Y-H, Ries M, Sugano N, Sedel L, Delauney C, Ben Nissan B, Donaldson T, Gustafson GA (2003). Current status of zirconia used in total hip implants. *The Journal of Bone&Joint Surgery* 85, 73-84.

Coastal and marine Geology program. A laboratory manual for x-ray powder diffraction. 2001. U.S. Department of the interior, U.S. Geological survey.

Coelho, A. A. TOPAS-Academic. 2004.

Colomban P, Havel M (2002). Raman imaging of stress-induced phase transformation in transparent ZnSe ceramic and sapphire single crystals. *Journal of Raman Spectroscopy* 33, 789-795.

Craig RG, Powers JM (2002). 'Restorative Dental Materials', Mosby Inc, St. Louis.

Craig RG, Ward ML (1997). Mechanical properties. In 'Restorative dental materials'. p. 56, Mosby, St. Louis.

Curtis AR, Wright AJ, Fleming GJP (2006). The influence of simulated masticatory loading regimes on the bi-axial flexure strength and reliability of a Y-TZP dental ceramic. *Journal of Dentistry* 34, 317-325.

Curtis AR, Wright AJ, Fleming GJP (2005). The influence of surface modification techniques on the performance of a Y-TZP dental ceramic. *Journal of Dentistry* 1-12.

Della Bona A, Anusavice KJ, Hood JA (2002). Effect of ceramic surface treatment on tensile bond strength to a resin cement. *The International Journal of Prosthodontics* 15, 248-253.

Della Bona A, Anusavice KJ, DeHoff PH (2003). Weibull analysis and flexural strength of hot-pressed core and veneered ceramic structure. *Dental Materials* 19, 662-669.

Della Bona A, Borba M, Benetti P, Cecchetti D (2007). Effect of surface treatments on the bond strength of a zirconia-reinforced ceramic to composite resin. *Brazilian Oral Research* 21, 10-15.

Della Bona A, van Noort R (1995). Shear vs. tensile bond strength of resin composite bonded to ceramic. *Journal of Dental Research* 74, 1591-1596.

DeLong R, Goodkind RJ, Douglas WH (1984) Corrosion-fatigue of the bond between nickle-chrome casting alloys and porcelain. *The Journal of Prosthetic Dentistry* 52, 344-348.

Denissen H, Dozic A, van der Zel J, van Wass M (2000) Marginal fit and short-term clinical performance of porcelain-veneered CICERO, CEREC, and Procera onlays. *The Journal of Prosthetic Dentistry* 84, 506-513.

Denry IL (1996) Recent advances in ceramics for dentistry. *Critical Reviews in Oral Biology&Medicine* 7, 134-143.

Denry IL, Holloway JA (2005) Microstructural and crystallographic surface changes after grinding zirconia-based dental ceramics. *Journal of Biomedical Materials Research Part B: Applied Biomaterials* 76B, 440-448.

Denry IL, Kelly JR (2008) State of the art of zirconia for dental applications. *Dental Materials* 24, 299-307.

Denry IL, Rosenstiel SF, Holloway JA, Niemiec MS (1993) Enhanced Chemical Strengthening of Feldspathic Dental porcelain. *Journal of Dental Research* 72, 1429-1433.

Derand P, Derand T (2000). Bond strength of luting cements to zirconium oxide ceramics. *The International Journal of Prosthodontics* 13, 131-135.

Deville S, Chevalier J, Dauvergne C, Fantozzi G (2005). Microstructural investigation of the aging behaviour of (Y-TZP)-Al2 O3 composites. *Journal of the American Ceramic Society* 88, 1273-1280.

Deville S, Chevalier J, Gremillard L (2006). Influence of surface finish and residual stresses on the aging sensitivity of biomedical grade zirconia. *Biomaterials* 27, 2186-2192.

Diego AA, dos Santos C, Landim KT, Elias CN (2007). Characterization of ceramic powders used in the InCeram systems to fixed dental prosthesis. *Material Research* 10, 47-51.

Dozic A, Kleverlann CJ, Meegdes M, van der Zel J, Feilzer AJ (2003). The influence of porcelain layer thickness on the final shade of ceramic restorations. *The Journal of Prosthetic Dentistry* 90, 563-570.

Drummond JL (1991) CAD/CAM in dentistry. *NGCA'91 12th Annual Conference and Exposition Dedicated to Computer Graphics* 75-79.

Duckworth WH (1951). Precise tensile properties of ceramic bodies. *Journal of the American Ceramic Society* 34, 1-9.

Duwez P, Brown Jr FH, ell F (1951). The zirconia-yttria system. *Journal of the Electrochemical Society* 98, 356-362.

Duwez P, Odell F, Brown Jr FH (1952). Stablized of zirconia with calcia and magnesia. *Journal of the American Ceramic Society* 35, 107-113.

EN ISO 6872:1998 (1999) 'The European Standard EN ISO 6872:1998.'

Estafan D, Dussetschleger F, Agosta C, Reich S (2003). Scanning electron microscope evaluation of CEREC II and CEREC III inlays. *General Dentistry* 51, 450-454.

Farsi, S, Giordano, R, and Pober, R. Flexure strength of yttria partially stabilized colored/un-colored zirconia. IADR . 2006.

Ferrario VF, Sforza C, Zanotti G, Tartaglia GM (2004). Maximal bite forces in healthy young adults are predicted by surface electromyography. *Journal of Dentistry* 32, 451-457.

Fett T, Rizzi G (2004) '3-balls-on-3-balls test on ceramic disks: a finite element study.' Forschugszentrum Kalsruhe,No. FZKA 7052, Karlsruhe

Fu-Kang F, Kuznetsov AK, Keler ÉK (1963). Phase relationships in the system Y_2O_3-ZrO_2 Part 2. solid solution. *Institute of silicate chemistry, Academy of sciences of the USSR* 4, 601-610.

Garvie RC, Hannink RH, Pascoe RT (1975). Ceramic steel. *Nature* 258, 703-704.

Garvie RC, Urbani C, Kennedy DR, McNeuer JC (1984). Biocompatibility of magnesia-partially stabilized zirconia (Mg-PSZ) ceramics. *Journal of Materials Science* 19, 3224-3228.

Grossman DG (1985). Processing a dental ceramic by casting methods. In 'Proceedings of conference on recent developments in dental ceramics.'. pp. 19-40, American Ceramic Society, Columbus, Ohio

Guazzato M, Albakry M, Swain MV, Ironside J (2002). Mechanical properties of In-Ceram Alumina and In-Ceram Zirconia. *The International Journal of Prosthodontics* 15, 339-346.

Guazzato M, Proos K, Quach L, Swain MV (2004a). Strength reliability and mode of fracture of bilayered porcelain/zirconia (Y-TZP) dental ceramics. *Biomaterials* 25, 5045-5052.

Guazzato M, Quach L, Albakry M, Swain MV (2005a). Influence of surface and heat treatments on the flexural strength of Y-TZP dental ceramic. *Journal of Dentistry* 33, 9-18.

Guazzato M, Albakry M, Ringer SP, Swain MV (2004b). Strength, fracture toughness and microstructure of a selection of all-ceramic materials. Part I. Pressable and alumina glass-infiltrated ceramics. *Dental Materials* 20, 441-448.

Guazzato M, Albakry M, Ringer SP, Swain MV (2005b). Strength, fracture toughness and microstructure of a selection of all-ceramic materials. Part II. Zirconia-based dental ceramics. *Dental Materials* 20, 449-456.

Guess PC, Kulis A, Witkowski S, Wolkewitz M, Zhang Y, Strub JR (2008). Shear bond strengths between different zirconia cores and veneering ceramics and their susceptibility to thermocycling. *Dental Materials* doi:10.1016/j.dental.2008.03.028, 1-12.

Gupta TK, Bechtold JH, Kuznicki RC, Cadoff LH, Rossing BR (1977). Stabilization of tetragonal phase in polycrystalline zirconia. *Journal of Materials Science* 12, 2421-2426.

Heiserman DL (1992) 'Exploring Chemical Elements and Their Compounds, McGraw Hill, New York.

Helmer JD, Driskell TD (1969) 'Research on bioceramics. ' Symposium on use of ceramics as surgical implants, Clemson, South Carolina, Clemson University

Herzfield H (1916) German Patent 290,878 (May 29, 1914). ***Journal of The Society of Chemical Industrial*** **35, 634.**

Hjerppe J, Narhi T, Froberg K, Vallittu PK, Lassila LV (2008). Effect of shading the zirconia framework on biaxial strength and surface microhardness. ***Acta Odontologica Scandinavica*** **doi:10.1080/00016350802247123.**

Horiba Jobin Yvon. Raman spectroscopy. 2008.

Hulm BJ, Evans WJ (2000). Evaluation of the cyclic fatigue life of 3-mol%-yttria-stabilized zirconia bioceramic using biaxial flexion. ***Journal of the American Ceramic Society*** **83, 321-328.**

Hummer CD, Rothman RH, Hozack WJ (1995). Catastrophic failure of modular zirconia-ceramic femoral head components after total hip arthroplasty. ***Journal of Arthroplasty*** **10, 848-850.**

Isgro G, Pallav P, van der Zel JM, Feilzer AJ (2003). The influence of the veneering porcelain and different surface treatments on the biaxial flexural strength of a heat-pressed ceramic. ***The Journal of Prosthetic Dentistry*** **90, 465-473.**

ISO 6872 (1995) 'International standard for dental ceramic.'

Itinoche KM, Özcan M, Bottino MA, Oyafuso D (2006). Effect of mechanical cycling on the flexural strength of densely sintered ceramics. ***Dental Materials*** **21, 1-6.**

Johnson CA (1983). Fracture statics of multiple flaw distribution. In 'Fracture mechanics of ceramics'. pp. 365-386, Plenum Press, New York.

Jones DW (1985). Development of Dental Ceramic: An historical perspective. ***Dental Clinics of North America*** **29, 621-644.**

Josset Y, Oum´ Hamed Z, Zarrinpour A, Lorenzato M, Adnet JJ, Laurent-Maquin D (1999). ***In vitro*** **reaction of human osteoblasts in culture with zirconia and alumina ceramics.** ***Journal of Biomedical Materials Research*** **47, 493.**

Jung Y-G, Peterson IM, Kim DK, Lawn BR (2000). Lifetime-limiting Strength Degradation from Contact Fatigue in Dental Ceramics. ***Journal of Dental Research*** **79, 722-731.**

Kailer A, Nickel KG, Gogotsi YG (1999). Raman microspectroscopy of nanocrystalline and amorphous phases in hardness indentations. ***Journal of Raman Spectroscopy*** **30, 939-946.**

Katz G (1971) X-ray diffraction powder pattern of metastable cubic ZrO_2. ***Journal of the American Ceramic Society*** **54, 531.**

Kelly JR (2007). Developing meaningful systematic review of CAD/CAM reconstructions and fiber-reinforced composites. *Clinical Oral Implants Research* 18 (Auppl.3), 205-217.

Kelly JR (2004). Dental ceramic: current thinking and trends. *Dental Clinics of North America* 48, 513-530.

Kelly JR, Denry I (2008). Stabilized zirconia as a structural ceramic: An overview. *Dental Materials* 24, 289-298.

Kelly JR, Nishimura I, Campbell SD (1996). Ceramics in dentistry: Historical roots and current perspectives. *The Journal of Prosthetic Dentistry* 75, 18-32.

Kelly JR, Tesk JA, Sorensen JA (1995). Failure of all-ceramic fixed partial dentures *in vitro* and *in vivo*: analysis and modelling. *Journal of Dental Research* 74, 1253-1258.

Kern M, Wegner SM (1998). Bonding to zirconia ceramic: adhesion methods and their durability. *Dental Materials* 14, 64-71.

Kim B, Zhang Y, Pines M, Thompson VP (2007) Fracture of porcelain-veneered structures in fatigue. *Journal of Dental Research* 86, 142-146.

Kim DJ (1990). Effect of Ta_2O_5, Nb_2O_5, and HfO_2 alloying on the transformability of Y_2O_3-stabilised tetragonal ZrO_2. *Journal of the American Ceramic Society* 73, 115-120.

Kitazaki H, Takahashi H, Hasegawa S, Nishimura F (2001). Effect of amount of grinding on flexural strength of dental ceramics. *Journal of Medical and Dental Sciences* 48, 7-13.

Kohal RJ, Klaus G (2004) A zirconia implant-crown system: a case report. *The International Journal of Periodontics&Restorative Dentistry* 24, 147-153.

Kohal RJ, Klaus G, Strub JR (2006). Zirconia-implant-supported all-ceramic crowns withstand long-term load: a pilot investigation. *Clinical Oral Implants Research* 17, 565-571.

Kondoh J (2004). Origin of the hump on the left shoulder of the X-ray diffraction peaks observed in Y_2O_3-fully and partially stabilized ZrO_2. *Journal of Alloys and Compounds* 375, 270-282.

Kosmac T, Dakskobler A (2007). The strength and hydrothermal stability of Y-TZP ceramics for dental applications. *International Journal of Applied Ceramic Technology* 4, 164-174.

Kosmac T, Oblak C, Jevnikar P, Funduk N, Marion L (2000). Strength and reliability of surface treated Y-TZP dental ceramics. *Journal of Biomedical Materials Research* 53, 304-313.

Kosmac T, Oblak C, Jevnikar P, Funduk N, Marion L (1999). The effect of surface grinding and sandblasting on flexural strength and reliability of Y-TZP zirconia ceramic. *Dental Materials* 15, 426-433.

Kreidl NJ (1942) Zirconium oxide and thorium oxide in ceramics. *Journal of the American Ceramic Society* 25, 129-141.

Kreulen CM, Moscovich H, Dansen KA, Creugers NHJ (2000). Time-and-motion study on Class II copy-milled ceramic inlays. *Journal of Dentistry* 28, 429-436.

Kukiattrakoon B, Thammasitboon K (2007). The effect of different etching times of acidulated phosphate fluoride gel on the shear bond strength of high-leucite ceramics bonded to composite resin. *The Journal of Prosthetic Dentistry* 98, 17-23.

Lange FF (1982). Transformation toughening Part3 experimental observations in the ZrO2-Y2O3 system. *Journal of Materials Science* 17, 240-246.

Lawson S (1995). Environmental degradation of zirconia ceramics. *Journal of the European Ceramic Society* 15, 485-502.

Leach CA (1989). A Raman microprobe study of a magnesia partially stabilized zirconia fracture surface. *Journal of Materials Science* 24, 1380-1382.

Li JF, Watanabe R (1998). Phase transformation in Y_2O_3-partially-stabilized ZrO_2 polycrytals of various grain size during low-temperature aging in water. *Journal of the American Ceramic Society* 81, 2687-2691.

Li L-S, Pabst RF (1980). Subcritical crack growth in partially stabilized zirconia (PSZ). *Journal of Materials Science* 15, 2861-2866.

Li M, Feng Z, Ying P, Xin Q, Li C (2003). Phase transformation in the surface region of zirconia and doped zirconia detected by UV Raman spectroscopy. *Physical Chemistry Chemical Physics* 5, 5326-5332.

Liu PR (2005). A Panorama of dental CAD/CAM restorative system. *Compendium of Continuing Education in Dentistry* 26, 507-508.

Liu SY, Chen IW (1991). Fatigue of yttria-stabilized zirconia: I, fatigue damage, fracture origins, and lifetime prediction. *Journal of the American Ceramic Society* 74, 1197-1205.

Luthardt RG et al (2004). CAD/CAM-machining effects on Y-TZP zirconia. *Dental Materials* 20, 655-662.

Lüthy H, Filser F, Loeffel O, Schumacher M, Gauckler L, Hammerle C (2005). Strength and reliability of four-unit all-ceramic posterior bridges. *Dental Materials* 21, 930-937.

Lüthy H, Loeffel O, Hammerle CHF (2006). Effect of thermocycling on bond strength of luting cements to zirconia ceramic. *Dental Materials* 22, 195-200.

Marquardt P, Strub JR (2006). Survival rates of IPS empress 2 all-ceramic crowns and fixed partial dentures: results of a 5-year prospective clinical study. *Quintessence International* 37, 253-259.

Matinlinna JP, Lassila LVJ, Özcan M, Yli-Urpo A, Vallittu PK (2004). An Introduction to silanes and their clinical applications in dentistry. *The International Journal of Prosthodontics* 17, 155-164.

McLean JW (1967). The alumina reinforced porcelain jacket crown. *Journal of the American Dental Association* 75, 621-628.

McLean JW (1965). A higher strength porcelain for crown and bridge work. *British Dental Journal* 119, 268-272.

Meyenberg KH, Lüthy H, Schärer P (1995). Zirconia posts: a new all-ceramic concept for nonvital abutment teeth. *Journal of Esthetic and Restorative Dentistry* 7, 73-80.

Michel D, Mazerolles L, Perez Y Jorba M (1983). Fracture of metastable tetragonal zirconia crystals. *Journal of Materials Science* 18, 2618-2628.

Milleding P, Karlsson S, Nyborg L (2003). On the surface elemental composition of non-corroded and corroded dental ceramic materials in vitro. *Journal of Materials Science: Materials in Medicine* 14, 557-566.

Miura S, Inagaki R, Okuno O, Kimura K (2005) A study on the computer aided manufacturing system utilizing the tetragonal stabilized zirconia. *International Congress Series* 1284, 316-317.

Morena R, Beaudreau GM, Lockwood PE, Evans AL, Fairhurst CW (1986). Fatigue of dental ceramics in a simulated oral environment. *Journal of Dental Research* 65, 993-997.

Mörmann WH (2006). The evolution of the CEREC system. *Journal of the American Dental Association* 137, 7S-13S.

Mörmann WH, Brandestini M, Lutz F, Barbakow F (1989). Chair-side computer-aided direct ceramic inlays. *Quintessence International* 20, 329-339.

Morrell R, McCormick NJ, Bevan J, Lodeiro M, Margetson J (1999). Biaxial disc flexure-Modulus and strength testing. *British Ceramic Transactions* 98, 234-240.

Nakamura T, Kojima T, Wakabayashi K (2003). Marginal and internal fit of Cerec 3 CAD/CAM all-ceramic crowns. *The International Journal of Prosthodontics* 16, 244-248.

Nakayama S, Sakamoto M (1998). Improvement of mechanical properties of Y-TZP by the addition of B_2O_3-Al_2O_3-SiO_2. *Journal of Materials Science Letters* 17, 1431-1433.

O'Brien WJ (2002) Dental porcelain. In 'Dental materials and their selection'. (Ed. WJ O'Brien) pp. 210-224, Quintessence Publishing Co, Inc.

Ödman P, Andersson B (2001). Procera AllCeram crowns followed for 5 to 10.5 years: a prospective clinical study. *The International Journal of Prosthodontics* 14, 504-509.

Ohyama T, Yoshinari M, Oda Y (1999). Effects of cyclic loading on the strength of all-ceramic materials. *The International Journal of Prosthodontics* 12, 28-37.

Okiyama S, Ikebe K, Nokubi T (2003). Association between masticatory performance and maximal occlusal force in young men. *Journal of Oral Rehabilitation* 30, 278-282.

Özcan M, Vallittu PK (2003). Effect of surface condition methods on the bond strength of luting cement to ceramics. *Dental Materials* 19, 725-731.

Pallis K, Griggs JA, Woody RD, Guillen GE, Miller AW (2004). Fracture resistance of three all-ceramic restorative systems for posterior applications. *The International Journal of Prosthodontics* 91, 561-569.

Papanagiotou HP, Morgano SM, Giordano RA, Pober R (2006). In vitro evaluation of low-temperature aging effects and finishing procedures on the flexural strength and structural stability of Y-TZP dental ceramics. *The Journal of Prosthetic Dentistry* 96, 154-164.

Pashchenko VP, Nesterov AM, Brovkina GT, Mikhailenko GP, Klochai IF, Lisovskii AM (1994). Influence of the forming process and sintering conditions on the structure and properties of powder ferrite materials. *Powder Metallurgy and Metal Ceramics* 33, 66-69.

Piconi C, Maccauro G (1999). Review zirconia as a ceramic biomaterial. *Biomaterials* 20, 1-25.

Piconi C, Maccauro G, Muratori F, Del Prever B (2003). Alumina and zirconia ceramics in joint replacements. *Journal of Applied Biomaterials&Biomechanics* 1, 19-32.

Piwowarczk A, Ottl P, Lauer HC, Kuretzky T (2005). A clinical report and overview of scientific studies and clinical procedures conducted on the 3M ESPE Lava all-ceramic system. *Journal of Prosthodontics* 14, 39-45.

Pjetursson BE, Sailer I, Zwahlen M, Hämmerle CHF (2007). A systematic review of the survival and complication rates of all-ceramic and metal-ceramic reconstructions after an observation period of at least 3 years. Part I: single crowns. *Clinical Oral Implants Research* 18, 73-85.

Pletka BJ, Weiderhorn SM (1982). A comparison of failure predictions by strength and fracture mechanics techniques. *Journal of Materials Science* 17, 1247-1268.

Porter DL, Heuer AH (1977). Mechanisms of toughening partially stabilized zirconia (PSZ). *Journal of the American Ceramic Society* 60, 183-184.

Probster L, Diehl J (1992). Slip-casting alumina ceramics for crown and bridge restoration. *Quintessence International* 23, 25-31.

Qualtrough AJE, Piddock V (1999). Recent advanced in ceramic materials and systems for dental restorations. *Dental Update* 26, 65-72.

Qualtrough AJE, Piddock V (1995). Dental CAD/CAM: A millstone or a milestone? *Dental Update* 22, 200-204.

Quinn JB, Quinn GD, Kelly JR, Scherrer SS (2005). Fractographic analyses of three ceramic whole crown restoration failures. *Dental Materials* 1-10.

Quinn JB, Sundar V, Lloyd IK (2003). Influence of microstructure and chemistry on the fracture toughness of dental ceramics. *Dental Materials* 19, 603-611.

Raigrodski AJ, Chiche GJ, Potiket N, Hochstedler JL, Mohamed SE, Billiot S, Mercante DE (2006). The efficacy of posterior three-unit zirconium-oxide-based ceramic fixed partial dental prostheses: A prospective clinical pilot study. *The Journal of Prosthetic Dentistry* 96, 237-244.

Reed, J. S. and Lejus, A-M (1977). Effect of grinding and polishing on near-surface phase transformations in zirconia. *Materials Research Bulletin* 12, 949-954. 1977.

Reese MJ, Cox JM (1992). Delayed failure/subcritical crack growth of ceramics. *National Physical Laboratory* 4-30.

Reese MJ, Tetlow PL, Galiotis C (1992). Phase transformation around indentations in zirconia. *Journal of Materials Science* 11, 575-577.

Richerson DW (1992) 'Modern ceramic engineering: Properties, processing and use in design', Marcel Dekker Inc, New York, USA.

Ritter JE (1995). Predicting lifetimes of materials and material structures. *Dental Materials* 11, 142-146.

Rosenstiel SF, Land MF, Fujimoto J (2000). 'Contemporary fixed prosthodontics.', Mosby, St. Louis.

Ruiz L, Readey MJ (1996). Effect of heat treatment on grain size, phase assemblage, and mechanical properties of 3 mol% Y-TZP. *Journal of the American Ceramic Society* 79, 2331-2340.

Sadoun M (1988). All ceramic bridges with the slip casting technique. Presented at the Seventh International Symposium on Ceramics, Paris.

Sailer I, Fehér A, Filser F, Gauckler LJ, Lüthy H, Hämmerle CHF (2007a). Five-year clinical results of zirconia frameworks for posterior fixed partial dentures. *Quintessence International* 20, 383-388.

Sailer I, Pjetursson BE, Zwahlen M, Hämmerle CHF (2007b). A systematic review of the survival and complication rates of all-ceramic and metal-ceramic reconstructions after an observation period of at least 3 years. Part II: fixed dental prostheses. *Clinical Oral Implants Research* 18 (suppl.3), 86-96.

Sano H, Ciucchi B, Matthews WG, Pashley DH (1994) Tensile properties of mineralized and demineralized human and bovine dentin. *Journal of Dental Research* 73, 1205-1211.

Sato T, Shimada M (1985). Transformation of yttria-doped tetragonal ZrO_2 polycrystals by annealing in water. *Journal of the American Ceramic Society* 68, 356-359.

Scarano A, Di Carlo F, Quaranta M, Piattelli A (2003). Bone response to zirconia ceramic implants: an experimental study in rabbits. *Journal of Oral Implantology* 29, 8-12.

Schlegel A, Besimo C, Donath K (1991). The in-vitro study of the marginal fit accuracy of computer-milled titanium crowns. II. A histological-morphometric marginal-gap analysis. *Schweiz Monatsschr Zahnmed* 101, 1409-1414.

Scott HG (1975) Phase relationships in the zirconia-yttria system. *Journal of Materials Science* 10, 1527-1535.

Seal A, Dalui AK, Banerjee M, Mukhopadhyay AK, Phani KK (2001). Mechanical properties of very thin cover slip glass disk. *Bulletin of Materials Science* 24, 151-155.

Seghi RR, Sorensen JA (1995). Relative flexural strength of six new ceramic materials. *The International Journal of Prosthodontics* 8, 239-246.

Sekulic A, Furic K, Tonejc A, Tonejc AM, Stubicar M (1997). Determination of the monoclinic, tetragonal and cubic phases in mechanically alloyed ZrO_2-Y_2O_3 and ZrO_2-CaO powder mixtures by Raman spectroscopy. *Journal of Materials Science Letters* 16, 260-262.

Sertgöz A, Gemalmaz D, Alkumru H, Yoruc B (1995). Luting composite thickness of two ceramic inlay system. *The European Journal of Prosthodontics and Restorative Dentistry* 3, 151-154.

Shah, K, Holloway, J. A., and Denry, I. L (2008). Effect of coloring with various metal oxides on the microstructure, color, and flexural strength of 3T-YZP. *Journal of Biomedical Materials Research* doi10.1002/jbm.b.31107 .

Sheng XJ, Hu H, Jin ZH, Wang YL (2004). Preparation of glass-infiltrated 3Y-TZP/Al_2O_3/glass composites. *Materials Letters* 58, 1750-1753.

Shetty DK, Rosenfield AR, Bansal GK, Duckworth WH (1981). Biaxial fracture studies of a glass-ceramic. *Journal of the American Ceramic Society* 64, 1-4.

Shimizu K, Oka M, Kumar P, Kotoura Y, Yamamuro T, Makinouchi K, Nakamura T (1993). Time-dependent changes in the mechanical properties of zirconia ceramic. *Journal of Biomedical Materials Research* 27, 729-734.

Sierraalta, M, Odén, A, and Razzoog, M. E. Material Strength of Zirconia Produced with Two Methods. 32nd Annual Meeting and Exhibition of the AADR 450. 2003.

Siervo S, Bandettini B, Siervo P, Falleni A, Siervo R (1994). The CELAY system: a comparison of the fit of direct and indirect fabrication technique. *The International Journal of Prosthodontics* 7, 434-39.

Sobrinho LC, Cattell MJ, Knowles JC (1998a). Fracture strength of all-ceramic crowns. *Journal of Materials Science: Materials in Medicine* 9, 555-559.

Sobrinho LC, Glover RH, Knowles JC, Cattell MJ (1998b). Comparison of the wet and dry fatigue properties of all ceramic crowns. *Journal of Materials Science: Materials in Medicine* 9, 517-521.

Sorensen JA, Kang SK, Torres TJ, Knode H (1998). In-Ceram fixed partial dentures: three-year clinical trial results. *Journal of the California Dental Association* 26, 207-214.

Sorensen JA (2003). The Lava system for CAD/CAM production of high-strength precision fixed prosthodontics. *Quintessence of Dental Technology* 26, 57-67.

Sorensen J, Cruz M, Mito W, Raffeiner O, Meredith H, Foser H (1999). Survival rates of IPS empress 2 all-ceramic crowns and fixed partial dentures: results of a 5-year prospective clinical study. *Practical Periodontic and Aesthetic Dentistry* 11, 95-106.

Stangel I, Nathanson D, Hsu CS (1987). Shear strength of the composite bond to etched porcelain. *Journal of Dental Research* 66, 1460-1465.

Studart AR, Filser F, Kocher P, Gauckler LJ (2007a). Fatigue of zirconia under cyclic loading in water and its implications for the design of dental bridges. *Dental Materials* 23, 106-114.

Studart AR, Filser F, Kocher P, Gauckler LJ (2007b). *In vitro* lifetime of dental ceramics under cyclic loading in water. *Biomaterials* 28, 2695-2705.

Sundh A, Molin M, Sjogren G (2005). Fracture resistance of yttrium oxide partially-stabilized zirconia all-ceramic bridges after veneering and mechanical fatigue testing. *Dental Materials* 21, 476-482.

Sunnegårdh-Grönberg K, Peutzfeldt A, van Dijken JWV (2003). Flexural strength and modulus of a novel ceramic restorative cement intended for posterior restorations as determined by three-point bending test. *Acta Odontologica Scandinavica* 61, 87-92.

Suttor D, Bunke K, Hoescheler S, Hauptmann H, Hertlein G (2001). Lava-The system for all-ceramic ZrO2 crown and bridge framework. *International Journal of Computerized Dentistry* 4, 195-206.

Swain MV, Hannink RHJ (1989). Metastability of the martensitic transformation in a 12 mol% ceria-zirconia alloy: grinding studies. *Journal of the American Ceramic Society* 72, 1358-1364.

Teufer G (1962) Crystal structure of tetragonal ZrO_2. *Acta Crystallographica* 15, 1187.

Thompson JY, Anusavice KJ, Naman A, Morris HF (1994). Fracture surface characterisation of clinically failed all-ceramic crowns. *Journal of Dental Research* 73, 1824-1832.

Thordrup M, Isidor F, Horsted-Bindslev P (1994). Comparison of marginal fit and microleakage of ceramic and composite inlays: an *in vitro* study. *Journal of Dentistry* 22, 147-153.

Thurmond JW, Barkmeier WW, Wilwerding TM (1994). Effect of porcelain surface treatments on bond strengths of composite resin bonded to porcelain. *The Journal of Prosthetic Dentistry* 72, 355-359.

Tinschert J, Natt G, Mautsch W, Augthun M, Spiekermann H (2001). Fracture resistance of lithium disilicate-, alumina-, and zirconia- based three-unit fixed partial dentures: a laboratory study. *The International Journal of Prosthodontics* 14, 231-238.

Tinschert J, Zwez D, Marx R, Anusavice KJ (2000). Structural reliability of alumina-, feldspar-, leucite-, mica- and zirconia-based ceramics. *Journal of Dentistry* 28, 529-535.

Trost L, Stines S, Burt L (2006). Making informed decisions about incorporating a CAD/CAM system into dental practice. *Journal of the American Dental Association* 137, 33S-36S.

Tsalouchou E, Cattell MJ, Knowles JC, Pittayachawan P, McDonald A (2007). Fatigue and fracture properties of yttria partially stabilized zirconia crown systems. *Dental Materials* doi:10.1016/j.dental.2007.05.011.

Tsitrou EA, Northeast SE, van Noort R (2006). Evaluation of the marginal fit of three margin designs of resin composite crowns using CAD/CAM. *Journal of Dentistry* 35, 68-73.

Tylka DF, Stewart GP (1994). Comparison of acidulated phosphate fluoride gel and hydrofluoric acid etchants for porcelain-composite repaire. *The Journal of Prosthetic Dentistry* 72, 121-127.

Uo M, Sjogren G, Sundh A, Watari F, Bergman M, Lerner U (2003). Cytotoxicity and bonding property of dental ceramics. *Dental Materials* 19, 487-492.

van der Zel JM, Vlaar S, Ruiter WJ, Davidson C (2001). The CICERO system for CAD/CAM fabrication of full-ceramic crowns. *The Journal of Prosthetic Dentistry* 85, 261-267.

van Noort R (2002). 'Introduction to dental materials.', Mosby, London.

Venetskii S (1965) .The "clothing" of uranium rods. *Metallurgist* 9, 38-39.

Vult von Steyern P, Carlson P, Nilner K (2005). All-ceramic fixed partial dentures designed according to the DC-Zircon technique. A 2-year clinical study. *Journal of Oral Rehabilitation* 32, 180-187.

Vult von Steyern P, Jönsson O, Nilner K (2001). Five-year evaluation of posterior all-ceramic three-unit (In Ceram) FDPs. *The International Journal of Prosthodontics* 14, 379-384.

Wada T (1986). Development of a new adhesive material and its properties. Proceedings of the international symposium on adhesive prosthodontics. pp. 9-18. Academy of Dental Materials, Amsterdam, Netherlands, Chicago.

Wagner WC, Chu TM (1996). Biaxial flexural strength and indentation fracture toughness of three new dental core ceramics. *The Journal of Prosthetic Dentistry* 76, 140-144.

Watanabe M, Iio S, Fukuura I (1984). Ageing behaviour of Y-TZP. In 'Science and technology of zirconia II'. (Eds N Claussen, M Ruhle, and AH Heuer) pp. 391-398. The American Ceramic Society, Inc., Columbus, Ohio.

Weibull W (1951). A statistical distribution function of wide applicability. *Journal of Applied Mechanics* 18, 293-297.

Wen MJ, Mueller HJ, Chai J, Wozniak WT (1999). Comparative mechanical property characterization of 3 all-ceramic core materials. *The International Journal of Prosthodontics* 12, 534-541.

White SN, Li ZC, Yu Z, Kipnis V (1997). Relationships between static chemical and cyclic mechanical fatigue in a feldspathic porcelain. *Dental Materials* 13, 103-110.

Witke K, Österle W, Skopp A, Woydt M (2001). Raman microprobe spectroscopy and transmission electron microscopy of thermal sprayed ZrO_2 coatings before and after rub testing of outer air seals. *Journal of Raman Spectroscopy* 32, 1008-1014.

Wohlwend A, Strub JR, Schärer P (1989). Metal ceramic and all-porcelain restorations: current considerations. *The International Journal of Prosthodontics* 2, 13-26.

Yeo IS, Yang JH, Lee JB (2003). In vitro marginal fit of three all-ceramic crown systems. *The Journal of Prosthetic Dentistry* 90, 459-464.

Yoshimura M (1988) Phase stability of zirconia. *American Ceramic Society Bulletin* 67, 1950-1955.

Zembic I, Lüthy H, Schumacher M, Schärer P, Hämmerle CHF (2002) 2- and 3-year results of zirconia posterior fixed partial dentures, made by direct ceramic machining (DCM). *European Cells and Materials* 3 Suppl.1, 38.

Zeng K, Oden A, Rowcliffe D (1996). Flexure tests on dental ceramics. *The International Journal of Prosthodontics* 9, 434-439.

Zhang MX, Kelly PM (2002). Further study of the model for stress-induced martensitic transformation in Fe-Ni-C alloy and white cast iron. *Material Science and Engineering* A326, 282-287.

Zhang Y, Lawn BR (2005). Fatigue sensitivity of Y-TZP to microscale sharp-contact flaws. *Journal of Biomedical Materials Research Part B: Applied Biomaterials* 72, 388-392.

Zhang Y, Pajares A, Lawn BR (2004). Fatigue and damage tolerance of Y-TZP ceramics in layered biomechanical systems. *Journal of Biomedical Materials Research Part B: Applied Biomaterials* 71, 166-171.

Zhu Q, de With G, Dortmans LJMG, Feenstra F (2003). Subcritical crack growth behavior of Al_2O_3-glass dental composites. *Journal of Biomedical Materials Research Part B: Applied Biomaterials* 65, 233-238.

CHAPTER 9

Appendix

Appendix I The results

9.1 SEM images of the Lava™ specimen failed in subcritical crack growth test

9.1.1 Uncoloured specimen

9.1.1.1 Loading rate of 10 N.s^{-1}

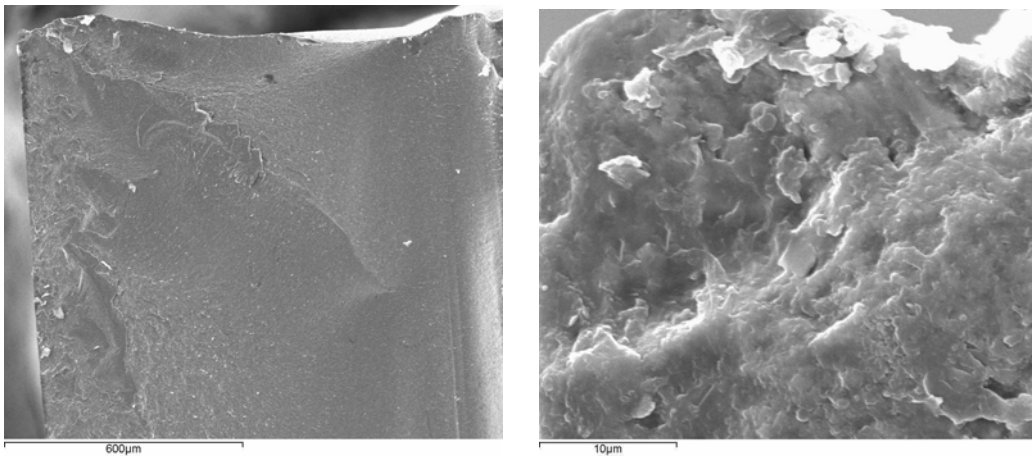

Figure 9.1. SEM image of fractured uncoloured Lava™ specimen after subcritical crack growth test using loading rate of 10 N.s^{-1}.

9.1.1.2 Loading rate of 1 N.s^{-1}

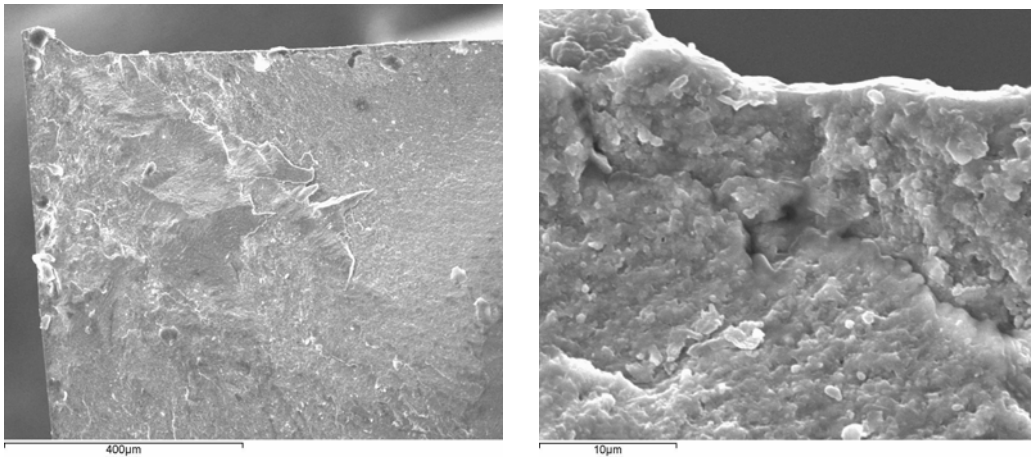

Figure 9.2. SEM image of fractured uncoloured Lava™ specimen after subcritical crack growth test using loading rate of 1 N.s^{-1}.

9.1.2 FS6

9.1.2.1 Loading rate of 10 N.s^{-1}

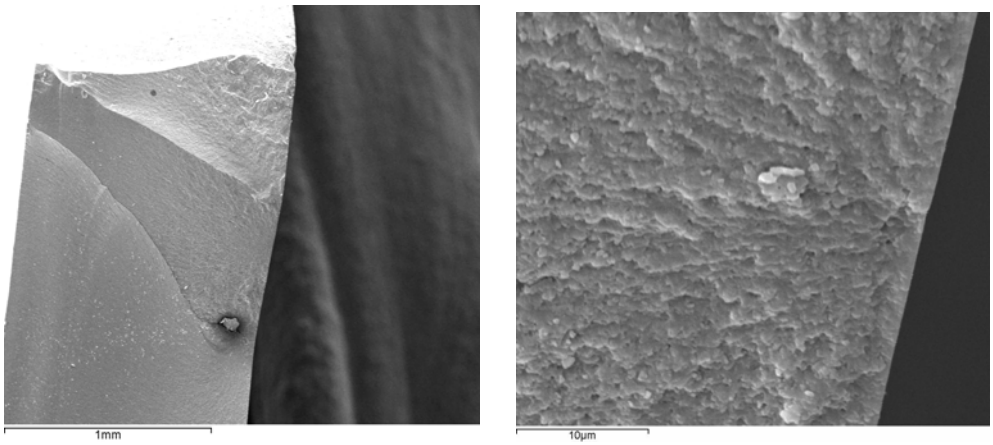

Figure 9.3. SEM image of fractured FS6 Lava™ specimen after subcritical crack growth test using loading rate of 10 N.s^{-1}.

9.1.2.2 Loading rate of 1 N.s^{-1}

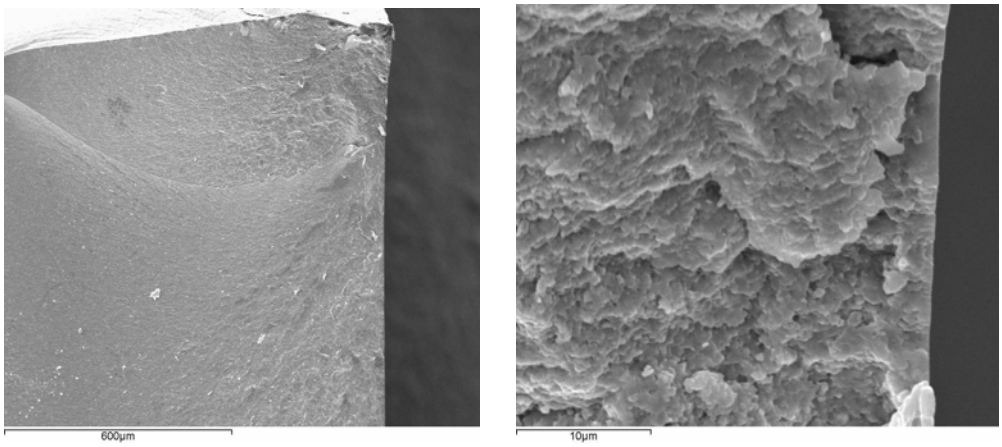

Figure 9.4. SEM image of fractured FS6 Lava™ specimen after subcritical crack growth test using loading rate of 1 N.s^{-1}.

9.2 Raman microscopic images of the fractured surface of Lava™ specimens

9.2.1 Tension side

9.2.1.1 Loading rate of 10 N.s^{-1}

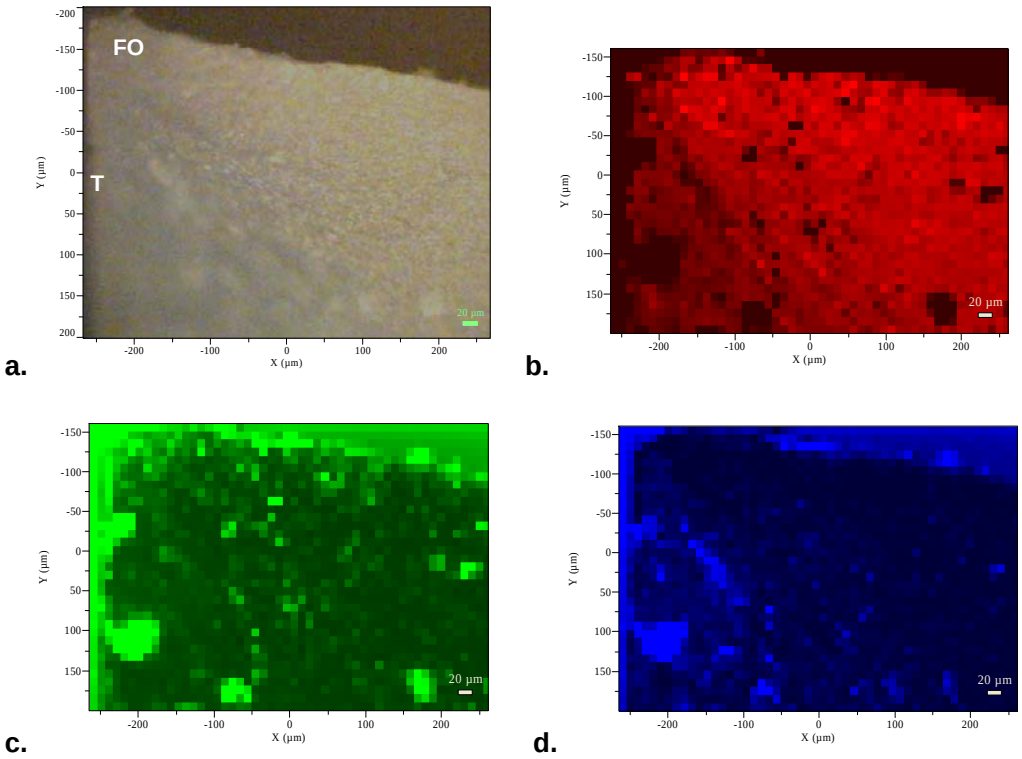

Figure 9.5. Visual image of one part of fracture surfaces at tension side after subcritical crack growth test using 10 N.s^{-1} obtained using the Raman microscope camera. FO is the fracture origin and T is the tensile side. Figures 10 b, c and d indicate the relative levels of tetragonal (b), cubic (c), and monoclinic (d) phases. Black regions indicate lower levels of each given phase.

9.2.1.2 Loading rate of 1 N.s^{-1}

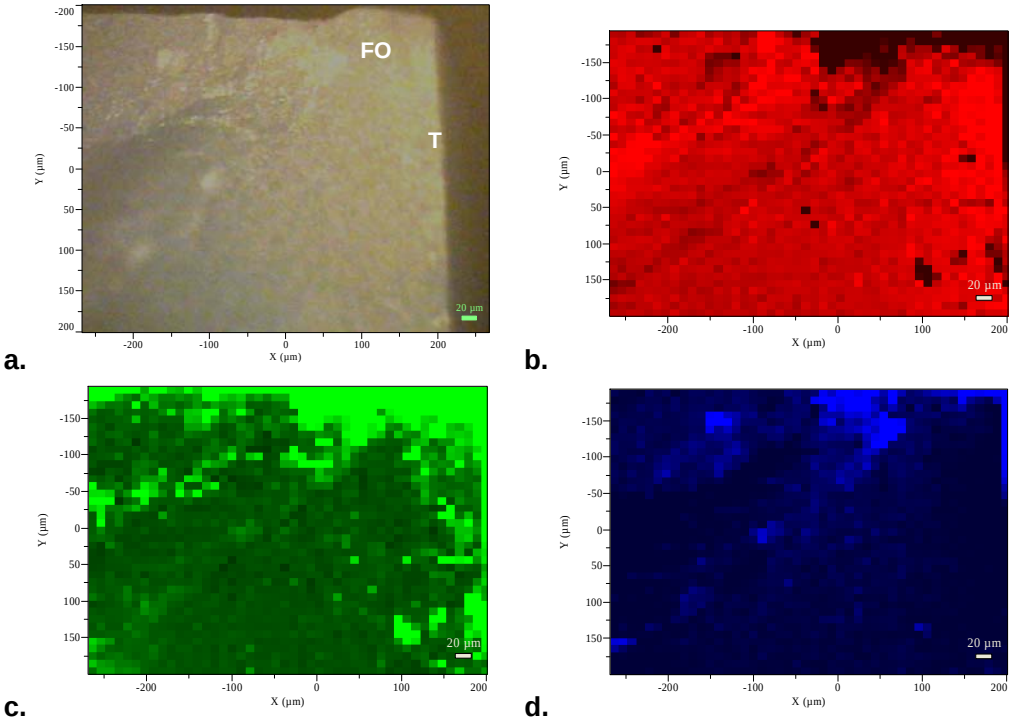

Figure 9.6. Visual image of one part of fracture surfaces at tension side after subcritical crack growth test using 1 N.s^{-1} obtained using the Raman microscope camera. FO is the fracture origin and T is the tensile side. Figures 10 b, c and d indicate the relative levels of tetragonal (b), cubic (c), and monoclinic (d) phases. Black regions indicate lower levels of each given phase.

9.2.2 Compression side

9.2.2.1 Loading rate of 10 N.s^{-1}

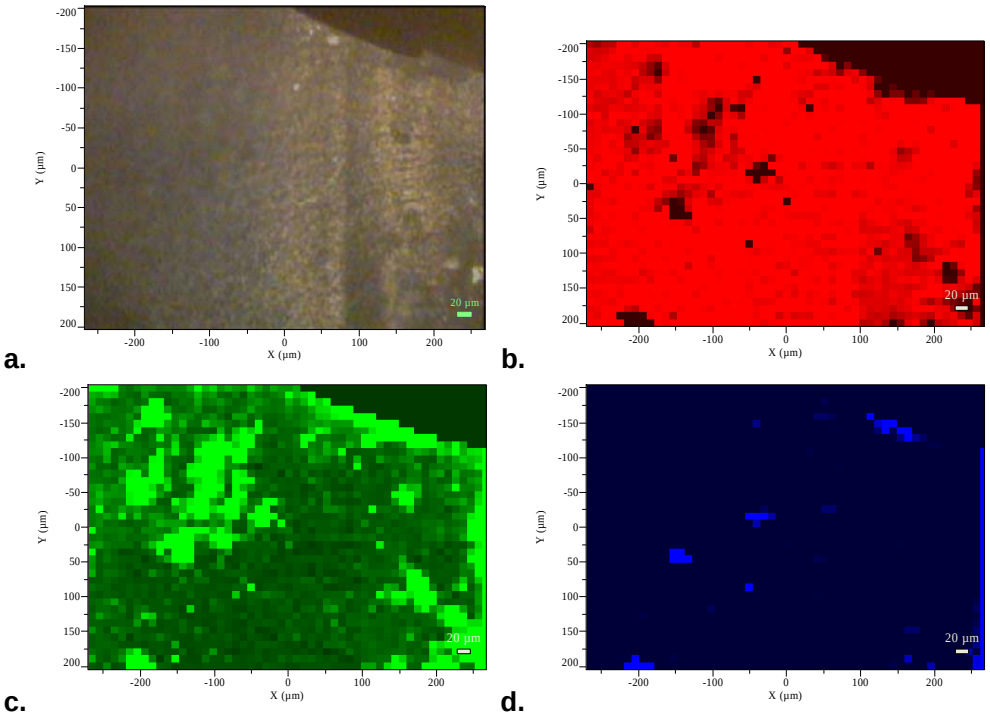

Figure 9.7. Visual image of one part of fracture surfaces at compression side after subcritical crack growth test using 10 N.s^{-1} obtained using the Raman microscope camera. Figures 10 b, c and d indicate the relative levels of tetragonal (b), cubic (c), and monoclinic (d) phases. Black regions indicate lower levels of each given phase.

9.2.2.2 Loading rate of 1 N.s^{-1}

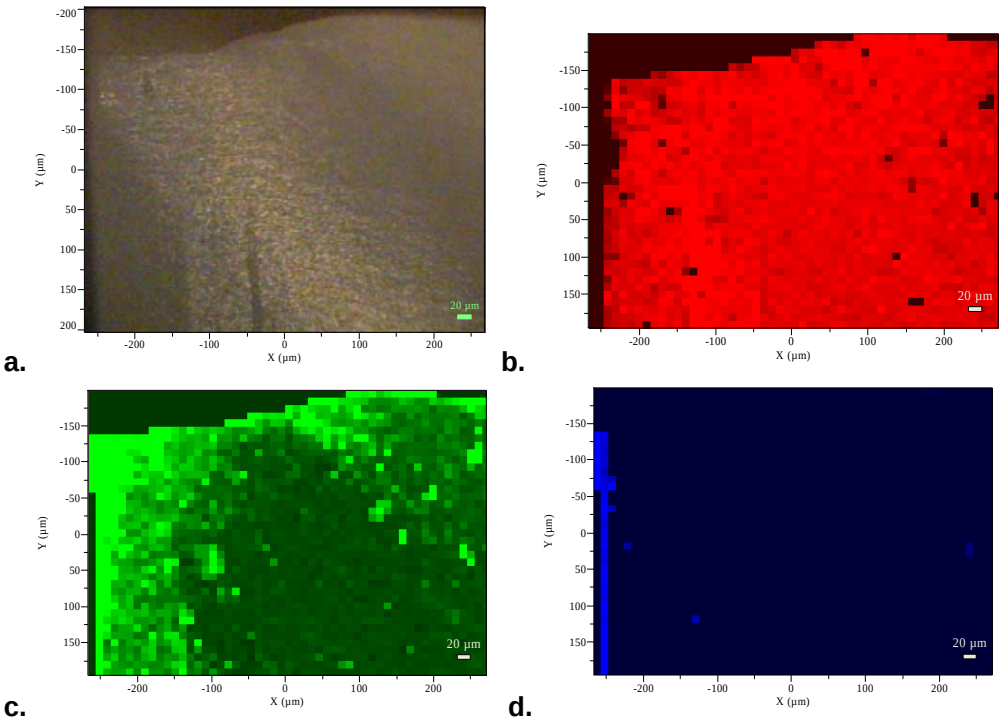

Figure 9.8. Visual image of one part of fracture surfaces at compression side after subcritical crack growth test using 1 N.s^{-1} obtained using the Raman microscope camera. Figures 10 b, c and d indicate the relative levels of tetragonal (b), cubic (c), and monoclinic (d) phases. Black regions indicate lower levels of each given phase.

9.3 The Raman intensity compared between tension and compression sides

9.3.1 Loading rate of 1 $N.s^{-1}$

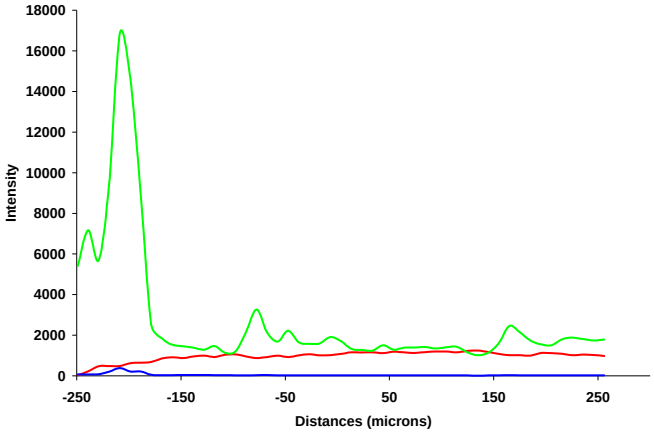

a.

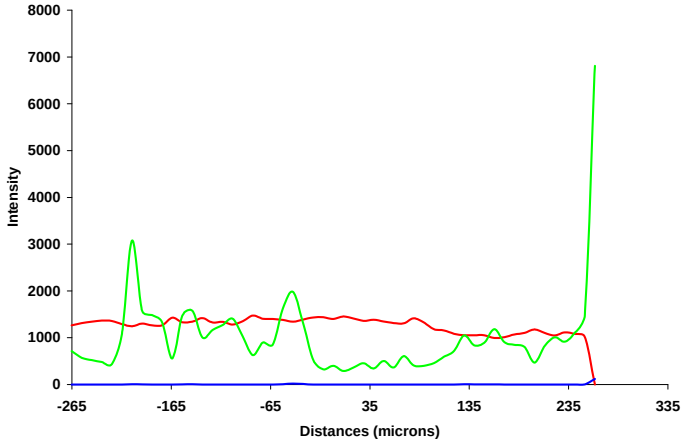

b.

Figure 9.9. Raman intensity of tetragonal (red), cubic (green) and monoclinic phases (blue) at the tension and compression sides of fractured Lava™ specimens after subcritical test using 10 $N.s^{-1}$ loading rate as a function of distance from the fractured area.

9.3.2 Loading rate of 1 $N.s^{-1}$

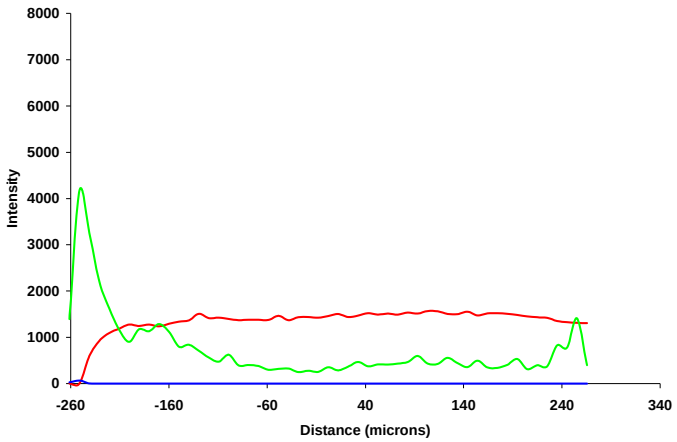

a.

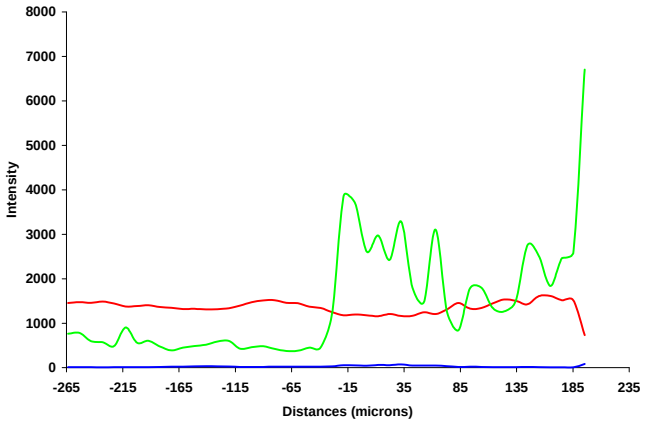

b.

Figure 9.10. Raman intensity of tetragonal (red), cubic (green) and monoclinic phases (blue) at the tension and compression sides of fractured Lava™ specimens after subcritical test using 1 $N.s^{-1}$ loading rate as a function of distance from the fractured area.

Appendix II List of Publications

1. Pittayachawan P, McDonald, A, Pettrie, A, Knowles, JC (2007). The biaxial flexural strength and fatigue property of Lava Y-TZP dental ceramic. *Dental Materials*, 23(8):1018-1029.

2. Pittayachawan P, McDonald A, Young A, Knowles, J.C (2008). Flexural strength, fatigue life, and stress-induced phase transformation study of Y-TZP dental ceramic. *Journal of Biomedical Materials Reasearch Part B Applied Biomaterials*, doi:10.1002/jbm.b.3164

3. Tslouchou E, Cattel MJ, Knowles, JC, Pittayachawan, P, McDonald, A (2008). Fatigue and fracture properties of yttria partially stabilized zirconia crown systems. *Dental Materials*, 24(3):308-318.